School of Biomedical Sciences

Curtin Health Innovation Research Institute (CHIRI) Biosciences Research Precinct

Role of Extracellular Matrix in Muscle Repair and Regeneration

Vishal Chaturvedi

This thesis is presented for the Degree of
Doctor of Philosophy
of
Curtin University

September 2014

Declaration

To the best of my knowledge and belief this thesis contains no material previously published by any other person except where due acknowledgement has been made. This thesis contains no material which has been accepted for an award of any other degree or diploma in any university.

Signature: Vishal Chaturvedi

Date: 1st September 2014

Contents

Declaration i

Abstract xi

Abbreviations xiii

Acknowledgements xvi

Publications arising from this thesis xviii

Presentations done during this thesis xix

Awards obtained during this thesis xx

Chapter 1: 1

Introduction and Literature Review 1

1.0 History of Tissue Engineering: 2

1.1 Muscle mass loss due to injury, disease or ageing 3

1.2 Skeletal muscle: 3

1.2.1 Structure of a skeletal muscle 3

1.2.2 Muscle repair and regeneration: 4

1.3 Extracellular matrix (ECM) in skeletal muscle: 10

1.3.1 Endomysium 10

1.3.2 Perimysium 12

1.3.3 Epimysium 12

1.4 Components of the ECM in skeletal muscle: 13

1.4.1 Collagen 13

1.4.2 Fibronectin 14

1.4.3 Laminin 14

1.4.4 Elastin 15

1.4.5 Proteoglycans (PGs) 15

1.5 Role of native extracellular matrix in muscle repair and regeneration: 18

1.6 Tissue engineering of skeletal muscle: 19

1.6.1 Bioscaffolds 20

1.6.2 Commercially supplied Natural Scaffolds for 2D and 3D TE applications in culture 24

1.6.3 Synthetic scaffolds 25

1.6.4 Developing hybrid materials as scaffolds 25

1.7 Extracellular matrix materials as a biological scaffold 26

1.8 Decellularization of tissues 27

1.8.1 Chemical decellularization methods 27

1.8.2 Physical 29

1.8.3 Biological 29

1.8.4 Whole organ decellularization 30

1.8.5 Decellularization of skeletal muscle 30

1.9 Other approaches used for skeletal muscle TE 33

1.9.1 Micropatterned substrates and self-assembled monolayers 33

1.9.2 Magnetic force based techniques 33

1.9.3 Hydrogels 34

1.10 Translational applications of the ECM scaffolds 34

1.10.1 Small intestinal submucosa (SIS) ECM 34

1.10.2 Clinical studies involving ECM scaffold for TE of muscle 36

1.11 Investigating Cell-Scaffold Interactions 37

1.11.1 Serum free culture 37

1.11.2 Atomic Force Microscopy 38

1.12 Conclusion 40

1.13 Aims of this project 42

Chapter 2: 44

Materials and Methods 44
2.1 Muscle sampling (mice and rats) 45
2.2 Decellularisation 45
2.2.1 Buffers and reagents 45
2.2.2 Decellularization of mouse skeletal muscle sections 47
2.2.2.1 Trypsin method 47
2.2.2.2 Sodium dodecyl sulphate (SDS) method 47
2.2.2.3 Phospholipase method 48
2.2.3 Whole muscle decellularization 48
2.2.4 Solubilisation of acellular skeletal muscle 49
2.2.4.1 Urea and RIPA buffer solubilisation 49
2.2.4.2 Acetic acid solubilisation 49
2.3 Protein Analysis 49
2.3.1 Gels, buffers and solutions for protein analysis 49
2.3.2 Protein quantification 51
2.3.2.1 Bicinchoninic acid (BCA) assay 51
2.3.2.2 Non-Interfering (NI) protein assay 52
2.3.3 SDS-PAGE 52
2.3.4 Coomassie blue staining 53
2.3.5 Electroblotting (protein transfer) 53
2.3.6 Western blotting 53
2.4. DNA analysis 54
2.4.1 Gels, buffers and solutions for DNA analysis 54
2.4.2 Agarose gel electrophoresis 54
2.4.3 DNA extraction and quantification 55
2.5 Immunofluorescence 55
2.5.1 Buffers, solutions and antibodies 55

2.5.2 Immunofluorescence staining procedure 56
2.6 Scanning electron microscopy....58
2.7 Tissue culture and cell based assays....61
2.7.1 Cell lines....61
2.7.2 Basic Tissue Culture Media and supplements 61
2.7.3 Serum free media....62
2.7.4 Freezing and thawing cell lines....62
2.7.5 Cell culture and maintenance....63
2.7.5.1 C2C12 murine myoblasts....63
2.7.5.2 HSMMs....63
2.7.5.3 Serum free culture of C2C12 cells....63
2.7.6 Proliferation and Differentiation of C2C12 cells on different matrices 64
2.7.7 Cell Proliferation (direct cell count) 64
2.7.8 Chloroform sterilisation of decellularised muscle scaffolds....65
2.7.9 Three-dimensional cell culture (C2C12 and HSMM)....65
2.7.10 Kwik Diff staining and imaging....65
2.7.11 Click-iT EdU cell proliferation assay 66
2.7.12 Immunofluorescence for myosin (differentiation marker) 66
2.7.13 Myotube width measurements (Image J) 67
2.8 RNA extraction and quantitative reverse transcription PCR (qRT-PCR) analysis 67
2.8.1 RNA extraction....67
2.8.2 RNA quantification and quality analysis....68
2.8.3 cDNA synthesis....69
2.8.4 Primers for qPCR....69
2.8.5 qRT-PCR and melt curve analysis....71
2.8.6 Primer efficiency calculation 71

2.8.7 Validation of reference genes 72
2.8.8 Gene expression analysis 72
2.9 Collection of silkworm species 72
2.9.1 Silk protein fibroin processing 73
2.9.2 Solubilisation of silk from freeze dried scaffolds for 2D culture 73
2.10 Cell culture and 2D cell based assays 73
2.10.1 Proliferation and Differentiation assays 74
2.10.2 alamarBlue dye assay for C2C12/HSMM cell proliferation 74
2.11 Immunofluorescence of 2D cultures 74
2.11.1 Etching of glass coverslips 74
2.11.2 Matrix protein expression 75
2.11.3 Differentiation of C2C12 and HSMM on silk - myosin expression 76
2.12 qPCR on 2D silk fibroin substrates 77
2.12.1 Gene expression analysis 77
2.12.2 RNA Isolation 77
2.12.3 cDNA synthesis and qRT-PCR analysis 77
2.13 3D cell based assays 79
2.13.1 Preparation of 3D silk scaffolds and HSMMs proliferation and differentiation 79
2.13.2 Immunofluorescence of filamentous actin (F-actin) and myosin 80
2.13.3 Scanning Electron Microscopy of 3D silk scaffolds (+/- HSMM cells) 80
2.13.4 Gene expression analysis of 3D cultures 80
2.13.4.1 RNA extraction 81
2.13.4.2 cDNA synthesis and qRT-PCR analysis 81
2.14 Statistical analysis 81
Development and characterization of an acellular skeletal muscle matrix with well-preserved extracellular matrix (ECM) components 84
3.1 Introduction 85

3.2 Results....86
3.2.1 Trypsin method....86
3.2.1.1 DNA remaining after decellularization....89
3.2.1.2 Retention of matrix proteins after decellularization....89
3.2.2 SDS method....91
3.2.2.1 DNA remaining after decellularization....91
3.2.2.2 Retention of matrix proteins after decellularization....91
3.2.3 Phospholipase method....95
3.2.3.1 DNA remaining after decellularization....95
3.2.3.2 Loss of cytoskeletal proteins following decellularization....95
3.2.3.3 Retention of matrix proteins after decellularization....98
3.2.4 Analyses of solubilised acellular muscle matrix....101
3.2.5 Western blots for PLA_2 method....103
3.2.6 Scanning electron microscopy (SEM) (section 2.6)....105
3.3 Discussion....107
3.4 Conclusion....112
3.5 Future Directions....113
Chapter 4:....115
Acellular skeletal muscle matrix supported serum free proliferation and differentiation of C2C12 murine myoblasts in *in vitro* 2D and 3D cultures4.1 Introduction....115
4.2 Results....118
4.2.1 Proliferation of C2C12 cells on different matrices....118
4.2.2 Differentiation of myoblasts into myotubes....121
4.2.3 qPCR Experimental workup:....121
4.2.4 Gene expression of myogenic markers in C2C12 cells on different matrices 131
4.2.5 C2C12 cell adhesion and proliferation on three-dimensional matrix scaffolds....132

4.2.6 Human skeletal muscle myoblast (HSMM) behaviour on solubilised muscle matrix and collagen I (section 2.7.5.2) 136

4.2.7 HSMM cell adhesion on three dimensional muscle matrix scaffolds 140

4.2.8 Immunostaining for secreted ECM proteins under serum free culture (section 2.11.2) 140

4.2.9 Immunostaining for Matrix deposition after cell removal (section 2.11.2) ... 140

4.2.10 Immunostaining for secreted ECM proteins on collagen type I and solubilised muscle matrix coated etched glass substrates (section 2.11.2) 144

4.3 Discussion 144

4.4 Conclusion 155

4.5 Future directions 155

Silk fibroin as a potential biomaterial for human skeletal muscle myoblast differentiation5.1 Introduction 157

5.2 Results 161

5.2.1 Solubilisation of silk fibroin (section 2.9.2) 161

5.2.2 Cyto-compatibility of different silk fibroins in serum-free culture conditions 162

5.2.3 C2C12 myoblasts fuse to form multinucleated myotubes on all 4 silk substrates 165

5.2.4 Secretion of matrix proteins in 2D serum free cultures (section 2.11.2) 168

5.2.5 Proliferation of Human skeletal muscle myoblasts (HSMMs) on 2D silk fibroin substrates (section 2.7.5.2) 173

5.2.6 Differentiation of HSMMs on 2D silk fibroin substrates 173

5.2.7 HSMM cell adhesion and spreading on four silk 3D scaffolds (section 2.13.1) 176

5.2.8 HSMM cell adhesion on solubilized muscle matrix coated *B. mori* silk scaffold 179

5.2.9 Matrix deposition by HSMMs on four silk 3D scaffolds 179

5.2.10 Scanning electron microscopy (SEM) of 3D silk scaffolds (section 2.13.3) .. 179

5.2.11 HSMMs differentiation on 3D silk scaffolds section (2.13.1) 184

5.2.12 Partially solubilised (or Unfixed) *B. mori* scaffold supported HSMM differentiation (section 2.13.1) 184

5.2.13 qPCR Experimental workup: 188

5.2.14 Relative mRNA levels of myogenic markers in HSMMs on 2D silk substrates (section 2.12) 192

5.2.15 Gene expression of myogenic markers in HSMMs on *B. mori* and *A. mylitta* 3D silk scaffolds (section 2.13.4) 192

5.2.16 3D muscle like tissue growth 195

5.3 Discussion 197

5.4 Conclusion 205

5.5 Future Directions 206

Chapter 6: 208

Atomic force microscopy: applications in muscle matrix biology 208

6.1 Introduction 209

6.2 Supplementary Materials and Methods 212

6.2.1 Cell culture or muscle tissue sectioning 212

6.2.2 Preparation of gelatine gel 212

6.2.2.1 Cross linking the gelatine gel with GAGs 212

6.2.3 AFM Probes used for imaging 212

6.2.4 Mounting the cantilever on scanner 214

6.2.5 Sample mounting 214

6.2.6 AFM imaging 214

6.2.6.1 Contact mode in air 214

6.2.6.2 Tapping mode in liquid 215

6.2.7 picoTREC Measurements 215

6.2.7.1 AFM tip functionalization 215

6.2.7.2 Antibody linking to the tips 216

6.2.7.3 Simultaneous topography and recognition imaging (TREC) measurements 216
6.2.8 Force spectroscopy and force volume imaging 217
6.2.9 Image Analysis 217
6.3 Results 217
6.3.1 Fine structure of cells and cell-matrix interactions were visualized using AFM 217
6.3.2 Muscle matrix ultrastructure visualized using AFM 220
6.3.3 AFM imaging of natural ECM proteins and scaffolds 223
6.3.4 picoTREC imaging of muscle sections (section 6.2.7.3) 223
6.3.5 Force spectroscopy imaging of muscle sections (section 6.2.8) 226
6.4 Discussion 226
6.5 Conclusion 231
Chapter 7: 233
Conclusion and Future Perspectives 233
7.0 Conclusion and Future perspectives 234
References: 241

Abstract

Extracellular matrix (ECM) molecules play important structural and mechanical roles in muscle tissue. They are also critical for normal muscle homeostasis, but it is poorly understood how individual matrix proteins like collagen type I or fibronectin, or a mixture of ECM proteins affects myoblast behaviour. Aspects of this question have been examined in this thesis using both acellular matrices from skeletal muscle and artificial scaffolds prepared from silk proteins. The ability of these surfaces to support myoblast proliferation and differentiation was examined using a murine myoblast cell line and primary human skeletal muscle myoblasts.

This study describes a new method for decellularisation of skeletal muscle that uses an enzyme called phospholipase A_2 and a mild detergent, sodium deoxycholate. This decellularisation method effectively removed all intact muscle cells, and the majority of the nuclear material and cytoplasmic proteins. The remaining acellular ECM contained most of the structural matrix proteins for example: collagens type I, III, IV and VI; major glycoprotein components like fibronectin and laminin-α2; and proteoglycans like perlecan, decorin, plus the retention of a heparan sulphate epitope. Scanning electron microscopy and atomic force microscopy revealed ultrastructural and nanotopographical differences in the control muscle and decellularised muscle matrices.

The mouse myoblast cell line, C2C12, was used to assess the functionality of the acellular matrix. Proliferation and differentiation of C2C12 cells on solubilized and three-dimensional skeletal muscle matrices in a serum free culture system were examined. Use of a serum free culture system removed any possibility that soluble ECM molecules in the culture medium have affected cell behaviour, or have modulated the contribution of the matrix protein substrates to myoblast differentiation. C2C12 mouse myoblasts proliferated on a muscle matrix substrate prepared from solubilized acellular muscle, but seemed to progress towards differentiation at a lower confluency when compared to C2C12 cells cultured on collagen type I and fibronectin coated surfaces. Gene expression data of a selection of genes responsible for myotube formation suggested a similar differentiation pattern on muscle matrix and fibronectin. Furthermore, three-dimensional acellular muscle matrix supported cell growth and provided physical

and chemical signals for cell alignment/orientation, suggesting that *in vivo* it is the muscle ECM that directs cell positioning.

The artificial scaffolds were prepared from silk fibroin of four insect species: the mulberry variety *Bombyx mori* and non-mulberry varieties *Antheraea mylitta*, *Antheraea assamensis*/*assama* and *Samia ricini*. These scaffolds were tested *in vitro* to determine if it may be possible to utilize scaffolds from a particular species as a biomaterial for future skeletal muscle tissue engineering *in vivo*. All the silk proteins, when solubilised and used as substrates, promoted the growth, proliferation and differentiation of C2C12 myoblasts in serum free cultures. Silk fibroin substrates also supported the differentiation of primary human skeletal muscle myoblasts (HSMMs) as was shown by immunostaining against antibodies to skeletal muscle slow myosin heavy chain and the glucose transporter 4. Scanning electron microscopy of the three-dimensional silk scaffolds revealed that the HSMMs spread across the scaffold pores and deposited matrix proteins onto the scaffold material. Differentiation of HSMMs on the three-dimensional scaffolds was triggered more readily on some scaffolds than on others. For example, on *B. mori* scaffolds HSMMs formed extremely long, well aligned myotubes that stained for myosin, whereas the myotubes formed on *A. mylitta* scaffolds appeared thicker and much shorter. The other two scaffolds from *A. assamensis* and *S. ricini* silk fibroin poorly supported differentiation of HSMMs. As a result, it is proposed that *B. mori* and *A. mylitta* scaffolds are most likely to be useful as three dimensional frameworks for skeletal muscle repair in *in vivo* muscle injury models.

Overall, the goal of this project was to use natural skeletal muscle matrices and silk bio-scaffolds to obtain information about ECM components that promote growth and differentiation of muscle precursor cells. This information will assist the development of a muscle specific scaffold that stimulates and enhances the repair and regeneration of aged or damaged skeletal muscle.

Abbreviations

The following abbreviations are used throughout this thesis:

^{o}C	Degrees Celsius
Aa	*Anthaerea assamensis*
Am	*Anthaerea mylitta*
AFM	Atomic force microscope/y
APS	Ammonium persulfate
ATCC	American Type Culture Collection
bFGF	basic fibroblast growth factor
BCA	Bicinchonic acid
Bm	*Bombyx mori*
BSA	Bovine serum albumin
ddH_2O	Double distilled water
dex	Dexamethasone
DMEM	Dulbecco's modified Eagle's medium
DMSO	dimethyl sulfoxide
dNTP	deoxyribonucleotide
DTT	Dithiothreitol
DNA	Deoxyribonucleic acid
ECM	Extracellular matrix
EDTA	Ethylenediamine tetra-acetic acid
EGF	Epidermal growth factor
FBS	Foetal bovine serum
FCS	Foetal calf serum
FGF	Fibroblast growth factor
FITC	Fluorescein isothiocyanate
GAPDH	Glyceraldehyde-3-phosphate dehydrogenase
HEPES	N-2 hydroxyethylpiperazine-N'ethanesulphonic acid
HRP	Horseradish peroxidase
HSMMs	Human skeletal muscle myoblasts
IGF	Insulin-like growth factor
IL	Interleukin
kb	Kilobase

kDa	Kilodalton
µ	micro
µM	micro molar
m	milli
M	molar
mA	milli Amperes
mM	milli molar
mAb	Monoclonal antibody
$MgCl_2$	Magnesium chloride
min	Minute
mRNA	messenger RNA
MW	Molecular weight
NI	Non-Interfering
NHS	N-hydroxy succinimide
nM	nanomolar
NP40	Nonidet P40
PAGE	Polyacrylamide gel electrophoresis
PBS	Phosphate buffered saline
PBS/BSA	PBS/0.5% (w/v) BSA
PBS-T	PBS-Tween
PCR	Polymerase chain reaction
PEG	Polyethylene glycol
PLA_2	Phospholipase-A_2
RNA	Ribonucleic acid
RT	Room temperature
qRT-PCR	Quantitative real time polymerase chain reaction
SD	Standard deviation
SDS	Sodium dodecyl sulfate
SDS-PAGE	Sodium dodecyl sulfate polyacrylamide gel electrophoresis
SEM	Standard error mean
SFM	Serum free media
SIS	Small intestinal submucosa
Sr	*Samia ricini*

TAE	Tris-acetate-EDTA gel running buffer
TE	Tissue Engineering
TEMED	N, N, N', N'- tetramethylethylenediamine
TNF	Tumor necrosis factor
Tris	Tris (hydroxymethyl) aminomethane
Tween 20	Polyoxyethlene sorbitan monolaurate
TX-100	Triton-X-100
U	Units of enzyme
UV	Ultraviolet
≥	greater than or equal to
>	greater than
≤	less than or equal to
<	less than

Acknowledgements

Firstly, I would like to sincerely thank my principal supervisor, Professor Deirdre Coombe for her invaluable guidance and constant support throughout the duration of this project. Her enthusiasm, scientific knowledge and expertise in cell biology has been invaluable and really allowed me to develop as an independent researcher.

I would also like to express my gratitude to my co-supervisor, Professor Miranda Grounds at the University of Western Australia. Her expertise in muscle biology has been invaluable during my PhD study. It is because of her that I got a chance to come and study at Curtin University. I met her in INDIA during a meeting at CCMB in 2010 and she pointed me in the direction of Professor Deirdre Coombe who graciously accepted an international student with no prior experience in extracellular matrix biology.

Extended thanks go to my co-supervisor/colleague Dr Danielle Dye who has always been cheerful and helpful at each and every step of my PhD. She has always extended her generous support whenever I came to her for lengthy conversations about my progress and any problems arising during the project.

I would also like to extend my sincere thanks to lab members of Molecular Immunology group, Ms Beverly Kinnear for her expertise and guidance in tissue culture; Mrs Sandra Stevenson for sorting out the accommodation and pickup from the airport when I first came to Australia. Also many past and current members of the laboratory have remained good friends. Thanks go to Bernadette Mc Erlaine, Xin Chen, Chee Wai Wong and all honours students.

I would like to acknowledge the Curtin University for generously providing the Curtin Strategic International Research Fellowship which allowed me to come and study at Curtin. Thank also goes to Dr Thomas Becker at the Nano Chemistry Research Institute, Curtin University for his able guidance in atomic force microscopy and the staff at the Curtin Electron Microscope Facility for their assistance with scanning electron microscopy.

Last but not the least, personal thanks to all my family and friends who have supported me through this journey; my parents for their endless encouragement and patience for sending me this far from the motherland; my brother and sister for their motivation; my friends Bhawna and Aparna for keeping me well fed and to Shyam and Abhijeet for all those weekend sessions which kept me entertained during the final stages of my writing.

Publications arising from this thesis

- **Vishal Chaturvedi,** Beverly F Kinnear, Danielle E Dye, Miranda D Grounds T.V.H. Kuppeveldt and Deirdre R Coombe. Acellular skeletal muscle matrix supports serum free proliferation and differentiation of C2C12 mouse myoblasts (Manuscript ready for submission, 2014)

- **Vishal Chaturvedi,** Deboki Naskar, Beverly F Kinnear, Danielle E Dye, Miranda D Grounds, Subhash C Kundu and Deirdre R Coombe. Natural biomaterial silk fibroins from mulberry and different non-mulberries support myoblast adhesion, proliferation, and differentiation (Manuscript under preparation for submission into *Acta Biomaterialia,* 2014)

- **Vishal Chaturvedi,** Danielle E Dye, Deirdre R Coombe and Miranda D Grounds. Bioactive scaffolds in skeletal muscle regeneration and tissue engineering. *Australian Biochemist Vol 42 No 3 December 2011*

Presentations done during this thesis

Oral

- "*Acellular muscle matrix supports serum-free proliferation and differentiation of C2C12 mouse myoblasts*" at the 23rd Annual Combined Biological Sciences Meeting (CBSM) held in UWA, Perth on 31st August 2013 and at Mark Liveris Health Sciences Research Student Seminar held in Curtin University, WA on 11th November 2013

Posters

- **Vishal Chaturvedi,** Beverly F Kinnear, Danielle E Dye, Miranda D Grounds Subhash C Kundu and Deirdre R Coombe. "*Silk fibroin, a natural biomaterial supports myoblast differentiation"* at the 38th Annual Scientific Meeting of the Matrix Biology Society of Australia and New Zealand, October 2014, Queenscliff, Victoria (Going to be presented)

- **Vishal Chaturvedi,** Beverly F Kinnear, Danielle E Dye, Miranda D Grounds and Deirdre R Coombe. "*Acellular muscle matrix supports serum-free proliferation and differentiation of C2C12 mouse myoblasts*" at the 3rd annual meeting of Australasian Society for Stem Cell Research held in Brisbane, from 27-29th of October 2013 and at the Indian Ocean Rim Muscle Colloqium held in Singapore, from 12-13th of December 2013

- **Vishal Chaturvedi,** Danielle E Dye, Miranda D Grounds and Deirdre R Coombe. *"Development of an acellular skeletal muscle matrix with well-preserved extracellular matrix (ECM)"* at Combined Biological Sciences Meeting held in University of western Australia, WA, Perth on 30th Aug 2012 and at Mark Liveris Health Sciences Research Student Seminar held in Curtin University, WA on 8th-9th November 2012

- **Vishal Chaturvedi,** Xin Chen, Danielle E Dye, Thomas Becker, Miranda D Grounds and Deirdre R Coombe. "*Atomic Force Microscopy: a novel technique with applications in Matrix Biology***"** in the International Proteoglycan conference held in Sydney from 16th-19th October 2011

Awards obtained during this thesis

2013	Ortho Cell student presentation award in the Regenerative Medicine category 23rd Annual Combined Biological Sciences Meeting, August 2013, University of Western Australia, Perth, WA
2013	National Stem Cell Foundation of Australia Conference Grant 6th Annual Scientific meeting Australasian Society for Stem Cell Research, October 2013, Brisbane, Queensland.
2011 – 2014 (CSIRS)	Curtin Strategic International Research Scholarship This PhD scholarship covered tuition fees and living stipend for 3.5 years

Chapter 1:

Introduction and Literature Review

1.0 History of Tissue Engineering:

The concept of tissue engineering (TE) evolved from a mythical Greek story where Prometheus is punished by Zeus for stealing fire from the Gods and giving it to mankind. Every day an eagle would eat his liver but it is said that Prometheus liver grew as much as it was eaten (Hesiod theogony, 1987). In the modern world context, the idea of using one tissue as a replacement for another was first attempted by Prof Alexis Carrel and Charles Lindbergh at the Rockefeller Institute for Medical Research when they transplanted blood vessels from dogs to the abdominal aorta of cats. In 1912 Alexis Carrel received the Nobel Prize for physiology or medicine for his work on "vascular suture and the transplantation of organs" [1]. It is against this background that the idea of TE emerged, where functional tissue is fabricated using living cells and scaffolds (natural and synthetic) that guide tissue development. The term TE was coined by Prof. Y C Fung (University of California, San Diego) in 1987 at a National Science Foundation meeting. The fields of TE and regenerative medicine were described as "emerging multidisciplinary fields involving biology, medicine, and engineering that are likely to revolutionize the ways we improve the health and quality of life for millions of people worldwide by restoring, maintaining, or enhancing tissue and organ function" (National Institute for Health, USA). The goals are to regenerate new biological tissue to replace diseased or aged tissue by using cells and extracellular matrix or scaffolds [2].

End-stage organ failure is a major cause of death worldwide. Organ transplantation is presently the only solution to this problem. However, even with the recent technological advancements in the field of reconstructive surgery, thousands of people die every year due to shortage of organs. In addition, after successful transplantation of an organ there are risks associated with chronic immune rejection, lifelong immunosuppression and destruction of the transplanted tissue over time. Although Australia is a world leader for successful transplant outcomes, it has one of the lowest donation rates in the developed world. Around 1600 people are on Australian organ transplant waiting lists (Donate Life report, 2011). A more recent Donate life report (2013) revealed the percentage of musculoskeletal transplants is a staggering 84% of all the tissue transplants performed,

thus, highlighting the need for alternative avenues for musculoskeletal repair and regeneration (Donate Life report, 2013) (http://www.donatelife.gov.au).

1.1 Muscle mass loss due to injury, disease or ageing

Skeletal muscle mass gradually decreases as people age, with 20-30% of the skeletal muscle mass lost between the ages of 40 and 80 years [3]. This is likely to be due to an age-related gradual decline in the regenerative response of the skeletal muscle to damage. Compared to young muscle, aged muscle responds with a delayed and sometimes only partly effective regeneration response to injury or overuse [4]. Data suggests that these age related changes in regeneration may be due to changes in the external environment rather than changes intrinsic to muscle satellite cells or to a decrease in the number of satellite cells [5-8]. A number of other factors may also contribute to muscle loss. Various muscle related disorders like Duchenne muscular dystrophy (DMD), dermatomyositis or polymyositis lead to a progressive reduction in muscle mass. Muscle fibre necrosis is the most common form of damage to muscle fibres, the other being muscle fibre atrophy. Muscle injuries are very common in sports, accounting for 10%-55% of sports injuries [9]. These statistics suggests that muscle repair and regeneration is an important issue which needs more focus and attention.

1.2 Skeletal muscle:

1.2.1 Structure of a skeletal muscle

Skeletal muscle performs diverse functions like walking, running, holding an object or maintaining the posture. If a skeletal muscle is damaged due to a disease or trauma, it can account for changes in lifestyle, restricting movement or sometimes causing muscle impairment and disability. Skeletal muscle consists of individual muscle cells called muscle fibres or myofibres. They are among the largest cells in the human body ranging from 10µm to 100µm in diameter. Each one contains many nuclei surrounded by a common cytoplasm and is formed by the fusion of myoblasts as these myoblasts terminally differentiate and cease dividing. Each muscle fibre runs along the entire length of the muscle, which can be as long as 35 cm in a human thigh. It contains many individual contractile subunits called myofibrils extending from one end of the fibre to

the other. Each cylindrical myofibril is surrounded by sarcoplasmic reticulum, a complex of membranes forming a network of hollow tubes [10]. The sarcoplasmic reticulum surrounds the myofibrils and holds a reserve of calcium ions needed for muscle contraction.

The principal cytoplasmic proteins of the myofibres are myosin and actin (also known as "thick" and "thin" filaments, respectively), which are arranged in a repeating unit called a sarcomere. This arrangement of actin and myosin gives skeletal muscle its characteristic striated appearance when a stained longitudinal section of a muscle is viewed under a light microscope [11]. The interaction of myosin with actin is responsible for muscle contraction. Skeletal muscle can produce contractions ranging from quick twitches to powerful sustained tensions [12]. Figure 1.1 shows the structure of a skeletal muscle [13].

1.2.2 Muscle repair and regeneration:

1.2.2.1 Satellite cells

Skeletal muscles have the ability to repair themselves after damage or loss due to injury, disease or ageing. This is due to the presence of a small population of cells called satellite cells or muscle stem cells. Satellite cells (SC) are mononuclear progenitor cells that are located on the outside of the muscle fibres between the basement membrane and the plasma membrane (sarcolemma) of muscle fibres and are responsible for the regenerative potential of skeletal muscle. Satellite cells were first observed in the Tibialis anticus muscle of a frog [14]. They are present in all mammalian voluntary muscles including the muscle spindles [15]. However, other involuntary muscles like cardiac striated muscle and smooth muscle do not contain satellite cells [16]. Although they are generally evenly distributed along a muscle fibre some studies suggest an increased number of satellite cells over at the myoneural junctions in association with soluble acetyl-cholinesterase (AChE) at the end of the fibres [17]. Satellite cell numbers vary according to the type of muscle. Lagord et al (1998) did an *in vitro* study to compare the proliferation and differentiation potential of satellite cells isolated from two different muscles from rats, extensor digitorum longus *(EDL)* and soleus. They found

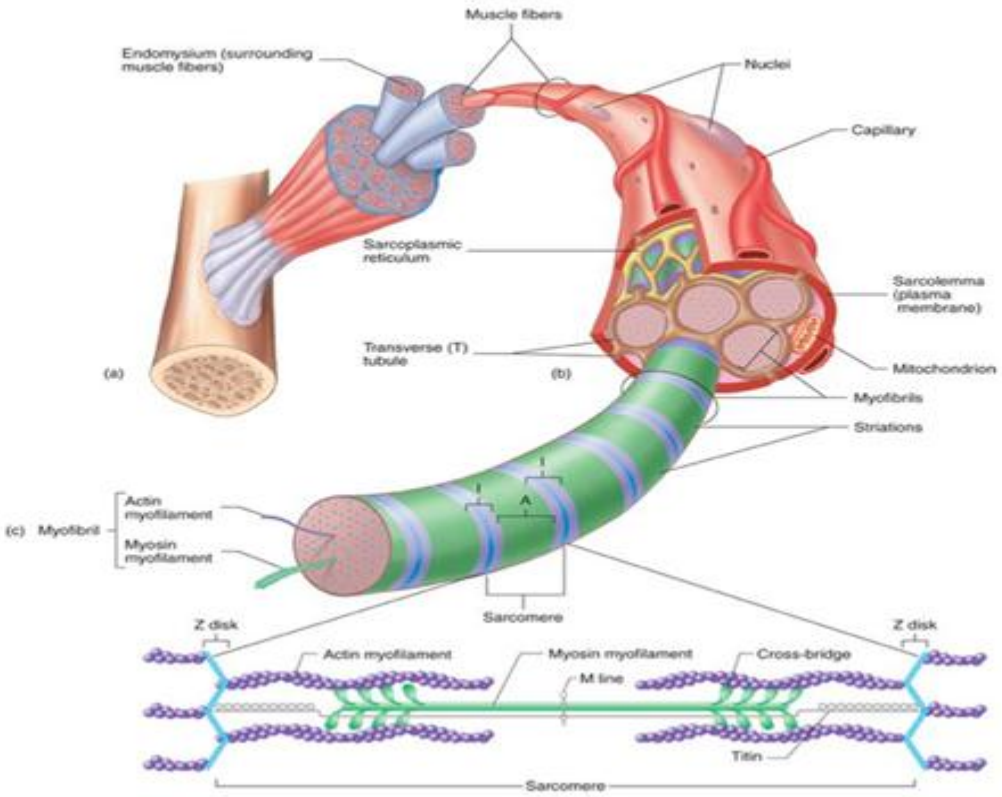

Figure 1.1 Structure of a skeletal muscle. Skeletal muscle consists of individual muscle cells called muscle fibres or myofibres. Each one contains many nuclei surrounded by a common cytoplasm and is formed by the fusion of myoblasts as they terminally differentiate and cease dividing. Each muscle fibre runs along the entire length of the muscle, which can be as long as 35 cm in a human thigh. It contains many individual contractile subunits called myofibrils extending from one end of the fibre to the other. Each cylindrical myofibril is surrounded by sarcoplasmic reticulum, a complex of membranes forming a network of hollow tubes. The sarcoplasmic reticulum surrounds the myofibrils and holds a reserve of calcium ions needed for muscle contraction. The principal cytoplasmic proteins of the myofibres are myosin and actin (also known as "thick" and "thin" filaments, respectively), which are arranged in a repeating unit called a sarcomere. This arrangement of actin and myosin gives skeletal muscle its characteristic striated appearance when a stained longitudinal section of a muscle is viewed under a light microscope. (Image adapted from [13])

that the satellite cell yield from soleus was 50% higher than EDL. After culturing these satellite cells on gelatin-coated culture dishes using normal growth media, they found that satellite cells from soleus muscles were more proliferative than the EDL derived satellite cells. However, the differentiation potential of EDL derived satellite cells was significantly higher than soleus derived satellite cells. Their study suggested that satellite cells have intrinsic differences which can affect the repair process of a muscle [18].

Once activated, satellite cells proliferate, migrate to the damaged area of the muscle, differentiate and fuse to form new muscle fibres which leads to an increase in the cross sectional area of the muscle [19]. Satellite cells are considered functionally heterogeneous in terms of their proliferative and myogenic potential. This is believed to be due to the effects of the different niches, or the microenvironment surrounding the cells [20, 21]. Although satellite cells play an indispensable role in skeletal muscle repair and regeneration, they are not the only cells capable of skeletal muscle repair. In recent years, several research groups have shown that other muscle derived stem-cells and circulating progenitor cells such as bone-marrow-derived cells have a potential for skeletal muscle repair [21-24]. Merritt and colleagues (2010) demonstrated the regenerative potential of bone-marrow derived mesenchymal stem cells (MSCs) *in vivo* [25]. They developed an injury model by creating a full thickness defect in the lateral gastrocnemius (LGAS) of Lewis rats. They implanted decellularized extracellular matrix (ECM) at the injury site and after 7 days seeded MSCs onto the ECM. They showed enhanced functional recovery of the muscle and 94% tension (maximum tetanic force per unit of muscle cross-sectional area) restoration when compared to the contralateral muscle after 42 days of implantation [25].

1.2.2.2 Skeletal muscle repair

Skeletal muscle repair is a highly synchronized process which follows a universal pattern independent of the type or severity of the injury [9] [26]. It can be divided into three phases:

1. Inflammatory phase: This is when rupture and necrosis of myofibres occurs and an inflammatory cell reaction is elicited. When a muscle is injured, myofibres rupture and

release their intracellular contents into the extracellular environment. This is triggered by an increased influx of Ca^{2+} through either, voltage gated Na^{2+} channels or through transient receptor potential channels. Increased Ca^{2+} levels activate Ca^{2+} dependent caspases like calpain, which leads to disintegration of the plasma membrane and other cell constituents. Increased cytosolic Ca^{2+} levels can also trigger membrane lipid peroxidation which is caused by an increase in the reactive oxygen species (ROS) levels [27]. What follows is the entry of plasma proteins into the damaged myofibres which leads to the activation of the complement cascade, resulting in the release of chemotactic factors that direct firstly, the migration of neutrophils followed by the infiltration of macrophages. Two distinct populations of macrophages (M1 and M2) have been identified in injured muscle tissue [28]. M1 macrophages secrete pro-inflammatory cytokines like tumor necrosis factor alpha (TNF-α) and interleukin-1 beta (IL-1β) and phagocytose the necrotic tissue. M2 macrophages cease the inflammation reaction by releasing anti-inflammatory cytokines like IL-10 and promote myoblast proliferation and differentiation by releasing growth factors like platelet derived growth factor (PDGF), basic fibroblast growth factor (bFGF) and other cytokines at the injury site [29-31]

2. Repair phase: Activation of muscle precursor cells leads to the formation of new muscle fibres and a simultaneous formation of scar tissue. Following muscle injury, multiple signals trigger the activation of satellite cells. Sphingosine-1 seems to trigger the initial activation, as when it is not present, satellite cells cannot enter the cell cycle and the repair process is defective [32]. Hepatocyte growth factor (HGF) also plays a role in satellite cell activation by binding to its receptor, c-met, on satellite cells and thereby inhibiting their differentiation into myotubes [33]. Activated satellite cells undergo asymmetric division to form two groups of cells, quiescent new stem cells and myogenic precursor cells (MPCs). MPCs will migrate through the damaged basal lamina and differentiate, fusing either with existing myoblasts or with damaged myofiber ends to form new muscle fibres. Simultaneously, infiltration of fibroblasts into the wound site with an excessive deposition of ECM molecules, mainly collagens, leads to the formation of a connective tissue scar. Scar tissue develops in between the stumps of two

regenerating myofibres and myotendinous junctions are formed within the scar tissue [9].

3. Remodelling phase: Reorganization of the muscle fibres is the next step and muscle function is restored by the remodelling of the scar tissue. Here in this phase, regenerated fibres are marked by the presence of centrally located nuclei and an intact basal lamina plays a major role in this stage of the repair process. Satellite cells and myotubes can fuse to form a myofibre if the basal lamina is intact. New muscle fibres develop connections with the surrounding ECM and their morphology changes during the process, forming forked or split fibres outside the basal lamina [34]. It is also essential for newly developed muscle fibres to develop neuromuscular junctions to avoid muscle atrophy.

1.2.2.3 Growth factors for myoblast proliferation and differentiation

Muscle ECM contains a multitude of growth factors which are secreted by the muscle cells and progenitor cells in response to an injury. Immune cells, neurons and associated vasculature also release growth factors to the injury site and this complex mix of growth factors plays a key role in determining the outcome of the muscle repair process. Key factors involve in the proliferation and differentiation of the myoblasts includes: hepatocyte growth factor (HGF) [35], insulin like growth factor-1 (IGF-1) [36], platelet derived growth factor (PDGF-AA, PDGF-BB), basic fibroblast growth factor (bFGF) [37], vascular endothelial growth factor (VEGF) and nerve growth factor (NGF).

In vitro studies have proposed a major role for IGF-1 in myoblast proliferation and muscle growth. IGF-1 promotes the proliferation of satellite cells thereby altering a range of myogenic markers. Interestingly, direct injection of IGF-1 into the muscle enhances muscle regeneration potential while systemic injection leads to muscle hypertrophy [36, 38]. Although the exact molecular mechanism of how IGF-1 interacts with other molecules and affects the proliferation of satellite cells is not known, there is one study which shows the involvement of PI3K pathway and Akt activation in this process [39]. Other studies have shown HGF is involved in satellite cell proliferation [33, 35] and the expression of HGF increases with the severity of the muscle injury [40,

41]. However, an inhibitory role for HGF has also been suggested because if it is injected directly into the muscle at its differentiation stage, it inhibits myotube formation and does not support muscle repair and regeneration [42].

In addition to growth promoting factors there are growth inhibiting factors residing among the molecules within the muscle ECM. Major growth inhibitory factors are transforming growth factor-α and –β1 (TGF-α, TGF-β1) and myostatin which is a member of the TGF-β superfamily [43]. TGF-β1 primarily acts to inhibit the proliferation and differentiation of myoblasts by blocking their recruitment to the injury site [44, 45]. It also induces the formation of scar tissue at the site of muscle injury which further hampers the muscle regeneration process [9].

1.2.2.4 Different genes involved in muscle differentiation

Formation of myofibers during embryonic development and muscle regeneration is a complex process and a number of different genes are involved in the process of muscle differentiation. The Myogenic regulatory factors (MRFs) are a group of basic helix-loop-helix factors which were discovered in the late 1980's [46-48]. They acts as transcriptional regulators by binding to DNA consensus sites called E- boxes; the basic domain of the MRF binds to DNA and the helix-loop-helix heterodimerizes with E proteins which are transcriptional activator proteins [49]. These factors are the master regulators of skeletal myogenesis and are highly conserved along the skeletal muscle lineage. Four MRFs regulate myogenesis: MyoD, myogenic regulatory factor 5 (Myf5), Myogenin (MyoG) and MRF4. Myf5 is the first regulatory factor to be expressed during mouse embryogenesis at day 8 [50], followed by myogenin and MRF4 at days 8.5 and 9 respectively. MyoD is the last to be expressed at day 10.5 [51]. MRF null mutations and MRF knockouts in different mouse models have increased our understanding of how these factors function *in vivo*. Rudnicki et al (1992) demonstrated that myoD null mice ($myoD^{-/-}$) showed normal muscle development with no adverse effects on the physiology and morphology of skeletal muscles [52]. However, the mutation led to a prolonged increase in the expression levels of myf5 [52]. Similarly, myf5 null mice ($myf5^{-/-}$) also displayed a normal muscle phenotype with no change in the levels of myoD, myogenin or MRF4. However, these mice died perinatally due to their abnormal rib development

and an inability to breathe [53]. The above mouse models and a myoD/myf5 double knockout suggest a functional redundancy in these two genes as only the absence of both genes cause an abnormality in skeletal muscle formation [54]. Myogenin knockout mice ($myoG^{-/-}$) suggest a possible role for myogenin in the later stages of differentiation as these mice were capable of forming myoblasts but were unable to form myotubes [55].

1.3 Extracellular matrix (ECM) in skeletal muscle:

ECM is the structural scaffold of the connective tissue and comprises a dense meshwork of interacting molecules including structural proteins like collagen and elastin, glycoproteins like fibronectin, vitronectin and laminin; proteoglycans such as biglycan, decorin and tenascin, as well as signalling molecules like cytokines and growth factors. The composition of the ECM varies from one tissue type to another; different proteins and proteoglycans combine in various proportions to provide a specific organization to the tissue. For example, a tissue like skin has more elastic ECM than bone which has a very stiff ECM. The interstitial connective tissue around muscle fibres accounts for between 1 and 10% of muscle mass. It assists in the proper alignment of muscle cells, provides a scaffold for nerves, blood and lymphatic vessels [4], and transfers force generated within the muscle fibres to move the skeleton [56]. Anatomically, muscle ECM can be divided into endomysium (around the muscle cell), perimysium (around groups of muscle cells) and epimysium (around the whole muscle) (Figure 1.2).

1.3.1 Endomysium

Each muscle fibre is surrounded by a layer of highly ordered connective tissue, the endomysium. It is composed of a dense meshwork of collagen fibres that are 60nm-120nm in diameter and it forms a continuous sheath covering the full length of the myofibres [57]. The basic understanding of muscle cell endomysium structure and function comes from the work of Purslow and Trotter (1992, 1994) with feline and bovine muscle [58, 59]. They showed that the endomysium is responsible for transmitting force generated within the sarcomeres of myofibres to the tendon and adjacent myofibres. Jarvinen and colleagues (2002) studied the connective tissue arrangement in three rat muscles (soleus, tibialis anterior and gastrocnemius) under

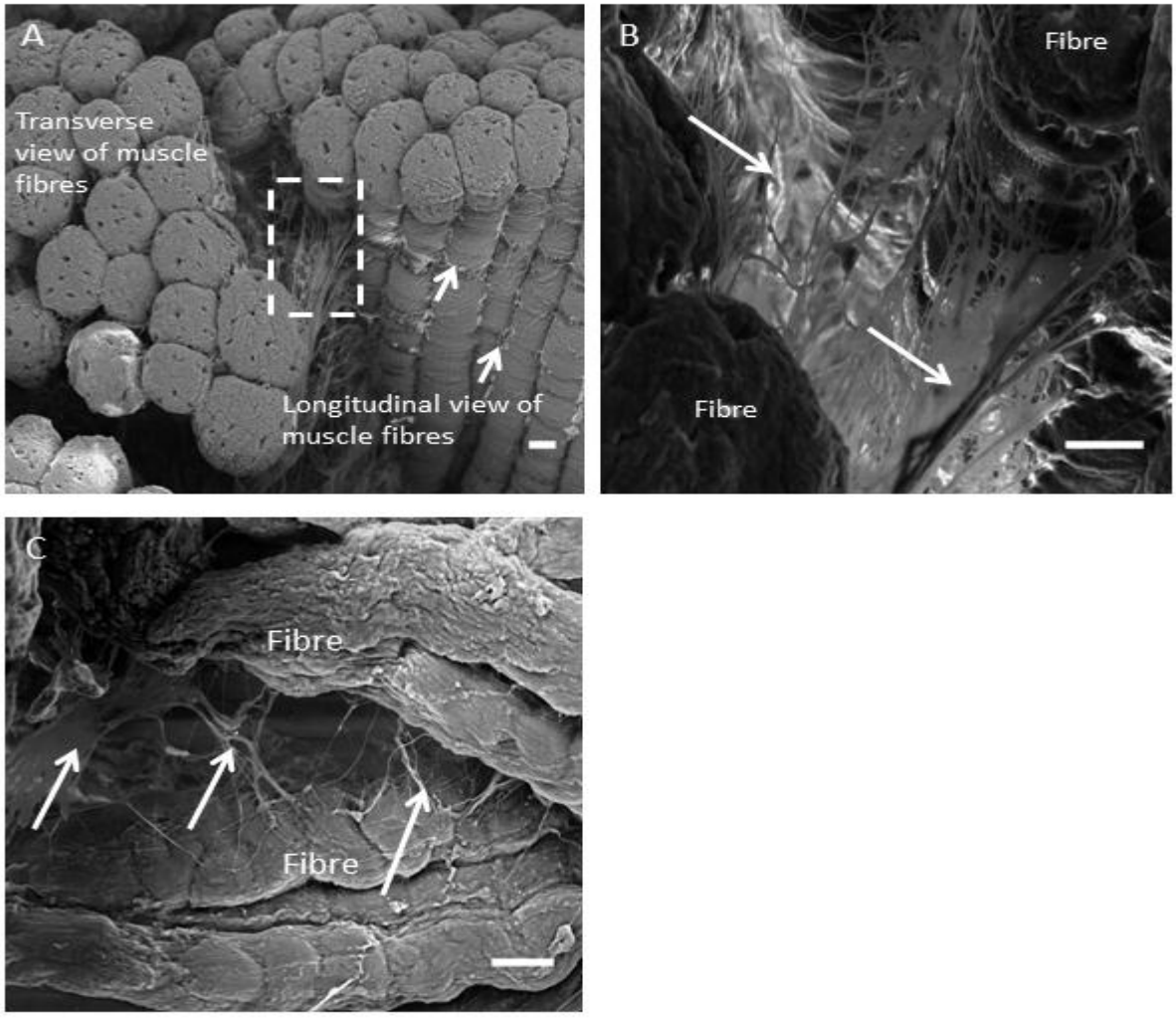

Figure 1.2 Scanning electron micrographs showing skeletal muscle ECM from the quadriceps muscle of 3 month old Sprague Dawley rats. Muscles were cryo-sectioned and formaldehyde fixed, dehydrated in graded series of ethanol, dried and observed under a scanning electron microscope. (A) Group of muscle fascicles showing the underlying arrangement of perimysium (white box) and endomysium (short white arrows). (B) Enlarged view of white box in the subsequent image reveals meshwork of collagen fibrils (white arrows) between the muscle fibres. (C) Longitudinal muscle fibres connected with discrete patches of ECM along the length (white arrows). Scale bar-20µm for A-C.

normal conditions and when rats were immobilized for three weeks [60]. Scanning electron microscopy revealed three separate networks of collagen fibres in the endomysium; (a) collagen fibres running along the surface of muscle fibres in parallel to the orientation of muscle fibres, (b) collagen fibres running perpendicularly to the muscle fibres and connecting two adjacent fibres, and (c) collagen fibres connected to neural and vascular networks. Immobilization led to an increase in (a) endomysial collagen, mainly deposited on the sarcolemma of muscle fibres and (b) number of perpendicular collagen fibres in the endomysium [60].

1.3.2 Perimysium

The perimysium encloses a number of myofibres into bundles or fascicles and it contains capillaries, nerves and lymphatics that run through the muscle. Arterioles and venules are found in this region along with intramuscular nerve branches. Compared to the collagen fibres in endomysium, perimysial collagen fibres are tightly woven, have a thicker diameter (600nm-1800nm) and extend along and across the muscle fibres [57]. Passeurix and colleagues (2006) analysed the structural organization of perimysium in bovine skeletal muscles and they found structures, 150µm-200µm long, called perimysial junctional plates (PJPs). These PJPs connect the endomysium to the perimysium [61]. The higher order arrangement of perimysium remains unknown as there are very few studies that strictly define these structures [62].

1.3.3 Epimysium

The entire muscle is encircled by a sheath of dense, irregular connective tissue, the epimysium, which protects muscles against friction from other muscles and bones. This layer can be dissected from the muscle allowing it to be mechanically tested. Gao et al (2008) developed a micromechanical model to describe the age related changes in the epimysium of old and young rats [63]. They found that the epimysium from old rats was much stiffer than that of the young rats. This finding may have implications in understanding the role of muscle ECM in ageing populations and under some pathophysiological conditions [63].

1.4 Components of the ECM in skeletal muscle:

The ECM in skeletal muscle is composed of structural and adhesion proteins such as collagens, laminins, fibronectin, vitronectin and a variety of proteoglycans (PGs). The ECM is an important constituent of the satellite cell niche and it also plays an indispensable role in skeletal muscle repair processes.

1.4.1 Collagen

Collagen is the most abundant protein in mammals and comprises 25% -35% of the total body protein content [64]. It is also the major structural protein in skeletal muscle ECM and accounts for 1-10% of muscle mass dry weight and nearly 90% of the dry weight of most muscle ECM. To date, twenty eight different types of collagens composed of at least 46 different polypeptide chains, have been identified in vertebrates [65]. A polypeptide chain in a collagen molecule consists mainly of a regular sequence of amino acids Gly-X-Y where X is often proline and Y is hydroxyproline. Each polypeptide chain in turn forms an extended left-handed polyproline type-II helix, stabilized by its high imino-acid content. All collagens share a basic molecular structure comprised of 3 polypeptide alpha (α) chains wound in a right-handed triple-helical conformation to form a coiled coil [64]. This repeat occurs in all types of collagen, although it is disrupted at some locations within the triple helical domain of non-fibrillar collagens [66].

Fibrillar collagens include Type I, II and III and the minor types V and XI. Two additional members of the collagen family, XXIV and XXVI have recently been identified [67]. Type I and III collagen fibrils predominate in adult endo-, peri-, and epimysium. Type I collagen is predominantly present in the perimysium, whereas Type III is more evenly distributed between epimysium and endomysium [68]. These studies were primarily qualitative and it is unclear whether collagen ratios differ in muscles with different functions. This is in part due to difficulties in isolating various regions of ECM. Currently available biochemical techniques do not quantify or differentiate collagen types very accurately. In addition to their structural biomechanical function, collagens also bind to growth factors like transforming growth factor β (TGF-β) and IGF-1 and -2,

and affect cell functions such as proliferation and differentiation through these interactions [69].

1.4.2 Fibronectin

Fibronectin is a high molecular weight glycoprotein that exists as a 450 kDa dimer of two identical chains, with molecular weight of 220-230 kDa each, which are covalently linked in an antiparallel manner by two interchain disulfide bridges at the C-terminal end [70]. Fibronectin exists mainly in 2 forms:

1. A soluble dimeric form known as plasma fibronectin is present in the blood and other body fluids. Blood plasma contains 300-400 µg/ml of fibronectin [71] which is produced by hepatocytes.

2. A highly insoluble matrix form exists as disulfide-bonded multimers and is plentiful in most embryonic and adult mesenchymal tissues, and particularly in loose connective tissue. Fibronectin's role in embryonic development is critical as it has been shown that inactivation of the fibronectin gene leads to embryonic lethality in mice [72]. Integrins, the key receptors that link the ECM to the internal cellular environment and help in signalling bidirectionally across the plasma membrane may bind to fibronectin. Integrin-fibronectin binding interactions are key regulators of cell-matrix interactions [73]. Fibronectin binds to collagen, laminin and other molecules of the ECM and it plays a key role in cell adhesion, migration and differentiation [74].

1.4.3 Laminin

The laminins are large heterotrimeric molecules (400-900 kDa) composed of three chains: α, β and γ each of which occur in multiple forms and variously combine to generate 16 different laminin subtypes. These molecules have a cruciform or T-shaped appearance and are a major component of all basement membranes [75]. In skeletal muscle, laminins containing the α2 chain are a major component of basement membrane, with laminin-2 (α2β1γ1) being the major form around the sarcolemma of mature myofibres, while laminin-4 (α2β2γ1) occurs at neuromuscular junctions (where the synapses connects nerves to muscle) and myotendinous junctions (where myofibers are connected to the tendon) [76].

Laminins play a key role in transmitting the contractile force from the muscle fibre to the ECM through binding to the dystrophin glycoprotein complex [77]. In the absence of laminin, transfer of the contractile force of the myofibre to the interstitial connective tissue fails to occur. Laminin α2 is of central importance as it is required for maintaining the stability and structural organization of mature muscle. Genetic defects in the laminin α2 chain can cause severe congenital muscular dystrophy in humans [78]. Cell surface receptors or integrins also binds to laminin and mediate cell signalling across the cell membrane [76].

1.4.4 Elastin

Elastic fibres are essential components of an ECM that imparts flexibility and elasticity to several organs including skin, lungs, tendon, ligaments, arteries, cartilage and blood vessels in all vertebrates [79, 80]. Elastin constitutes 90 % of the elastic fibre with the remaining 10 % constituting of microfibrils including proteins like fibrillin-1, fibrillin-2 and membrane associated glycoprotein [79]. Elastin is formed by cross-linking of tropoelastin, a 60-70 kDa molecule which exists as a monomer in solution [81]. Various molecules such as glycosaminoglycans bind to tropoelastin [82] and proteoglycans (PGs) like biglycan and decorin also interact with tropoelastin [83]

1.4.5 Proteoglycans (PGs)

Proteoglycans are proteins modified by the covalent attachment of one or more glycosaminoglycan (GAG) chains. They include molecules such as perlecan, decorin biglycan and syndecans [74]. GAG molecules are attached to their protein core by a specific trisaccharide composed of two galactose residues and a xylose residue. The trisaccharide linker is coupled to the protein core through an *O*-glycosidic bond to a serine residue in a serine-glycine motif in the protein. Proteoglycans are structurally diverse, some PGs like syndecans are integral membrane glycoproteins where as others like perlecan are ECM components. As well as differing in the amino acid sequence of their core protein, they also possess different numbers of GAG chains attached to the protein core. Proteoglycans are found in all connective tissues, in the ECM and on the surfaces of many cell types. They perform a multitude of functions and the major

ones include: assisting in the maturation of specialized tissues, influencing cell growth and modulating growth-factor activities [84].

1.4.5.1 Glycosaminoglycans (GAGs)

GAGs are large complex carbohydrate molecules comprising long unbranched chains of repeating disaccharide units composed of an amino sugar (N-acetyl glucosamine or N-acetyl galactosamine) and a uronic acid (glucuronic acid or iduronic acid). The most common GAGs in muscle are heparan sulfates (HS), chondroitin sulfates (CS) and dermatan sulfates (DS) [74], and these are found both within the matrix and on the surface of muscle cells. Chondroitin sulfate contains the disaccharide unit N-acetylgalactosamine and glucuronate with on average one sulphate group per disaccharide, while DS chains contain different proportions of iduronic acid in place of glucuronate and a similar degree of sulfation [85].

Heparin is a hydrophilic, linear unbranched GAG consisting of repeating units of uronic acid, either L-iduronic or D glucuronic acid in a proportion of approximately 9:1, which is linked to glucosamine residues via 1-4 linkage [86]. Heparan Sulphate is similar to heparin in its structure and contains the disaccharide unit of N-acetylglucosamine alternating with a uronic acid, however the degree of sulfation is much less in HS than in heparin. During biosynthesis, the HS chains are covalently linked to their core proteins to form heparan sulphate proteoglycans (HSPGs) and HSPGs are the major PGs in the basement membrane and on cell surface in skeletal muscle [86].

Glycosaminoglycans have been implicated in cell behaviours such as proliferation, differentiation, adhesion and migration due to their ability to bind growth factors and cytokines. The binding of growth factors to GAGs is primarily an electrostatic interaction whereby the negative charge of the GAG chain binds basic regions of growth factors and cytokines. The binding of growth factors and cytokines to GAGs protects these proteins from degradation and presents them to their cell surface receptors [87]. Spatiotemporal regulation of PGs in the ECM and on the cell surface creates a specific environment around muscle cells that regulates myogenesis; in particular by regulating the availability of different growth factors. Barbosa et al (2004) quantified the

composition of different GAGs during myogenesis of C2.7 mouse cells and found that during myogenic differentiation, levels of HS GAGs were increased [88]. They also investigated the effect of a dextran polymer, ReGeneraTing Agent (RGTA) which is a GAG mimetic on the amount of GAG species during myoblast growth and differentiation and found that RGTA increased the total amount of GAGs without affecting their degree of sulfation [88].

1.4.5.2 Biglycan

Biglycan is a member of the small leucine rich proteoglycan (SLRP) family and consists of a core protein of 42 kDa and two CS chains [89]. Biglycan is highly expressed in young and regenerating muscles of both mice and humans [90, 91]. In addition to skeletal myofibres it is also expressed in the pericellular region of a variety of other tissues like articular cartilage, sub-perichondral regions, periosteum and renal tubular epithelia [89]. Previous studies have shown that biglycan plays a role in matrix organization followed by muscle remodelling by binding to various growth factors like TNF-α, and TGF-β [92, 93]. Biglycan also binds to α-dystroglycan of the dystrophin associated protein complex through its two GAG chains [94]. The implications of this interaction have not yet been elucidated; however, it may play a role in localizing signalling molecules to the plasmalemma of the muscle fibre. Other studies have shown that biglycan interacts with other matrix molecules like collagen I [95], collagen VI [96] and the elastin microfibril network (i.e. tropoelastin) [97] suggesting a role for this proteoglycan in matrix assembly.

1.4.5.3 Perlecan

Perlecan is a member of the heparan sulphate proteoglycan (HSPG) family and consists of a protein-core of about 400 kDa and three 100 nm long heparan sulfate chains of 35-40 kDa each [98]. It was the first basement membrane proteoglycan to be characterized, and was first isolated from the mouse Englebroth-Holmes-Swarm (EHS) tumor [99] [98]. Hassell and colleagues (1980) coined the term Perlecan (Perl-beads and can-Glycosaminoglycan) due to its appearance like ‘beads on a string’[100]. It has been shown that perlecan binds to the acetyl-cholinesterase (AChE) and is essential for its localization to the NMJs [101-103]. Although, it is difficult to study the developmental

role of perlecan in placental mammals because of embryonic lethality of perlecan gene knockouts [104], the work of Zoeller et al (2008) suggests a potential role of perlecan in human myopathies. In addition, perlecan has been shown to play a role in muscle development in other systems. Using zebrafish as a model system, perlecan morphants showed a severe myopathy characterized by abnormal orientation and reduced amounts of actin filaments and disorganized sarcomeres [105]. Recent studies in drosophila have shown that perlecan regulates Wnt signalling at the NMJs [106].

1.4.5.4 Decorin

Decorin is also a member of the SLRP family and shares 57% homology, and is somewhat similar in structure, to biglycan except that it contains, either a CS chain or DS chain at its N-terminal end [107]. *In vitro* studies have shown that decorin binds to myostatin and entraps it in the ECM. Myostatin is a member of the TGF- β family of proteins and is a negative regulator of skeletal muscle growth [108, 109]. Recently, Li et al (2007) demonstrated using mouse models that decorin activated the differentiation of the murine myoblast cells, C2C12 *in vitro* and enhanced muscle regeneration by upregulating the expression of p21, follistatin, peroxisome proliferator-activated receptor gamma coactivator-1-alpha (PGC-1α) and downregulating myostatin expression [110]. The core protein of decorin contains binding sites for collagen I and fibronectin [111]. Goetsch et al (2011) showed that decorin modulated C2C12 migration in an *in vitro* wound repair model and has a synergistic effect on the migration of myoblasts when added in combination with collagen I [112].

1.5 Role of native extracellular matrix in muscle repair and regeneration:

The first report to imply a role of ECM in muscle repair and regeneration was published in 1966 by Hauschka and Konigsberg [113]. This study showed there was an enhanced proliferation of embryonic chick myoblasts on a collagen substrate compared to cells grown on tissue culture plastic. Later, Hartley et al (1990) showed that Matrigel (a commercially available ECM) enhanced myoblast attachment and differentiation, but not proliferation [114]. Although ECM molecules play important structural and mechanical roles in muscle tissue, it has become clear that the interactions between

muscle cells and the surrounding ECM are critical for normal muscle homeostasis as well as the activation of satellite cells and subsequent repair and regeneration of muscle tissue [74]. Although it is well known that the ECM is essential for normal myogenesis and muscle regeneration, few studies have attempted to identify the specific factors that are critical to these processes. There are a few reports that describe the interaction between the ECM and growth factors in muscle. Kricker et al (2003) showed the interaction of HS-proteoglycans with growth factors such as fibroblast growth factors (FGFs), hepatocyte growth factor (HGF) and TGF-β [115]. Fiorotto et al (2003) found that the large family of IGF-1 binding proteins (IGF-BPs) in the ECM varies with age and gender [116]. It has also been shown that hyaluronan (a non-sulfated glycosaminoglycan) acts as an inhibitor of myoblast differentiation with no effect on myoblast attachment or proliferation [117].

1.6 Tissue engineering of skeletal muscle:

Skeletal muscle tissue comprises 40-50% of the human body mass and may be lost due to traumatic injury, surgical ablations or as a result of a musculoskeletal disorder [118]. When a traumatic injury results in a significant loss of muscle, the natural repair processes are unable to bridge the gap between the remaining muscle tissue, leading to the accumulation of scar tissue, cosmetic deformity and a loss of muscle function. A current treatment option available for repairing the damaged muscle tissue is "autologous grafting" which is the relocation of muscle tissue from an autologous site to the site of the defect. However, autologous transfers are not completely successful due to limitations in the supply of tissue and can result in donor-site morbidity, causing functional loss and volume deficiency [119]. Another method of muscle repair is the injection of a suspension of satellite cells or myoblasts to the site of injury but this was found to also have a modest therapeutic outcome due to poor retention, survival and integration of grafted cells [120]. Skeletal muscle tissue engineering provides a promising alternative for these treatments with minimal functional loss. Bach et al (2004) defined skeletal muscle tissue engineering as "an interdisciplinary approach, using cell biology and engineering principles to generate functional muscle tissue by

initiating neo-organogenesis from mononucleated stem cells (e.g. myoblasts) to differentiated myofibres" [119].

1.6.1 Bioscaffolds

An important pre-requisite for skeletal muscle tissue engineering is a scaffold to support the organization, growth and differentiation of cells in the process of forming a functional tissue. It is a great challenge to find a suitable matrix or scaffold for skeletal muscle TE purposes. An ideal skeletal muscle scaffold should be biocompatible, biodegradable (with non-toxic degradation products), porous and have the correct balance of stability and elasticity [121, 122]. Scaffolds should also mimic the ECM of skeletal muscle, thereby increasing the probability that surrounding cells will be stimulated to proliferate, migrate and differentiate correctly [123]. Currently, there are limited materials available that both meet these criteria and are easy to manufacture. A range of bio-degradable and non-biodegradable materials have been developed and tested in skeletal muscle tissue engineering applications. These can be classified into: natural and synthetic scaffolds. In the past decade, there have been significant advancements in the development of such scaffolds.

1.6.1.1 Natural scaffolds

Natural scaffolds consist of proteins and polysaccharides. These include natural structural proteins such as collagen, fibronectin, elastin, fibrin, and laminin and polysaccharides like chitosan, alginate and hyaluronan [124]. Alginate is a polysaccharide from marine organisms that can be prepared into three-dimensional porous scaffolds. Fibroblasts seeded on these scaffolds remained spherical in contrast to the flat morphology seen when they are seeded onto culture dishes [125]. Guerret et al. (2003) used collagen as a scaffold for dermal tissue engineering. They implanted Apligraf® (a bioengineered skin composed of a bovine collagen network containing living human fibroblasts overlaid with a human keratinocyte derived differentiated epithelium) into athymic mice. Examination of the implant by immunohistochemistry (IHC) and transmission electron microscopy (TEM) revealed that the graft provided living and bioactive cells to the wound site even after one year past grafting [126]. Other clinical studies have similarly shown that collagen can be a useful scaffold for

regenerating cells [126-128]. In addition to these purified natural products, natural ECMs such as that derived from decellularized porcine small intestinal submucosa (SIS) has been used with some success to repair muscle defects in abdominal wall and load bearing skeletal muscle [129, 130].

Natural scaffolds have advantages over their synthetic counterparts in terms of their excellent physiological and mechanical properties that resemble natural tissues and their biodegradability. However, potential limitations of these scaffolds include a risk of viral infection from animal derived products, an unstable material supply and deterioration which accompanies long term implantation [131]. In recent years, natural silk has become an emerging biomaterial for TE purposes.

1.6.1.2 Natural Silk as a Biomaterial

Silk is a natural biopolymer produced by the silk glands of some arthropods. Although spiders, fleas, bees and scorpions produce silk the main source is from the larvae of silkworms of various Lepidoptera. Two major groups of silkworm are economically and commercially important, namely bombycidae (mulberry) and saturniidae (non-mulberry) [132]. The domesticated mulberry species *Bombyx mori*, the major species used in the textile industry, is found throughout the world, whereas the wild non-mulberry species are found in specific geographical regions. The widely available non-mulberry varieties are *Antheraea mylitta* (Tropical tasar), *Antheraea assamensis/assama* (Muga) and *Philosamia/Samia ricini* (Eri); all of which are found in the Indian subcontinents. Some other species like *A. pernyi* (Chinese temperate oak tasar) and *A. yamamai* (Japanese oak tasar) are also important. Silk proteins obtained from cocoon of *B. mori* are of two types: the hydrophilic water soluble protein called sericin, which uniformly covers the fibrous hydrophobic protein fibroin. It is the fibroin protein that makes up textile fibers. Sericin is a glycoprotein with a molecular weight in the range of 24-400 kDa and constitutes 20-30% of the total weight of the cocoon [133]. Silk fibroin is a semi-crystalline fibrous protein; it is the key component of silk and constitutes 78 % of the total cocoon weight. The *B. mori* fibroin consists of a heavy (H) chain (390 kDa) and a light (L) chain (26 kDa) connected by a disulphide bond formed between cysteine-20 at the carboxyl terminal of the heavy chain (C20) and cysteins-172 of the light chain (C172) [134]. A 30

kDa glycoprotein, P-25, is non-covalently linked to the H-L chain complex through hydrophobic interactions [135]. The sequence of the H chain reveals a highly repetitive glycine rich core flanked by non-repetitive sequences. It is the repeating GAGAGS motif that is the main component of the highly ordered β-sheet crystalline units which give rise to the strength and toughness of silk, whilst the non-crystalline regions contribute to silk's elasticity [136].

Fibroin proteins from other silkworm species have slightly different structures. For example, *A. mylitta* fibroin is a homodimer of a H-chain of 197 kDa, *A. assama* fibroin is a heterodimer comprising chains of 220 kDa and 20 kDa and fibroin from *S. ricini* consists of a heterodimer of chains of approximately 245 kDa and 210 kDa [137, 138]. These differences as well as the underlying amino acid sequence differences between the mulberry and non-mulberry species contribute to the different properties of these silk fibroin proteins. In contrast to *B. mori* the β-sheets of non-mulberry species generally arise from poly-alanine repeats which give rise to their very high tensile strength and when in aqueous solution α-helical as well as random coil structures are found, whereas *B. mori* silk fibroin in aqueous solution is primarily random coils [138]. In addition, fibroin from *A. mylitta* possesses RGD sequences, but *B. mori* fibroin does not. Probably as a consequence the organisation of the actin cytoskeleton, cell spreading and the binding force between cells and substratum was higher on films of *A. mylitta* fibroin compared to cells on *B. mori* fibroin films [139].

Traditionally silk is mainly used in the textile industry; however silk also has medical applications, particularly for making sutures. Properties such as high tensile strength, elasticity, thermal stability and biocompatibility make silk a useful biomaterial. Silk proteins have also been used by the biomedical field for applications like implantable biomaterials, drug delivery vehicles and medical devices because of their mechanical robustness, inertness and biodegradability.

Most of the commercial silk used for textiles and sutures is obtained from *B. mori*. However, attention is gradually focusing on the indigenous species (*A. mylitta, A.*

assamensis/assama and *S. ricini*) as an alternative source of silk proteins. These species can be naturally reared and the water based processing and easy formatting of the silk proteins from these species make them very attractive to the tissue engineering and biomedical fields [138, 140, 141]. Fibroin scaffolds and materials, prepared from regenerated protein solutions possess characteristics which are key requirements of a standard biomaterial. These matrices can be engineered and employed as constructs for different applications in tissue engineering such as for bone [142-144], cartilage [145, 146], cardiac [141], liver [147] and skin tissue engineering. Three-dimensional (3D) fibroin scaffolds are also utilized as in vitro tumor and metastasis model [148, 149]. Silk biomaterials can be moulded in various forms such as hydrogels, membranes, nets, sponges and scaffolds. Useful information about cell interactions with silk is mostly gathered by coating thin films of solubilised silk in two-dimensional (2D) in vitro cell culture however, 3D silk scaffolds provides a better alternate, which mimics the in situ cell-matrix interactions and other microenvironments [148].

1.6.1.3 Bio-compatibilty and bio-degradability of Silk

Any foreign material before being used as a biomedical implant needs to be tested for its immuno-modulatory properties, with silk being no exception. The immunogenic potential of silk fibroin and sericin proteins have been tested using both, *in vitro* and *in vivo* model systems. Panilaitis et al (2003) investigated the innate immune response of solubilised silk extracts and intact silk fibres using murine macrophage cells (RAW 264.7) in an *in vitro* system for 1 and 7 days [150]. Silk fibres or solubilised silk failed to elicit an immune response measured by TNF-α release. Even sericin proteins were not able to activate the macrophages. However, a suspension of irregularly shaped silk fibroin particulates measuring 10 µm-200 µm in diameter resulted in an increased expression of TNF-α in a dose dependent manner [150].

For any biological implant to be a successful candidate for tissue transplantation purposes, it should be bio-degradable without releasing any toxic products during the degradation process. *In-vivo* degradation rates and inflammatory responses to 3D silk fibroin scaffolds implanted in muscle pouches of nude and Lewis rats have been investigated by Wang et al (2008) [151]. Scaffolds used in this study were either

prepared using an all-aqueous process or using an organic solvent, hexafluoroisopropanol (HFIP). The results showed that aqueous derived scaffolds degraded completely between 2-6 months while HFIP-derived scaffolds were stable for more than a year. Interestingly, the immune responses to both the scaffolds were mild and the implants were well tolerated by the rats [151]. Another study showed a time dependent degradation of electrospun silk fibroin scaffolds when the scaffolds were treated with an enzyme solution of protease XIV *in vitro*. The same scaffolds when implanted intramuscularly and subcutaneously were degraded within 8 weeks [152].

1.6.2 Commercially supplied Natural Scaffolds for 2D and 3D TE applications in culture

A number of natural scaffolds have made their way from bench to bedside in recent years and are now commercially available. A popular natural scaffold for 3D TE is Matrigel (Becton Dickinson Biosciences, San Jose, CA, USA) which is derived from the murine EHS tumor. It is a basement membrane preparation and primarily consists of laminin, collagen IV and entactin. It is mainly used for 3D culture *in vitro.* For example, it has been used as a substrate for culturing endothelial cells to study the role of various growth factors during angiogenesis [153]. Although, Matrigel supports cell growth and differentiation, its composition has not been well-defined and it varies from batch to batch. Hence, it is not an appropriate matrix for *in vivo* TE applications.

Hyaluronic acid (HA) hydrogel scaffolds include HyStem for culturing stem cells and Extracel (Glycosan BioSystems, Salt Lake City, UT, USA) for general cell culture. Other natural scaffolds include different alginate-based systems such as AlgiMatrix (Invitrogen) or the peptide based self-assembling-gel, Puramatrix developed in the laboratory of Shuguang Zhang at Massachusetts Institute of Technology and marketed by 3D Matrix Inc. (Waltham, MA, USA). PuraMatrix is an amino acid–based hydrogel consisting of 16-mer oligopeptides that self-assemble into nanofibers and form a matrix under physiological salt concentrations [154].

1.6.3 Synthetic scaffolds

Synthetic scaffolds are materials which are chemically synthesized in the laboratory. [123, 155]. The number of synthetic scaffolds on the market has been increasing annually [156]. Their material properties of flexibility and controlled manufacture make them attractive for TE applications. Additionally, they can be manufactured cheaply and there is minimum batch to batch variation [157]. However, they lack cell-recognition signals and unless modified with cell-recognition sequences do not support the growth of cells. The most widely used synthetic polymers for skeletal muscle applications are poly (α-hydroxy acids), e.g. poly-lactic acid (PLA), poly-glycolic acid (PGA), poly-caprolactone (PCL) and their copolymers [124, 158].

1.6.4 Developing hybrid materials as scaffolds

Natural scaffolds like Matrigel support cell growth but due to the complexity of these ill-defined matrices, it is difficult to understand the underlying cell-signalling mechanisms. Synthetic materials are chemically well-defined but they do not support cell adhesion and proliferation on their own. Therefore, there is a need to design synthetic materials that are well defined and their mechanical and material properties can be controlled to achieve a desired outcome. The combination of synthetic polymers with ECM proteins may be a suitable option. Here, the material properties of the synthetic materials are controlled and constant, and bioactivity is provided by the ECM proteins. Examples include powdered small intestinal submucosa (SIS) combined with poly (D, L-lactide-co-glycolide) to create tissue-engineered bone [159] and the combination of urinary bladder matrix (UBM) with a poly (ester-urethane) urea (PEEU) to create an elastomeric scaffold [160].

Gilmore and colleagues (2009) used the conducting polymer, polypyrrole, coated with ECM GAG components like HA and CS to stimulate the proliferation of C2C12 myoblasts *in vitro* and compared the effects with those of non-ECM coated materials [161]. They showed that Polypyrrole/HA based substrates supported the proliferation of C2C12 myoblasts but did not support their adhesion and differentiation. On the other hand Polypyrrole/CS based substrates effectively supported both proliferation and differentiation of myoblasts [161]. This study suggests that different physical properties

of the material support different stages of skeletal muscle myogenesis and that GAGs attached to synthetic materials can be a viable option for skeletal muscle TE. It is possible that GAG components like heparin and HS, when coated on a substrate could impart a higher degree of support for myoblast proliferation and differentiation as HS binds and presents various growth factors to their cell surface receptors. Although HS coated polycaprolactone (PCL) has been used for bone tissue engineering with mesenchymal stem cells [162], to date, there are no reports of HS coated materials being used for skeletal muscle TE.

Kaji et al (2010) developed an alumina based scaffold for skeletal muscle TE [163]. They demonstrated electrically induced contraction of C2C12 myotubes when C2C12 myoblasts were cultured on an alumina based substrate, containing an atelocollagen top layer and a PDMS (poly-dimethylsiloxane) layer below the surface of the alumina membrane [163]. This micropoous substrate has a Young's modulus (measurement of elasticity) of 14.8 kPa which closely resembles that of normal muscle. Previous studies also showed that myotubes differentiate and striate on substrates with muscle-tissue like stiffness [164]. As contraction plays a pivotal role in muscle functionality [12], it is important to design materials that support the contractility of muscle, so that functionality is restored.

Recently, an alginate gel based scaffold was developed, and used to treat muscle injury in an ischaemic mouse model [165]. In this case, C2C12 cells and myogenic progenitor cells were mixed with this gel, which contained the growth factors, vascular endothelial growth factor (VEGF) and IGF-1 and implanted into the injury site. The controlled release of VEGF and IGF-1 from these scaffolds enhanced the repair process of the muscle, improved contractile function and stimulated neovascularization.

1.7 Extracellular matrix materials as a biological scaffold

The use of the ECM as a scaffold for constructive tissue remodelling has been supported by both, preclinical animal studies and human clinical applications. A number of clinical products now on the market are composed of ECM derived from xenogenic or allogenic tissues. A recent review by Crapo et al (2011) provides a list of all biologic ECM

derived materials used in clinics for a wide number of applications from treating irreparable wounds or severe burns to heart valve replacements [166].

There is a considerable list of tissues from which ECM can be derived and it ranges from vascular tissues like heart valves [167-169] and blood vessels [170, 171] to skeletal tissues like tendons [172], ligaments [173], skeletal muscle [174-176] and skin [177]. SIS-ECM and UBM are the most comprehensively studied and their mechanical, structural and biological properties have been well defined. Although the exact mechanism by which ECM enhances site specific tissue remodelling is unknown, it is clear the composition and structure of the ECM plays a pivotal role in determining the outcome of the repair process [166].

1.8 Decellularization of tissues

Decellularization (removal of cells) of tissues and organs is a promising, relatively new technique to obtain an ECM from tissues, where the complex 3D ultrastructure of the matrix is largely retained [178] (Figure 1.3). To obtain a 3D ECM suitable for implantation, it is essential to remove all cellular components from the tissue so that only the ECM remains. The efficiency of decellularization depends upon the origin of the tissue, its thickness, lipid content, density and the methods (physical, chemical or enzymatic) used to remove the cells [166]. Preferably, the method should not adversely affect the composition, biological activity and mechanical integrity of the remaining matrix. Incomplete decellularization can elicit adverse immune reactions due to remnants of cell membrane epitopes or allogenic DNA [179]. The presence of DNA can also hinder subsequent quantification of the cell population seeded on the matrix. Complete (100%) decellularization of a tissue or organ is not feasible; therefore the emphasis is on maximising the loss of cells from the tissue and minimizing the damage to the ECM, so it remains as close to its native structure and composition as possible. Several methods have been used to decellularize different tissues.

1.8.1 Chemical decellularization methods

To decellularize organs and tissues, the most commonly used chemical agents are detergents. These detergents may be ionic like sodium dodecyl sulphate (SDS) and

Sodium deoxycholate, non-ionic (Triton X-100) or zwitterionic (CHAPS). They solubilize cell membranes and disrupt the DNA-protein or lipid-protein interactions.

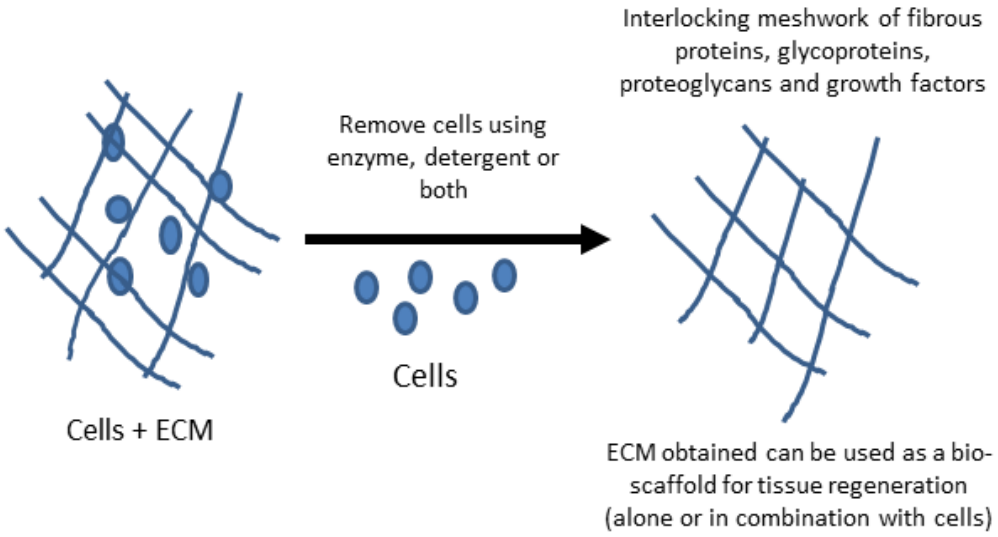

Figure 1.3 Schematic representation of the decellularisation procedure. Decellularisation (removal of cells) is a relatively new technique to obtain ECM from tissues while retaining the complex 3D ultrastructure of the matrix. Tissues can be decellularised using physical, chemical or enzymatic methods. Preferably, the decellularization method should not adversely affect the composition, biological activity and mechanical integrity of the remaining matrix. However, it should effectively remove all the cellular material from the tissues to avoid immune reactions.

Alcohols (ethanol and methanol) and other solvents (acetone) have also been used for removing cells from lipid predominant tissues like adipose tissue [180], and heart valves [181]. However, alcohols will fix the tissue, which can alter the mechanical properties and ultrastructure of the remaining ECM.

1.8.2 Physical

Decellularization can also be achieved by a temperature shock to the cells. There are a few reports of using temperature differences or freeze-thaw cycles for effective cell lysis, although subsequent processing is required to clear the cellular and membranous remains from the tissues [182, 183]. Several cycles of freeze-thaw are required for effective decellularization and this seems to only partly affect the topology and structure of the remaining ECM [184]. High hydrostatic pressure (>600MPa) treatment has also been used to decellularize porcine aortic blood vessels [185].

1.8.3 Biological

Biological agents include enzymes like trypsin, collagenase, nucleases, lipase, dispase, thermolysin and non-enzymatic agents including chelating agents like EDTA and EGTA. Trypsin is most commonly used as a decellularization agent due to its ability to cleave multiple proteins because of its serine protease activity, but when preservation of GAG components in the ECM is an aim, trypsin is not the preferred choice as it can cleave the core protein of proteoglycans and so release the GAG chains [175]. Trypsin can also cleave some of the collagens [168]. Nucleases (DNases and RNases) also form an integral part of decellularization protocols as they help in the removal of nucleotides after cell lysis.

There are reports suggesting the use of chelating agents like EDTA and EGTA in decellularization protocols but these agents are seldom effective in removing cells when used alone [186]. They are usually used in combination with enzymes [185, 187, 188] or detergents [189, 190]. The advantage of using these chelating agents is that they sequester metal ions like Mg^{2+} required for matrix metalloproteinase (MMP) activity and

hence they help to protect the ECM from MMPs released from the cells, which may damage the ECM ultrastructure and remove growth factors.

1.8.4 Whole organ decellularization

The idea of whole organ regeneration was first proposed by Langer and Vacanti (1993) and recently, there has been considerable development in new techniques for whole organ decellularization. Preservation of ECM molecules in a 3D form may provide valuable insights about the cell-ECM interactions and the role ECM molecules play *in vivo*. Recent progress in whole organ decellularization techniques are a leap forward in this area. Three groups have successfully used a whole organ perfusion decellularization technique to produce scaffolds for a bioartificial heart [191], a bioartificial liver [192] and a bioartificial lung [193]. The decellularized liver, when recellularized with hepatocytes and cultured *in vitro*, showed normal expression levels of cytochrome P450 and metabolic activity including urea synthesis and albumin secretion [192]. The heart scaffold, when connected to a bioreactor, showed sustained contractions and when stimulated electrically it could generate pump functions equivalent to 2% of a normal heart [191]. Interestingly, when the decellularized lung was orthotopically transplanted in rats, it supported gas exchange from 45 min to 2 hours [193]. Encouragingly, all three decellularized organs regained significant normal physiological activity. These organs are highly vascularized and need to be connected to the blood supply to provide metabolic function; therefore it is vital to obtain these matrices in a 3D form. However, obtaining a skeletal muscle matrix in the form of a whole organ is difficult due to the presence of long muscle fibres and the complexity of the muscle connective tissue.

1.8.5 Decellularization of skeletal muscle

Decellularized skeletal muscle is a promising system to study the role of extracellular matrix in muscle regeneration. After removal of the muscle cells, the ECM ultrastructure should retain the remnants of endomysial tubes, and neural and vascular pathways that can promote alignment and fusion of myoblasts and stimulate neurovascular growth [194]. Early attempts to decellularize skeletal muscles have incorporated harsh physical methods with enzymes like trypsin [175] and strong detergents like SDS [174]. Stern et al (2009) used trypsin and Triton X-100 to decellularize hamstring and quadriceps

muscles of rats and they showed that with this method the levels of GAGs in the decellularized matrix were below the limits of detection. DeQuach et al (2010) used 1% SDS as decellularizing agent and showed loss of most of the basement proteins, for example, collagen IV, fibronectin and laminin from the matrix. Recently, however, Gillies et al (2011) published a method for decellularizing skeletal muscle without detergents or proteolytic enzymes and in this case there was only a slight reduction in the GAG content of the matrix [176].

Following all of the above mentioned methods of decellularization, the sulfated GAGs in the matrix were measured but to our knowledge, which extracellular matrix proteoglycans (decorin, biglycan, perlecan) were retained after decellularization has not been examined. Considering the significance of proteoglycans and their GAG chains in skeletal muscle repair and regeneration, it is imperative to develop new methods of decellularization where most of the ECM molecules including the GAGs are preserved.

1.8.5.1 Powdered form

In recent years several research groups have presented techniques where skeletal muscle ECM has been extracted, converted to a powdered form and used as a substrate to promote the growth and differentiation of myoblasts *ex vivo*. Stern et al (2009) extracted skeletal muscle ECM from thigh muscles (quadriceps and hamstring) of 4-7 month old adult rats and used it as a surface coating to study the influence of skeletal muscle ECM on the regenerative potential of myogenic cells [175]. To make an ECM extract suitable for coating surfaces, muscle tissue was frozen at -80ºC and cut into thin slices of 500 µm followed by washing in ultrapure water for 2 days. After washing, the tissue was incubated in 0.05% trypsin/EDTA for 1 h and trypsin neutralized overnight by DMEM/10% FBS. Finally the tissue was washed in Triton X-100 for 5 days and then rinsed in water and PBS for 2 days and 1 day respectively. After decellularization, tissue was cut into small pieces, lyophilized, and powdered into a matrix. Powdered matrix was then dissolved in 2M urea for 3 days and dialyzed against water for 3 days. Finally, the matrix solution was lyophilized until dry and then dissolved in 0.1 % acetic acid for use as a coating [175].

Surfaces coated with muscle ECM prepared as described promoted the growth and differentiation of muscle progenitor cells and myoblasts in culture. Western blot analyses of extracts from these cells revealed higher expression levels of phospho-Erk 1 and 2, myogenin and MyHC on ECM coated surfaces compared to extracts of cells cultured on uncoated surfaces [175]. Erk 1 and 2 are members of the mitogen activated protein kinase (MAPK) family of proteins and have been shown to play a role in the proliferation and differentiation of muscle cells [195, 196]. Myogenin is a member of a family of transcription factors involved in early stage myogenic differentiation, while MyHC is a marker of the final stage of myogenic differentiation after the fusion of cells into multinucleated myotubes [197]. Alhough the decellularization method was effective in removing cells from the muscle it did lead to a loss of GAG components from the matrix. Thus while the ECM extract used in this study had a desirable effect on the proliferation and differentiation of myogenic cells, these effects may be further enhanced by developing a method that preserves skeletal muscle ECM in a more native state where the GAGs have remained attached to the matrix [175].

DeQuach et al (2010) developed a different method to obtain a powdered ECM from porcine skeletal and cardiac muscles suitable for coating on tissue culture dishes [174]. Muscle tissue was cut into pieces of $1cm^3$, rinsed briefly in deionized water and 1% SDS in PBS was used to decellularize the muscle tissues until the tissue became transparent. It was then rinsed thoroughly with PBS to remove the detergents. Decellularization was confirmed by the absence of nuclei as revealed by haematoxylin and eosin staining. The decellularized matrix was lyophilized, milled into a powder, digested with pepsin solubilised through pepsin digestion and dissolved in 0.1M acetic acid to prevent self-assembly. Characterization of this skeletal muscle matrix preparation using Time-of-Flight Secondary Ion Mass Spectrometry (TOF-SIMS) showed the presence of collagen I, II, VI and proteoglycans like decorin as well as heparan sulfates in the matrix [174].

The basement membrane is a highly specialized ECM that is sandwiched between parenchymal cells and connective tissue. Collagen IV is the major component of the basement membrane while laminin and fibronectin function as linker molecules between type IV collagen in the basement membrane and the sarcolemma (muscle fibre

membrane) [62]. Although De Quach et al (2010) also showed enhanced differentiation of mouse C2C12 myoblasts on surfaces coated with this ECM preparation when compared to collagen coated surfaces [174], they did not investigate the contractile properties of the myoblasts. This would have been interesting given the lack of basement membrane components in their acellular matrix and particularly the laminins, as laminins play a key role in transmitting the contractile force to the ECM through binding to the dystrophin glycoprotein complex [74]. These examples clearly suggest that there is a need to develop new methods to decellularize skeletal muscles where the key components of ECM are preserved.

1.9 Other approaches used for skeletal muscle TE

1.9.1 Micropatterned substrates and self-assembled monolayers

Huang et al (2004) cultured C2C12 myoblasts on micropatterned PDMS substrates with 10 μm wide grooves and found that C2C12 cells aligned themselves along the direction of the microgrooves, fused to form long and unbranched myotubes with uniform diameter [198]. In contrast, on non-patterned surfaces C2C12 cells were randomly oriented and the myotubes formed were non-uniform in diameter and oriented along various directions [198]. Gingras et al (2009) used different micropatterned polydimethylsiloxane substrates (fabricated by photolithography) for culturing C2C12 myoblasts *in vitro* and demonstrated that all substrates with varying geometries allowed fusion of myoblasts, but only a few substrates allowed proper alignment and orientation of myotubes [199].

1.9.2 Magnetic force based techniques

Yamamoto et al (2009) developed a method for culturing aligned myotubes (C2C12) in culture using magnetic force [200]. In this method, C2C12 cells were cultured in the presence of magnetite cationic liposomes (MCLs) with a magnet attached at the bottom of each well and a linear magnetic field was applied to the wells [200]. Although, it led to the formation of multi-layered thin sheets (250 μm) of cells, the cell sheets shrank considerably and failed to maintain their shape until differentiation. Positioning of a silicon plug at the centre of each well allowed the sheets to grow for 6 days without

breakage and immunohistochemical analysis revealed that the cells were properly aligned around the silicone rings. Further culturing of the cell sheets for 6 days in differentiation medium caused multinucleated myotubes to form [200].

1.9.3 Hydrogels

Photo-polymerizable HA based hydrogels containing satellite cells (SCs) or myogenic progenitor cells (MPCs) have been successfully used to engineer functional skeletal muscle *in vivo* [201]. In this study, Tibialis anterior muscles of C57Bl/6J mice were partially amputated and photo-cross-linked HA based gels (HA-PI), loaded with either freshly isolated SCs or MPCs, or isolated single muscle fibers were implanted at the injured site. Histological and morphological assessment of the repaired muscle showed a higher number of regenerated muscle fibers, characterized by centrally located nuclei, when fibers or SCs were used with HA-PI. Myogenic progenitor cells also yielded more regenerating fibers than HA-PI alone [201]. Functionality of the repaired muscle was also assessed after 6 weeks by measuring the absolute tetanic force (150 Hz) and these results showed that HA-PI loaded with SCs yielded the maximum force and hence the best functional recovery. Further, immunolabelling of the repaired muscle by α-bungarotoxin and von Willebrand factor revealed respectively formation of NMJs and blood vessels at the repair site [201].

1.10 Translational applications of the ECM scaffolds

Over the years, ECM based biomaterials derived from animal (xenograft) or human sources (allograft) have been successfully used to treat burns [202-205], wounds [206-208], abdominal wall defects [209-211] and ruptured tendons [212, 213].

1.10.1 Small intestinal submucosa (SIS) ECM

Studies in the past have shown that SIS-ECM scaffolds promote functional skeletal muscle regeneration in a rat-abdominal wall defect [130] and musculotendinous junction repair of gastrocnemius muscles [214] in a canine model. However, the extent of injury was minimal in both cases. The anatomical location and the extent of the muscle injury may also play a major role in the regenerative response. Recently, Turner et al (2012) showed that a complex quadriceps injury in a canine model can significantly alter the

repair process of the skeletal muscle [215]. Quadriceps is a complex muscle comprising four parts: rectus femoris, vastus lateralis, vastus medialis and vastus intermedius. The complex injury to the quadriceps muscle of dogs included removal of the distal one-third of vastus lateralis, removal of the medial half of the vastus medialis (distal one-third) and the associated quadriceps tendon (proximal half). A SIS-ECM scaffold was implanted into the site of defect and the regenerative response was monitored for 6 months after implantation. Histochemical analyses revealed that the initial phase of muscle regeneration (1 month) showed similar results to previous studies [214] and was marked by infiltration of mononuclear and spindle shaped cells. However, the final response (after 6 months) included deposition of dense connective tissue (mainly collagen) and the formation of bony and cartilaginous structures within the graft [215].

It appears the age of the animal from which the ECM is harvested affects the ECM scaffold properties and plays a crucial part in determining the outcome of the repair process. Recently, Tottey et al (2011) showed that SIS-ECM isolated from pigs of different ages (3, 12, 26 or >52 weeks) showed distinct mechanical, structural and biological properties [216]. Growth factor analysis for the amount of bFGF and VEGF revealed that SIS-ECM derived from 12 week old animals had the most bFGF (per mg dry weight) while SIS-ECM derived from 3 week old animals had the lowest. The VEGF content was equivalent in SIS-ECM from 12 and 26 week old animals, but in SIS-ECM from 3 week and >52 week old animals it was much lower [216]. The elastic modulus of SIS-ECM derived from 12 or 26 weeks old animals was much higher than that derived from 3 or >52 weeks old animals.

Taken together, age of the animal (from which ECM is harvested) and anatomical location of the injury (Tibialis Anterior vs Quadricpes/Soleus vs Gastrocnemius) may have different effects on the regenerative response of a muscle. There is no indication that these two factors (age and location of injury) have been explored together. Designing animal models with both factors in mind would help to improve our knowledge about differential treatment response at different ages.

Although SIS-ECM has been used for various clinical studies in the past, there is one study which suggests that SIS-ECM is not a complete acellular matrix. Zheng et al (2005) investigated Restore^{TM} SIS membrane for the presence of DNA and other cellular remnants [217] using histological and PCR methods and thus showed the presence of DNA and mast cells in the SIS-ECM. Further, when this SIS-ECM was implanted into mice or rabbits, it elicited an immune response characterized by fibrosis and infiltration of lymphocytes into the implant site [217]. This study suggests that although SIS-ECM has been approved by the Food and Drug Administration (FDA) for clinical use, further preclinical investigation needs to be done before it is used as a surgical material.

For any muscle graft to be compatible and successful, the engineered muscle graft should mimic the structure of the native muscle at the cellular and molecular level. The muscle fibres should be uniformly aligned and densely packed within an appropriate and well organized ECM [218]. In addition to the parallel alignment of muscle fibres, innervation of the engineered tissue and formation of functional vascular bundles is indispensable for a functional graft [194]. Despite the promising applications for tissue engineered skeletal muscle that have been described, culturing functional and mature muscle tissue still remains an unsolved puzzle. An important hurdle that has yet to be overcome is the inability of skeletal muscle cells to develop into fully mature muscle fibres within engineered muscle constructs.

1.10.2 Clinical studies involving ECM scaffold for TE of muscle

There have been very few clinical studies on the application of ECM based biomaterials for skeletal muscle TE. Currently, there is only one clinical report of the successful implantation of a biological scaffold in a patient for the purpose of regenerating functional muscle tissue [129]. The patient was 19-year old military person who sustained injuries in the right thigh as a result of a bomb explosion. This type of injury characteristically leads to volumetric muscle loss. The patient suffered a right-femur fracture associated with large quadriceps muscle loss. At first, the treatment involved an autologous bone graft and a latissimus muscle flap was also grafted to the damaged area. Over time, the fracture healed, but even after 3 years of surgery, the patient was not able to recover completely and reported muscle weakness in the right leg [129].

Seemingly, the muscle loss was irreparable by normal muscle regeneration or autologous grafting. Finally, the surgeons used a tissue engineering approach and implanted a biological scaffold composed of a multilayered porcine SIS-ECM into the damaged muscle area. A 15 cm incision was made on the right thigh exposing vastus medialis and 5 sheets of SIS-ECM were implanted into 12x10 cm pockets created between the muscle belly. The patient was discharged on the 5^{th} day post-surgery and after 4 weeks resumed physical therapy. Post-operatively, computer tomography (CT) scans showed new tissue growth at the implant site and the patient showed a marked increase in the isokinetic muscle function (peak torque, total work and average power) in the repaired limb [129]. This example is encouraging for developing muscle specific scaffolds which might provide better repair.

1.11 Investigating Cell-Scaffold Interactions

Although the ultimate goal of developing a muscle-specific scaffold is to support the growth and repair of a muscle *in vivo,* important cues can be obtained by developing an artificial microenvironment *in vitro* for muscle growth. Thus, in recent years there have been several technological advancements in the field of skeletal muscle TE which includes development of (a) serum free culture, (b) sensitive methods such as quantitative real-time polymerase chain reaction (qRT-PCR) to measure cell differentiation, and (c) atomic force microscopy to visualize and quantify cell-scaffold interactions at nanometre resolution.

1.11.1 Serum free culture

Currently, foetal bovine and horse sera are used for respectively myoblast proliferation and differentiation in tissue culture systems. However, these sera provide an ill-defined mixture of growth factors to the medium which makes it difficult to assess the contribution of individual growth factors and ECM molecules on myoblast growth and differentiation. By developing a serum-free media formulation, the effect of specific ECM molecules, cytokines and growth factors on muscle development in culture can be studied.

Only a few studies have attempted to study the role of different growth factors in skeletal muscle differentiation by developing a serum free culture system [219]. Das et al (2009) used a serum free culture system for i*n vitro* skeletal muscle TE. In this study, C2C12 rat myoblasts were cultured in a defined serum free environment with known amounts of growth factors. The cells differentiated and the myotubes were able to maintain their phenotype for 70-90 days in culture [220]. This long term maintenance of the cultured myotubes was due to the presence of NBactiv4 media, a formulation created by adding creatinine, oestrogen and cholesterol to B27/Neuro-basal media, a media which was originally used for increasing the lifespan of foetal hippocampal neurons [221].

Although, studies have been done previously using ECM as a coating material to promote the proliferation and differentiation of myoblasts in culture, traditional serum supplemented media was used to support myoblast growth. In these cases it is difficult to assess that whether the growth of myoblasts is due to the ECM coating or due to factors present in the serum. To date, there are no reports of using a serum free culture system to assess the effect of decellularized skeletal muscle ECM on myoblast proliferation and differentiation.

1.11.2 Atomic Force Microscopy

Visualization of 3D cell-scaffold interactions presents a challenge to standard light and confocal scanning microscopy methods most often used by cell biologists. To better understand the role of scaffolds in muscle repair and regeneration, the 3D ultrastructure of these materials, as well as cell-scaffold interactions at nanometer levels should be determined. For decades, electron microscopy (EM) has been used to visualize tissue ultrastructure, but routine EM methods irreversibly denature biomolecules both during specimen preparation because of the use of harsh chemical fixation procedures and during imaging because of the interaction of electron beam with the tissue [222] .

Atomic force microscopy, an alternative to EM, was invented in the mid-1980s. Atomic force microsopes (AFMs) belong to a class of scanning probe microscopes that record

interactions between a probe and a surface. A typical AFM consists of a silicon or silicon nitride cantilever with a sharp tip (or probe) at the end to scan a specimen surface. When the tip scans the surface, molecular interactions between the tip and the surface cause a deflection in the cantilever which is measured by an array of photodiodes. Since AFMs operate in physiologically appropriate solution conditions and can perform quantitative, non-destructive, high resolution imaging [223], they have obvious advantages over EM.

Atomic force microscopy can be used to characterize the topography of both synthetic and natural scaffold materials, and the interaction of cells with these scaffolds. Graham et al. (2010) recently developed a new method using cyropreservation and cryosectioning of tissue samples to preserve and visualize bio-molecular structures, including ECMs *in situ* [224]. Using this technique, it was possible to visualize the macromolecular structures of fibrillar collagens in skin, cartilage and intervertrebal disc; elastic fibres in the aorta and lung; as well as desmosomes and mitochondria. We envisage this method being particularly useful for analyses of both natural muscle ECM as well as synthetic scaffolds that have been modified, with ECM proteins to enhance their functional attributes.

Atomic force microscopy images yield information about the shape and volume of the molecule being imaged, but information about the type of molecule is missing. A possible solution can be provided by simultaneous topography and receptor imaging [225]. Using this technique, it is possible to generate single molecule maps of specific types of molecules in a complex sample while simultaneously carrying out high-resolution topography imaging [225]. In this mode the AFM tip contains a covalently coupled antibody molecule so that it will function as a molecular sensor. A highly developed feedback loop allows sample topography measurement with the simultaneous mapping of antibody recognition sites on the surface of the sample. This imaging mode may be used to investigate receptor binding sites and their distribution on natural biological surfaces.

In addition to imaging biological samples AFM can also be used to measure the elastic properties of a cell or a tissue by a process of force measurement. The first report of force measurements by AFM was by Paul Hansma and colleagues in 1992 [226]. They measured the interaction forces between the cantilever and a glass surface in water. Later, Tao et al (1992) investigated the elastic properties of bone and cartilage. Their method was quantitative in nature and gave a direct correlation between the elastic properties of the material and its force distance curves [227]. Engler et al (2004) investigated the elastic properties of myoblasts cultured on different substrates of varying stiffness using AFM [164]. Myoblasts were cultured on collagen strips attached to glass or polymer gels of different elasticity. Although the myoblasts fused into myotubes irrespective of substrate flexibility, actin/myosin striations appeared only in myotubes cultured on gels with stiffness closer to normal muscle (passive Young's modulus, E ~ 12 kPa). Myoblasts did not fuse and striate on much stiffer or softer gels than that of normal muscle hence, indicating that substrate stiffness is a critical factor for differentiation of striated muscle [164]. Later, the same group demonstrated the significance of matrix elasticity on stem cell fate [228]. Mesenchymal stem cells (MSCs) were cultured on collagen coated gels of varying elasticity that mimicked brain, muscle and bone matrix in their stiffness. The MSCs differentiated into a neuronal morphology with filopodia branching and spreading when cultured on soft matrices that mimic brain elasticity; medium stiffness gels promoted the differentiation of MSCs to spindle shaped myogenic cells and the high stiffness gels led to osteogenic differentiation [228].

Limited work has been done in this field of AFM and it has only occasionally been applied to measure the elastic forces of muscle samples. Designing scaffolds of matching stiffness to muscle tissue and implanting these scaffolds at the muscle injury site may improve cell-scaffold interactions to enhance the outcome of the muscle repair processes.

1.12 Conclusion

The idea of "dynamic reciprocity" or cell-ECM crosstalk was first proposed by Bissel et al in 1982 [229], where she postulated that ECM alters gene expression in cells and

thereby regulates cell growth and differentiation. Cells are in contact with the ECM via cell surface receptors called integrins that signal or transmit the message from outside of the cell to inside the cell [230]. Traditional 2D tissue culture has been a useful model system to study cell-matrix interactions and the associated factors which modulate these interactions. However, there is a need to improve our understanding of cell-matrix interactions and designing 3D culture systems, which closely mimic the *in-vivo* cell microenvironment, will help in this regard. Studies have shown that cell-adhesion complexes in "3D matrices" differ markedly in terms of structure and function from their counterparts on 2D substrates. Cell-signalling events also differ between 3D matrices and 2D flat substrates [231]. Another study measured the gene expression levels of three integrin subunits (α1, β1 and β3) and ECM molecules (collagen I, collagen III and tropoelastin) of vascular smooth muscle cells cultured on 2D substrates and 3D matrices composed of pure collagen type I and fibrin. On all 3D matrices, a marked increase in gene expression was observed as compared to that on 2D substrates [232].

Constructing 3D artificial microenvironments may provide valuable insights into cell-material interactions. Although the idea sounds interesting, constructing these materials poses a significant challenge in terms of material elasticity, pore size and biophysical constraints which may inhibit cell migration. For tissue repair and regeneration, migration of cells is necessary for angiogenesis and vascularization. Microarchitecture of a scaffold can affect the migratory capabilities of a cell which in turn may affect the remodelling response of an injured tissue. Harley et al (2008) showed that mouse fibroblast migration rate decreased as the pore size of "collagen-GAG" scaffolds increased from 90 to 150 μm [233].

For several years, the importance of ECM in tissue regeneration has been well known. However, there is still paucity of information on the underlying mechanism that how cell-matrix interactions contribute towards the regenerative response of an injured tissue. There is an unmet need to develop better 3D cell-based models which can replicate the *in vivo* settings very closely and can bridge the gap between 2D cell culture studies and *in vivo* animal models. Developing better 3D skeletal muscle tissue based models will

also be very helpful in identifying suitable therapeutic drug targets and testing candidate drugs for their ability to improve muscle function. These models will also enable us to better understand cell-matrix interactions and furthermore provide valuable insights for a clinical setting.

1.13 Aims of this project

This thesis aimed to investigate the contribution of ECM in regulating myoblast proliferation and differentiation by:

- Development of a novel method of skeletal muscle decellularization.
- Functional characterization of the solubilised and whole muscle decellularised ECM using C2C12 murine myoblasts in 2D and 3D serum free cultures.
- Use of silk fibroin as an alternative biomaterial using primary human skeletal muscle myoblasts in 2D and 3D cultures.

1.14 Hypothesis

Natural skeletal muscle matrices and silk bio-scaffolds provide information about ECM components that promote growth and differentiation of muscle precursor cells.

Chapter 2:

Materials and Methods

2.1 Muscle sampling (mice and rats)

Female C57Bl/6J mice aged 3 months were obtained from the Animal Resource Centre (Perth, Australia). The mice were delivered to Curtin University and allowed to acclimate for one week. All animal procedures were carried out in strict accordance with the guidelines of the National Health and Medical Research Council of Australia and approved by the Curtin Animal Ethics Committee (AEC 2011-73A). Mice were anesthetized with 2% isoflurane and euthanized by cervical dislocation. Rats were euthanized by intraperitoneal overdose (50mg/100g body weight) of pentobarbitone sodium (Lethabarb) and obtained, post- euthanasia, from Dr Christine Cooper, Curtin University. Following euthanasia, the quadriceps, gastrocnemius, soleus, tibialis anterior and extensor digitorum longus muscles from both legs of the mice and rats were removed. Muscles were either snap frozen in liquid nitrogen, or embedded for cryosectioning and frozen using isopentane cooled with liquid nitrogen. All samples were stored at -80ºC.

2.2 Decellularisation

2.2.1 Buffers and reagents

All chemical reagents for buffers used in decellularisation of skeletal muscle and solubilisation of the muscle extract were purchased from Sigma Aldrich (St Louis, MO) unless otherwise stated.

Phosphate Buffered Saline (PBS)

1x PBS (137 mM NaCl, 2.0 mM KCl, 10.0 mM Na_2HPO_4, 1.8 mM KH_2PO_4) was prepared by dissolving 80.0 g NaCl, 2.0 g KCl, 14.4 g Na_2HPO_4 and 2.4 g KH_2PO_4 in 800 ml of double distilled water (ddH_2O). pH was adjusted to 7.4 using HCl and volume made up to 1 litre using ddH_2O and sterilized by autoclaving.

1M Tris buffer (TB) (pH 8.0) stock solution

12.11 g of Tris base (Amresco, Solon, OH) was dissolved in 100 ml of ddH_2O and pH was adjusted to 8.0 using HCl.

0.5 % Sodium deoxycholate (w/v) in 20 mM Tris buffer

0.5 g sodium deoxycholate was dissolved in 80 ml of 20 mM Tris buffer (pH 8.0) and the final volume adjusted to 100 ml using 20 mM Tris buffer (pH 8.0)

3.4 M Sodium Chloride in Tris buffer

19.86 g of NaCl (Amresco) was dissolved in 80 ml of 20 mM Tris buffer (pH 8.0) and the final volume adjusted to 100 ml using 20 mM Tris buffer (pH 8.0)

2.0 M NaCl in PBS

11.7 g of NaCl was dissolved in 80 ml of 1x PBS (pH 7.4) and the final volume was made up to 100 ml using PBS

0.1 M Ethylenediaminetetraacetic acid (EDTA)

1.86 g of EDTA was dissolved in 40 ml of ddH_2O, NaOH was added to dissolve EDTA and pH was adjusted to 7.4. The final volume was made up to 50 ml using ddH_2O.

0.2 % Sodium-dodecyl-sulphate (SDS) (w/v)

0.2 g of SDS (APS, Auckland, New Zealand) was dissolved in 80 ml of ddH_2O and the final volume was made up to 100 ml using ddH_2O.

1.0 % Triton X-100 (v/v) in PBS

1.0 ml Triton X-100 (Amresco) was dissolved in 80 ml of PBS and the final volume was made up to 100 ml using PBS.

DNase I reaction buffer (10X)

DNase I reaction buffer (10x) (Promega) consisted of 400 mM Tris-HCl (pH 8.0), 100mM $MgSO_4$ and 10mM $CaCl_2$. To prepare a 1x buffer solution, DNase I reaction buffer (10x) was diluted in ddH_2O.

Radioimmunoprecipitation assay (RIPA) buffer

RIPA buffer consisted of 20 mM Tris HCl (pH 7.5), 150 mM NaCl, 1.0 mM EDTA, 1.0 mM EGTA (Sigma Aldrich), 1% NP-40 (Sigma Aldrich), and 1% sodium deoxycholate. Buffer was kept ice cold and supplemented with 1x cOmplete protease inhibitor cocktail (Roche) immediately prior to use.

Urea buffer

UREA buffer consisted of 40.0 mM Tris HCl (pH 7.5), 5M urea, 2M thiourea (Sigma Aldrich), 0.1% SDS and 1% CHAPS (Sigma Aldrich). Buffer was kept ice cold and supplemented with 1x cOmplete protease inhibitor cocktail (Roche) immediately prior to use.

Acetic acid buffer (0.1 M)

57 µL of glacial acetic acid (17.4 M) was added to 10 ml of ddH_2O.

2.2.2 Decellularization of mouse skeletal muscle sections

2.2.2.1 Trypsin method

Muscle sections were rinsed in PBS for 2 h, incubated in 0.05 % trypsin (Sigma-Aldrich) for 20 min before the trypsin was inhibited by Dulbecco's modified eagles medium (DMEM, Life Technologies, Carlsbad, CA) containing 10 % fetal bovine serum (FBS, HyClone, Thermo Fisher Scientific, Waltham, MA) for 1 h. Sections were then washed in PBS/1 % Triton X-100 (Sigma-Aldrich) for 30 min and then with PBS for 1 h.

2.2.2.2 Sodium dodecyl sulphate (SDS) method

Muscle sections were rinsed in distilled water for 2 h and treated with 0.2 % SDS in PBS containing 50 mM EDTA and 1 x cOmplete protease inhibitor (Roche, Mannheim, Germany) for 75 min at 4^{o}C with buffer replaced every 20 min. Sections were then washed with 2 M NaCl/50 mM EDTA/1x protease inhibitors/20 mM Tris, pH 7.4 for 10

min at 4°C followed by 100 mM NaCl/20 mM Tris for 1 h at 4°C. Finally, sections were washed twice with 20 mM Tris/0.15M NaCl buffer for 30 min each.

2.2.2.3 Phospholipase method

Muscle sections were rinsed in PBS for 30 min followed by incubation in a phospholipase A_2 (PLA_2, 170 U/ml)(Sigma-Aldrich), 0.5 % sodium deoxycholate (Sigma-Aldrich) solution in 20 mM Tris buffer (pH 8.0)/0.15M NaCl containing 1x cOmplete protease inhibitor for 30 min. Muscle sections were then washed in 3.4 M NaCl/20mM Tris for 2 h, rinsed 2x in PBS for 5 min each, treated with DNaseI (75 U/ml) (Promega, Madison, WI) in 1x DNase I reaction buffer for 1 h at 37°C and then washed 3x in PBS for 15 min each.

2.2.3 Whole muscle decellularization

Rat tissue was used for whole muscle decellularization to produce sufficient material for analysis and tissue culture studies. The muscle was weighed, sliced into 0.5 mm pieces and rinsed in PBS containing 1x cOmplete protease inhibitor for 2 h at 4ºC. After washing, sections were treated with PLA_2 (170 U/ml), 0.5 % sodium deoxycholate in 20 mM Tris buffer (pH 8.0)/0.15M NaCl containing 1x cOmplete protease inhibitor (Roche) for 18 h at room temperature (RT) until the tissue appeared transparent. The tissue samples were washed with 3.4 M NaCl/20 mM Tris/1x protease inhibitor for 24 h at 4ºC (buffer changed every 8 h) and then rinsed in PBS for 1 h at 4ºC. The samples were treated with DNAse I (75 U/ml) in 1x DNase I reaction buffer at 37ºC for 24 h and washed in PBS for 12 h at 4ºC (3 buffer changes) and stored at 4ºC until further use. Decellularised muscle samples were used in two- or three-dimensional culture (2D/3D). For 2D culture experiments, decellularized muscle samples were air dried on tissue paper and weighed before and after vacuum drying for 3 h (Integrated SpeedVac^R, Thermo Fisher Scientific). The ECM was then solubilized in 0.1 M acetic acid/20 mM EDTA for 7 days at 4ºC with mixing and the protein concentration was measured using the Pierce BCA protein assay kit (Pierce Biotechnology, Rockford, IL). For 3D culture, decellularised muscle samples were stored in PBS and sterilised before use (Section 2.7.8)

2.2.4 Solubilisation of acellular skeletal muscle

2.2.4.1 Urea and RIPA buffer solubilisation

Untreated and PLA_2 decellularised muscles were solubilised either in urea or RIPA buffers for 4 h or O/N at 4ºC. After incubation, the tissue lysate was centrifuged at 12,000 rpm for 20 min at 4ºC. The supernatant was carefully aspirated without disturbing the insoluble tissue debris and transferred to a clean microtube and stored at -20ºC. Protein concentrations were then measured by either BCA (Pierce Biotechnology, Rockford, IL) or Non- Interfering (NI) protein assay (G-Biosciences, St Louis, MO) (see Section 2.3.2.1 for the protocol).

2.2.4.2 Acetic acid solubilisation

Decellularized muscle samples were air dried on tissue paper and weighed (wet weight) in eppendorf tubes. The muscle samples were dried using an Integrated SpeedVac^R apparatus (Thermo Fisher Scientific) for 3 h and then weighed again (semi-dry weight). The dried ECM was solubilized using 0.1 M acetic acid/20 mM EDTA for 7 days at 4ºC with mixing. After incubation, the tissue lysate was centrifuged at 12,000 rpm for 20 min at 4ºC. The supernatant was carefully aspirated without disturbing the insoluble tissue debris and transferred to a clean microtube, before storing at 4^{o}C. The protein concentration was measured at days 1, 3, 5 and 7 using the Pierce BCA protein assay kit (Pierce Biotechnology, Rockford, IL) (see Section 2.3.2.2 for the protocol).

2.3 Protein Analysis

2.3.1 Gels, buffers and solutions for protein analysis

All chemical reagents for buffers used for protein analysis were purchased from Sigma Aldrich unless otherwise stated.

SDS-PAGE resolving and stacking gels

SDS-PAGE resolving gels were prepared by combining an acrylamide/bis-acrylamide solution (29:1 ratio, Bio-Rad laboratories, Hercules, CA) with 0.375 M Tris-HCl (pH

8.8), 0.1% w/v SDS and ddH_2O. The acrylamide/bis-acrylamide was added in sufficient quantities to produce gel solutions of 6%, 7.5%, 10% or 12% acrylamide. Just prior to pouring, 0.1% w/v ammonium persulfate and 0.2% (v/v) TEMED (both from Amresco) were added to the gel solution. The gel mixture was immediately poured between two glass plates (mini-gel) assembled in a gel caster (Hoefer, San Fransisco, CA) leaving 2 cm space at the top of the glass plates for the stacking gel. The resolving gel was overlaid with 25% ethanol and allowed to polymerize at room temperature (RT).

Stacking gels were prepared by combining 4 - 5% acrylamide/bis-acrylamide (29:1), 125mM Tris-HCl (pH 6.8), 0.1% w/v SDS and ddH_2O. Just prior to pouring, 0.1% v/v ammonium persulfate and 0.2% (v/v) TEMED were added to the gel mixture. The stacking gel solution was immediately poured between the glass plates on top of the polymerized resolving gel and the well casting comb put in place. The stacking gel was left to polymerize at room temperature before removing the comb. Wells were washed with ddH_2O to remove any unpolymerized gel.

SDS-PAGE running buffer

SDS-PAGE running buffer was prepared as a 10x stock solution containing 250mM Tris-HCl, 2M glycine and 1% (v/v) SDS diluted in ddH_2O; adjusted to pH 8.3 using 1M NaOH. 1x gel running buffer was prepared fresh for each run by diluting the stock solution 1:10 with ddH_2O.

Sample loading buffer

Sample loading buffer was prepared as a 2x stock consisted of 160mM Tris-HCl (pH 6.8), 4% (v/v) SDS, 20% (v/v) glycerol and 0.2% (v/v) bromophenol blue (Bio-Rad, Hercules, California) in ddH_2O.

Coomassie Brilliant Blue (CBB) staining solutions

Coomassie staining solution was prepared by dissolving 50 mg of Coomassie Brilliant Blue-R 250 (Bio-Rad) in a solution consisting of 40 ml methanol, 10 ml glacial acetic

acid and 50 ml ddH_2O. The solution was filtered prior to use. The de-staining solution consisted of 40 ml methanol, 10 ml glacial acetic acid and 50 ml ddH_2O.

Western blotting electrotransfer buffer

Western blotting transfer buffer was prepared as a 10x stock solution containing 250mM Tris-HCl and 2M glycine and the pH adjusted to 8.3 using 1M NaOH. 1x blotting buffer was prepared fresh for each electrotransfer by diluting 10x stock solution with ddH_2O, and then adding 20% of methanol to the diluted solution.

PBS-Tween (PBST) buffer

0.1 ml of Tween-20 was added to 100 ml of 1xPBS buffer to yield a 0.1% (v/v) PBST buffer.

Blocking buffer (Western blotting buffer)

Blocking buffer was prepared by dissolving 5.0 g of skimmed milk powder in 90 ml of PBST buffer and the volume was made up to 100 ml using PBST buffer to yield a solution of 5% (w/v) skimmed milk in PBST. This buffer was freshly prepared for each use.

2.3.2 Protein quantification

2.3.2.1 Bicinchoninic acid (BCA) assay

The working reagent (WR) was prepared by mixing 50 parts of BCA Reagent A with 1 part of BCA Reagent B (50:1, Reagent A: B). Bovine serum albumin (BSA)(Sigma Aldrich) was used as a standard. 10 mg of BSA was dissolved in 1 ml of 1x PBS or 0.1M acetic acid to yield a 10.0 mg/ml stock, and serially diluted to yield concentrations ranging from 0.1 mg/ml to 4.0 mg/ml. 10 µL of each sample (standard or unknown sample) was pipetted into a 96 well plate (Nunc, Thermo Fisher Scientific) and 200µL of the WR was added to each well and mixed thoroughly. The plate was covered and incubated at 37°C for 30 minutes before being brought to RT. Absorbance was measured at 590 nm on an Enspire plate reader (Perkin Elmer, Waltham, MA). A standard curve was generated by plotting the mean absorbance for each BSA standard versus its

concentration in mg/mL and this curve used to determine the protein concentration of each unknown sample.

2.3.2.2 Non-Interfering (NI) protein assay

The NI protein assay (GBiosciences) was performed according to the manufacturer's instructions. Briefly, a set of BSA protein standards was prepared from a BSA stock (2.0 mg/ml) to yield concentrations ranging from 0 - 50 µg/ml. 10 µl of protein sample (unknown concentration) was aliquoted into a 1.5 ml microtube containing 0.5 ml of universal protein precipitation agent (UPPA I) buffer . The mixture was vortexed briefly and incubated at RT for 5 min before the addition of 0.5 ml of UPPA II. The mixture was then, vortexed briefly and centrifuged at 10,000 g for 5 min to pellet the precipitated protein. The supernatant was discarded and 100 µl of copper solution (Reagent I) and 400 µl of deionized water were added to the pellet and vortexed until the protein pellet dissolved. Finally, 1 ml of reagent II was added to the tube, mixed thoroughly, incubated at RT for 20 min and absorbance was measured at 480 nm. A standard curve was prepared by plotting the average measurement for each BSA standard versus its concentration in mg/mL. The standard curve was used to determine the protein concentration of each unknown sample (see below).

2.3.3 SDS-PAGE

Solubilised ECM extracts of decellularised muscle were separated by electrophoresis on a 7.5 % SDS-PAGE using 10 µg of collagen I (Sigma Aldrich) as a control standard. Proteins were separated on the basis of molecular weight under non-reducing conditions using SDS-PAGE as described by Laemmli (1970)[234]. The polyacrylamide gels (7.5% running, 5% stack) were placed in a Mighty Small SE250 apparatus (Hoefer, Scientific Instruments, CA, USA) and the chamber filled with 1x running buffer. Before loading the protein samples, 1 volume of 6x loading buffer was added to 5 volumes of protein samples and heated at 95ºC for 10 min. Pre-stained high molecular weight markers (Spectra multicolour broad range protein ladder, Thermo Fisher Scientific) were also loaded on each gel. The proteins were electrophoresed at a constant current of 120V for

90 min. Following electrophoresis; gels were either stained with Coomassie blue or transferred to a PVDF membrane via electroblotting.

2.3.4 Coomassie blue staining

SDS-PAGE gels were incubated overnight in Coomassie staining solution at room temperature with gentle rocking. The stained gel was transferred into a destaining solution and gently agitated until the background became clear. The gel was then imaged using the ChemiDoc^{TM} MP System (Bio-Rad) or placed between two moistened sheets of clear cellophane film, clamped between two plastic frames and allowed to dry overnight.

2.3.5 Electroblotting (protein transfer)

Following electrophoresis, proteins separated via SDS-PAGE were transferred to a Immobilon-P PVDF membrane (Millipore, Bedford, MA, USA) using a wet blotting apparatus (Hoefer, Scientific Instruments, CA, USA). Electroblotting was either performed at 400 mAmp for 1 h at 4ºC and 20V for overnight at 4ºC, or at 200 mAmp for 2 h at room temperature (RT). The membrane was then blocked for 2 h at RT or overnight at 4ºC in blocking buffer.

2.3.6 Western blotting

Following blocking, the membrane was incubated in primary antibodies diluted in blocking buffer. Antibodies used were against collagen I (1:1500), collagen VI (1:2500), fibronectin (1:1500), perlecan (1:5000) and laminin α2 (1:3000), myosin (1:1000) and β-tubulin (1:1500) for 2h at RT. Collagen I, collagen VI and perlecan were all rabbit polyclonal antibodies. Fibronectin (EP5) and laminin α2 (4H8-2) were mouse and rat monoclonal antibodies respectively (Refer Table 2.1). Membranes were washed 4 times in 0.1 % Tween-20 in PBS (PBST) for 5 min each and incubated in 0.1 % PBST containing anti-rabbit, anti-mouse or anti-rat horseradish peroxidase (HRP) conjugated secondary antibodies at (1:2000, 1:1000 and 1:1000 dilutions respectively)(Refer Table

2.2). Membranes were washed 4 times in 0.1% PBST for 5 min each and incubated in Western Lightning® Plus-ECL substrate (Perkin Elmer, Waltham, MA) for 5 min. Membranes were scanned and imaged using the ChemiDoc^{TM} MP System (Bio-Rad).

2.4. DNA analysis

2.4.1 Gels, buffers and solutions for DNA analysis

All chemical reagents for buffers used for DNA analysis were purchased from Sigma Aldrich unless otherwise stated.

Tris-Acetate-EDTA (TAE) gel running buffer

Tris-Acetate-EDTA (TAE) buffer was prepared as a 50x stock by combining 242 g Tris base, 57.1 ml glacial acetic acid and 100 ml 0.5M EDTA (pH 8.0) in ddH_2O to a volume of 1 litre. 1x TAE buffer (pH 8.0) was prepared by diluting the stock solution 1:50 with ddH_2O.

DNA gel loading buffer (6x)

DNA gel loading buffer (6x) was prepared by adding 3.9 mL glycerol, 500 µL 10% (w/v) SDS, 200 µL 0.5 M EDTA (pH 8.0), 0.025 g bromophenol blue (Bio-Rad) and 0.025 g xylene cyanol to 5 ml of ddH_2O and the volume was made upto 10 ml using ddH_2O.

Agarose gels

Agarose gels (1, 1.5 or 2%) were prepared by dissolving molecular biology grade agarose in 1x TAE buffer and bringing the solution to the boil. 2µl of Midori Green (Nippon Genetics, Deuren, Germany) was added per 50 ml of gel solution to detect DNA.

2.4.2 Agarose gel electrophoresis

Agarose gels were made to the desired concentration and samples were mixed with 6x gel loading buffer prior to loading in the wells of the gel. Samples were then

electrophoresed in 1x TAE buffer using a Wide Mini Sub Cell and Power Pack (Bio-Rad) until the marker was completely resolved. The gel was visualized using a UV trans-illuminator and imaged using a Gel Doc Imaging System (Vilber, Adelab Scientific, Adelaide, Australia)

2.4.3 DNA extraction and quantification

DNA was extracted from 10 µm thick control and decellularized muscle sections by scraping 40 sections off glass slides using a total volume of 300µl of 1x PBS for 40 sections. Muscle sections (control and decellularized) from mid belly regions of the muscle were selected to minimize the variation in the starting amount of DNA. The material was collected in a 1.5 ml microtube and centrifuged at 12,000g for 10 min. DNA was extracted using the Master Pure kit (Epicentre, Illumina, Madison, WI) according to the manufacturer's instructions. Briefly, control and decellularised muscle sections were incubated in 600µl of tissue and cell lysis solution containing 2.0 µl of proteinase K (50 mg/ml)(Sigma Aldrich) and incubated at 65ºC for 45 min until the tissue was digested. Samples were cooled to 37ºC and 2.0 µl of 5.0 µg/ml RNase A was added to the sample and incubated at 37ºC for 30 min. Samples were kept on ice for 5 min, 300 µl of MasterPure complete (MPC) protein precipitation reagent was added and the mixture centrifuged at 10,000 g for 10 min at 4ºC. The supernatant was collected and DNA precipitated by adding 1 ml of isopropanol to the supernatant and centrifuging at 10,000g for 10 min at 4ºC. The pellet was rinsed in 70% ethanol twice, dried and dissolved in 35 µl of TE buffer. DNA was quantified using the Nanodrop (Thermo Fisher Scientific) by measuring the absorbance at A_{260} and visualised on a 1.5% agarose gel to check the DNA quality.

2.5 Immunofluorescence

2.5.1 Buffers, solutions and antibodies

4% Paraformaldehyde

4.0 g of paraformaldehyde (PFA) powder was added to 100 ml of 1x PBS and heated at 65ºC for 5 min. 1 drop of 10M NaOH was added to the above solution to enable the PFA

to dissolve into solution. The solution was then cooled to RT, the pH was adjusted to 7.3 using dilute HCl and solution stored at 4ºC. The solution was stored only for 2 weeks at 4ºC and prepared fresh thereafter.

Antibody blocking solution

Fetal bovine serum (FBS) and BSA were added to 1 x PBS at 10% (v/v) and 1% (v/v), respectively.

Antibodies

See Tables 2.1, 2.2 and 2.3

Antibody isotype controls

Antibody isotype controls and only secondary antibody controls for respective antibodies verified the lack of non-specific staining (Figure 2.1) for all the three methods.

2.5.2 Immunofluorescence staining procedure

Muscle sections were fixed in 4% paraformaldehyde in PBS for 10 minutes and then incubated in antibody blocking solution overnight at 4^{o}C. Sections were washed 3 times with PBS (5 min each) and incubated in primary antibody (Table 2.1) diluted in antibody blocking solution for 2 h at RT. All the antibodies used for immunofluorescence experiments were tested at different dilutions (1:50, 1:100 and 1:200) before selecting 1:100 as the dilution used for all further experiments. Following incubation in primary antibody, sections were washed 3 times with PBS (5 min each) and incubated in secondary antibody (Table 2.2) diluted in blocking solution for 1 hour. The samples were then washed in PBS and mounted in a DAPI-containing mounting media (Vectashield, Vector Laboratories, Burlingame, CA). Images were captured with a Zeiss Axioskop fluorescent microscope (Carl Zeiss, Oberkochen, Germany) using Spot Advanced software (SPOT Imaging Solutions, Sterling Heights, MI). All the images were acquired at the same gain and exposure settings and were processed using the same

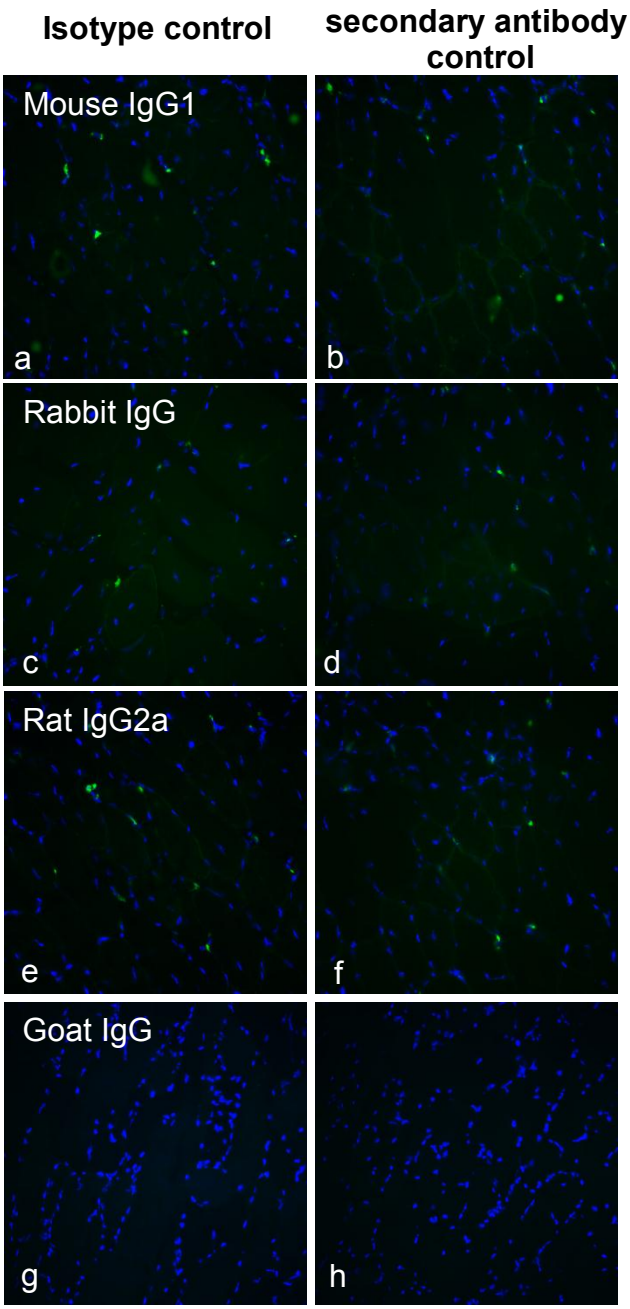

Figure 2.1 Immunofluorescence labeling of untreated triceps muscle sections of 3 month old female C57/black mice. Muscle sections were fixed using 4% paraformaldehyde and stained with antibodies against isotype controls: mouse IgG1 (a), Rabbit IgG (c), Rat IgG2a (e) and Goat IgG (g). Secondary antibodies were**:** goat anti-mouse alexa fluor 488 antibody (a, b); goat anti-rabbit FITC conjugated antibody (c, d); goat anti-rat FITC conjugated antibody (e, f) and Dylight 549 conjugated anti-goat IgG antibody (g, h). Nuclei are stained with DAPI (blue).

parameters to refine the images. The blocking solution for anti-decorin antibody was 10% normal donkey serum in PBS. Antibody isotype controls and secondary antibody controls were used to verify the specificity of each primary antibody. FBS was used for blocking in immunohistochemistry experiments and it contains high levels of soluble ECM proteins like fibronectin and other proteoglycans. The results described in Figure 3.2 and Figure 3.6. show that there is no evident staining for fibronectin (Fig 3.2) and decorin and biglycan (Fig 3.6) which suggest that FBS was not contributing to any false positives.

The presence of DNA in decellularized sections (section 2.2.2) was assessed qualitatively using DAPI (4',6-diamidino-2-phenylindole**)** (1.0µg/ml in PBS). Control and decellularized sections were mounted in a Vectashield and images captured as described above.

2.6 Scanning electron microscopy

Control and decellularised muscle sections were fixed in 4% paraformaldehyde for 30 min at RT and subsequently dehydrated in ethanol solutions of increasing concentration (30% to 100% in ddH_2O), for 15 mins per concentration. Muscle sections were then dried at room temperature and sputter coated with platinum (5 nm) using an Emitech K575 × Sputter Coater (Cressington, Redding, CA) and data collected using an EVO Scanning Electron Microscope (Carl Zeiss). Sample coating and the scanning electron microscopy was performed with the technical assistance of Mrs. Elaine Miller at the Curtin University Electron Microscope Facility.

Table 2.1. Primary antibodies

Antibody	Species, Isotype	Reacts against	Clonality, Clone name	Applications	Manufacturer, catalogue no.
collagen type I	Rabbit IgG	Mouse, Rat, Horse, Human	Polyclonal	IHC, ICC, WB	Abcam (ab292)

collagen type III	Rabbit IgG	Mouse, Rat, Cow, Human	Polyclonal	IHC, WB	Abcam (ab7778)
collagen type IV	Rabbit IgG	Mouse, Rat, Cow, Human	Polyclonal	IHC, ICC, WB	Abcam (ab6586)
collagen type VI	Rabbit IgG	Mouse, Rat, Cow, Human	Polyclonal	IHC, ICC, WB	Abcam (ab6588)
Fibronectin	Rabbit IgG	Mouse, Rat, Cow, Human	Polyclonal	IHC, ICC,	Abcam (ab2413)
Fibronectin	Mouse IgG1	Rat, Human	Monoclonal, EP5	WB	SantaCruz (SC-8422)
Laminin α2	Rat IgG_1	Mouse, Human	Monoclonal, 4H8-2	IHC, ICC, WB	Abcam (ab11576)
Desmin	Mouse IgG1	Rat, Cow, Human	Monoclonal, DE-U-10	IHC, ICC	Abcam (ab6322)
Myosin (slow muscle)	Mouse IgG	Human, rat, feline	Monoclonal, NOQ7.4.D	IHC, ICC, WB	Millipore(MAB1628)
Biglycan	Goat Ig	Mouse, Rat	Polyclonal	IHC	Abcam (ab58562)
Decorin	Sheep IgG	Chicken, Cow, Human	Polyclonal	IHC	Abcam (ab35378)
Perlecan	Rabbit IgG	Mouse, Rat, Human	Polyclonal	IHC, ICC, WB	Prof. John Whitelock University of NSW, Sydney

EV3C3	Mouse	Rat, Human	Monoclonal	IHC	Prof Toin Van Kuppeveldt Radboud University, The Netherlands
β-tubulin	Rabbit IgG	Mouse, Rat, Human,	Polyclonal	WB	Abcam (ab6046)
Vinculin	Mouse IgG1	Human, Rat, Bovine	Monoclonal hVIN-1	ICC	Sigma (V 9131)

Table 2.2 Secondary antibodies

Name, species, isotype	**Reacts against**	**Conjugated**	**Applications**	**Manufacturer, Catalogue no.**
Goat anti-mouse Ig	mouse Ig, mainly IgG	HRP	WB	Dako (P0447)
Goat anti-rabbit Ig	rabbit Ig, mainly IgG	HRP	WB	Dako (P0448)
Rabbit anti-rat Ig	rat Ig, mainly IgG	HRP	WB	Dako (P0450)
Goat anti-rabbit Ig	Rabbit Ig	FITC	IHC	Sigma (F9887)
Goat anti-rabbit Ig	Rabbit Ig	Alexa-fluor 488	IHC, ICC	MP (A-11008)
Goat anti-rabbit Ig	Rabbit Ig	Alexa-fluor 546	IHC	MP (A-11035)
Goat anti-rat Ig	Rat Ig	FITC	IHC	Sigma (F6258)
Goat anti-mouse Ig	Mouse Ig	Alexa-fluor 488	ICC	MP (A-11001)
Goat anti-mouse Ig	Mouse Ig, mainly IgG	unconjugated	Blocking	Dako
Donkey anti-goat Ig	Mouse Ig	Dylight 549	IHC	Jackson Immunoresearch
Donkey anti-sheep Ig	Mouse Ig	Dylight 549	IHC	Jackson Immunoresearch

Table 2.3 Isotype Control antibodies

Name, species, isotype	Applications	Manufacturer, Catalogue no.
Rat IgG2a	IHC, ICC	Zymed (02-9688)
Rabbit IgG	IHC, ICC	Invitrogen (02-6102)
Sheep IgG	IHC	Jackson Immunologicals (D13-000-003)
Mouse IgG2a	IHC, ICC	Dako (X0943)
Mouse IgG1	IHC, ICC	Dako (X0931)

2.7 Tissue culture and cell based assays

2.7.1 Cell lines

The C2C12 murine myoblast cell line was purchased from the American Type Culture Collection (ATCC, Manassas, VA). Human skeletal muscle myoblasts (HSMMs) were purchased from Lonza (Basel, Switzerland). HSMMs were obtained from normal human donors usually from the quadriceps or psoas muscles.

2.7.2 Basic Tissue Culture Media and supplements

Dulbecco's modified Eagle's medium (DMEM) was purchased in 500 ml bottles (pre-prepared, without L-Glutamine) from Life Technologies (Carlsbad, CA). Skeletal Muscle Growth Media-2 (SkGM™-2 Medium) was purchased from Lonza. Ham's F-10 and Ham's F-12 media, both without L-Glutamine were purchased from Sigma-Aldrich. Stock solutions of HEPES (1M), L-Glutamine (200mM) and sodium pyruvate (100mM) were purchased from Life Technologies. Fetal Bovine Serum (FBS) was purchased from HyClone (Thermo Fisher Scientific). DMEM working media solutions were prepared by adding the stock solutions of HEPES, L-Glutamine and sodium pyruvate at a 1:100 dilution into DMEM, and supplementing with 10% FBS to produce a final media solution containing DMEM, 10 mM HEPES, 1 mM sodium pyruvate, 2 mM glutamine and 10% FBS.

2.7.3 Serum free media

Serum free base media was prepared by adding DMEM and Ham's F10 in a 1:1 ratio, supplemented with HEPES, L-Glutamine and sodium pyruvate as described above. Monothioglycerol (MTG) was added to the media to a final concentration of 0.1 mM. Serum free media (SF) proliferation media was prepared by supplementing serum free base media with 50 ng/ml epidermal growth factor (EGF), 25 ng/ml fibroblast growth factor (bFGF), 1.0 µM/ml dexamethasone, 0.12 IU/ml insulin, 1.0 µg/ml heparin and 0.5% BSA. Serum free differentiation medium consisted of DMEM/F10 in a ratio of 1:1 supplemented with 50 ng/ml epidermal growth factor (EGF), 25 ng/ml insulin growth factor (IGF-1), 1.0 µM/ml dexamethasone and 0.5% BSA. Growth factors were purchased from from Peprotech (Rocky Hill, NJ), dexamethasone, insulin and BSA were all from Sigma-Aldrich and heparin was from Celsus Laboratories (Cincinnati, OH).

2.7.4 Freezing and thawing cell lines

Freezing

Cells were harvested, resuspended in appropriate FBS containing tissue culture media (see sections 2.7.5.1, 2.7.5.2) and then pelleted by centrifugation at 1000 rpm for 5 min. Media was carefully removed from the cell pellet by pipetting. The cell pellet was gently resuspended in 0.5 ml of freeze media (50% DMEM or SkGM-2, 40% FCS, 10% DMSO) and transferred into cryogenic vials (Corning, Tewksbury, MA). The cryogenic vials were then placed at -80ºC before being transferred to a liquid N_2 cylinder.

Thawing

Cells in cryogenic vials were warmed quickly by immersing the vial in a 37ºC water bath. 1 ml of warm complete tissue culture media (either DMEM or SkGM-2) was added drop wise to the cells. The cell solution was then transferred into a 25cm^2 tissue culture flask (Nunc, Thermo Fisher Scientific) and a further 4 ml of warm tissue culture media was slowly added. The flask was monitored every 2 hours and media was changed after the cells attached to the flask (4-6 h).

2.7.5 Cell culture and maintenance

2.7.5.1 C2C12 murine myoblasts

C2C12 myoblasts were subcultured in DMEM complete media and housed in a humidified 37^{o}C incubator equilibrated at 5 % $CO_{2.}$ C2C12 myoblasts were passaged when they reached 60-70% confluence and cells less than 20 passages old were used for all experiments. Briefly, media was discarded from the T_{25} flask and cells were washed with PBS before 500 µl of 0.05% trypsin-EDTA (Life Technologies) was added to the flask and incubated at 37ºC for 5 min or until the cells detached. Cells were pelleted by centrifugation at 1000 rpm for 5 min in DMEM complete media. Media was removed; cells were resuspended in 1 ml of DMEM complete media and counted using a haemocytometer. C2C12 myoolasts were at 4 x 10^4 cells per T_{25} flask for maintenance, or at 3500 - 7000 cells/cm^2 in a well for further experiments.

2.7.5.2 HSMMs

HSMM were maintained in SkGM™-2 Medium containing human epidermal growth factor (hEGF), Dexamethasone, L-glutamine and 10% FBS. SkGM-2 media was prepared and used according to the manufacturer's instructions. Cells were subcultured once they reached 50-70% confluency. Briefly, media was discarded from the flask and cells were washed with PBS (HyClone, Ca^{2+} and Mg^{2+} free). PBS was removed and 750 µl of TE (trypsin-EDTA) was added to the T_{25} flask and incubated at 37ºC for 5 min or until the cells detached. Cells were pelleted by centrifugation at 1000 rpm for 5 min in 5 ml of SKGM-2 media. Media was removed and cells were counted using a haemocytometer. Cells were seeded at a density of 3500 cells/cm^2 for a T_{25} flask or at 1 x 10^4-1.5 x 10^4 cells/cm^2 for seeding in wells. HSMM cells less than 6 passages old were used in all further experiments.

2.7.5.3 Serum free culture of C2C12 cells

C2C12 cells were harvested from serum-containing media using the following protocol. Briefly, media was removed from the flask and cells were rinsed with 5 ml PBS and then

5 ml of 2.5mM EDTA. 0.5 ml of warm 0.05% trypsin/EDTA diluted 1:10 in 2.5mM EDTA (0.9 ml EDTA+0.1 ml trypsin/EDTA) was then added per T25 flask and incubated at 37ºC for 5 min. Cells were pelleted down with 4.5 ml DMEM/10% FCS at 1100 rpm for 5 min. Pellet was washed thrice with 5 ml of DMEM/F10 base media + 0.5 % BSA by centrifuging at 1100 rpm for 5 min to remove any remaining serum. Cells were counted in 2 ml of base media and seeded at required densities in serum free proliferation media (section 2.7.3).

2.7.6 Proliferation and Differentiation of C2C12 cells on different matrices

Wells of a 24 well plate (Nunc) were coated with 10µg/cm^2 of the solubilised ECM derived from skeletal muscle (section 2.2.3), 10µg/cm^2 of collagen I (Sigma C8919) and 10.0µg/cm^2 of fibronectin (Sigma F0895) diluted in PBS (1x), incubated at 37ºC for 2 h, washed twice with PBS and then sterilized under UV light for 20 min. C2C12 myoblasts were plated at a density of 7,000 cells/well in serum free medium and maintained at 37ºC and 5% CO_2. Myoblasts were maintained in the serum supplemented or serum free proliferation medium for the first three days, after which they were transferred to serum supplemented or serum free differentiation medium. Cells were monitored for morphological changes and phase contrast images were taken on days 1, 3, 5 and 7 following the addition of differentiation medium. Control wells contained cells grown in serum free proliferation media supplemented with 10% foetal calf serum (FCS) and serum free differentiation media containing 2% horse serum (HS).

2.7.7 Cell Proliferation (direct cell count)

Direct cell counts were performed from cells cultured in 24 well plates unless otherwise stated. Cells were counted using the Z™ Series COULTER COUNTER® (Beckmann Coulter, Indianapolis, IN) and cell concentrations were calculated from a live cell count only, as gates were set to remove dead cells and cellular debris from the analysis. To count, cells were harvested from the plastic using 0.05% trypsin/EDTA and resuspended in DMEM/10% FBS (0.5 ml or 1 ml, depending on the number of cells). 100µl, 200 µl

or 400 µl of this cell suspension was diluted in 10 ml of isotonic saline and 500 µl of this sample counted. The cell concentration was then calculated after adjusting for the dilution factor.

2.7.8 Chloroform sterilisation of decellularised muscle scaffolds

10 ml chloroform was combined with sterile 1x PBS to make a 2L solution. Whole, decellularised scaffolds were placed in pre-wetted dialysis tubing containing 5 ml tissue culture grade PBS and sealed at both ends. The dialysis bag containing the scaffolds was dialysed against 2L of chloroform/PBS at 4ºC overnight. The scaffolds were then dialysed against an additional 2 changes of chilled chloroform/PBS, each for 30 min at 4ºC. Next, the scaffolds were removed from the dialysis tubing using sterilised tweezers and stored in 10 ml of sterile tissue culture grade PBS at 4ºC until required.

2.7.9 Three-dimensional cell culture (C2C12 and HSMM)

Longitudinal and transverse samples of decellurarised rat muscle scaffolds were cut using a sterilized razor blade and placed into the wells of a 24 well plate. C2C12 or HSMM were harvested and re-suspended in SF media (C2C12) or SKGM-2 plus FBS (HSMM). Media (50 µl) containing $1x10^4$ cells was dripped gently onto the scaffold, to minimise dispersal of cells into the well, and the cells were allowed to adhere to the scaffold for 30 min in a tissue culture incubator. Following this, the scaffolds were carefully transferred to a new well, 1.5 ml of media (SF or SKGM-2) was added and cells were cultured for 7 and 14 days, with media replaced after every third day. After 7 and 14 days of culture, cells and scaffolds were stained with Kwik Diff stain (Thermo Fisher Scientific)

2.7.10 Kwik Diff staining and imaging

Kwik-Diff staining of the decellularised scaffolds was performed according to the manufacturer's instructions. In brief, media was removed from each well and 500 µl of solution 1 (fixative) was added. Scaffolds were incubated at RT for 1 min and then

solution 1 replaced by solution 2 (eosin) for 30 sec. Solution 2 was removed and 500 µl of solution 3 (methylene blue) was added to each well and plate incubated for 1 min at RT. Wells were washed with ddH_2O three times (1 min each). Samples were left in ddH_2O water to de-stain for 3 days, with water replaced regularly. Samples were imaged using Zeiss Axioskop bright field microscope (Carl Zeiss) using Spot Advanced software (SPOT Imaging solutions). Images were taken at 100x, 200x and 400x magnification.

2.7.11 Click-iT EdU cell proliferation assay

Click-iT® EdU (Life Technologies) cell proliferation assay was performed on the whole muscle scaffolds seeded with C2C12 myoblasts. This assay labels recently synthesized DNA of cell nuclei with the coloured thymidine analogue EdU. Detection is based on a covalent reaction between an alkyne (EdU) and an azide (Alexa Fluor 488), catalyzed by copper. At day 3 of proliferation and day 6 of differentiation, half of the serum-free proliferation media was replaced fresh media containing 20 µM EdU and incubated for 24 h. The media was then removed and scaffolds fixed in 4 % paraformaldehyde in PBS for 10 min, washed twice with 3% BSA and permeabilized with 0.5 % Triton X-100 for 10 min. After permeabilization, the scaffolds were washed twice with 3 % BSA and incubated in 100 µl of Click-iT reaction cocktail (1X Click-iT reaction buffer - 90 µl, $CuSO_4$ - 2 µl, Alexa fluor azide - 0.25 µl and reaction buffer additive - 10 µl) for 30 min at RT in the dark. After incubation, the scaffolds were washed with 3% BSA and incubated in DAPI/PBS (1 µg/ml) for 10 min. Scaffolds were imaged using a Nikon A1+ confocal microscope (Nikon, Tokyo, Japan) using NIS-Elements AR analysis version 4.10 software. 69 z-stack images (2 µm each) were taken and merged to generate a single image showing the distribution of cells across the scaffold.

2.7.12 Immunofluorescence for myosin (differentiation marker)

Differentiation of C2C12 myoblasts was assessed by immunoflourescence. C2C12 myoblasts were cultured on etched glass coverslips and on Day 4 and 8 of differentiation

were fixed in 4 % paraformaldehyde in PBS for 10 min, permeabilized in 0.1 % Triton X-100/PBS for 5 min at RT and then blocked in 10 % FBS/1% BSA in PBS for 1 h at RT. Cells were washed 3 times with PBS (5 min each) and incubated in primary antibody (Slow Muscle Myosin, Millipore, Table 2.1) diluted in blocking solution (10 % FBS/1% BSA) in PBS for 2 h at RT before being washed 3 times with PBS (5 min each) and incubated in secondary antibody (anti-mouse Alexa Flour 488) diluted in blocking solution (10 % FBS/1% BSA) in PBS for 1 h at RT. The samples were then washed 3 times in PBS for 5 min each and incubated in DAPI (1µg/ml in PBS) solution for 5 min. The coverslips were then mounted in a mounting media (Vectashield) and sealed with nail varnish. Images were captured with a (Zeiss Axioskop) fluorescent microscope using Spot Advanced software.

2.7.13 Myotube width measurements (Image J)

Phase contrast images of myotubes with a scale bar of 100 µm were imported in ImageJ. A line was drawn along the scale bar by clicking on the "straight line drawing tool" followed by "Analyze" and "Measure", which indicated the pixel length (134) that corresponded to the 100 µm scale bar. The straight line drawing tool was then used to measure the width of each myotube in pixels before converting to a length in µm. For each myotube, three measurements were made along the myotube and a mean width generated. 25 independent myotubes were measured from 5 different images for each time point. The values were exported to Microsoft excel and plotted as bar graphs with standard errors.

2.8 RNA extraction and quantitative reverse transcription PCR (qRT-PCR) analysis

2.8.1 RNA extraction

RNA was isolated from cells cultured in SF proliferation or differentiation media in wells coated with collagen I (10µg/cm^2), fibronectin (10µg/cm^2) or solubilised muscle matrix (10µg/cm^2), using the ISOLATE RNA KIT (Bioline, Alexandria, Australia). Cell

culture medium was removed from the wells and 450 µl Lysis Buffer R was added to each well. The sample was resuspended by gently mixing with a pipette and incubated at RT for 3 min. The sample was then pipetted into a spin column (R_1) in a 2ml collection tube and centrifuged at 12,000 rpm for 2 min. DNase I (1U/sample) was added to the filtrate and incubated at 25º C for 10 min. 450 µl of 70% ethanol was added to the filtrate and mixed well by pipetting before the filtrate/ethanol mixture was applied to a spin column (R_2) in a 2ml collection tube and centrifuged at 12,000 rpm for 2 min. The filtrate was discarded and spin column R_2 was placed in a new collection tube. The spin column was washed with 500 µl buffer AR, centrifuged at 10000 rpm for 1 min and transferred to a new collection tube before being washed with 700 µl buffer BR, centrifuged at 10000 rpm for 1 min and transferred to an elution tube. To elute the RNA, 50µl RNase-free water was added directly to the spin column membrane, incubated at RT for 1 min and centrifuged at 8000 rpm for 1 min.

2.8.2 RNA quantification and quality analysis

The yield and purity of RNA was measured by light absorption at 260nm using a Nanodrop DN-100 spectrophotometer (Thermo Fisher Scientific). RNA was also analysed using a LabChip GXII (Perkin Elmer) according to the manufacturer's instructions. Briefly, 75 µl of HT RNA Dye concentrate was mixed with 425 µl of HT RNA gel matrix and vortexed to mix. The gel-dye mix was then carefully transferred to a spin filter and centrifuged at 9200 rpm for 10 min at RT and stored at 4°C until further use. Sample buffer was prepared (for 96 samples) by adding 620 µl RNA sample buffer to 5580 µl of RNAse free water. 4 µl of RNA ladder and 2 µl of each sample was pipetted into individual wells of a microtiter plate (Axygen) and heated at 70°C for 2 min, then immediately snap cooled on ice for 5 min. 46 µl of sample buffer was added to each well and the plate centrifuged at 1250 rpm for 1 min at RT. 96 µl of sample buffer was added to the RNA ladder well. The ladder tube was inserted into the ladder slot on the LabChip GX instrument. 750 µl of sample buffer was added to the buffer tube, which was placed into the buffer slot on the instrument. The chip was allowed to come to room temperature, the foil cover removed and the chip surfaces dried using a pipette

tip attached to a vacuum line. Active wells of the chip (1, 3, 4, 7, 8 and 10) were thoroughly rinsed with nuclease free water twice. 75 µl of Gel-Dye solution was added to chip well 3, 7 and 8 and 120 µl of Gel-Dye was added to chip well 10. 120 µl of HT RNA marker was added to well 4 and the chip was placed in the instrument to start the assay.

2.8.3 cDNA synthesis

RNA (300 ng) was reverse transcribed using the Tetro cDNA synthesis kit (Bioline) to according to the manufacturer's instructions. 20 µl reactions were performed, each containing 300 ng of total RNA, 0.5 µl each of Oligo (dT) and Random Hexamer, 1µl 10mM dNTP mix, 4µl RT Buffer (5x), 1µl Ribosafe RNase Inhibitor and 1µl Tetro Reverse Transcriptase (200u/µl), with the final volume made up to 20µl with DEPC-treated water. Samples incubated for 10 min at 25°C followed by 30 min at 45°C. The reaction was terminated by incubating the samples at 85°C for 5 min before the samples were immediately chilled on ice. 30 µl of RNase free water was then added to make a 50 µl solution (neat cDNA) which was further serially diluted to produce 1/5, 1/10, 1/25, 1/125 and 1/625 dilutions for use in quantitative reverse transcriptase PCR (qRT-PCR) reactions.

2.8.4 Primers for qPCR

Primers were selected for four reference genes (RG) and seven genes of interest (GOI) (Table 2.4) primarily using the PrimerBank database [235] and purchased from Geneworks (Hindmarsh, Australia).

Table 2.4 Primers used in qPCR

Gene		Sequence (5'-3')	NCBI ref	PrimerBank ID	T_M (°C)	Length (bp)
SDHA	F	TGG GGA GTG CCG TGG TGT CA	NM_023281		60	100
	R	TGC CCC GTA GCC CCC AGT AG			60	

ACTAB	F	GTG ACG TTG ACA TCC GTA AAG A	NM_007393	145966868c1	60	245
	R	GCC GGA CTC ATC GTA CTC C			61	
TBP	F	CCT TGT ACC CTT CAC CAA TGA C	NM_013684	172073170c2	61	119
	R	ACA GCC AAG ATT CAC GGT AGA			61	
GAPDH	F	AGG TCG GTG TGA ACG GAT TTG TGT	NM_008084		54	139
	R	AGA CCA TGT AGT TGA GGT C			50	
MYOG	F	CGA TCT CCG CTA CAG AGG C	NM_031189	162287254c3	62	137
	R	GTT GGG ACC GAA CTC CAG T			61	
MYF5	F	GCC TTC GGA GCA CAC AAA G	NM_008656	240120094c2	61	187
	R	TGA CCT TCT TCA GGC GTC TAC			61	
ACTA1	F	CCC AAA GCT AAC CGG GAG AAG	NM_009606	133893192c1	62	89
	R	GAC AGC ACC GCC TGG ATA G			62	
ACTAC1	F	CTG GAT TCT GGC GAT GGT GTA	NM_009608	14192922a1	54	173
	R	CGG ACA ATT TCA CGT TCA GCA			52	
MYH1	F	CGG AGT CAG GTG AAT ACT CAC G	NM_030679	82524273c2	57	153
	R	GAG CAT GAG CTA AGG CAC TCT			54	
MYH3	F	ATG AGT AGC GAC ACC GAG ATG	NM_001099635	153792648c1	61	119
	R	ACA AAG CAG TAG GTT TTG GCA T			61	
MYH7	F	ACT GTC AAC ACT AAG AGG GTC A	NM_080728	18859641a1	53	114
	R	TTG GAT GAT TTG ATC TTC CAG GG			53	

SDHA- Succinate dehydrogenase complex, subunit A; ACTAB- β-actin; TBP- Tata binding protein; GAPDH- Glyceraldehyde-3 phosphate dehydrogenase; MYF5- Myogenic factor 5; MYOG-Myogenin; ACTA1- Actin, alpha 1, skeletal muscle; ACTAC1- Actin, alpha 1, cardiac muscle; MYH1- Myosin heavy chain-1; MYH3- Myosin heavy chain-3; MYH7- Myosin heavy chain-1

2.8.5 qRT-PCR and melt curve analysis

qRT-PCR reactions (10 µl total volume) consisted of 5 µl SyBr Green Lo-RoX Mix (Bioline), 2 µl template cDNA, 1 µl forward/reverse primer (20 ng/µl) and 2 µl RNase free H_2O. Reactions were performed on a ViiA™ 7 Real-Time PCR system (Applied Biosystems) with fast 96-well block using the following cycling conditions: initial denaturation at 95ºC for 2 min, 40 cycles of denaturation at 95ºC for 5 sec and annealing and extension together in 1 step at 60ºC for 20 sec, followed by a melt step ranging from 55-95ºC. The 4 RG and 7 GOI (Table 2.4) were analysed in C2C12 cells cultured on col I (10 µg/cm^2) and matrix (10 µg/cm^2) coated wells in serum free media, at days day 1, 4 and 8 of differentiation.

To assess the specificity of the primers, melt curve analysis was performed for all genes by heating the completed qPCR reactions from 55°C to 95°C and a fluorescence reading taken every 0.5°C. The rate of change of the relative fluorescence units (RFU) with time (T) (-d(RFU)/dT) was plotted on the Y-axis, versus the temperature on the X-axis. A peak was generated at the melting temperature (Tm) of each amplified product.

2.8.6 Primer efficiency calculation

Five-fold dilutions of neat cDNA were prepared to yield dilutions of 1/5, 1/25, 1/125 and 1/625. Each dilution was amplified for each primer pair to create an efficiency curve. The log template dilution (*x*-axis) was plotted against the cycle threshold (C_T) value obtained for each dilution (*y*-axis) using Microsoft Excel. Efficiency (E) of each primer in the exponential phase was calculated by substituting the slope of the line in the equation $E=10^{(-1/slope)}$. All reactions were performed in triplicates with the mean C_T value used in the statistical analysis.

2.8.7 Validation of reference genes

For selection of the most stable gene(s), all four reference genes were tested using Normfinder [236] and Bestkeeper [237] software. Briefly, the qRT-PCR of four reference genes was performed as described above. C_T values obtained from qPCR were exported into Microsoft Excel. The most stable gene was *SDHA*.

2.8.8 Gene expression analysis

Gene expression (fold change) was calculated using the $2^{-\text{delta delta CT}}$ method as described by Livak and Schmittgen [238]. Briefly, the qPCR of different genes was performed as described above and C_T values obtained exported into Microsoft Excel. Expression levels for *MyoG*, *Myf5*, *MYH1*, *MYH3*, *MYH7*, *ACTA1* and *ACTAC1* were normalized to *SDHA* expression values and fold change determined using $2^{-\text{deltadeltaCT}}$ method, according to the equation below. Day x is either 4 or 8 days of differentiation and day 1 represents the 1X expression of the target gene normalized to reference gene SDHA.

$$\Delta\Delta CT = (CT, GOI - CT, SDHA)Day\ x - (CT, GOI - CT, SDHA)Day\ 1.$$

Fold changes in gene expression were log transformed as the gene expression data is normally log distributed [239]. Mean ± SE of 4 replicates were shown. A Wilcoxon signed rank test was performed comparing the ΔCT data from day 1 of differentiation to day 4 and day 8 of differentiation to determine whether the differences in expression observed were statistically significant.

2.9 Collection of silkworm species

Bombyx mori (*B. mori*) cocoons were collected from Debra Sericulture Farm, Midnapore, West Bengal. *Antheraea mylitta* (*A. mylitta*) 5^{th} instar late larvae collected just before spinning were obtained from our IIT Kharagpur Farm. *Antheraea. assamensis* (*A. assamensis*) and *Samia. ricini* (*S. ricini*) 5^{th} instar larvae were collected from Jorhat, Assam and Coochbehar, West Bengal, India.

2.9.1 Silk protein fibroin processing

The regenerated fibroin solution was prepared from both mulberry and the different non-mulberry sources using two distinct methods. Schematic representation of silk protein fibroin isolation from mulberry and non-mulberry species, and the preparation of 3D fibroin scaffolds are shown in Fig 5.1. Fibroin was isolated from *B. mori* cocoons using a standard protocol described elsewhere [240], whereas fibroin from non-mulberry sources was isolated by squeezing the glands of 5^{th} instar larva immediately prior to the spinning of their cocoons, before following the steps described previously [138, 140, 241]. The regenerated 2% fibroin solutions from the four species were used to fabricate 3D porous sponges using the described freeze drying technique [242]. Collection of the silkworm species and silk processing was performed by Professor Subhash C Kundu and colleagues at IIT, Kharagpur, INDIA.

2.9.2 Solubilisation of silk from freeze dried scaffolds for 2D culture

The silk fibroin scaffolds were solubilised in PBS to produce a fibroin solution used to coat tissue culture polystyrene plates. Scaffolds were placed in 1.5 ml microtubes and weighed. 500 µl PBS was added to each tube, incubated at 42ºC for 30 min with rocking, and then centrifuged at 9000 rpm for 10 min at 4ºC. Supernatants were transferred to a fresh tube and re-centrifuged. Protein content of the supernatants was measured using a BCA protein assay (Pierce Biotechnology). The solubilised silk was stored at 4ºC until used. Routinely, 10 µg/cm^2 silk fibroin was used to coat either tissue culture plastic (TCP) or etched glass surfaces.

2.10 Cell culture and 2D cell based assays

All cells were housed in a humidified 37^{o}C incubator equilibrated at 5 % CO_2. The murine myoblast cell line, C2C12 (ATCC, Manassas, VA) and HSMM cells were routinely cultured as previously described (section 2.7.5).

2.10.1 Proliferation and Differentiation assays

Wells of a 24 well tissue culture plate (Nunc) were coated with 10 µg/cm^2 of either *B. mori*, *A. mylitta*, *A. assamensis* or *S. ricni* solubilised silk fibroin; or collagen I or fibronectin (Sigma-Aldrich). Plates were incubated at 37ºC for 2 h, washed with PBS and sterilized under UV light for 20 min. C2C12 myoblasts were plated at a density of 7,000 cells/well in SF growth medium and cultured for 3 days before being transferred to SF differentiation medium. Phase contrast images were taken using a Zeiss Axiovert (Carl Zeiss) microscope and Spot Advanced software (SPOT^{TM} Imaging solutions) on days 1, 2 and 4 of proliferation as well as days 1, 4, 6 and 7 in SF differentiation media.

2.10.2 alamarBlue dye assay for C2C12/HSMM cell proliferation

C2C12 cells were seeded in 96-well plates (Nunc) at a density of 1x10^3 cells per well in SF growth media (200 µl) and cultured for 3 days. After 24, 48 and 72 h in culture, 20 µl of alamarBlue reagent was added and the cells were incubated at 37^{o}C with 5% CO_2 for 4 h. The fluorescence intensity of each well was then measured at excitation and emission wavelengths of 560 nm and 600 nm respectively (EnSpire Multimode plate reader, Perkin Elmer). Similarly, HSMMs were cultured in a 48-well plate (Corning Inc., Corning, NY) at a seeding density of 1x10^3 cells per well in SkGM-2 media/10% FCS (500 µl) and cultured for 10 days. After 2, 5, 8 and 10 days of proliferation, 50 µl of alamarBlue reagent was added to the wells and fluorescence measured as described. Blank media served as a negative control and relative cell numbers were represented as relative fluorescence units (RFU) per well. Previous experiments indicated the cell numbers obtained were in the linear range of an alamarBlue standard curve.

2.11 Immunofluorescence of 2D cultures

2.11.1 Etching of glass coverslips

Round glass coverslips (13 mm diameter) (ProScitech, Thuringowa, Australia) were stored in 100% ethanol. Coverslips were treated with freshly prepared etch solution (6.0 g NaOH dissolved in 24 ml ddH_2O, with the volume made up to 60 ml using 95%

ethanol) for 30 min at RT. After treatment coverslips were washed extensively with ddH_2O dried at RT, sterilised by UV light and used in experiments.

Atomic force microscopy (AFM) was used to examine the surface topography of the etched glass coverslips. The coverslips were washed and dried under a stream of nitrogen, mounted on magnetic steel stubs and AFM imaging was performed using a Nanoscope IIIa (Digital Instruments Inc., Santa Barbara, CA) atomic force microscope with V-shaped silicon nitride cantilevers, using contact mode and a long range scanner. A variety of scans (5µm x 5µm) were performed at random locations on the glass surface. Untreated coverslips washed with ethanol were used as a control.

2.11.2 Matrix protein expression

The expression of matrix proteins by C2C12 myoblasts was investigated by seeding 3.5 x 10^3 cells/cm^2 cells on etched glass coverslips either uncoated or coated with collagen type I or solubilized muscle matrix. Cells were cultured for 3 days, washed with PBS and coverslips were fixed with 4% paraformaldehyde in PBS (PFA/PBS), then blocked in 10 % FBS/1% BSA/PBS for 1h at RT. Cells were washed in PBS and incubated in primary antibodies recognising the extracellular matrix molecules: collagen I, collagen IV, collagen VI, fibronectin and perlecan (refer Table 2.1). Primary antibodies were used at a concentration between 2 µg – 4 µg. Cells were washed with PBS and incubated in secondary antibody (anti-rabbit Alexa Flour 488) diluted in blocking solution for 1 h. Coverslips were washed extensively in PBS and mounted in a DAPI-containing mounting media (Vectashield, Vector Laboratories). The control antibodies were rabbit IgG and mouse IgG (Life Technologies). Images were captured with a Nikon A1+ confocal microscope (Nikon, Tokyo, Japan) using NIS-Elements AR analysis version 4.10 software. All images were acquired at the same gain and exposure settings and were modified using same brightness and contrast settings.

The expression of matrix proteins by C2C12 myoblasts was examined by seeding cells on etched glass coverslips in a 12-well plate in DMEM/F10 SF and allowing the cells to grow for 3 days in proliferation medium. After 3 days, the media was changed to a

differentiation medium and the cells were cultured for another 6 days. At day 3 of roliferation and day 6 of differentiation, immunostaining was then performed as described above.

The deposition of matrix proteins was explored by immunofluorescent staining of matrices following removal of the cells. For these experiments, C2C12 myoblasts (3.5 x 10^3 cells/cm^2) were seeded on etched glass coverslips placed in a 12-well polystyrene plate in SF growth medium. Cells were maintained for 3 days in culture, allowing the cells to deposit ECM on the coverslips. After 3 days in culture, cells were removed by treating the coverslips with 0.5 % Triton X-100/PBS and 20mM NH_4OH for 2 min at RT, before washing three times with ice cold PBS to remove any cell debris. The coverslips were then fixed with 4% paraformaldehyde and incubated in primary antibodies recognising collagen I, collagen IV, collagen VI, fibronectin and perlecan as described above, but omitting the permeabilization step.

The deposition of matrix proteins on silk fibroin substrates was explored by culturing C2C12 myoblasts on either *B. mori, A. mylitta, A. assamensis* or *S. ricni* soluble silk fibroin (all at 10 µg/cm^2) on an etched glass coverslip placed in a 12-well polystyrene plate in SF growth medium. Immunostaining was then performed as described above.

2.11.3 Differentiation of C2C12 and HSMM on silk - myosin expression

C2C12 anti-myosin immunostaining was performed as described earlier (refer to section 2.7.12). Similarly, HSMMs were seeded at a density of $15x10^3/cm^2$ on etched coverslips coated with a fibroin protein, collagen I or fibronectin (all at 10 µg/cm^2) in SkGM-2 media and cultured for 3 days. The media was then changed to differentiation media (DMEM/F12/2%HS) and after day 7 and day 10 in differentiation media, HSMMs were fixed and immunostained for slow muscle myosin and GLUT 4 (Table 2.1) as described for the C2C12 myoblasts (section 2.7.12). Images were captured using fluorescent microscopy (Zeiss Axioskop) and Spot Advanced software with a 40 x objective. Total number of nuclei and number of myotubes were counted in 6 random fields of view

(>250 nuclei) and Fusion index (FI) was calculated according to the formula = (No. of nuclei within myotubes with two or more nuclei/ Total no. of nuclei) * 100. At least two independent experiments were performed for FI and myotube number calculations and the data represented here is from one of those experiments.

2.12 qPCR on 2D silk fibroin substrates

2.12.1 Gene expression analysis

For gene expression analysis, HSMMs were seeded on *B. mori* and *A. assamensis* scaffolds at a cell concentration (6×10^3 cells/cm^2) in a 12-well plate and cultured for 4 days in proliferation medium. Then the medium was changed to a differentiation one and cells were cultured for another 14 days in differentiation medium, with cells harvested at day 1, day 7 and day 14 of differentiation.

2.12.2 RNA Isolation

RNA was isolated usin the ISOLATE RNA KIT as described before (section 2.8.1).

2.12.3 cDNA synthesis and qRT-PCR analysis

Reverse transcription was performed on 500 ng of HSMM RNA using the Tetro cDNA synthesis kit (Bioline) according to the manufacturer's instructions. qPCR reactions were performed using SensiFAST SYBR Lo-Rox kit (Bioline), with triplicate reactions containing 5 µl SYBR Green Lo-RoX Mix, 2 µl template cDNA, 1 µl forward/reverse primer (25 ng/µl) and 2 µl RNase free H_2O. Reactions were performed on a ViiA™ 7 Real-Time PCR system (Applied Biosystems) with fast 96-well block using the cycling conditions: denaturation at 95ºC for 2 min, 40 cycles of denaturation at 95ºC for 5 sec and annealing and extension together in 1 step at 60ºC for 20 sec, followed by a melt step ranging from 55-95ºC. Primers were selected for three reference genes and five genes of interest (Table 4.1) using the PrimerBank database [235] and purchased from Geneworks (Hindmarsh, Australia). Of the three reference genes, *TBP* was found to

have the most stable expression according to Normfinder [236] and Bestkeeper [237] software. Expression levels for *MyoD1*, *Myf5*, *MYH1*, *MYH7*, *and ACTA1* were normalized to *TBP* expression values and fold change determined using $2^{-\text{delta delta Ct}}$ method with baseline expression at day 1 of differentiation. Mean ± SE of 4 replicates are shown.

Table 2.5 Primers used in HSMM qRT-PCR

Gene		**Sequence (5'-3')**	**NCBI ref**	PrimerBank ID	**T_M (°C)**	**Length (bp)**
SDHA	F	TGG CAT TTC TAC GAC ACC GTG	**NM_004168**	156416002c3	54	77
	R	GCC TGC TCC GTC ATG TAG TG			56	
ACTAB	F	TCC CTG GAG AAG AGC TAC G	**NM_001101**		53	
	R	GTA GTT TCG TGG ATG CCA CA			52	
TBP	F	CCC GAA ACG CCG AAT ATA ATC C	**NM_003194**	285026518c2	55	80
	R	AAT CAG TGC CGT GGT TCG TG			54	
MYOD1	F	CGG CAT GAT GGA CTA CAG CG	**NM_002478**	77695919c2	56	133
	R	CAG GCA GTC TAG GCT CGA C			55	
MYF5	F	CTG CCA GTT CTC ACC TTC TGA	**NM_005593**	156104905c1	54	78
	R	AAC TCG TCC CCA AAT TCA CCC			54	
ACTA1	F	GGC ATT CAC GAG ACC ACC TAC	**NM_002478**	47078293c1	56	84
	R	CGA CAT GAC GTT GTT GGC ATA C			55	
MYH1	F	GGG AGA CCT AAA ATT GGC TCA A	**NM_005963**	115527081c2	53	106
	R				50	

		TTG CAG ACC GCT CAT TTC AAA				
MYH7	F R	TGG ATG TGA GTG AAC TTG GGG GCA CCC AGA CTC GCT TCT T	**NM_020884**	291045202c2	54 53	108

2.13 3D cell based assays

2.13.1 Preparation of 3D silk scaffolds and HSMMs proliferation and differentiation

The 3D silk scaffolds were fixed by treating with 90% ethanol for 1 h and then with 70 % and 50 % ethanol for 30 min each. Scaffolds were washed twice in PBS for 30 min each and placed in a 24-well plate in SkGM-2 media for 2 h at 37ºC for pre-conditioning. The scaffolds were air dried under UV light for 20 min then placed in the wells of a 24-well plate. HSMMs in SkGM-2 media (25 µl, containing 7.5 x 10^4 cells) were added onto the scaffold and allowed to adhere for 30 min in a CO_2 incubator. Scaffolds were then transferred to a new well, 2 ml of SkGM-2 medium was added and the cells were cultured for either 2 or 5 days with the SkGM-2 media being replaced every third day.

Following 5 days of proliferation, HSMMs were switched to differentiation medium (DMEM/F10/2% HS) and cultured for a further 10 or 11 days, with the differentiation medium replaced every third day. The scaffolds were fixed and processed either for Scanning Electron Microscopy (SEM) or immunofluorescence.

For HSMM differentiation and myosin immunostaining, cells were seeded at a higher cell density (5 x 10^5 cells/scaffold) and cultured for 4 or 7 days in proliferation medium and then the medium was changed to a differentiation medium and cells were cultured for a further 10 days.

2.13.2 Immunofluorescence of filamentous actin (F-actin) and myosin

3D scaffolds processed as described above were stained with either Rhodamine phalloidin (10 Units/ml, Molecular Probes) diluted in PBS or slow muscle myosin (Table 2.1) antibody, counterstained with DAPI and placed on a glass slide. For 3D imaging of scaffolds, 15-25 z-stack images (either 5 µm or 10 µm stack) were taken using a Nikon A1+ confocal microscope (Nikon, Tokyo, Japan) and merged to generate a single image. For each scaffold, six images were captured at different locations and representative images are shown.

For myosin immunostaining and imaging large areas of the silk scaffold, 50 z-stack images (2.5 µm stack) were taken using an UltraVIEW VoX Spinning Disc Confocal Microscope (PerkinElmer) and the images were stitched together using the Volocity software (PerkinElmer). The length of the myotubes was measured using the line tool measurement.

2.13.3 Scanning Electron Microscopy of 3D silk scaffolds (+/- HSMM cells)

All four 3D silk scaffolds (with or without HSMM cells) were fixed in 4 % PFA for 30 min at RT and then dehydrated in ethanol solutions of increasing concentration (30 % - 100 %) for 20 min per concentration, freeze dried using a ScanVac (LaboGene, Lynge, Denmark), mounted on aluminium stubs and sputter coated with platinum (10 nm) using a 208HR sputter coater (Cressington, Redding, CA). Data were collected using either a Neon 40EsB Scanning Electron Microscope (Carl Zeiss) or MIRA SEM (TESCAN, Brno, Czech Republic). Sample coating and imaging was performed with the assistance of technical staff at the Curtin Electron Microscope Facility.

2.13.4 Gene expression analysis of 3D cultures

For gene expression analysis, HSMMs were seeded on *B. mori* and *A. mylitta* scaffolds at a cell concentration (5×10^5 cells/scaffold), cultured for either 4 or 7 days in proliferation medium and 4 or 10 days in differentiation medium, with cells harvested at day 4 of proliferation, day 2 and day 10 of differentiation.

2.13.4.1 RNA extraction

RNA was isolated using TRI Reagent (Sigma-Aldrich), as per the manufacturer's instructions, as the protein content of the silk scaffold meant the spin column extraction method used in 2D culture was unsuitable. Briefly, the media was discarded and the silk scaffolds were placed in a 2 ml eppendorf tube. The scaffolds were then homogenized in 1.5 ml of TRIzol reagent by repeated pipetting and incubated at -80ºC overnight. The next day, the samples were thawed at RT for 15 min and 0.3 ml of chloroform was added to each tube, before vortexing for 10 sec and incubating at RT for 5 min. Tubes were then centrifuged at 12, 000 g for 20 min to separate the lower phenol-chloroform phase from the upper aqueous phase. The aqueous phase was transferred to a new tube, 0.75 ml of 100% isopropanol was added, and the mixture was incubated for 15 min at RT. Tubes were then centrifuged at 12,000 g for 10 min, the supernatant was removed and the RNA pellet was washed with 1 ml of 75 % ethanol. Samples were vortexed briefly, centrifuged at 12,000 g for 5 min, the supernatant removed and the pellet was air dried for 10 min at RT. The RNA pellet was resuspended in 40 µl-60 µl of RNase free water and incubated at 55 ºC for 15 min. RNA concentration and purity was assessed using a Nanodrop spectrophotometer. All RNA samples had an A260/A280 ratio of > 1.8

2.13.4.2 cDNA synthesis and qRT-PCR analysis

cDNA synthesis was performed as described in section 2.12.3. Expression levels for *MyoD1, Myf5, MYH1, MYH7, and ACTA1* were normalized to *TBP* expression values and fold change determined using $2^{-\text{delta delta Ct}}$ method with baseline expression either at day 4 of proliferation or day 2 of differentiation. Mean ± SE of 4 replicates are shown.

2.14 Statistical analysis

Data were collected with 3-4 independent replicates per data point from 2 representative experiments and represented as mean ± standard deviation (SD). Analysis for cell proliferation experiments were performed using one-way analysis of variance (ANOVA) followed by Tukey's post-hoc test with SPSS statistics software v22.0 (IBM corporation, NY). P-value ($p<0.05$) was considered statistically significant. For qPCR data analysis,

Wilcoxon's signed-rank test was performed and significance (P) values shown at each time point with *P<0.05.

Chapter 3:

Development and characterization of an acellular skeletal muscle matrix with well-preserved extracellular matrix (ECM) components

3.1 Introduction

The ECM is the non-cellular material surrounding cells in tissues. It provides both a structural scaffold and biochemical cues for tissue morphogenesis. It comprises of a dense meshwork of interacting molecules including structural proteins like collagen and elastin, glycoproteins like fibronectin, vitronectin and laminin; proteoglycans such as biglycan, decorin and tenascin, and signalling molecules, like cytokines and growth factors. To obtain a three-dimensional ECM suitable for either implantation as a bio-scaffold or to study cell-matrix interactions in a laboratory, removal of all cellular components from the tissue is necessary so that only the ECM remains. Decellularization (removal of cells) is a promising and relatively new technique to obtain ECM from tissues. The efficiency of decellularization depends upon the origin of the tissue, its thickness, lipid content, density and the methods (physical, chemical or enzymatic) that are used to remove the cells [166]. Preferably, the method should not adversely affect the composition, biological activity and mechanical integrity of the remaining matrix while effectively removing DNA and cellular remnants. It should be understood that complete decellularization of a tissue or organ is not feasible, therefore the emphasis is on maximising the loss of cells from the tissue and minimizing the damage to the ECM, so the ECM remains as close to its native structure and composition as possible.

Perfusion of organs/tissues with decellularizing agents is a commonly used technique to remove the majority of immunogenic cellular and nuclear material and to obtain bio-scaffolds with well-preserved ECM components. Perfusion of the decellularizing fluid through relevant vasculature, for example: pulmonary artery and trachea in lung [193] and portal vein in liver [243], enables cellular components of the tissue to be removed relatively quickly (within a few hours) leading to an isolated matrix bio-scaffold. In addition, tracks previously occupied by the vasculature of the organs/tissues are also well preserved, which has further implications in revascularization of the scaffold when used for implantation *in vivo*. However, obtaining a skeletal muscle matrix in the form of a whole organ is difficult due to the presence of long muscle fibres and the complexity of the muscle connective tissue. A possible solution is to decellularize

skeletal muscle by cutting small pieces of muscle and immersing in decellularizing agents to increase the surface area of tissue interacting with buffers.

Muscle ECM prepared by decellularizing skeletal muscle can be used to study the role of ECM in muscle formation. This ECM can be used as a three-dimensional bio-scaffold or it may be lyophilized and solubilized to use as a coating on coverslips to test the ability of the matrix to support cell growth and formation of muscle fibres *in vitro*. A variety of published protocols have been used to decellularize skeletal muscle to obtain a functionalized ECM scaffold [174-176]. Generally these protocols have incorporated enzymes like trypsin [175] and strong detergents like SDS [174]. Recently, a method for decellularizing skeletal muscle without detergents or proteolytic enzymes was described [176], and using this method although there was a slight reduction in the GAG content of the matrix other ECM components remained intact. These published studies measured the sulfated GAGs in the matrix but, to our knowledge, none have investigated which ECM proteoglycans (decorin, biglycan, perlecan) are retained after decellularization.

The aim of the study described in this chapter is the development of a method to obtain a three dimensional muscle scaffold with well-preserved ECM components which can be utilized in subsequent studies (next chapter) to understand the role of the ECM proteins in regulating muscle myoblast behaviour. Described here is the development of a method to effectively remove the cells from muscle ECM and characterization of the ECM components remaining after decellularisation. Three methods (Trypsin, SDS and Phospholipase A_2) were compared with respect to efficacy of decellularization and retention of matrix proteins.

3.2 Results

3.2.1 Trypsin method

The trypsin method was initially attempted using triceps muscles harvested from 3 months old Duchenne muscular dystrophic (mdx) female mice. These mice have a point mutation in the dystrophin gene, which causes the gene to stop synthesis of dystrophin.

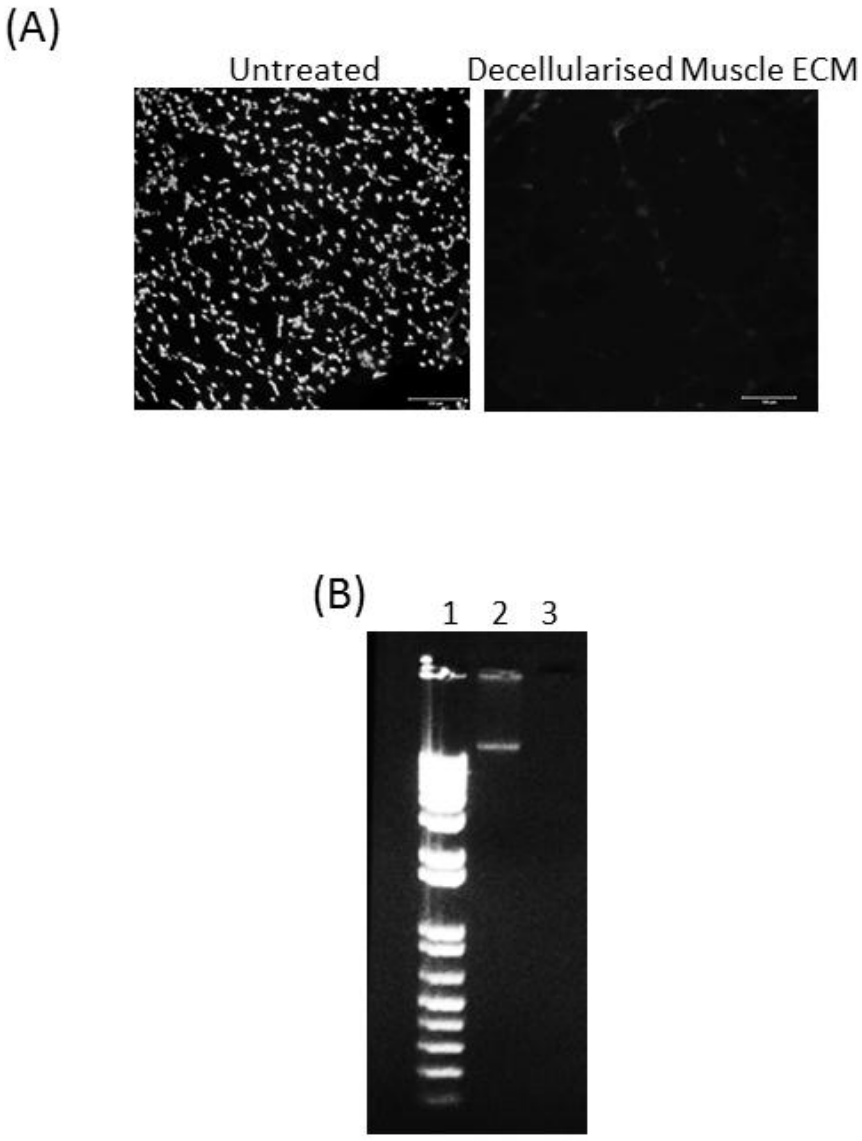

Figure 3.1 Qualitative and quantitative analysis of cellular material after trypsin decellularisation from quadriceps muscle sections of 3 month old female C57 black mice. (A) DAPI staining in untreated and decellularised muscle sections treated with trypsin. Scale bar-100μm. (B) Gel showing DNA isolated from equal quantities (40 sections) of untreated muscle and muscle decellularised using trypsin. Genomic DNA was separated on a 1.5% agarose gel. Lane 1= 1 kb plus DNA ladder; Lane 2= Untreated muscle; Lane 3= decellularised muscle.

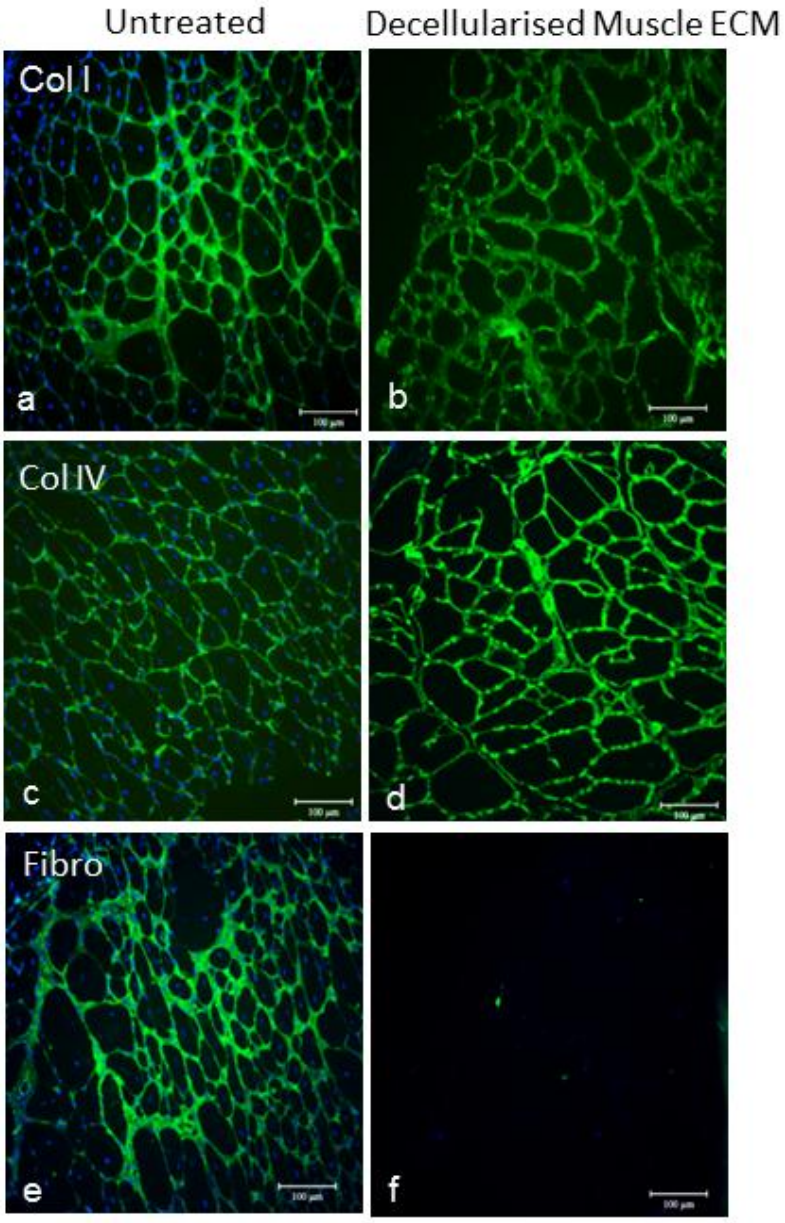

Figure 3.2 Immunofluorescence labeling of untreated and trypsin decellularised triceps muscle sections of 3 month old female mdx mice. Sections were fixed and stained with antibodies against structural and basement membrane components of ECM collagen I (a, b), collagen IV (c, d) and fibronectin (e, f). The antibodies recognising collagen I, collagen IV or fibronectin were all rabbit polyclonal antibodies. The secondary antibody was a goat anti-rabbit FITC conjugated antibody. Nuclei are stained with DAPI (blue). Scale bar-100µm.

As a result, in early stages of their life, these mice exhibit muscle degeneration followed by regeneration and fibrosis as they age. The archival tissue was provided by Prof. Miranda Grounds, School of Anatomy, Physiology and Human Biology, University of Western Australia. Briefly, triceps muscle sections from mdx mice and quadriceps muscle sections from C57/black mice were treated with trypsin and Triton-X 100 and washed with PBS to decellularize the muscle tissue (see detailed method in section 2.2.2.1).

3.2.1.1 DNA remaining after decellularization

A dye, DAPI which stains DNA and RNA was used to assess the loss of cells from the muscle tissue. The trypsin method of decellularization was effective in complete removal of cells as indicated by the loss of DAPI staining in the decellularized tissue when compared to normal muscle samples (Figure 3.1 A). Decellularization was further confirmed by quantitative analysis of the DNA extracted from native and decelluralized muscle sections (see methods in section 2.4.3). The DNA extracted from a total of 40 native and decellularized sections was pooled in 40 µl of TE buffer and the concentration of DNA was determined using a spectrophotometer. Quantitative analysis of the DNA content show that the amount of DNA was reduced from 120.2 ng/µl in native muscle to 46.0 ng/µl after decellularization (62% decrease). When run on a 1.5% agarose gel (section 2.4.2), native muscle DNA showed a clear band of genomic DNA while there was nothing visible in the lane where DNA from decellularized sections was loaded, suggesting that any DNA present was degraded (Figure 3.1 B).

3.2.1.2 Retention of matrix proteins after decellularization

Immunohistochemistry was used to determine the ECM molecules remaining following decellularisation (see methods in section 2.5.2). Stronger staining of the collagen type I and collagen type IV antibodies was apparent in the decellularized matrices (Figure 3.2 b, d) compared to the normal muscle samples (Figure 3.2 a, c). The epitopes recognised by the anti-fibronectin antibody were completely lost in the decellularized matrix suggesting that trypsin treatment was removing/degrading fibronectin in the matrix

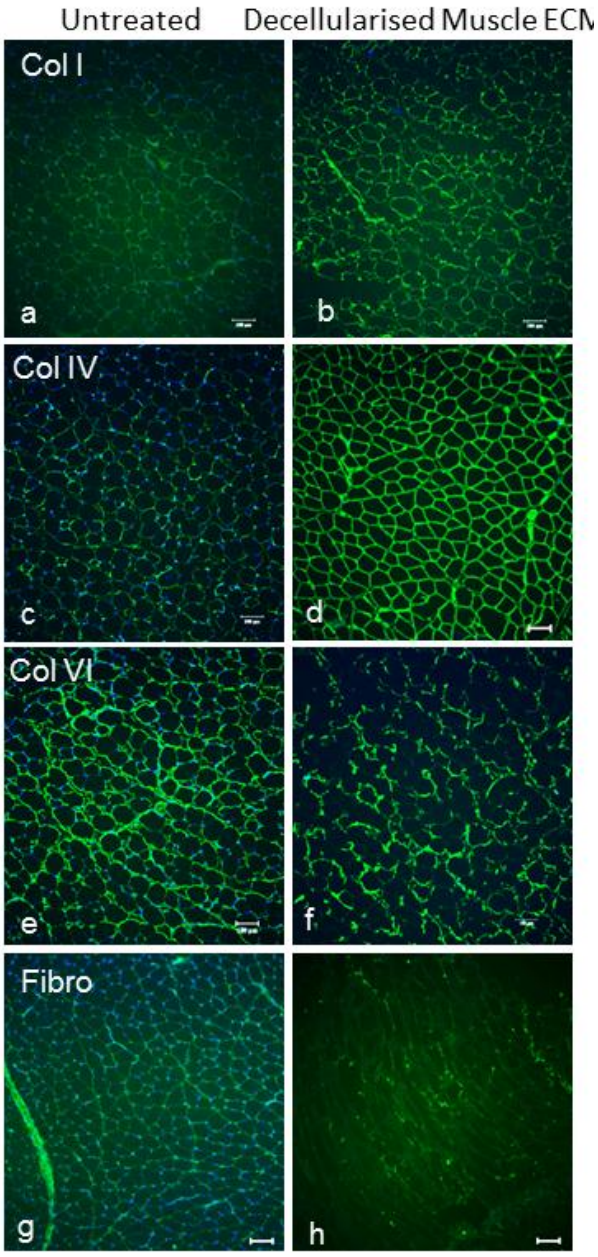

Figure 3.3 Immunofluorescence labeling of untreated and trypsin decellularised quadriceps muscle sections of 3 month old female C57 black mice. Sections were fixed and stained with antibodies against structural and basement membrane components of ECM collagen I (a, b), collagen IV (c, d), Collagen VI (e, f) and fibronectin (g, h). The antibodies recognising Collagen I, Collagen IV, Collagen VI and Fibronectin were all rabbit polyclonal antibodies. The secondary antibody was a goat anti-rabbit alexa fluor 488 conjugated antibody. Nuclei are stained with DAPI (blue). Scale bar-100µm.

(Figure 3.2 f). These experiments were repeated using quadriceps muscle harvested from 3 month old C57/black female mice. Immunohistochemistry similarly showed epitopes for collagens type I, IV and VI were preserved in the decellularised muscle matrix but fibronectin epitopes were lost (Figure 3.3). Since, fibronectin appeared to be lost during trypsin decellularization and the goal was to preserve most of the matrix components in the decellularised matrix including the glycoproteins, the SDS method was tried.

3.2.2 SDS method

In brief, triceps muscle sections from mdx mice and quadriceps muscle sections from C57/black mice were decellularised using a combination of SDS/EDTA and then washed in a solution of NaCl (2M) before finally washing with PBS (see methods in section 2.2.2.2).

3.2.2.1 DNA remaining after decellularization

As DAPI staining showed traces of DNA in the decellularized sections (Figure 3.4 A) it appeared the 0.2 % SDS method was not effective in completely removing all cellular components. DNA was extracted from the decellularized sections and resuspended in 40 µl of TE buffer (see methods in section 2.4.3). Quantitative analysis of the DNA content showed that the amount of DNA was reduced from 106.2 ng/µl in native muscle to 56.0 ng/µl after decellularization. Although, there was a decrease (48%) in the amount of DNA remaining in the decellularised tissue, when run on a 1.5 % agarose gel, a clear band of genomic DNA can be seen in both control and decellularised tissue lanes (Figure 3.4 B).

3.2.2.2 Retention of matrix proteins after decellularization

Results from immunostaining experiments showed that collagens type I, IV and VI appeared to be staining more strongly in the decellularized sections (Figure 3.5 b, d, f) than in the normal muscle sections (Figure 3.5 a, c, e). The glycoprotein, fibronectin was also well preserved in both the normal (Figure 3.5 g) and decellularized muscle matrix (Figure 3.5 h). Epitopes on the heparan sulphate proteoglycan, perlecan were preserved

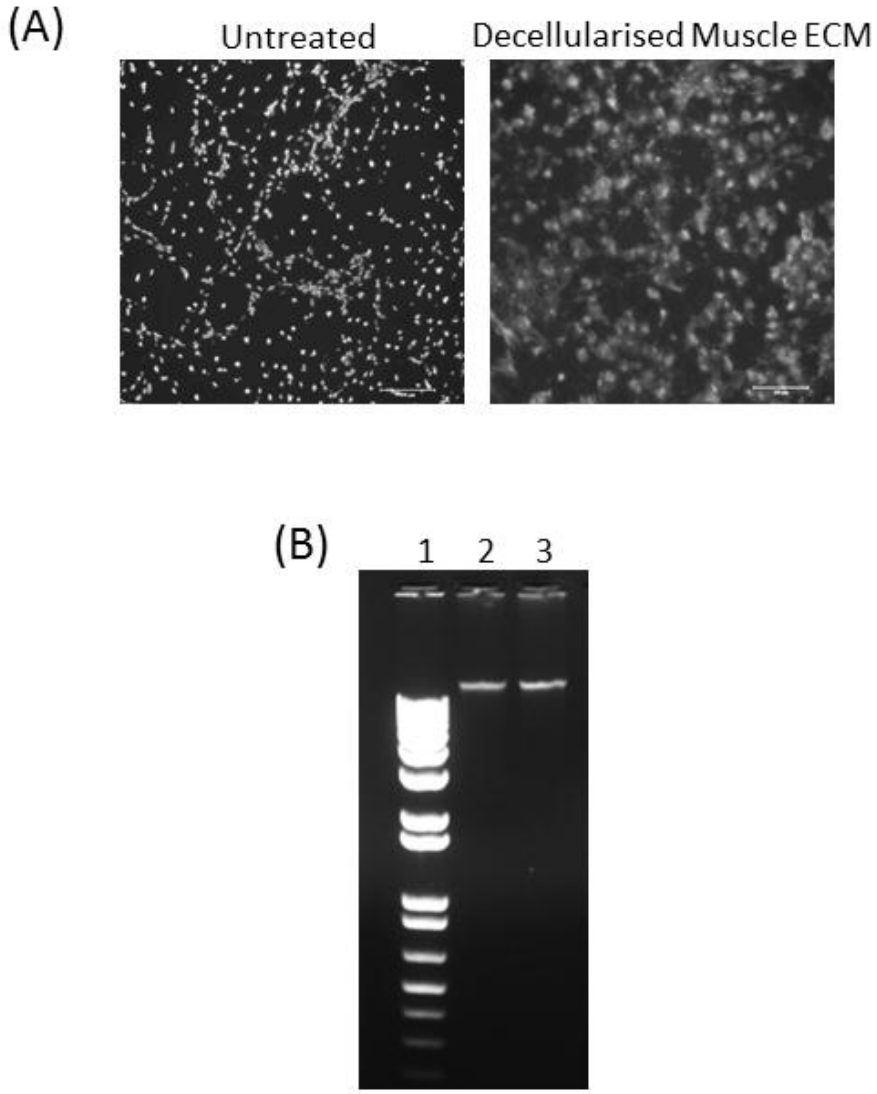

Figure 3.4. Qualitative and quantitative analysis of cellular material after SDS decellularisation from quadricpes muscle of 3 month old female C57 black mice. (A) DAPI staining in untreated and decellularised muscle sections treated with 0.2% SDS. Scale bar-100µm. (B) Gels showing DNA isolated from equal quantities (40 sections) of untreated muscle and muscle decellularised using SDS. Genomic DNA was separated on a 1.5% agarose gel. Lane 1= 1 kb plus DNA ladder; Lane 2= Untreated muscle; Lane 3= decellularised muscle.

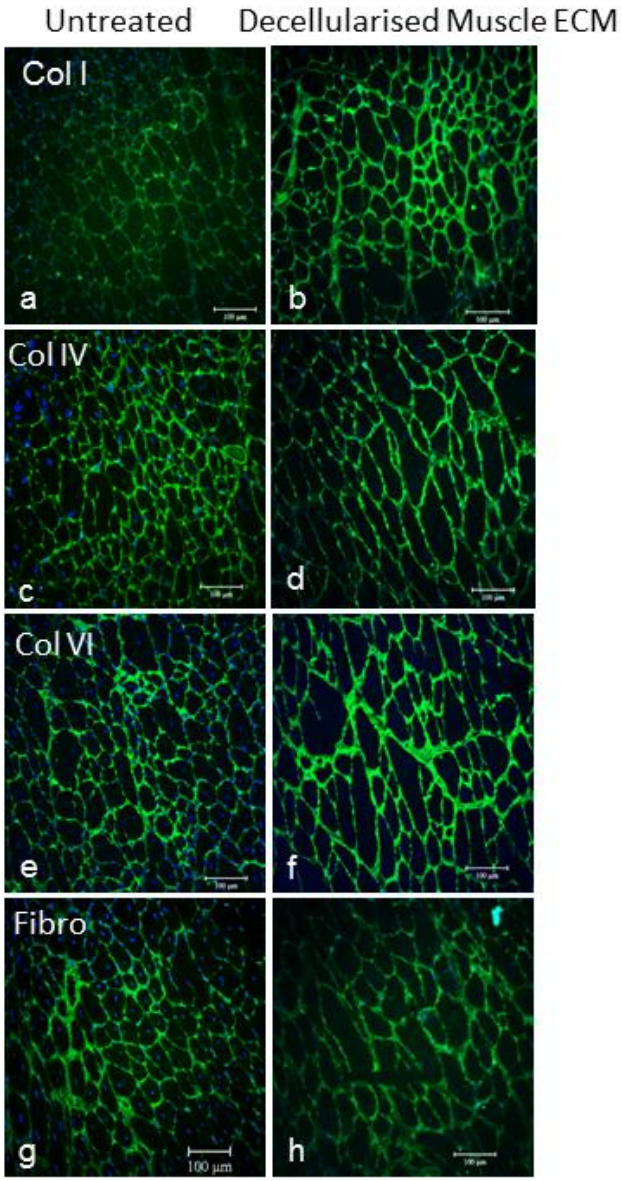

Figure 3.5 Immunofluorescence labeling of untreated and SDS decellularised triceps muscle sections of 3 month old female mdx mice. Muscle sections were fixed and stained with antibodies against structural and basement membrane components collagen I (a, b), collagen IV (c, d), Collagen VI (e, f) and fibronectin (g, h). The antibodies recognising Collagen I, Collagen IV, collagen VI and Fibronectin were all rabbit polyclonal antibodies. The secondary antibody was a goat anti-rabbit FITC conjugated antibody. Nuclei are stained with DAPI (blue). Scale bar-100µm.

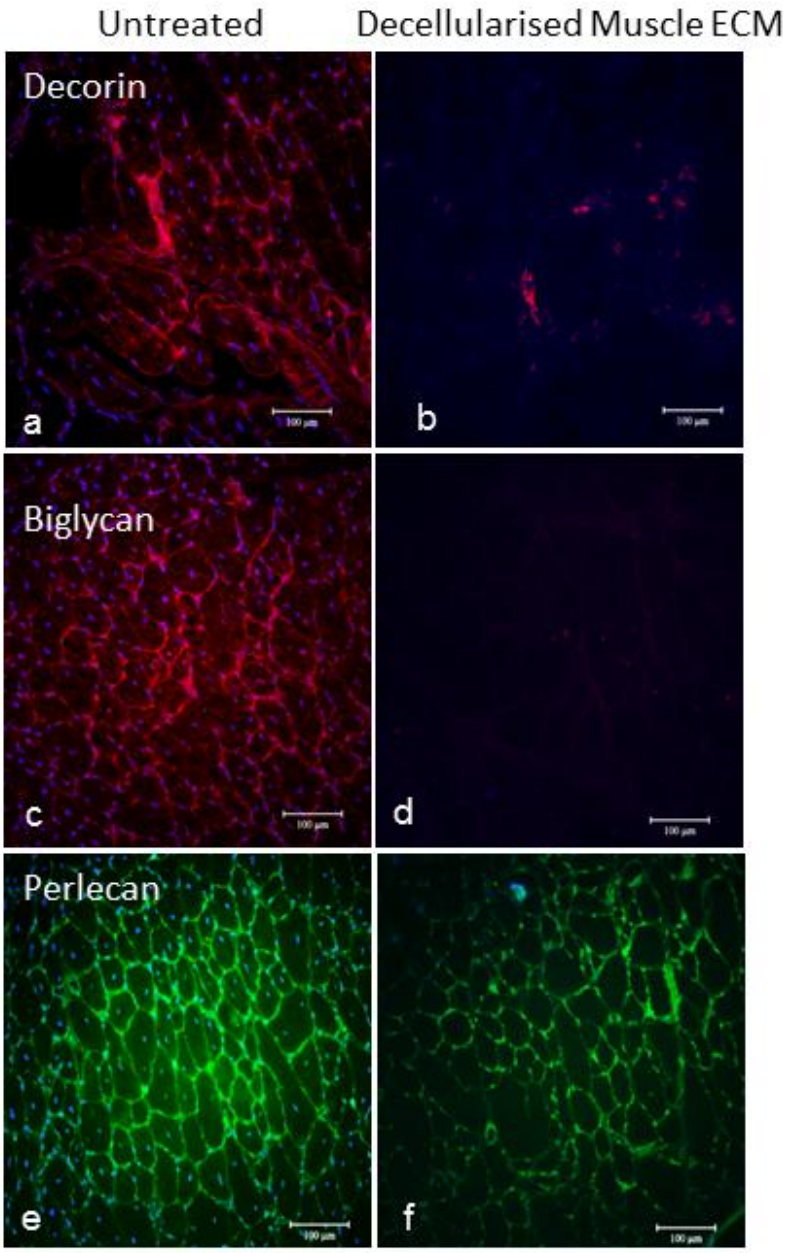

Figure 3.6. Immunofluorescence labeling of untreated and SDS decellularised triceps muscle sections of 3 month old female mdx mice. Muscle sections were fixed and stained with antibodies against proteoglycan components of ECM: decorin (a, b), biglycan (c, d) and perlecan (e, f). The antibodies recognising decorin, biglycan and perlecan were sheep, goat and rabbit polyclonal antibodies respectively. Secondary antibodies were: Dylight 549-conjugated donkey anti-sheep antibody (a, b); Dylight 549 conjugated anti-goat IgG antibody (c, d), and goat anti-rabbit FITC conjugated antibody (e, f). Nuclei are stained with DAPI (blue). Scale bar-100μm.

in the decellularized matrix as is evident from the comparable levels of immunostaining in decellularised and control sections (Figure 3.6 e-f), but immunostaining of small leucine rich proteoglycans, decorin and biglycan in the decellularized sections (Fig 3.6 b, d) was markedly less compared to the controls (Figure 3.6 a, c).

3.2.3 Phospholipase method

Briefly, gastrocnemius and quadriceps muscle sections from C57/black mice were decellularized using combination of an enzyme (Phospholipase A_2) and a detergent sodium deoxycholate (see methods section 2.2.2.3).

3.2.3.1 DNA remaining after decellularization

DAPI staining revealed a loss of punctate nuclei in the treated muscle (Figure 3.7 A). Decellularization was further confirmed by a quantitative analysis of the DNA extracted from native and decellularized sections (see methods in section 2.4.3). Quantitative analyses showed that the amount of DNA was reduced from 161.35 ng/µl in native muscle to 39.35 ng/µl after decellularization (76.6 % decrease). When run on a 1.5% agarose gel, DNA extracted from native muscle gave a clear band of genomic DNA, while nothing was visible in the lane where DNA extracted from decellularized sections was loaded (Figure 3.7 B). DNA was also extracted from untreated and decellularized pieces of quadriceps muscle (of equal weights before treatment) from C57/black mice. The amount of DNA were quantified spectrophotometrically and normalized to the wet weight of muscle (before and after treatment). Quantitative analysis revealed an 81.0 % loss after decellularisation (Figure 3.7 C). Further, the PLA_2 method was also used to decellularise gastrocnemius muscle from C57/black mice and DNA quantification results showed a 87.7 % decrease in the amount of DNA after decellularisation (data not shown).

3.2.3.2 Loss of cytoskeletal proteins following decellularization

Since, there was a greater reduction in the amount of DNA remaining after decellularisation with the PLA_2 method compared to that seen following the trypsin and

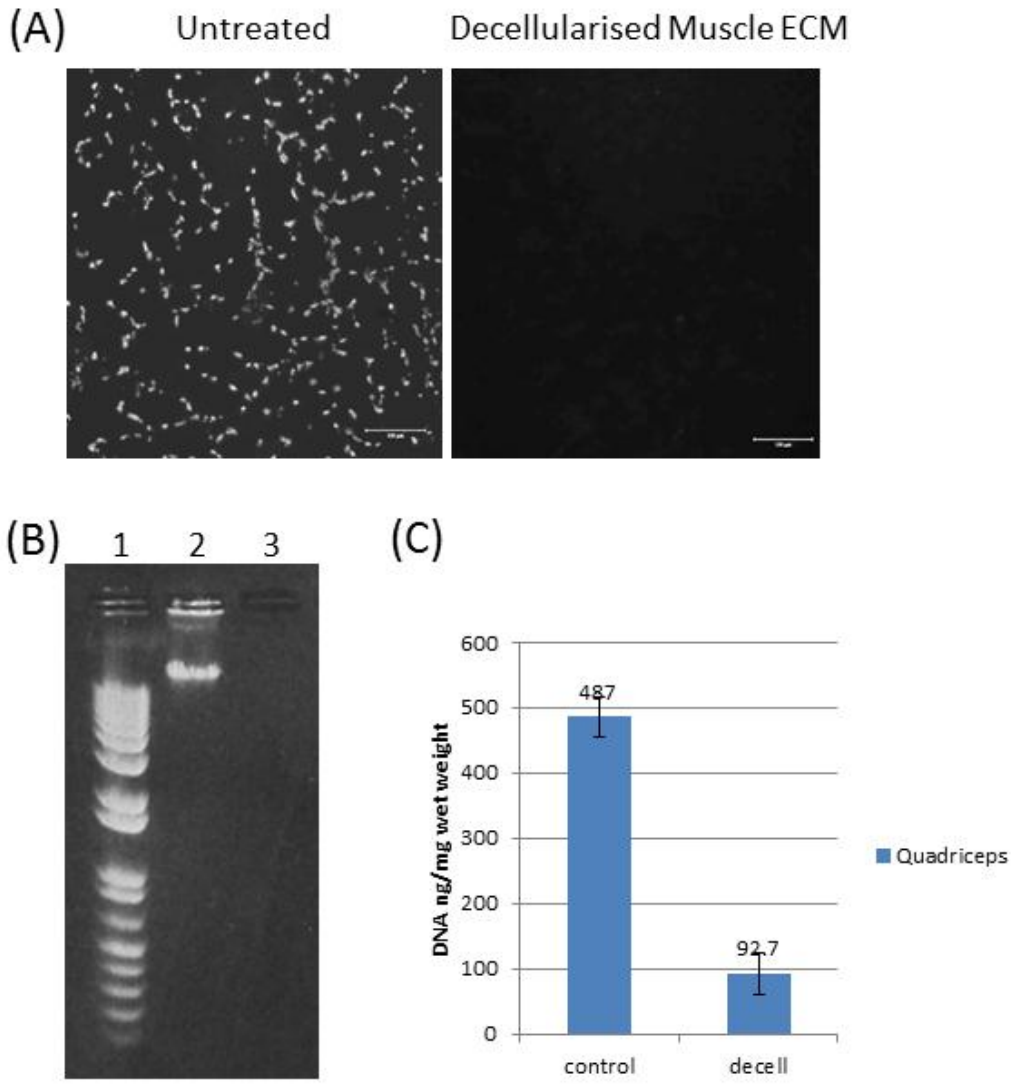

Figure 3.7. Qualitative and quantitative analysis of cellular material after PLA_2 decellularised quadriceps muscle sections of 3 month old C57 black mice. (A) DAPI staining in untreated and decellularised muscle sections treated with PLA_2. Scale bar-100μm. (B) Gels showing DNA isolated from equal quantities of untreated muscle and muscle decellularised using PLA_2. Genomic DNA was separated on a 1.5% agarose gel. Lane 1= 1 kb plus DNA ladder; Lane 2= Untreated muscle; Lane 3= decellularised muscle. (C) Quantification of DNA present in the muscle before and after decellularisation. Mean values are shown.

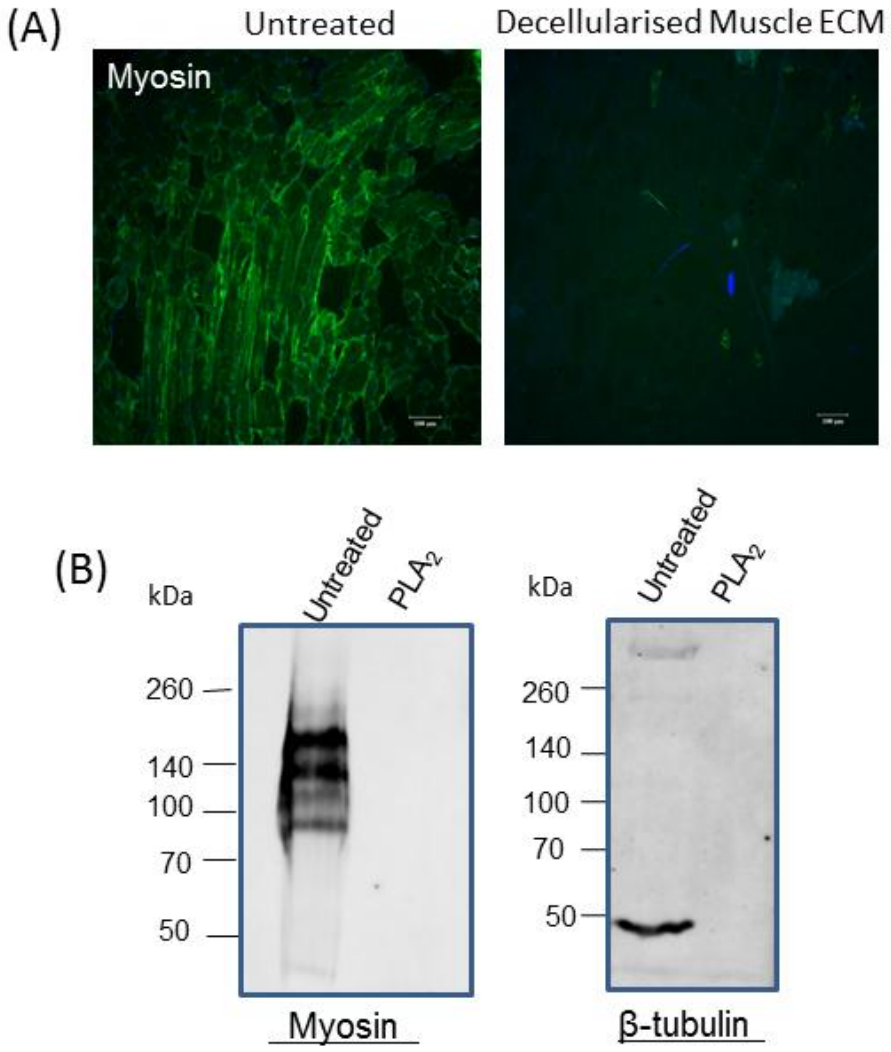

Figure 3.8 Loss of cytoskeletal proteins after PLA_2 decellularisation. A. Immunofluorescence labelling of untreated and PLA_2 decellularised muscle sections for myosin (slow muscle). B Untreated and PLA_2 -treated muscle extracts were solubilized in urea buffer and equal amounts of protein were separated by SDS-PAGE and Western blot analysis was performed using antibodies against the intracellular proteins myosin and β-tubulin. Anti-myosin (NOQ7.5.4D) and anti-β-tubulin were mouse monoclonal and rabbit polyclonal antibodies respectively. The conjugated secondary antibodies: IHC, a goat anti-mouse alexa fluor 488 antibody, Western blots, a goat anti-mouse HRP antibody and a goat anti-rabbit HRP antibody were used for myosin and β-tubulin antibody detection respectively.

SDS treatments, the ECM from the PLA_2 method was chosen for further analysis. Immunohistochemistry showed loss of myosin (a crucial contractive protein in muscle) staining from the decellularized sections (Figure 3.8 A). Western blotting (section 2.3.6) was used to confirm the loss of cytoskeletal components and intracellular proteins from the decellularised matrix. Protein extracts from untreated and PLA_2 decellularised muscles were solubilized in RIPA buffer and equal amounts of protein were separated on a 7.5% SDS PAGE, blotted and probed for myosin and β-tubulin. Western blots for myosin revealed two distinct bands at 220 kDa and 140 kDa in the control lane containing extracts of untreated muscle while no band can be seen in the lane containing extracts from the decellularised tissue, indicating that myosin had been removed from the decellularised muscle. Similar results were obtained when the blots were probed with an antibody recognising β-tubulin; no band was visible at the 50 kDa mark in the lane containing the decellularised extract whereas this band was evident in the control tissue lane (Figure 3.8 B).

3.2.3.3 Retention of matrix proteins after decellularization

Imunofluroescence experiments revealed the major structural proteins of the matrix, collagen type I and collagen type III, were well preserved in the endomysium around each muscle fibre with possibly an increase in the intensity of collagen type III staining in the interstitial connective tissue after decellularization (Figure 3.9 b, d). Positive staining for the basement membrane components, collagen type IV, collagen type VI, laminin α2 and fibronectin was also observed in the acellular ECM prepared using PLA_2 (Figure 3.9 f, h, j, l). The muscle cross-sections maintained their polyhedral tubular organization even after decellularization indicating that the overall structure of the ECM was preserved. Although the immunofluorescent staining of the proteoglycans decorin and perlecan was less strong than that of the collagens a similar level of signal was seen in the decellularized sections as in the untreated control sections indicating these molecules were preserved in the matrix (Figure 3.10 a-d). EV3C3 is mAb that recognises a GAG epitope on heparan sulphate chains and positive staining with this antibody revealed this epitope was also intact after decellularization with a signal comparable to that seen with control muscle matrix (Figure 3.10 e-f). In one or more of

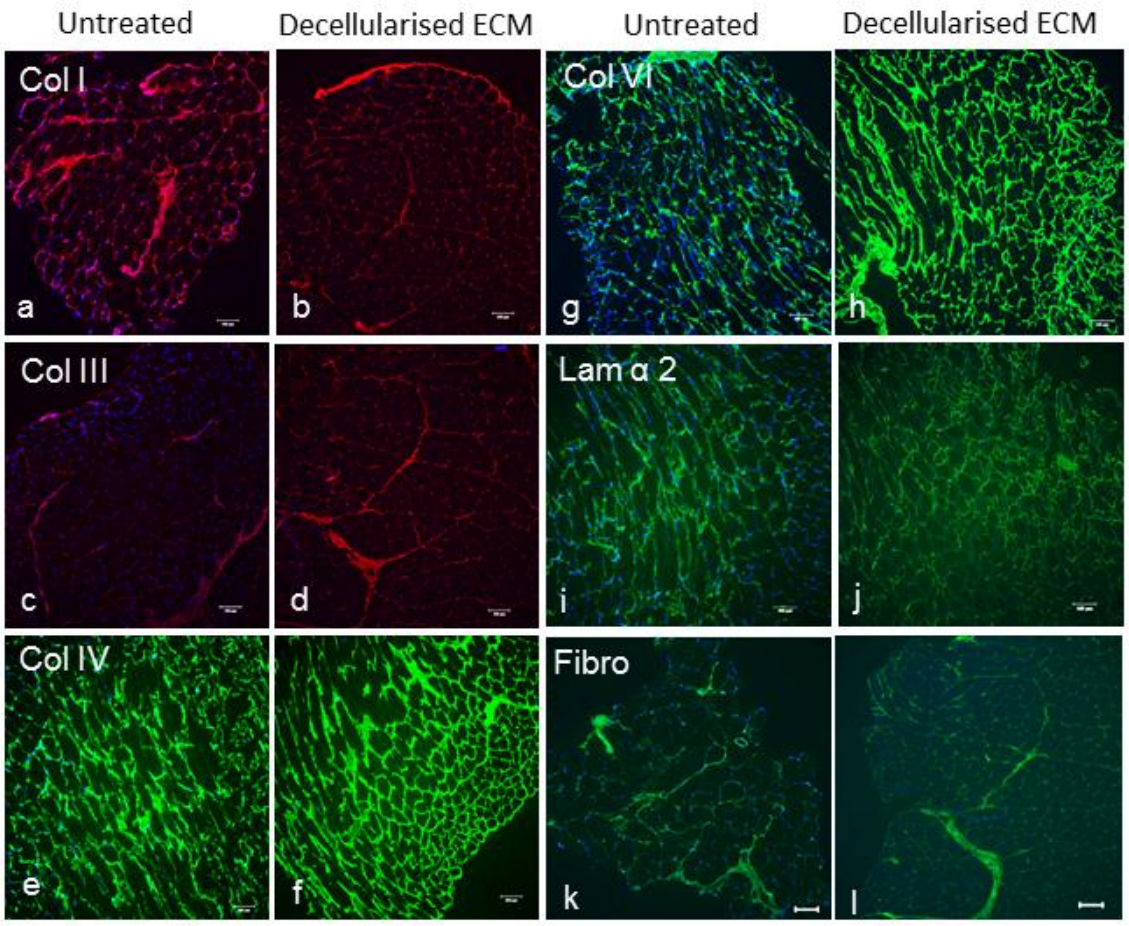

Figure 3.9. Immunofluorescence labelling of untreated and PLA_2 decellularised quadriceps muscle sections of 3 month old C57 black mice. Sections were fixed and stained with antibodies against structural and basement membrane components of ECM: collagen I (a, b), collagen III (c, d), collagen IV (e, f) collagen VI (g, h), laminin α2 (i, j) and fibronectin (k, l). The antibodies recognising all the ECM components except the laminin chain were rabbit polyclonal antibodies. The anti-laminin-α2 (4H8-2) was a rat monoclonal antibody. Secondary antibodies were: goat anti-rabbit FITC conjugated antibody (e, f, g, h, k and l); a goat anti-rabbit Alexa fluor 546 conjugated antibody (a, b, c, d), and a goat anti-rat-IgG FITC conjugated antibody (I, j). Nuclei are stained with DAPI (blue). Scale bars- 100μm

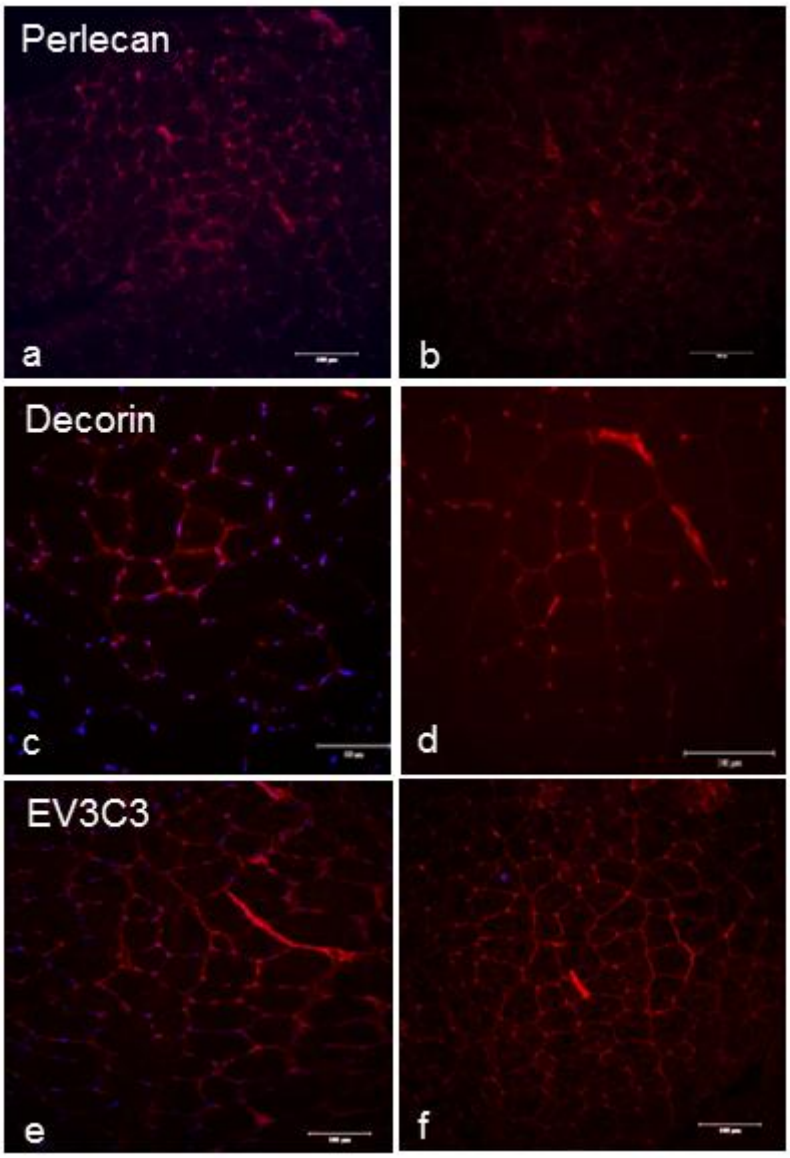

Figure 3.10. Immunofluorescence labelling of untreated (a, c, d) and PLA_2 decellularised (b ,d ,f) quadriceps muscle sections of 3 month old C57 black mice. Sections were fixed and stained with antibodies against the proteoglycan perlecan (a, b), decorin (c, d) and a GAG epitope, EV3C3 (e, f). Perlecan and Decorin were rabbit and sheep polyclonal antibodies respectively and EV3C3 was a phage display mouse monoclonal antibody. Secondary antibodies used were: Dylight 549-conjugated donkey anti-sheep (c, d), and goat anti-rabbit TRITC (a, b). Rabbit Anti-VSV-G and goat anti-rabbit TRITC antibodies were used for EV3C3 (e, f). Nuclei are stained with DAPI (blue). Scale bars: 100 μm for a-d, 50 μm for e-f.

the other decellularization methods decorin, fibronectin and collagen VI stained less intensely than in the untreated control sections. This was not the case following the PLA_2 decellularization procedure and for this reason this decellularization method was adopted for the rest of the study.

3.2.4 Analyses of solubilised acellular muscle matrix

The solubilisation of ECM is problematical as a majority of the proteins exist in cross-linked or aggregated forms [244]. Accordingly, three different solubilisation buffers were tested: RIPA, Urea and 0.1M acetic acid (section 2.2.4). Initially, untreated muscle was solubilized in RIPA buffer either for 4h or O/N at 4ºC and the solubilized proteins (20 µg) were resolved on 7.5% SDS-PAGE (section 2.3.3) and stained with Coomassie Brilliant Blue (section 2.3.4). RIPA buffer solubilized the muscle proteins and a protein concentration of 6.0 mg/ml was obtained from 40 mgs of muscle tissue (wet weight). However the SDS-PAGE analysis revealed only a few clearly resolved bands and the majority of the proteins appeared as unresolved smears (Figure 3.11).

Untreated muscle and decellularised muscle matrix were solubilized in Urea buffer in an attempt to obtain proteins that could be better resolved on SDS-PAGE. The tissue was placed in Urea buffer for either for 4h or O/N at 4ºC. Since urea interferes in the BCA assay, a non-interfering (NI) protein assay (section 2.3.2.2) was used to measure the concentration of the solubilized proteins. This assay indicated that UREA buffer was able to better solubilize the native muscle than the RIPA buffer with concentrations of 8-9 mg/ml being regularly obtained. However, as occurred with the RIPA solubilized muscle samples when 20 µg of protein from untreated muscle was run on 7.5 % SDS-PAGE Coomassie Brilliant Blue staining revealed that most of the proteins were not resolved and appeared as smears and this was the case regardless as to whether the extraction time was 4h or overnight. In contrast, proteins (8.0 µg) extracted from PLA_2 decellularized muscle resolved as a small number of bands of around 260 kDa plus some faint bands of a higher molecular weight (Figure 3.11).

Finally, muscle tissue from both untreated and PLA_2 treated muscle was solubilized in 0.1M acetic acid buffer containing 20mM EDTA for 7 days at 4ºC. The extraction time

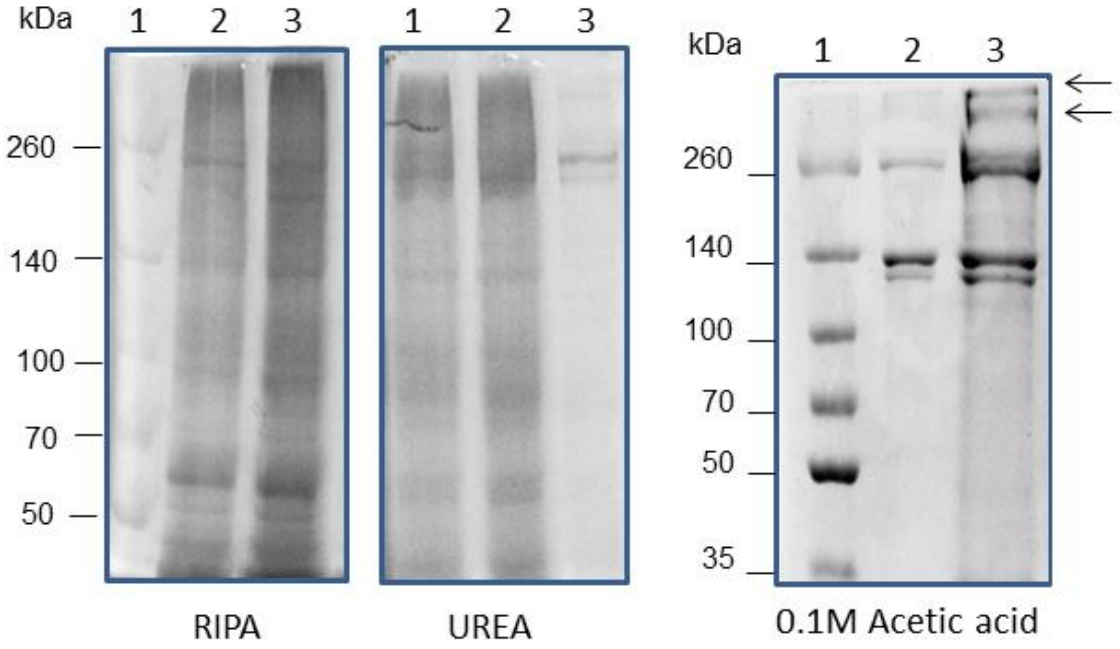

Figure 3.11 Muscle proteins and decellularised ECM solubilisation using different buffers. Whole muscles and PLA_2 decellularised ECM proteins were solubilised in RIPA, UREA and 0.1M acetic acid buffers and resolved on a 7.5 % SDS-PAGE and visualized by Coomassie Brilliant Blue staining. RIPA Lane1: Marker; Lane 2: untreated muscle solubilised for 4h; Lane 3: untreated muscle solubilised O/N. UREA Lane1: untreated muscle solubilised for 4h; Lane 2: untreated muscle solubilised for O/N; Lane 3: PLA_2 decellularised matrix solubilised for O/N. Acetic acid Lane1: Marker; Lane 2: Collagen I standard; Lane 3: PLA_2 decellularised matrix. Arrows show high molecular weight bands.

was determined by measuring the protein concentration after solubilizing the muscle tissue for 1, 3, 5 and 7 days in 0.1M acetic acid and measuring the protein concentration using a BCA assay (section 2.3.2.1) (Table 3.1). After 7 days of solubilisation in 0.1M acetic acid the protein concentration of muscle extracts reached a maximum of 0.7 mg/ml for decellularized tissue and 4.0 mg/ml for intact tissue. The proteins solubilized from PLA_2 decellularised ECM resolved on 7.5% SDS-PAGE as two bands at approximately 260 kDa, two bands at around 140 kDa and additional high molecular weight bands at >260 kDa). A comparison of the banding pattern of this extract with that of the same concentration of a collagen I standard, run on the same gel, revealed a very similar banding pattern, that is the collagen I standard also gave rise to bands around 260 and 140 kDa (Figure 3.11). The absence of low molecular weight proteins showed that decellularised ECM extract has lost most of the cytoplasmic proteins.

Table 3.1. Solubilised muscle ECM protein yield at different time points

No. of days in solubilisation buffer	Absorbance at 560 nm	Concentration (mg/ml)
1	0.152	0.15
3	0.184	0.24
5	0.313	0.5
7	0.456	0.7

3.2.5 Western blots for PLA_2 method

Extracts from untreated and PLA_2 decellularized muscles solubilized using 0.1M acetic acid were analysed using Western blotting (section 2.3.6) to assess the extent of preservation of collagen I, collagen VI, laminin α2, perlecan and fibronectin. Two distinct bands were evident on the collagen I blot, one at ~140 kDa which is probably the α1 chain, and a possible trimer above 260kDa. Staining with the antibody

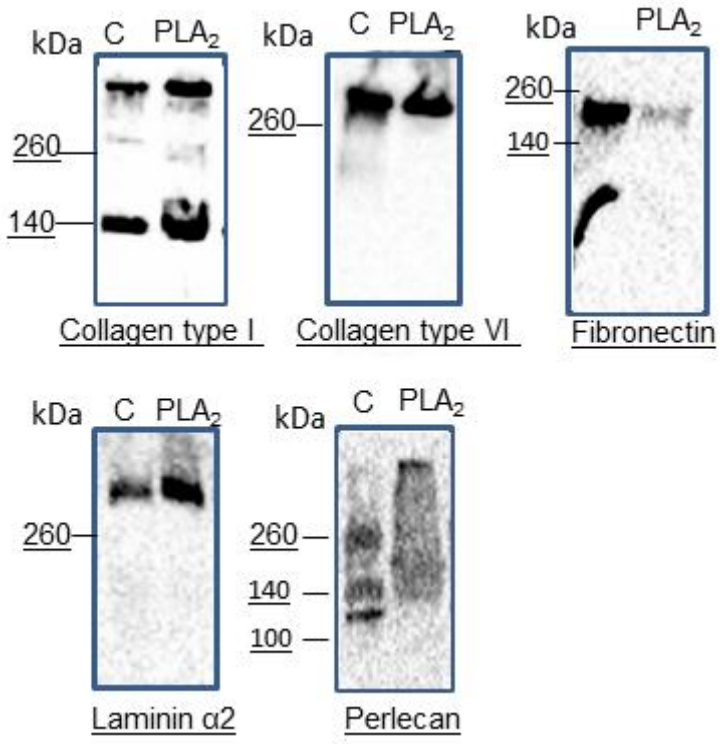

Figure 3.12. Western blot analysis of PLA_2 decellularised matrix. Untreated and PLA_2 treated muscle extracts were prepared by solubilising the ECM proteins in 0.1M acetic acid. Protein (40 µg) was loaded in both (untreated and PLA_2) lanes and resolved on 4-15% Mini-PROTEAN TGX gradient gels. Proteins were transferred to a PVDF membrane (Immobilon-P) and Western blot analysis was performed using antibodies recognising collagen I, collagen VI, fibronectin, laminin α2 and perlecan. The anti-collagen I, anti-collagen VI and anti-perlecan antibodies were rabbit polyclonal antibodies. Anti-laminin-α2 (4H8-2) and anti-fibronectin (EP5) were rat and mouse monoclonal antibodies respectively. Secondary antibodies used were goat anti-mouse HRP antibody for the fibronectin blot, goat anti-rabbit HRP antibody for collagen I, collagen VI and perlecan blots and rabbit anti-rat HRP antibody for the laminin α2 blot.

recognising collagen VI, indicated one band above 260kDa that was similar in intensity for extracts from both untreated and PLA_2 decellularised muscle. Fibronectin was detected as a 200 kDa band, although with lower signal intensity in the decellularized extract compared to untreated muscle extract. A band staining with the Laminin α2 antibody was at the top of the gel (~400kDa) with an increased amount in the extract from decellularised muscle compared to the untreated muscle extract. A novel finding is the preservation of some perlecan in the decellularised ECM extract. Multiple bands were revealed with the anti-Perlecan antibody in the untreated sample (>260kDa and at 140 kDa), but a single high molecular weight band at the top of the gel appeared in the decellularised extract (Figure 3.12).

3.2.6 Scanning electron microscopy (SEM) (section 2.6)

Structural changes following the process of decellularisation were investigated using SEM, which was performed on both, untreated and decellularised muscles. Five samples each of untreated and decellularised mouse muscle sections (60 µm thick) and representative samples of whole rat quadriceps muscles were examined. Untreated muscle samples show a hexagonal, compact fibre arrangement while decellularised samples show hollow tubular structures, indicating the loss of cells (Figure 3.13).

Table 3.2 ECM proteins in Native Muscle and Acellular Muscle

ECM protein	Native muscle	Method of decellularisation		
		Trypsin	SDS	PLA_2
Col I	+	++	++	++
Col III	+	NT	NT	++
Col IV	+	++	++	++
Col VI	+	+	+	++
Fibronectin	+	-	+	+
Perlecan	+	NT	+	+
Biglycan	+	NT	-	NT
Decorin	+	NT	-	+
HS EV3C3 epitope	+	NT	NT	+

+ present, - absent, ++ present with an increased intensity, NT not tested

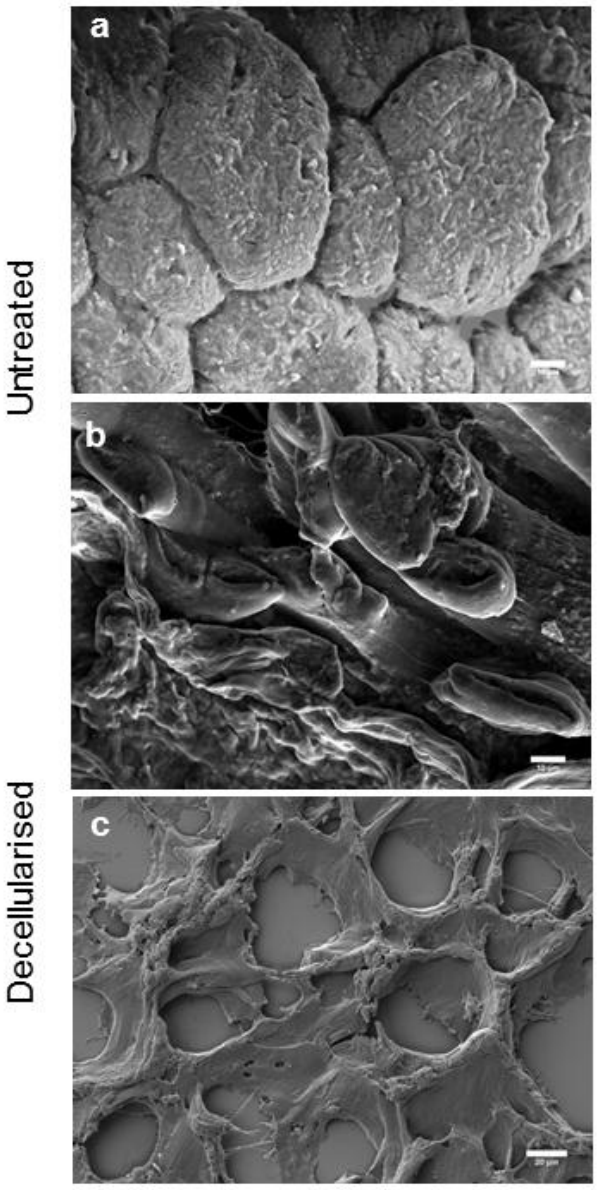

Figure 3.13 Scanning electron micrographs of untreated (a) and PLA_2 decellularized (b, c) rat quadriceps muscles. SEM imaging was performed on full thickness chunks of muscle (a, b) (approximately 0.5 mm thick, cut using a sharp razor blade) and muscle sections (c) (60 µm thick, cut using a cryostat). Scale bars: 10µm (a, b) and 20µm (c).

3.3 Discussion

This chapter describes the development of a method to obtain a skeletal muscle ECM scaffold with well-preserved matrix components including the proteoglycans. Of the three methods that were explored, a phospholipase based method provided the best balance between removal of cells and cellular components like DNA and the preservation of ECM components.

The first method tested used a proteolytic enzyme, trypsin. This method was effective in decellularizing the muscle tissue (Fig 3.1) and by immunohistochemistry it appeared as if collagens type I, type IV and type VI were preserved, but immunohistochemistry also suggested that the matrix glycoprotein, fibronectin, was destroyed (Fig 3.2 and 3.3). Previously, trypsin was used as a decellularization agent due to its serine protease activity but it can also cleave the core proteins of proteoglycans and so release GAG chains [175]. Stern et al (2009) used trypsin and Triton X-100 to decellularize hamstring and quadriceps muscles of rats and showed that the levels of GAGs in the decellularized matrix were below the limits of detection [175]. Although Stern et al (2009) did not perform an immunohistochemical examination of the decellularised muscle ECM; they measured the collagen content as a percentage of total protein content and found it to be 72% in the decellularised ECM. Although no intact cells were seen using this method strands of disrupted DNA and RNA were evident [245].

Since, the main goal was to preserve most of the ECM components in the remaining matrix including fibronectin, a detergent based method was tried. A method using the anionic detergent SDS was used. This detergent assists in the decellularization process by solubilizing the cell membrane and disrupting DNA-protein or lipid-protein interactions. Others have found that although SDS removes cells from dense tissues more effectively than other chemical agents it can adversely affect the ultrastructure of the remaining ECM [168, 246] and may lead to the removal of growth factors [177]. In our study, DNA quantification results indicated that the SDS method did not efficiently remove all of the DNA from the muscle tissue (Fig 3.4), although by immunohistochemistry it was evident that most of the ECM components including all

the collagens and fibronectin were retained (Fig 3.5 and 3.6). Other workers have used a variety of methods to decellularize skeletal muscle and to analyse the decellularized matrix. DeQuach et al (2010) used Time-of-Flight Secondary Ion Mass Spectrometry (TOF-SIMS) to characterize the matrix remaining following decellularization of porcine intercostal muscle using 1% SDS. They showed the presence of collagens, fibronectin, laminin, fibrinogen, fibrillin-1 and fibrillin-5, proteoglycans such as decorin, lumican and HS GAGs in this matrix [174]. They assessed whether cellular material remained by sectioning the decellularised matrix and staining with hematoxylin and eosin. Although they reported loss of all cells, using this method it would be difficult to determine whether cell fragments or strands of DNA remained, as were evident in our study when we used SDS to decellularize quadriceps muscle, although we did use a lower concentration of SDS (0.2%). Interestingly, DeQuach et al (2010) also decellularized cardiac tissue using the same 1% SDS procedure and their analyses revealed tissue specific differences in the cardiac matrix and skeletal muscle matrix, and for both tissues significant quantities of GAGs were measured in the acellular matrices [174]. In an attempt to produce an acellular muscle matrix that retains both the biochemical and mechanical properties of intact tibialis anterior muscle Gillies et al. (2011) developed a procedure involving cell lysis by osmotic shock, latrunculin B treatment to disrupt actin, high ionic strength salt treatment to depolymerize myosin and finally DNase treatment [176]. In this case, although the proteins in decellularised muscle were greatly decreased from those in intact muscle some myosin fragments and a small amount of actin remained. The collagen content was consistent with that of intact muscle but the GAG content was reduced by approximately half [176], possibly because cell surface GAGs would have been included in the GAGs measured from intact muscle.

The final method examined was a modification of the method used by Wang et al. (2011) and involved a combination of enzyme, detergent and nucleases [243]. This method, coined the “phospholipase method” consisted of sequential incubation of mouse Quadriceps muscle in phospholipase A_2 and sodium deoxycholate; a high ionic strength solution and DNase I [243]. This method avoided the use of proteases or strong ionic detergents like SDS that could degrade the ECM. This method was originally used by

Wang et al. (2011) to prepare an acellular liver matrix using perfusion of the decellularisation reagents. In this case preservation of growth factors, cytokines and extracellular components of the matrix were reported [243]. This present study is the first to use a phospholipase in the decellularization reagents for skeletal muscle.

PLA_2 decellularisation successfully removed most of the cellular material, as shown by DNA and cellular protein analysis (Figs 3.7 and 3.8) and appeared to be a better method than the previous two methods. SEM images of decellularized muscles suggested that while the PLA_2 method successfully removed the muscle fibres from the tissue, the overall architecture of the remaining matrix was well maintained (Fig 3.13). Similar to our observations with acellular quadriceps muscle, scanning electron microscopy of the acellular tibialis anterior muscle obtained by the method of Gillies et al (2011) revealed hollow tubular extracellular matrix structures, indicating retention of the tissue architecture [176]. Using the PLA_2 method immunohistochemistry revealed all the collagens examined (type I, III, IV and VI) were present in the decellularised matrix (Fig 3.9). Interestingly in some instances the staining intensity increased in the decellularised matrix, which may imply more antigenic sites were exposed following the loss of cells (Figure 3.9 and Table 3.2). The Western blotting data for collagens type I and VI in the solubilised ECM extracts indicated intact α1chains as well as high molecular weight collagen trimers (Figure 3.12).

Collagens type I and III are the major structural proteins in skeletal muscle ECM and constitute major portions of endomysium and perimysium [68]. In addition to their structural biomechanical function, collagens also bind to different growth factors like transforming growth factor β (TGF-β) and insulin like growth factor (IGF 1 and 2), and affect diverse cell functions such as proliferation and differentiation through these interactions [69]. *In vitro* studies suggest a possible role for IGF-1 in satellite cell proliferation [33] whereas *in vivo* studies show that IGF-1 induces hypertrophy in muscle [247] and its direct injection in muscle improves the process of muscle regeneration [36]. TGF-β1 plays a role in determining the fibre type formation during muscle development [248, 249] and also induces the myogenic cells into myofibroblasts leading to the formation of scar tissue within the regenerating muscle [250]. Recently,

Urciulo et al (2013) showed that collagen VI plays an important role in regulating the self-renewal capacity of the satellite cells and it forms an essential component of the satellite cell niche [251]. Once activated, satellite cells proliferate, migrate to the damaged area of the muscle, differentiate and fuse to form new muscle fibres which leads to an increase in the cross sectional area of the muscle. Collagen VI also seems to be important for regulating the mechanical properties of muscle as studies using a Col6a 1-/- mice model indicated an increase in elasticity and reduced stiffness of skeletal muscle [251]. The data indicates good collagen retention with the PLA_2 method which has the added advantage that this enables preservation of collagen-binding molecules such as laminins, fibronectin, proteoglycans and GAGs, that in turn preserve cytokines and growth factors bound to them [243].

Immunohistochemistry results also showed that the two major basement membrane glycoproteins, laminin-α2 and fibronectin were preserved in the decellularised matrix (Figure 3.9). A result that was confirmed by the western blotting data, although there appeared to be a decrease in the levels of fibronectin in the solubilised acellular ECM extracts (Figure 3.12). In skeletal muscle, laminins containing the α2 chain are a major component of the basement membrane, with laminin-2 (α2β1γ1) being the major form around the sarcolemma of mature myofibres, while laminin-4 (α2β2γ1) occurs at neuromuscular junctions and myotendinous junctions [76]. These laminins bind α7β1 integrin, the major laminin receptor in skeletal muscle, to activate the phosphatidylinositol 3-kinase/Akt and the Ras/Raf/MEK/Erk signalling pathways. This has the effect of promoting myotube survival and stability by up regulating suppressors of apoptosis and down regulating the expression of pro-apoptotic molecules [252]. Laminins also bind to non-integrin cell surface receptors like α-dystroglycan and control the transmission of contractile force from the muscle fibre to the ECM [77]. Mice lacking the laminin α2 subunit have severely impaired muscle regeneration and muscular dystrophy, which can be rescued if the link between the basement membrane and dystroglycan is restored [253]. Fibronectin binds to collagen, laminin and other molecules of the ECM to play a key role in myoblast adhesion, migration and differentiation [74]. Like collagen VI, fibronectin is a key component of the satellite cell

niche and loss of fibronectin severely reduces the pool of satellite cells because fibronectin is involved in stimulating Wnt7a signaling which induces satellite cell expansion [254]. Fibronectin binds to the integrins-α5β1 and αvβ3 and controls the organization of cell-matrix adhesions and fibronectin fibrillogenesis [255]. These integrins are easily detected in myoblasts and are considered to play a crucial role during myogenic differentiation [256].

It was particularly encouraging that using this phospholipase method to decellularize muscle resulted in the retention of the proteoglycans, perlecan and decorin, as well as a heparan sulfate epitope that was detected by the EV3C3 antibody [257]. Western blot data also showed preservation of perlecan in the solubilised muscle matrix (Figure 3.12). The proteoglycan perlecan is an integral component of the muscle basement membrane where it binds collagen IV through its core protein. Knockout mouse studies have suggested that perlecan is important for maintaining the muscle mass of fast fiber type muscle probably through its regulation of myostatin signalling and expression. Loss of perlecan also seemed to increase the sensitivity of muscles to mechanical stress [258]. In addition, perlecan is essential for the functioning of the neuromuscular junctions as it binds and localizes acetyl-cholinesterase to the neuromuscular junctions [102]. Another proteoglycan present in the acellular muscle matrix was decorin, the core protein of which contains binding sites for collagen I and fibronectin. The N-terminal domain of decorin's core protein binds myostatin and suppresses myostatin signaling, thereby enhancing the proliferation and differentiation of myogenic cells [109]. Moreover, the intra-muscle injection of a peptide from this region of decorin induced muscle hypertrophy [259]. Recently, Li et al (2007) demonstrated that decorin activated the differentiation of C2C12 cells *in vitro* and enhanced muscle regeneration in two mouse models by upregulating the expression of p21, follistatin, peroxisome proliferator-activated receptor gamma coactivator-1-alpha (PGC-1α) and down regulating myostatin expression [110]. Decorin also binds TGF-β through a core protein region and this interaction inhibited TGF-β activity triggered in response to muscle injury [260]. The GAG chains of perlecan and decorin and other matrix proteoglycans play important roles in myogenesis. Of particular importance are the HS chains because of their ability

to bind and sequester growth factors like FGF-2 and HGF. Both of these growth factors stimulate skeletal muscle cell proliferation and inhibit differentiation [84]. Collectively these studies outline roles played by collagens, laminin-α2, fibronectin, perlecan, decorin and HS chains in myoblast development and highlight the importance of preservation of these components if a fully functional decellularized ECM from muscle is the goal.

Generally it is impossible to directly compare the efficacy of the various decellularization methods as different types of tissue were used and the analyses of the acellular matrices differed from study to study. However, when a direct comparison of different methods has been made it is clear that the decellularization method has a marked effect on the extracellular matrix components retained, on the removal of DNA and RNA remnants, and on the organization of the collagen fibres [176, 261]. Moreover, the quality of the acellular matrix produced was reflected in the morphology, proliferation and integrin expression levels of cells grown on these surfaces [176, 261]. Although PLA_2 decellularisation method preserved most of the ECM components tested, including perlecan and a GAG epitope, accurate quantification of the GAG components and any growth factors remaining in the decellularised ECM was not done. It would be interesting to evaluate these two components of the matrix thoroughly as growth factors forms an integral part of ECM niche and their binding to PGs and GAGs is well known [87, 88, 115, 117].

3.4 Conclusion

With the aim of obtaining a three dimensional decellularized muscle scaffold which could further be utilized to study cell behaviour and cell-matrix interaction *in vitro*, skeletal muscle tissue was decellularized using three different methods. In each case the ECM scaffold obtained had different matrix components preserved and different levels of cellular DNA remaining. Of the three methods tested, the phospholipase method provided the best balance between loss of cell components and preservation of ECM components.

3.5 Future Directions

The contribution of ECM to muscle repair and regeneration is an area of increasing interest and more research is being undertaken to understand more about the cell-ECM-growth factor interactions and their role in tissue repair [262]. However, less attention has been paid to the fact that the same tissue can vary in its ECM composition in different situations: for example, healthy versus diseased, young versus old or the same tissue type but in a different anatomical location for example, in case of muscle, a soleus muscle versus a tibialis anterior muscle, or a gastrocnemius versus a quadriceps muscle. Limited work has been published of a direct comparison of ECM obtained after decellularisation of muscle from different aged animals. It would be intriguing to investigate whether there are any significant differences in ECM obtained from mice of different ages and if so how these differences may affect myoblast proliferation and differentiation.

In this study, immunohistochemistry technique was used to assess the preservation of ECM proteins in the decellularised matrix. However, using immunohistochemistry, it is difficult to quantify the amount of ECM proteins remained in the matrix due to the semi-quantitative nature of this technique. In future, a thorough biochemical approach to quantify the amount of collagens (Sircoll assay kit, Biocolor assays) and GAGs (Blyscan Assay kit, Biocolor assays) must be used.

Every technique that has been used to assess DNA removal (DAPI staining, Nanodrop and gel electrophoresis) has a certain threshold level. For example, if the DNA was detected in the decellularized matrix using Nanodrop (20ng/µl), it is possible that the same sample when electrophoresed on an agarose gel failed to detect any measurable levels of DNA as the amount of DNA was below the limits of detection under a UV transilluminator and secondly, there is a probability that the DNA was degraded. In future, better methods such as those available in the market (Quant-iT PicoGreen dsDNA assay kit) may be used to quantify the DNA.

Chapter 4:

Acellular skeletal muscle matrix supported serum free proliferation and differentiation of C2C12 murine myoblasts in *in vitro* 2D and 3D cultures

4.1 Introduction

Acellular ECM scaffolds obtained from muscle have been investigated by other workers to assess their effects on myoblasts both in tissue culture and *in vivo* in animal models. An understanding of the efficacy with which these ECM scaffolds become repopulated by host myogenic cells *in vivo* is crucial for determining whether they can be used in future translational applications in human muscle [174, 175]. *In vitro* testing of scaffolds can provide valuable insights into the cell-ECM interactions and a measure of the cyto-compatibility of the scaffolds. The examination of myogenesis on scaffold materials in tissue culture have traditionally used foetal bovine and horse sera as a source of growth factors to stimulate myoblast proliferation, fusion and differentiation. However, these sera contain a diversity of ill-defined components, making it difficult to assess the contribution of different growth factors and ECM molecules at the various stages of myogenesis. Furthermore, cells cultured in animal sera are increasingly being viewed unsuitable for human transplantation applications [263] [264]. The use of alternative artificial serum-free media to promote myogenesis is desirable as a way of avoiding both the undefined nature of sera and possible batch to batch variability, as well as potential regulatory issues associated with the use of animal materials to culture cells to be used for transplantation. Serum-free media formulations have been tested for myoblast proliferation and differentiation previously [220, 265-267]. Fujita et al (2010) evaluated protein expression, glucose metabolism, sarcomere formation and generation of active tension during different stages of muscle differentiation in several serum free media: DMEM containing either Ham's F-12, AIM-V, 0.2 % Ultroser G, 0.1 % sericin or AIM-V/0.1% Ultroser G [268, 269]. All the media except DMEM/F-12 were able to induce sarcomere formation in differentiated myotubes, but there was more active tension generation in AIM-V media as compared to the media containing horse serum [268]. The authors suggested that serum free media was better in promoting the differentiation of C2C12 myoblasts than the serum-containing media. The above study suggests that the serum free media tested so far have showed variable results and therein lies the opportunity for improvement in formulation of serum free media for muscle cell culture.

Traditional two-dimensional tissue culture is a useful model system to study cell-matrix interactions and the associated factors which modulate these interactions, for example how cells at different stages of differentiation respond to different types of matrix glycoproteins, and the physical and mechanical properties of a substrate. Studies of cell behaviour on substrates of a pure matrix glycoprotein, like fibronectin [270] [271], a laminin [271, 272] or a collagen [273] are relatively common, but studies of cell behaviour during differentiation on substrates comprising the mix of glycoproteins found in their natural tissue ECM are just beginning. In the case of myoblasts these studies have been conducted in the presence of serum [174, 175], which contains soluble matrix proteins that can adhere to the substrate proteins. This makes it difficult to determine the exact contribution of a matrix glycoprotein substrate on the differentiation process.

Previous studies have indicated that cell behaviour on a 2-dimensional (2D) matrix glycoprotein substrate is not identical to that seen when the glycoprotein is in a three-dimensional (3D) scaffold. For example, cell-adhesion complexes in "3D matrices" differ markedly from their counterparts on 2D substrates in their structure and function, and cell-signalling events can also differ between 3D matrices and 2D flat substrates [231]. For these reasons there is a need to improve our understanding of cell-matrix interactions by designing 3D culture systems which closely mimic the *in-vivo* cell microenvironment.

This chapter describes the functional characterisation of the decellularized skeletal muscle matrix, prepared in the previous chapter. To avoid the confounding effects of serum, a serum-free medium (developed in our lab) that supports myoblast differentiation in tissue culture, when these cells are provided with a matrix glycoprotein substrate, was used. We hypothesized firstly, that a substrate of solubilised muscle matrix would regulate myoblast differentiation differently than a substrate of a pure matrix glycoprotein, and secondly, that the correct 3D arrangement of ECM components from a muscle matrix would affect cell behaviour differently from a solubilized ECM under *in vitro* conditions. Hence, this study used the serum-free medium, to investigate the formation of differentiated myotubes from mouse and human myoblasts either on

surfaces coated with solubilised skeletal muscle ECM, or on intact acellular skeletal muscle matrices.

4.2 Results

4.2.1 Proliferation of C2C12 cells on different matrices

To compare the ability of substrates of various ECM proteins to support cell adhesion and growth the murine myoblast cells, C2C12, were cultured on collagen I, fibronectin or solubilised rat muscle matrix coated plastic dishes in our serum free medium (section 2.7.5.3). Solubilized rat quadriceps muscle matrix (sections 2.2.3 and 2.3.4) was used for these coating experiments as it was not possible to obtain sufficient matrix material from the smaller mouse muscles. It was found C2C12 myoblasts adhered to, spread and proliferated on all matrices (Fig 4.1 a–i). By day 3 the cells were almost 70% confluent, and by day 4 the cells became confluent on all 3 substrates. In contrast, on uncoated tissue culture plastic C2C12 cells in the serum-free medium did not adhere to the substrate; they had a rounded morphology and aggregated together adhering to each other rather than the substrate (Fig 4.1. j-k). Without a matrix protein substrate, proliferation was poor, the aggregates failed to thrive, and after 4 days many of the cells had died. Cell proliferation was quantified by culturing C2C12 cells in serum free proliferation medium for 7 days on collagen I, fibronectin and solubilised muscle matrix substrates in a 24-well plate, with the cells being harvested and counted each day using a Z™ Series Beckmann coulter counter (section 2.7.7) (Fig 4.2). Interestingly, C2C12 myoblasts proliferated at a similar rate on collagen I and fibronectin coated surfaces with cells reaching approximately 2.5 x 10^5 million at day 3 in the wells of a 24-welled plate from an initial seeding number of 7.0 x 10^3 cells/well. On muscle matrix coated surfaces, the cells proliferated at a slower rate and reached to 2 x 10^5 cells by day 4 and plateaued thereafter. C2C12 myoblasts began to differentiate on day 4 which may explain the plateau in cell numbers seen on muscle matrix, and to a lesser extent on fibronectin and collagen.

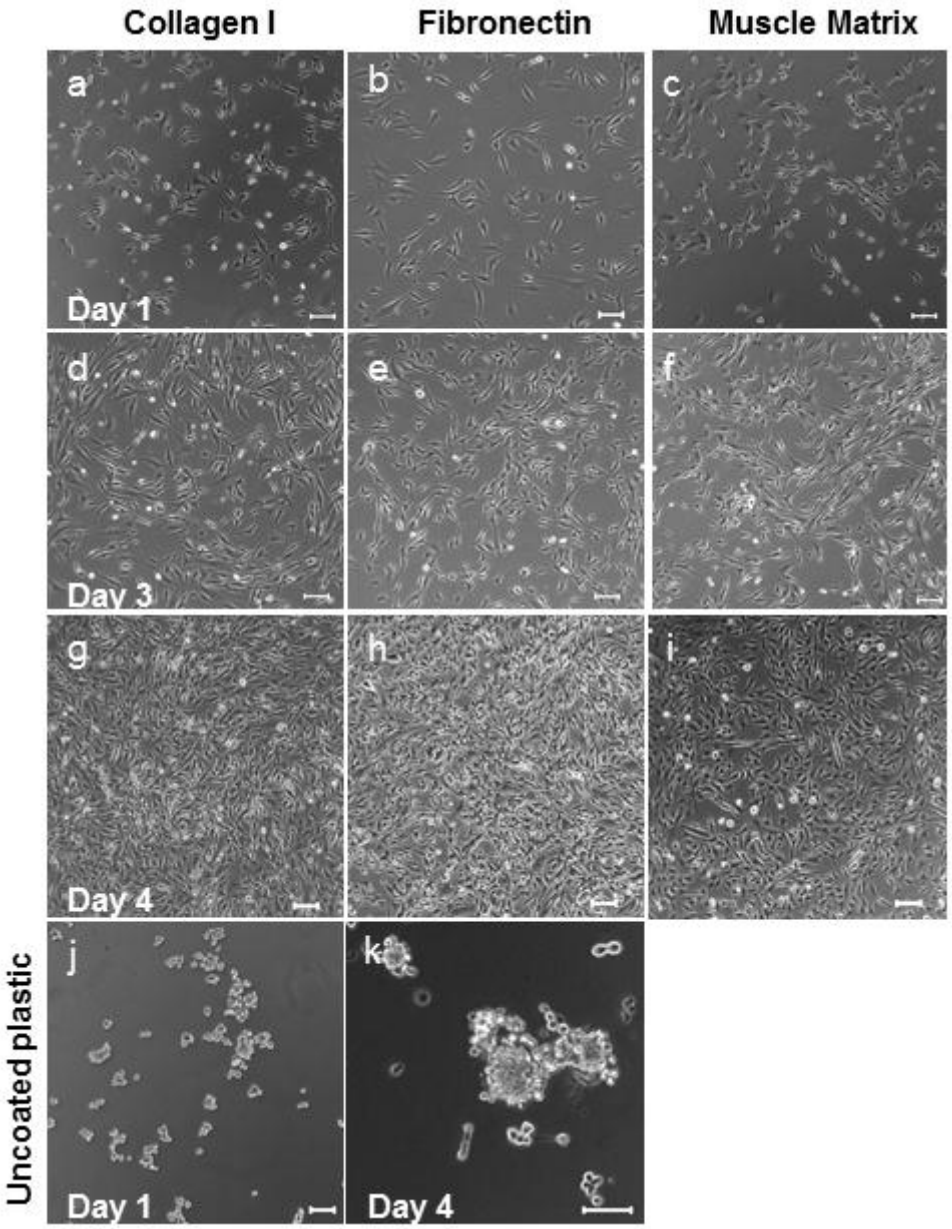

Figure 4.1. Phase contrast images of proliferating C2C12 cells cultured on collagen I (a, d, g), fibronectin (b, e, h) solubilised muscle matrix (c, f, i) and uncoated plastic (j, k) for 1, 3 and 4 days in serum free proliferation medium. C2C12 cells (3.5×10^3 cells/cm^2) were seeded in wells of a 24-well plate coated with either collagen I (10 µg/cm^2), fibronectin (10 µg/cm^2), solubilised muscle matrix (10 µg/cm^2) or uncoated plastic and cultured for 4 days in serum free medium. Images were captured at day 1, 3 and 4 after seeding, with a Zeiss Axiovert bright field microscope at an overall magnification of 120x using Spot Advanced software. Scale bars - 100 µm for a-k.

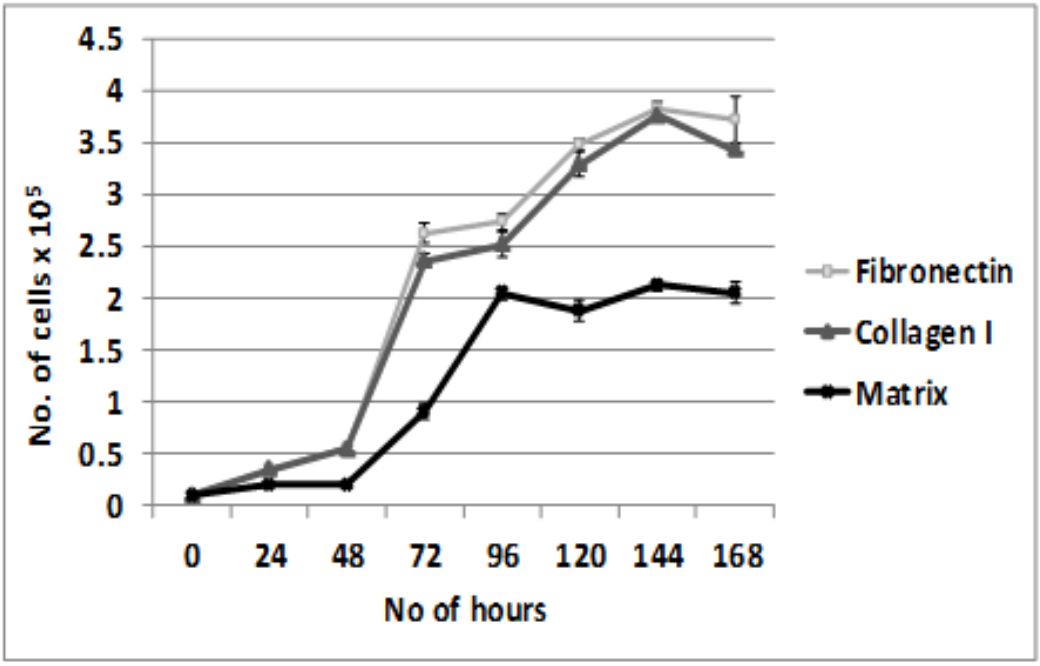

Figure 4.2. Proliferation of C2C12 cells in serum free proliferation medium was assessed on collagen I, fibronectin and solubilised muscle matrix. C2C12 cells (3.5×10^3 cells/cm^2) were seeded in wells of a 24-well plate coated with either collagen I (10 µg/cm^2), fibronectin (10 µg/cm^2) or solubilised muscle matrix (10 µg/cm^2), and cultured for 7 days in serum free medium. After every 24 h, cells were removed from the plastic using 0.05% trypsin/EDTA and counted using the Z™ Series COULTER COUNTER®

4.2.2 Differentiation of myoblasts into myotubes

To examine the effect of muscle matrix on the differentiation of C2C12 myoblasts, cells were cultured on muscle matrix, fibronectin and collagen I coated surfaces for 12 days. They were cultured in serum free proliferation medium until almost confluent (90%-100% confluency) (proliferation day 4), and then switched into serum-free differentiation medium for the remaining 8 days (differentiation day 8). Phase contrast microscopy of the cells after 4 days in differentiation medium clearly showed fusion of myoblasts into myotubes with a similar capacity on collagen I (Figure 4.3. a, d) and fibronectin (Figure 4.3. b, e). However on muscle matrix coated surfaces myotubes appeared much thicker than on the other substrates (Figure 4.3. c, f). Immunostaining with a mAb to myosin heavy chain 7 (MyHCB) (section 2.7.12) revealed that the myoblasts differentiated and fused to form myotubes on all the ECM substrates with similar capacity (Figure 4.4). By day 6 in differentiation media, striations appeared on the myotubes, which are indicative of assembly into sarcomeres.

Myotube width was also measured at days 4 and 6 in differentiation medium using image J analysis software (section 2.7.13) (Figure 4.5). This analysis revealed that myotube width increased from day 4 to day 6 and this increase was similar on both collagen type I and muscle matrices, but no visible difference in myotube width was found in myotubes formed on fibronectin.

4.2.3 qPCR Experimental workup:

(a) RNA concentration and quality

RNA was isolated from C2C12 myoblasts cultured for 3 days in proliferation media or for 1, 4 or 8 days in differentiation media on wells coated with collagen I (10 µg/cm^2), fibronectin (10 µg/cm^2) or solubilized matrix (10 µg/cm^2) using the ISOLATE RNA KIT (section 2.8.1). Since the RNA was to be used for qPCR experiments, RNA concentration and purity was assessed by measuring the absorbance spectrophotometrically (section 2.8.2) and obtaining the ratio of A_{260}/A_{280} nm. For all the RNA samples, A_{260}/A_{280} values were between 1.9 and 2.1. As an additional quality control step the quality of RNA was also measured using LabChip® GX II and all

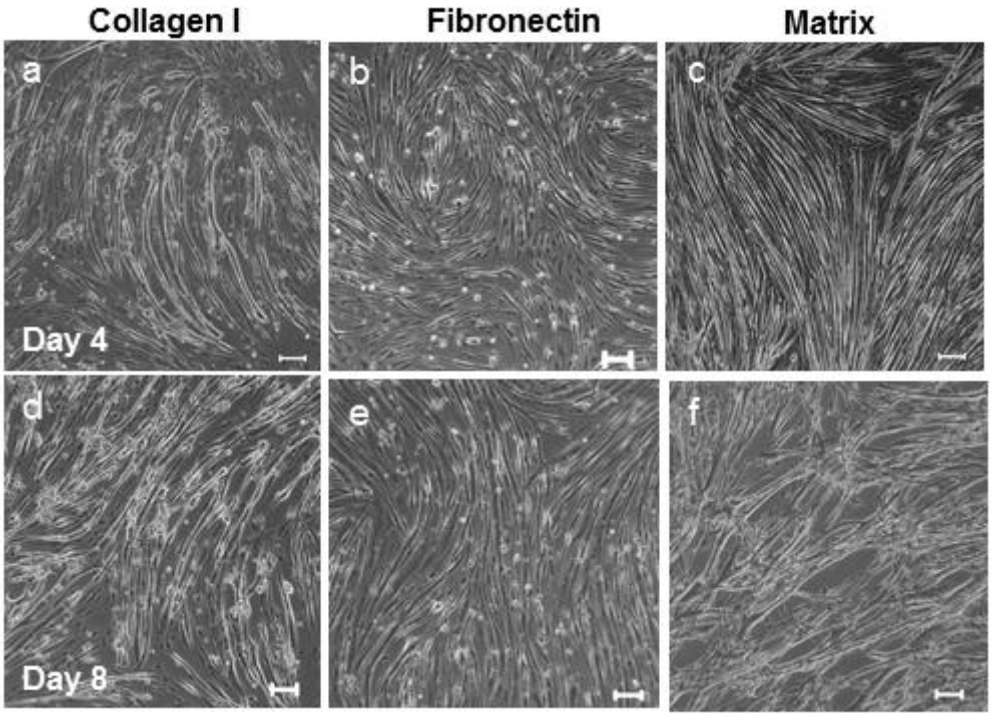

Figure 4.3. Phase contrast images of C2C12 cells cultured on collagen I (a, d), fibronectin (b, e) and solubilised muscle matrix (c, f) in serum free differentiation medium. C2C12 cells (3.5×10^3 cells/cm^2) were seeded in wells of a 24-well plate coated with either collagen I (10 µg/cm^2), fibronectin (10 µg/cm^2) or solubilised muscle matrix (10 µg/cm^2), and cultured for 4 days in serum free proliferation medium. After 4 days, the medium was changed to a culture medium designed to stimulate differentiation and the cells were cultured for another 8 days. Images were captured at day 4 and 8 of differentiation with a Zeiss Axiovert bright field microscope at an overall magnification of 120x using Spot Advanced software. Scale bars - 100 µm for a-f.

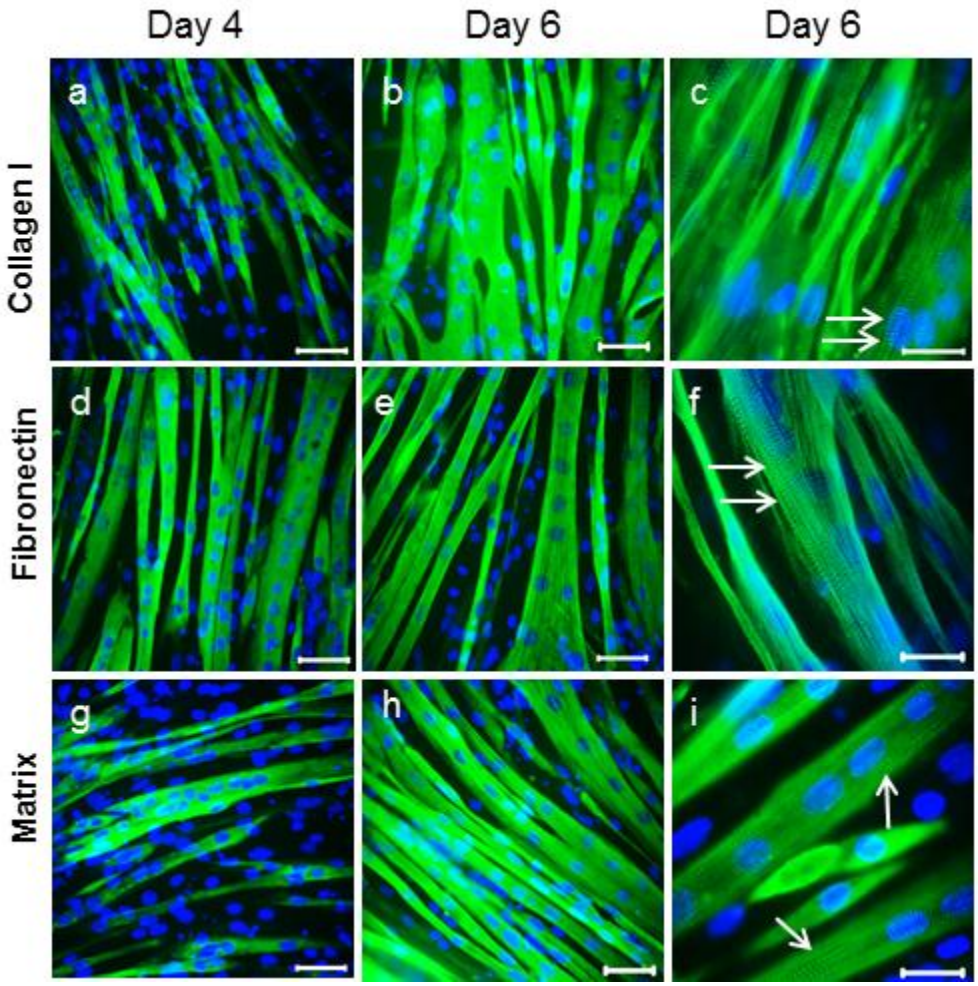

Figure 4.4. Immunofluorescence images of C2C12 cells cultured on collagen I (a-c), fibronectin (d-f) and solubilised muscle matrix (g-i) at 4 and 6 days in serum free differentiation medium. C2C12 cells (3.5×10^3 cells/cm^2) were seeded in wells of a 24-well plate coated with either collagen I (10 µg/cm^2), fibronectin (10 µg/cm^2) or solubilised muscle matrix (10 µg/cm^2), and cultured for 4 days in serum free proliferation medium. After 4 days, the medium was changed to a medium designed to stimulate differentiation and the cells were cultured for another 8 days. Post-differentiation, cells were fixed with 4% paraformaldehyde and stained for myosin (green) and imaged using a Zeiss Axioskop fluorescent microscope at an overall magnification of 480x using Spot Advanced software.The antibody recognising myosin was a mouse monoclonal (NOQ7.5.4D) antibody. The secondary antibody used was a goat anti-mouse alexafluor 488 conjugated antibody. Scale bars - 50 µm for a-i.

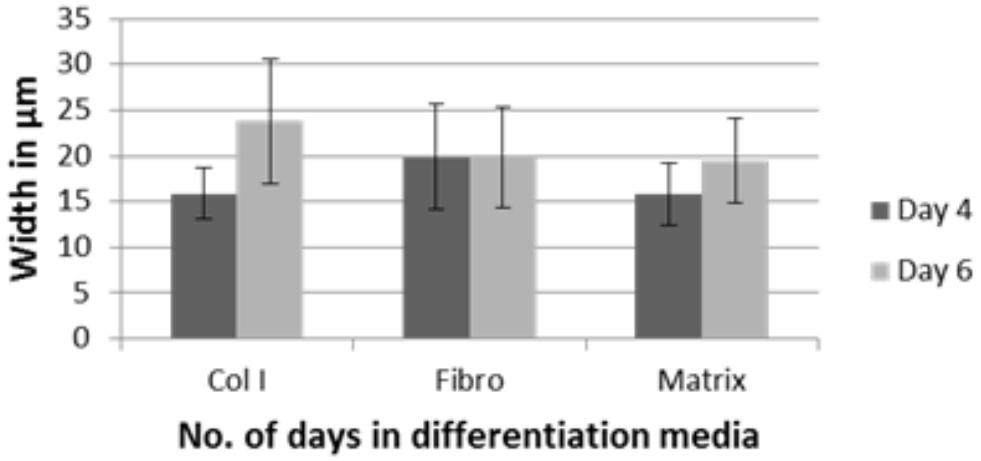

Figure 4.5. Myotube width was measured using ImageJ software. C2C12 cells (3.5×10^3 cells/cm^2) were seeded in wells of a 24-well plate coated with either collagen I (10 µg/cm^2), fibronectin (10 µg/cm^2) or solubilised muscle matrix (10 µg/cm^2), and cultured for 4 days in serum free proliferation medium. Then the medium was changed to a medium designed for differentiation and the cells were cultured for another 8 days. Myotube width of 25 myotubes was calculated using ImageJ software. Values are the mean±SD of 25 myotubes on days 4 and 6.

samples were found to have a RNA quality score (RQS) of > 8.0.

(b) Melt Curve Analysis (section 2.8.5)

Melt curve analysis allows identification of the melting temperature of the amplified sequence within each sample. The appearance of a single sharp peak indicates that only a single sequence was amplified during the thermal cycling reaction. Primer-dimers usually appear as small peaks beside the sharp peak, as they usually have a lower melting temperature due to their short length. In my experiments as the amplified DNA within the sample became single stranded, a sharp decrease in the SYBR green fluorescence intensity was observed. As can be seen in figure 4.6 and figure 4.7, melt curve histograms for all four reference genes and seven genes of interest (Table 2.4) respectively from cDNA samples of C2C12 cells in days 1, 4 and 8 of differentiation, a prominent single peak was detected for each primer pair indicating gene specific annealing.

(c) Primer efficiency calculations (section 2.8.6)

Briefly, five-fold dilutions (1/5, 1/25, 1/125 and 1/625) of neat cDNA (from cultures day 1 and day 4 of myotube differentiation) were prepared and were amplified for each primer pair (four reference genes and seven genes of interest) in a qPCR reaction. Efficiency of each primer was calculated using the equation $E=10^{(-1/slope)}$ where a value of 2.0 represents a perfect primer with product doubling after every cycle. The reaction efficiencies derived from these experiments are shown in Table 4.1 and the respective curves are shown in Figure 4.8-4.9. Primer efficiencies between 90% and 110 % are generally acceptable for gene quantification analysis.

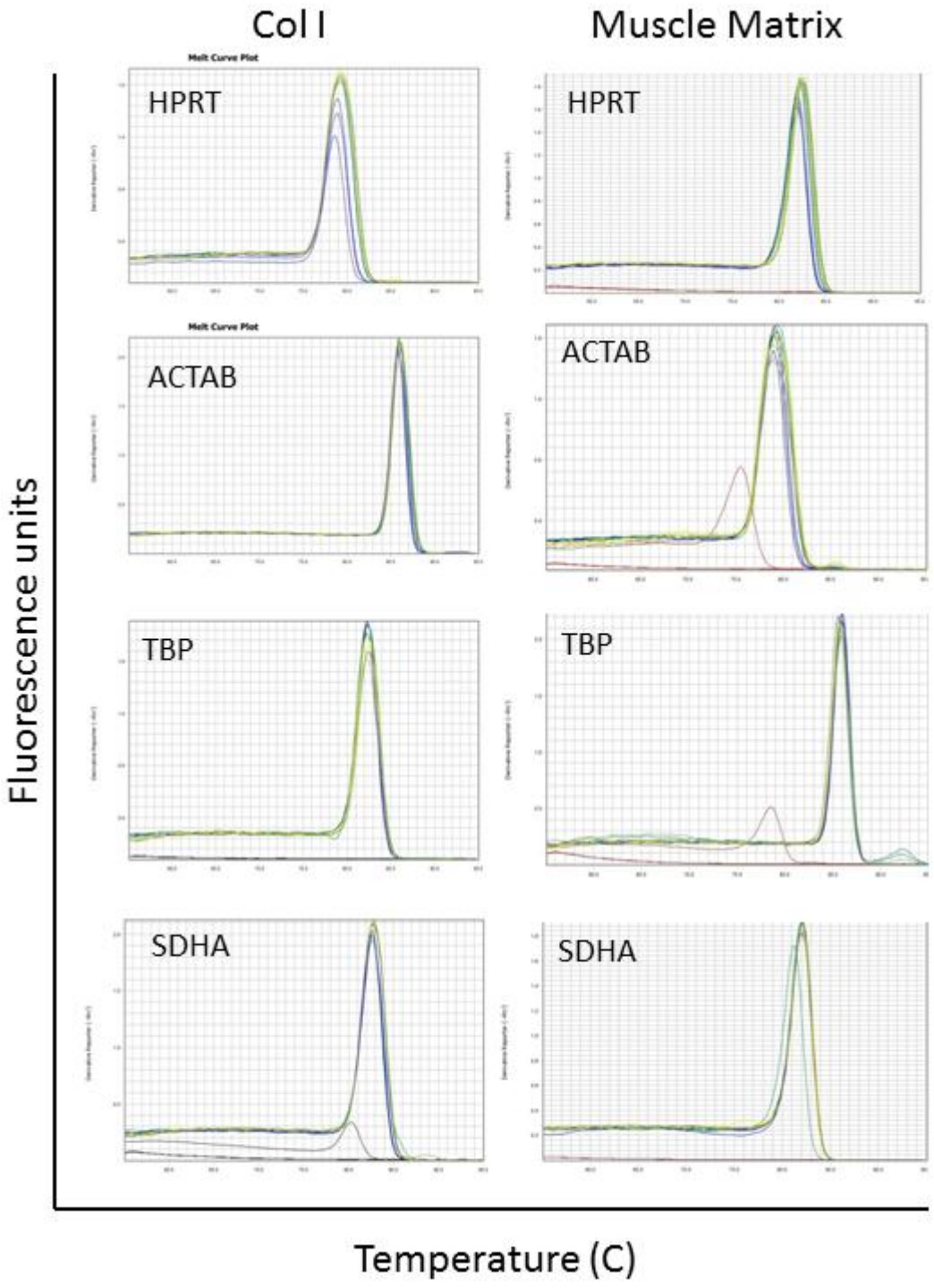

Figure 4.6. Melt curve analysis of reference genes for C2C12 cells cultured on collagen I and muscle matrix. To assess the specificity of the primers, melt curve analysis was performed after every qRT-PCR run. Fluorescence (y-axis) is plotted versus temperature (x-axis). Melt curves show the temperature where two strands of DNA separate.

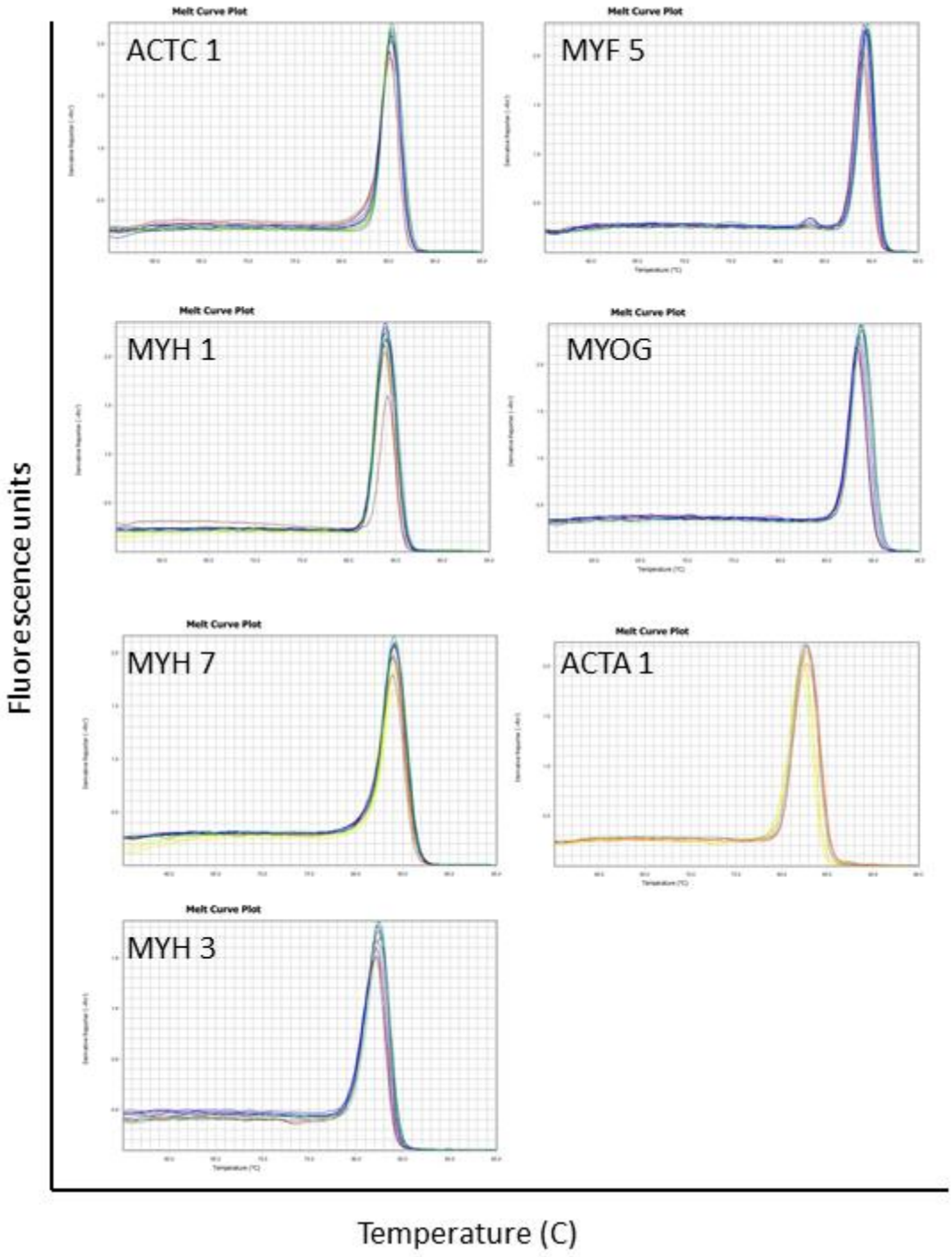

Figure 4.7. Melt curve analysis of genes of interest for C2C12 cells cultured on collagen I. To assess the specificity of the primers, melt curve analysis was performed after every qRT-PCR run. Fluorescence (y-axis) is plotted versus temperature (x-axis). Melt curves show the temperature where two strands of DNA separate.

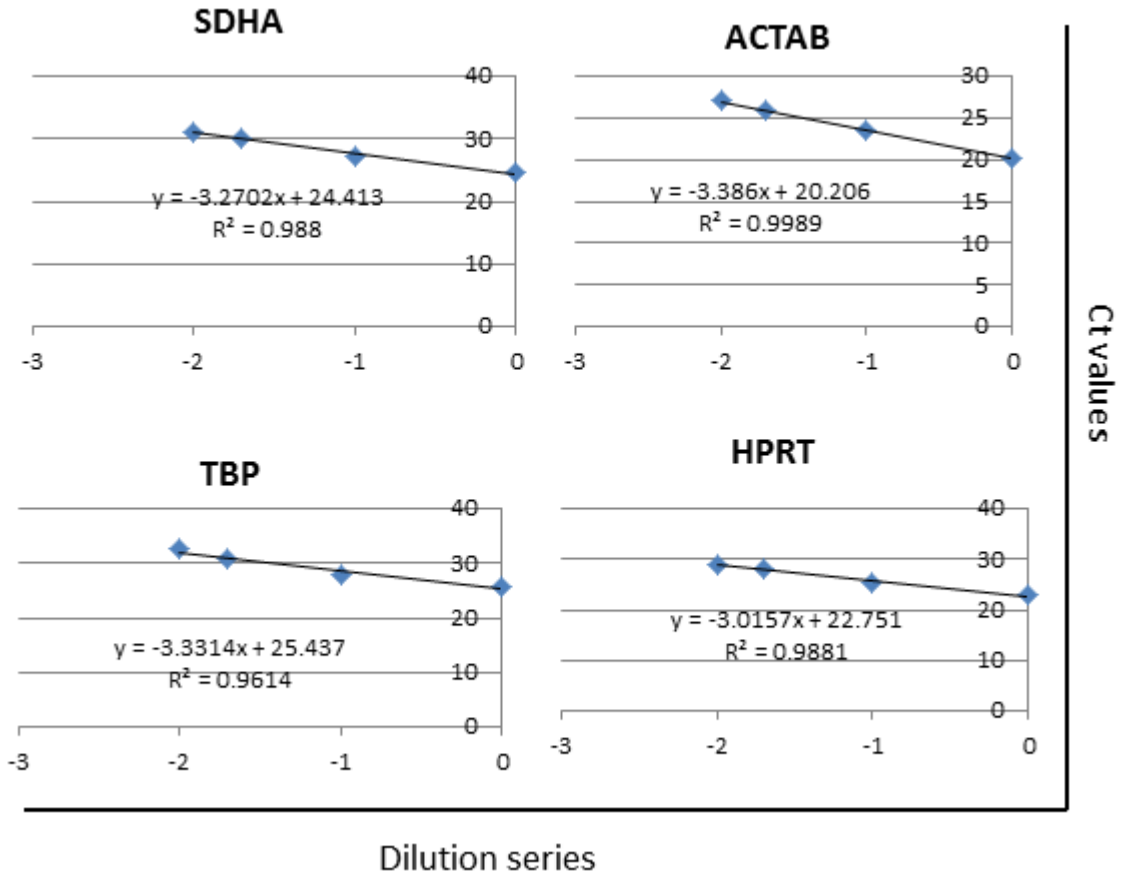

Figure 4.8. Primer efficiency calculation of four reference genes for C2C12 cells cultured on collagen I. To assess the efficiency of the primers, five-fold dilutions of cDNA (day 1 differentiation) was done and qPCR was performed. Ct values were plotted (y-axis) versus dilution series (x-axis) to determine the primer efficiency.

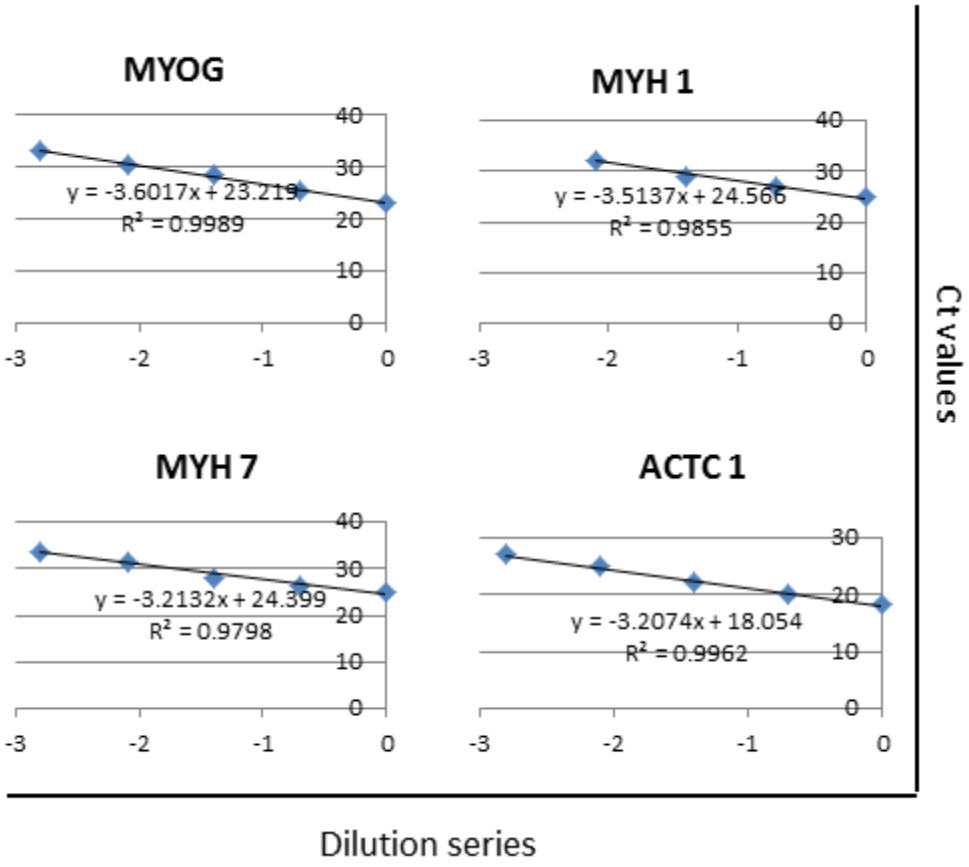

Figure 4.9. Primer efficiency calculation of four differentiation genes for C2C12 cells cultured on collagen I. To assess the efficiency of the primers, five-fold dilutions of cDNA (day 1 differentiation) was done and qPCR was performed. Ct values were plotted (y-axis) versus dilution series (x-axis) to determine the primer efficiency.

Table 4.1 Primer efficiencies of reference genes and genes of interest

Gene symbol	Amplification efficiency (%)
SDHA	102
ACTAB	97
TBP	100
HPRT	114
MYOG	90
MYF5	110
MYH 1	93
MYH 3	138
MYH 7	105
ACTA 1	122
ACTC 1	105

(d) Validation of reference genes (section 2.8.7)

In gene expression analysis using real time qPCR, reference genes (RGs), or housekeeping genes are included as internal controls, and it is assumed that expression of RGs should not change under the conditions of the experiment. However, expression of RGs may vary under different experimental conditions and if unrecognized this could result in an over- or under-estimation of gene expression. Thus, all RGs need to be validated for each experimental setting before performing the baseline correction for gene expression. Four reference genes (*SDHA, TBP, HPRT, and ACTAB*) were tested and analyzed using NormFinder [236] and BestKeeper [237] software.

(e) NormFinder

qRT-PCR was performed on cDNA obtained from cells cultured on collagen I, fibronectin and solubilized muscle matrix in serum free media at day 3 of proliferation and day 1 of differentiation. C_T values obtained after performing the qRT-PCR were placed in the NormFinder software and analysed. Table 4.2 shows the list of 4 candidate reference genes and their ranks, using the NormFinder programme to calculate

expression stability. The gene with the lowest expression stability is considered to be expressed with the greatest consistency. *SDHA* was found to have the most constant expression across all conditions with an expression stability value of 0.004 and was therefore used as the reference gene for normalization of data. The analysis for a combination of two genes yielded *SDHA* and *ACTAB* as the best combination with the stability value for best combination of two genes as 0.359.

Table 4.2 Stability values of 4 reference genes using the software Normfinder

Gene name	Stability value
TBP	0.088
SDHA	0.004
ACTAB	0.071
HPRT	0.025

(f) Bestkeeper

qRT-PCR was performed on cDNA obtained from cells cultured on collagen I, fibronectin and solubilized muscle matrix in serum free media at day 3 of proliferation and day 1 of differentiation. C_T values obtained after performing the qRT-PCR were placed in the Bestkeeper software and analysed. The reference gene with the lowest coefficient of variance ± standard deviation (CV±SD) is considered to be the most stable. Under serum-free culture conditions, *SDHA* and *ACTAB* were found to be the most stable reference genes with CV±SD values of 3.38±0.82 and 4.35±0.97. Although, *HPRT* and *TBP* also showed low CV±SD values of 4.59±1.22 and 3.68±1.06 respectively, the standard deviation was higher than 1 (starting template variation by a factor 2) in both cases making them unacceptable for normalization [237].

4.2.4 Gene expression of myogenic markers in C2C12 cells on different matrices

qRT-PCR was then used to examine the expression of seven genes that play important roles in different stages of myoblast differentiation (section 2.8.8). These were: myogenic factor 5 (*Myf5*) and myogenin (*MYOG*), both transcription factors belonging to the myogenic regulatory factor (MRF) family of proteins; three isoforms of myosin

heavy chain (*MYH1*, *MYH3* and *MYH7*); and two muscle actin isoforms (*ACTA1* and *ACTAC1*). Gene expression on days 1 (in differentiation medium), 4 (in differentiation medium) and 8 (in differentiation medium - myotubes) was assessed when C2C12 cells were cultured on collagen (Figure 4.10), fibronectin (Figure 4.11) and muscle-matrix (Figure 4.12).

Myf5 showed similar low levels of expression at days 1, 4 and 8 on collagen I (Fig 4.10). On fibronectin and muscle matrix coated surfaces, *Myf5* levels at day 8 were significantly lower than levels at day 1 (Figs 4.11 and 4.12). *MYOG* mRNA increased on muscle matrix coated surfaces to be at day 8 approximately 4-fold higher than at day 1 (Fig 4.12). In contrast, on collagen I and fibronectin coated surfaces, myogenin levels peaked at day 4 before declining at day 8 (Figs 4.10 and 4.11). A large increase was observed in the *MYH1*, *MYH7* and *ACTA1* expression from differentiation day 1 to differentiation day 4 and this was maintained at day 8 on all three matrices, suggesting strong differentiation. *MYH3* and *ACTC1* (which are expressed in immature muscle) also increased from differentiation day 1 to day 4, before decreasing at day 8 with the trend being similar on all 3 matrices (Fig 4.10-4.12). However, there was virtually no decrease in *MYH3* expression at day 8 on collagen I, whereas on fibronectin expression decreased to be the same as that on day 1 and on muscle matrix although the decrease was marked expression remained higher than that at day 1. These data, plus the fact that on muscle matrix *MYH1* did not increase from day 4 to day 8, tend to suggest that on muscle matrix differentiation is occurring earlier than on collagen I, but at about the same time as on fibronectin.

4.2.5 C2C12 cell adhesion and proliferation on three-dimensional matrix scaffolds

Decellularized 3D rat muscle scaffolds were used as a substrate to evaluate whether they supported proliferation and movement of C2C12 myoblasts in serum free culture (section 2.7.9). Cell proliferation was assessed by using the Click-iT EdU assay (section 2.7.11), which labels the recently synthesized DNA (proliferating cells) with the coloured thymidine analogue EdU [274]. This assay indicated many cells were

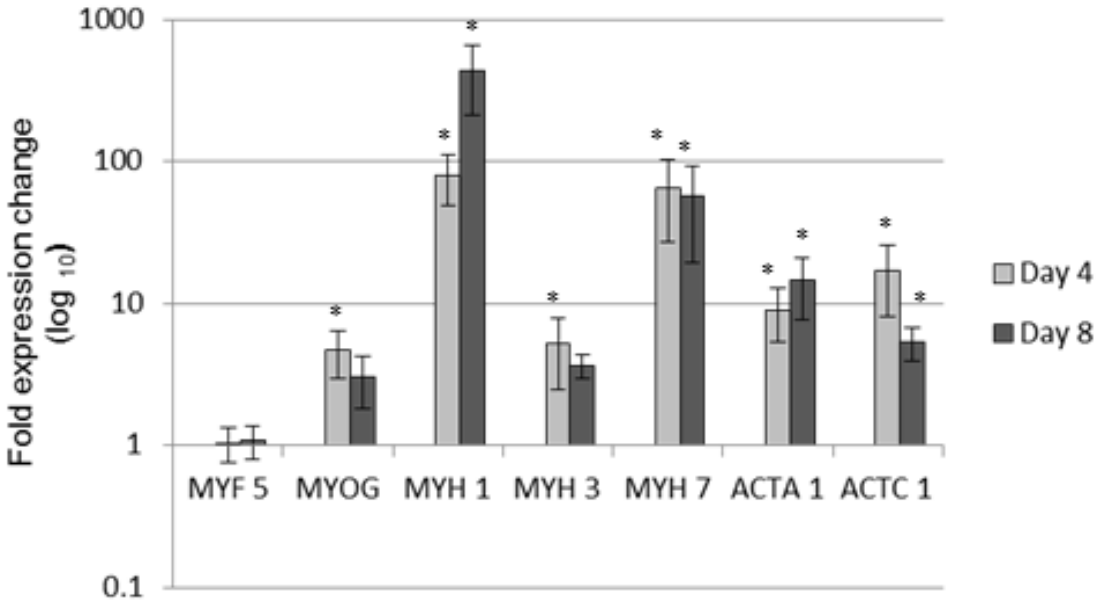

Figure 4.10. Quantitative real-time PCR was used to determine the expression of seven differentiation markers in differentiating C2C12 cells grown on collagen I at days 1, 4 and 8 of differentiation. C2C12 cells (3.5×10^3 cells/cm^2) were seeded in wells of a 24-well plate coated with collagen I (10 µg/cm^2) and cultured for 4 days in serum-free proliferation medium and for a further 8 days in differentiation medium. RNA was isolated from cells at day 1, day 4 and day 8 of differentiation. Relative expression levels for *MYF5, MYOG, MYH1, MYH3, MYH7, ACTA1, ACTC1* were normalized to the C_t value of the reference gene (*SDHA)* and fold change was determined using $2^{-\text{delta delta}}$ C_t method. Day 4 and Day 8 expression levels were normalized to Day 1 and $\log_{10}$ transformed. Mean ± SE of 4 biological replicates are shown. Wilcoxon's T-test was performed and significance (p) values shown at each time point. *p<0.05.

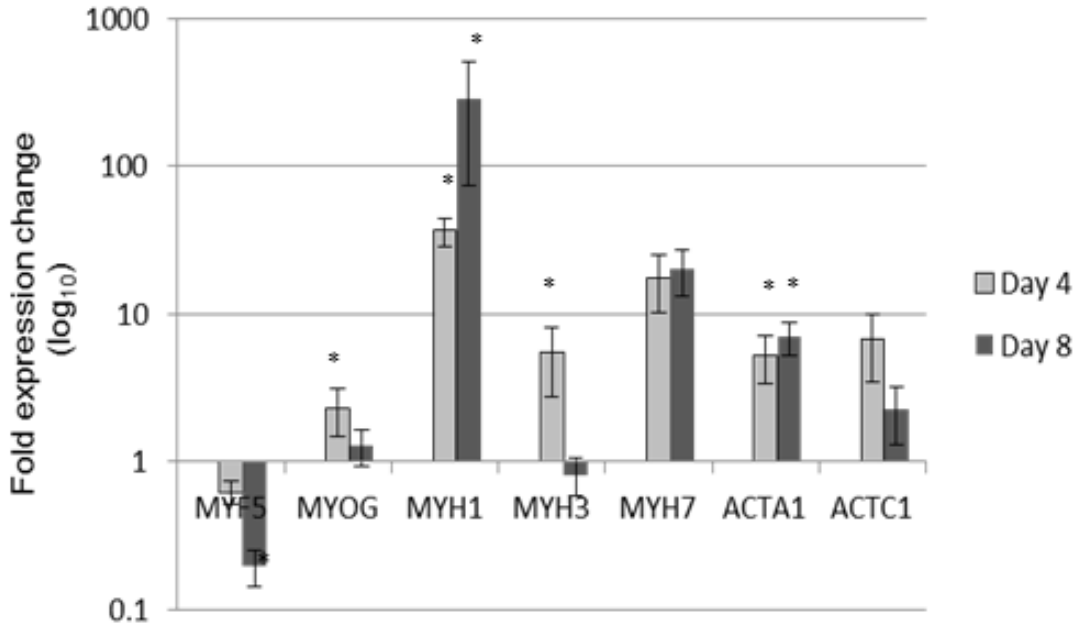

Figure 4.11. Quantitative real-time PCR was used to determine the expression of seven differentiation markers in differentiating C2C12 cells grown on fibronectin at days 1, 4 and 8 of differentiation. C2C12 cells (3.5×10^3 cells/cm^2) were seeded in wells of a 24-well plate coated with fibronectin (10 µg/cm^2) and cultured for 4 days in serum-free proliferation medium and for a further 8 days in differentiation medium. RNA was isolated from cells at day 1, day 4 and day 8 of differentiation. Relative expression levels for *MYF5, MYOG, MYH1, MYH3, MYH7, ACTA1, ACTC1* were normalized to the C_t value of the reference gene (*SDHA*) and fold change was determined using $2^{-\text{delta delta}}$ C_t method. Day 4 and Day 8 expression levels were normalized to Day 1 and $\log_{10}$ transformed. Mean ± SE of 4 biological replicates are shown. Wilcoxon's T-test was performed and significance (p) values shown at each time point. *p<0.05.

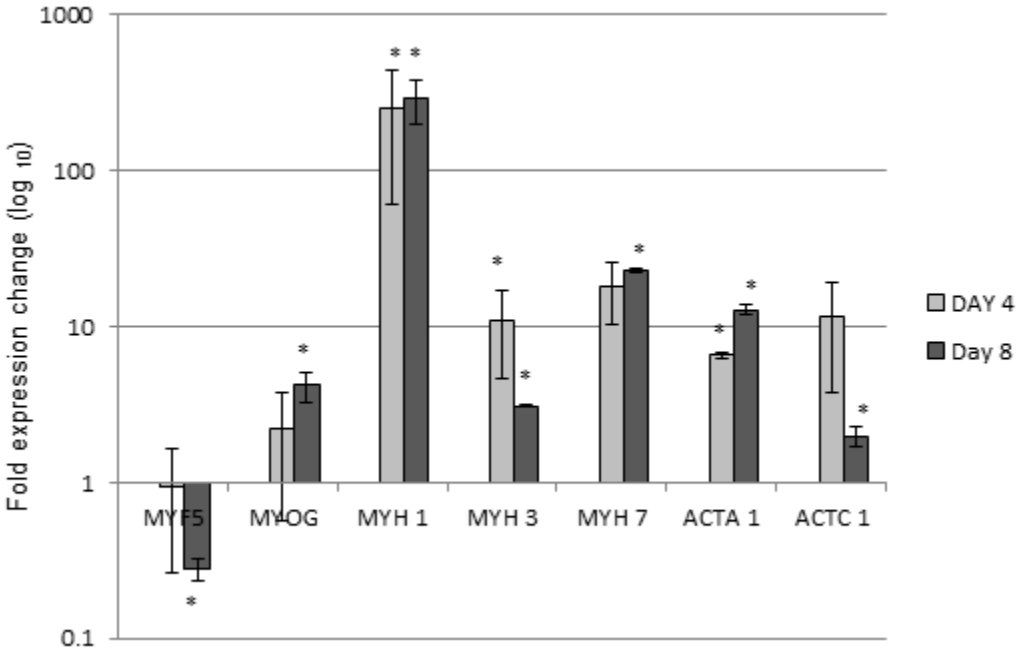

Figure 4.12. Quantitative real-time PCR was used to determine the expression of seven differentiation markers in differentiating C2C12 cells grown on solubilised muscle matrix at days 1, 4 and 8 of differentiation. C2C12 cells (3.5×10^3 cells/cm^2) were added in wells of a 24-well plate coated with solubilised muscle matrix (10 µg/cm^2) and cultured for 4 days in serum-free proliferation medium and for a further 8 days in differentiation medium. RNA was isolated from cells at day 1, day 4 and day 8 of differentiation. Relative expression levels for *MYF5, MYOG, MYH1, MYH3, MYH7, ACTA1, ACTC1* were normalized to the C_t value of the reference gene (*SDHA*) and fold change was determined using $2^{-\text{delta delta}}$ C_t method. Day 4 and Day 8 expression levels were normalized to Day 1 and $\log_{10}$ transformed. Mean ± SE of 4 biological replicates are shown. Wilcoxon's T-test was performed and significance (p) values shown at each time point. *p<0.05.

proliferating at day 3 after seeding on the intact acellular muscle matrix, in serum free proliferation medium (Fig 4.13. a). The three-dimensional colour coded image of the muscle scaffold provided evidence that the cells were distributed up to a depth of 138 μm into the muscle scaffold (Fig 4.13 b). Six days after switching to differentiation medium (i.e day ten of culture) the EdU assay was repeated and in contrast to proliferation day 3, the nuclei were elongated and there were no proliferating (EdU staining) cells present, which suggests that the cells ceased proliferation and were differentiating (Fig 4.13 c).

The Kwik Diff dye system (section 2.7.10), which stains both cell nuclei and cytoplasm, was used to stain C2C12 cells cultured on intact acellular muscle matrices for 7 -14 days in serum free proliferation medium. This revealed that the myoblasts became organised on the 3D matrix scaffolds lining up longitudinally, presumably along tracts of ECM material (Fig 4.14. a-b). C2C12 myoblasts organized in a circular pattern where the EMC had been cut in transverse section (Fig 4.14 c).

4.2.6 Human skeletal muscle myoblast (HSMM) behaviour on solubilised muscle matrix and collagen I (section 2.7.5.2)

The ability of a solubilized muscle matrix substrate to support the adhesion and growth of HSMMs was compared to a collagen I substrate. The HSMMs adhered to the muscle matrix, spread and expressed desmin after only a day in culture. In contrast, on collagen I the HSMMs did not express desmin at this time although a little desmin expression is evident at day 4 (Fig 4.15. a, b & c). In addition, the EdU assay indicated that more cells were proliferating on the muscle matrix substrate than on collagen I and desmin staining was more pronounced in those cells on the muscle matrix than on collagen I (Fig 4.15 b, d).

To determine whether cell density plays a key role in determining the differentiation pattern, HSMM cells were cultured at two different cell densities: $6x10^3$ cells/cm^2 and $15x10^3$ cells/cm^2 on collagen I and solubilized muscle matrix coated surfaces for 4 days in SkGM-2 proliferation medium and then for further 6 days in differentiation medium. Six days after switching to differentiation conditions at the lower seeding density only a

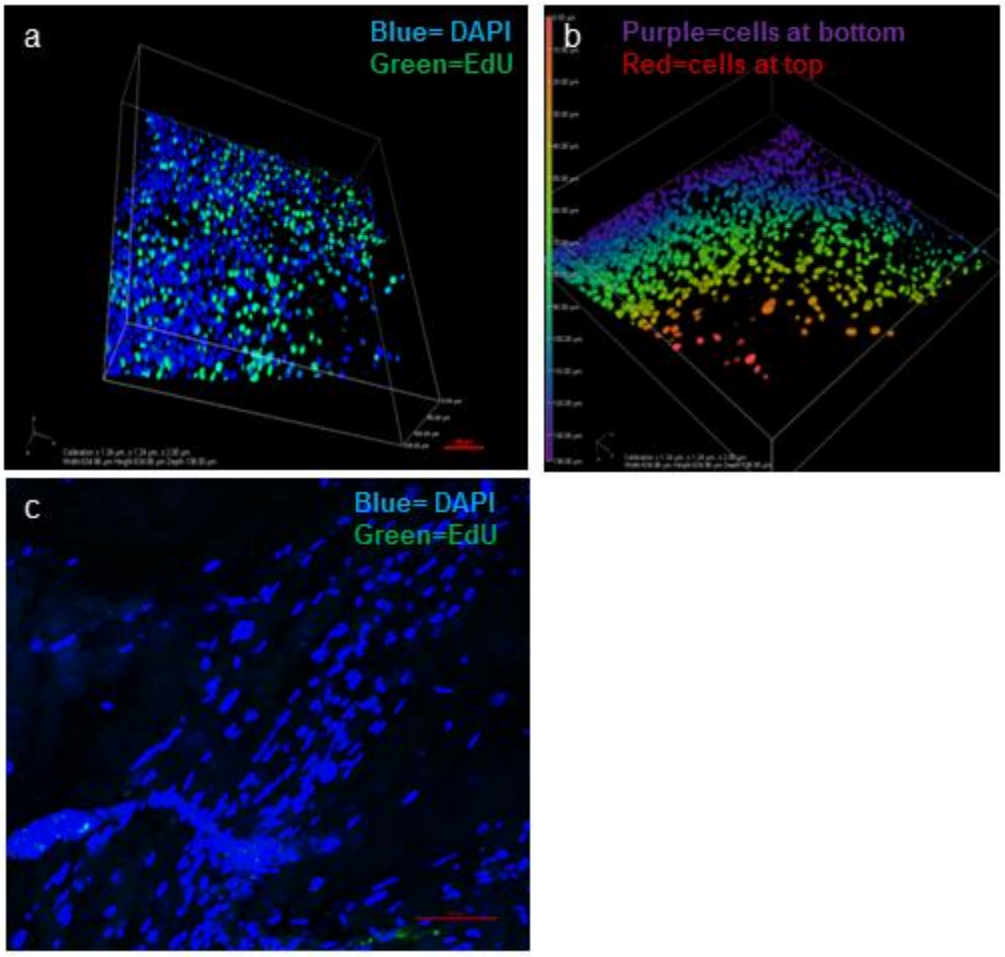

Figure 4.13. Proliferation and migration of C2C12 cells on decellularised whole muscle ECM. The click-iT EdU assay was performed on C2C12 myoblasts ($5x10^4$ cells/scaffold) cultured for 3 days in serum free proliferation medium (a) 3D image of proliferating C2C12 myoblasts; (b) The colour coded image shows the distribution and migration of cells into the scaffold after 3 days; (c) The EdU assay was performed on cells cultured for 3 days in proliferation medium and then followed by 6 days in differentiation medium. scale bar-100 µm, Nuclei are stained with DAPI (blue) (proliferating cells – green, all cells – blue).

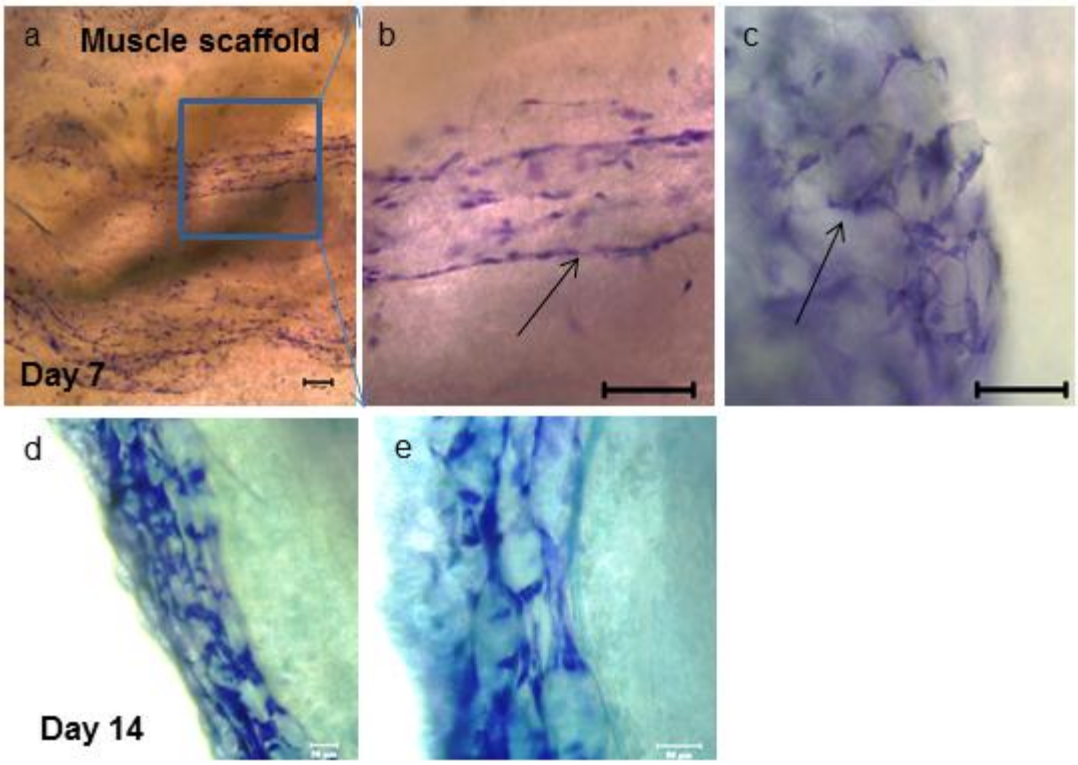

Figure 4.14. Three-dimensional culture of C2C12 cells on whole muscle scaffolds. C2C12 myoblasts ($5x10^4$ cells/scaffold) were grown for 14 days on decellularised whole muscle scaffolds ($1mm^2$) in serum free proliferation medium, stained with either Kwik-Diff or DAPI and imaged using bright field microscope (Zeiss-Axiovert). Scale bars 100 µm for (a-c) and 50 µm for (d-e). Cells appear purple in colour (a-e).

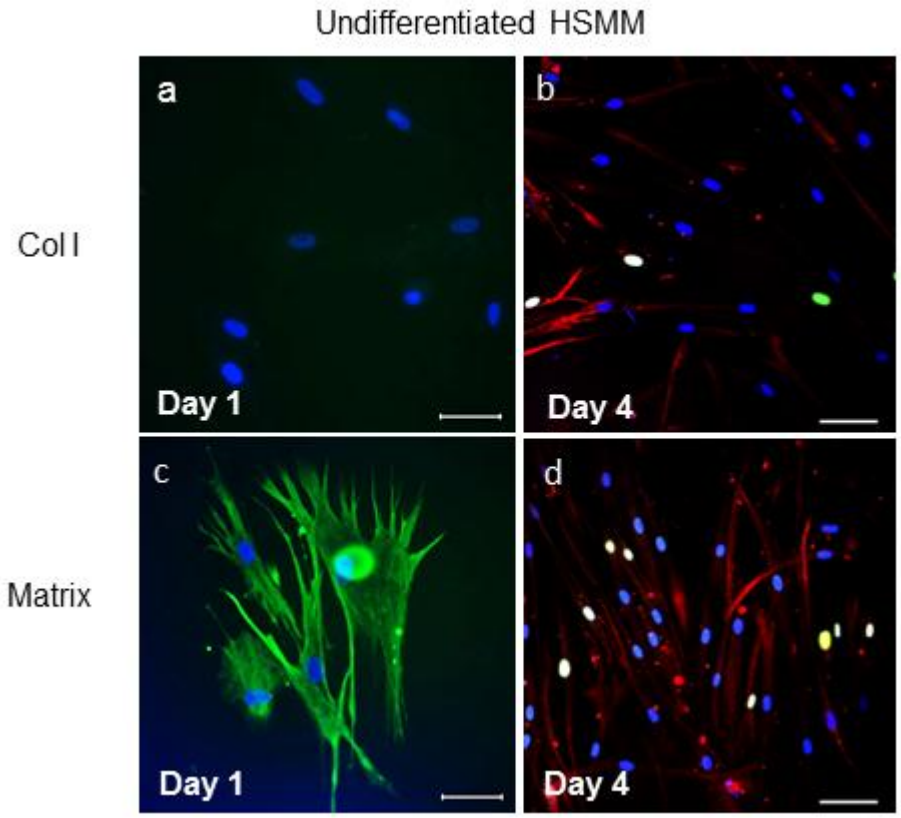

Figure 4.15. Human skeletal muscle myoblasts (HSMM) cell adhesion and proliferation on collagen I and muscle matrix. HSMMs ($5x10^4$) were cultured for 1 and 4 days in SkGM-2 medium on collagen I (10 µg/cm^2) (a-b) and matrix (10 µg/cm^2) (c-d) respectively, stained for desmin (green) (a, c) and desmin (red) + EdU (green) (b, d) and imaged using Zeiss Axioskop fluorescent (a, c) and Nikon A1 confocal microscope (b, d). Nuclei are stained with DAPI (blue). The antibody recognising desmin was a mouse monoclonal (DE-U-10) antibody. The secondary antibody used was a goat anti-mouse alexafluor 488 and 546 conjugated for (a, c) and (b, d) respectively. Scale bar- 50 µm for a, c and 100 µm for (b, d). (Proliferating cells – green, white and yellow, all cells – blue, desmin-green for a, c and red for b, d).

few myotubes expressed myosin on the matrix coated substrate, however, no myosin expressing myotubes were visible on collagen I coated surfaces (Fig 4.16 a, c). On the contrary, at the higher seeding density several multinucleated parallel myosin expressing myotubes were visible on both collagen I and muscle matrix coated surfaces (Fig 4.16. b, d).

4.2.7 HSMM cell adhesion on three dimensional muscle matrix scaffolds

Decellularized 3D rat matrix scaffolds were also used as substrate to test adhesion, spreading and viability of HSMM cells **(**section 2.7.9**)**. It was found that HSMM cells cultured for 2 weeks on decellularised (3D) matrix scaffolds grew along tracts of ECM (Fig 4.17 a-b) and Phalloidin staining after 3 days in culture indicated they were well spread with elongated F-actin fibres (Fig 4.17 c). Six days after switching to differentiation medium, nuclei became elongated and uniformly oriented suggesting cells were committed towards a differentiation lineage (Fig 4.17 d).

4.2.8 Immunostaining for secreted ECM proteins under serum free culture (section 2.11.2)

To determine whether C2C12 cells synthesize and secrete ECM proteins under serum free culture conditions, C2C12 cells were grown on etched glass coverslips for 3 days in proliferation medium and 6 days in differentiation medium and immunostained using antibodies against collagen type I, collagen type IV, fibronectin and perlecan (Fig 4.18). Undifferentiated cells secreted large amounts of all four matrix proteins and the staining pattern was similar for all four matrix protein antibodies. However, the arrangement of the matrix proteins was different in the differentiated myotubes when compared to the undifferentiated cell population (Fig 4.18). Collagen type I and IV were found distributed around the length of the myotubes while fibronectin appeared in a filamentous web-like pattern along the surface of the myotubes. Perlecan was distributed along the edges of the myotubes; on some myotubes the staining was quite intense but on others the staining appeared weak.

4.2.9 Immunostaining for Matrix deposition after cell removal (section 2.11.2)

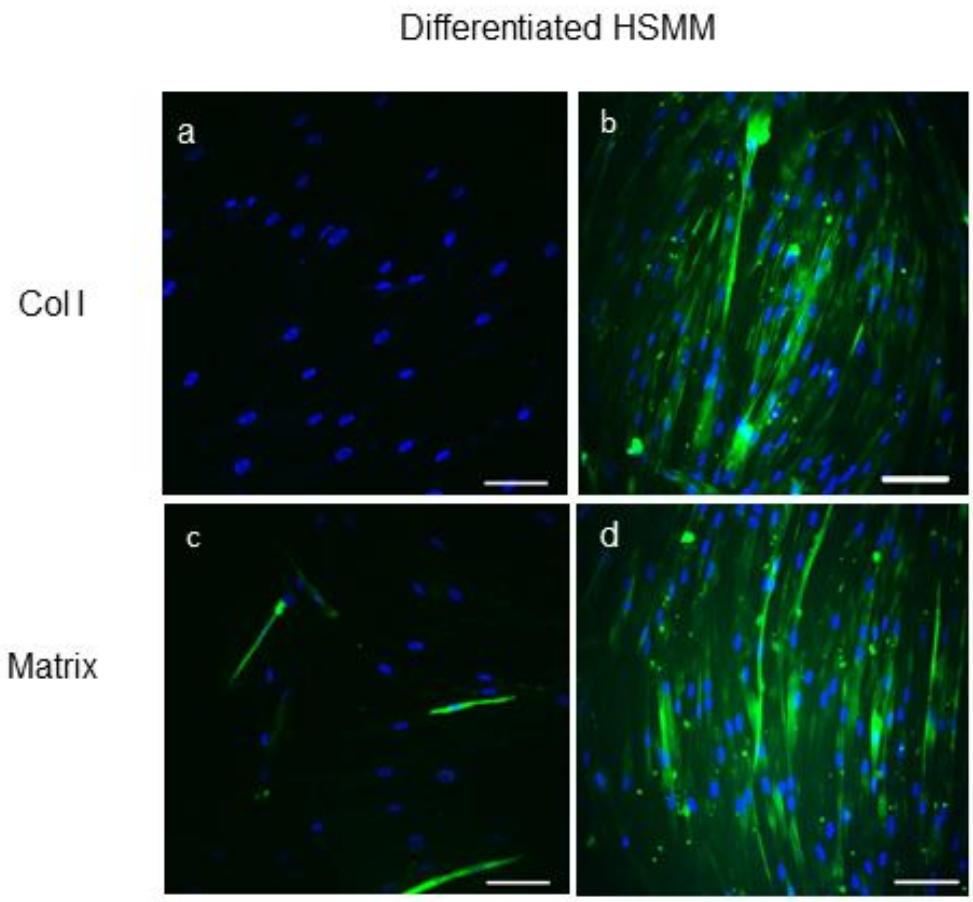

Figure 4.16. Immunostaining for myosin on differentiated HSMMs on collagen I and muscle matrix coated surfaces. HSMMs were seeded at two different densities, $6x10^3$ cells/cm^2 for (a, c) and $15x10^3$ cells/cm^2 for (b, d) on collagen type I and solubilized muscle matrix and cultured for 4 days in SkGM-2 proliferation medium. Then the medium was changed to a differentiation medium containing 2% HS and cells were cultured for another 6 days. Post-differentiation, cells were fixed with 4% paraformaldehyde and stained with myosin (green) and imaged using Nikon A1 confocal (a, c) and a Zeiss Axioskop fluorescent (b, d) microscope. The antibody recognising myosin was a mouse monoclonal (NOQ7.5.4D) antibody. The secondary antibody used was a goat anti-mouse alexafluor 488 conjugated antibody. Nuclei are stained with DAPI (blue). Scale bar- 100 µm for a-d.

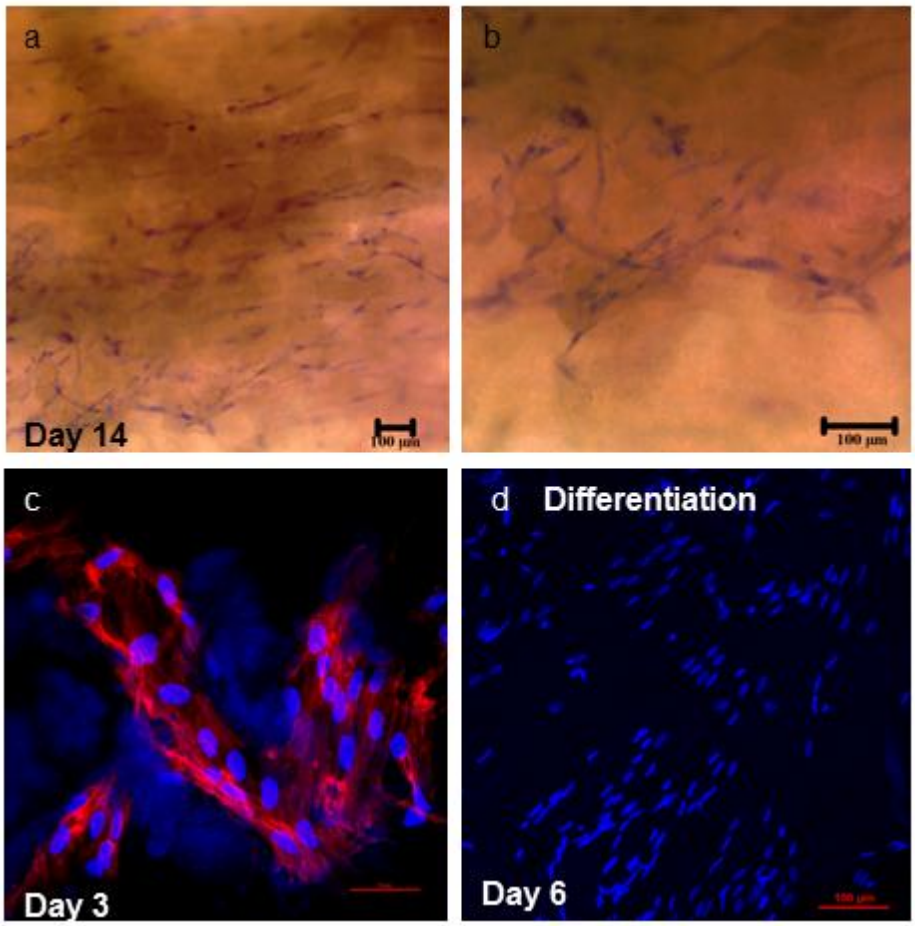

Figure 4.17. Three-dimensional culture of human skeletal muscle myoblasts (HSMMs) on whole muscle scaffolds. HSMMs ($5x10^4$ cells/scaffold) were cultured for 14 days on decellularised whole muscle scaffolds in SkGM-2 medium, stained with Kwik Diff and imaged using bright field microscopy (a, b). HSMMs were cultured for 3 days in SkGM-2 medium, stained with rhodamine phalloidin for F-actin (red) and DAPI (blue), and imaged using Nikon A1 confocal microscope (c-d). Scale bar 100 µm a, b and d, 50 µm for c.

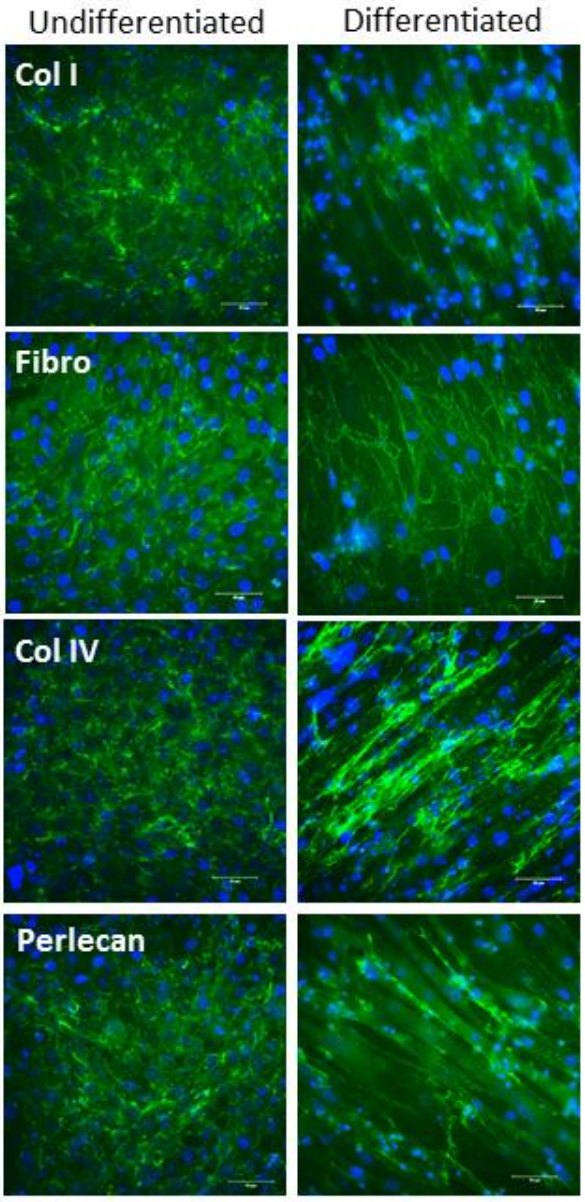

Figure 4. 18. Secretion and orientation of matrix proteins by C2C12 cells under serum free conditions on etched glass. C2C12 cells ($3.5x10^3$ cells/cm^2) were seeded on etched glass coverslips ($13mm^2$) in the wells of a 12-well plate and cultured for 3 days in serum free proliferation medium. After 3 days, the media was changed to a serum free differentiation medium and cells were cultured for another 6 days. Coverslips were fixed and stained with antibodies recognising Collagen I, Fibronectin, Collagen IV and Perlecan which were all rabbit polyclonal antibodies. Secondary antibody was a goat anti-rabbit alexafluor 488 conjugated for all primary antibody. Nuclei are stained with DAPI (blue). Scale bar-50μm.

To determine the pattern of matrix protein deposition on glass surface, C2C12 cells were cultured on etched glass coverslips for 3 days in proliferation media and then the cells were removed using 20mM NH_4OH/0.5% TX-100 in PBS (section 2.11.2) (Figure 4.19). No DNA remnants were found on the coverslips as evidenced by the absence of DAPI staining. Immunostaining was then performed for the ECM proteins collagen type I, collagen type IV, fibronectin and perlecan. Clear staining was observed for all four matrix protein antibodies, although the staining intensity was lower when compared to that seen when the cells were on the coverslips (compare Fig 4.18 and 4.19). Collagen I staining was patchy and it appeared that collagen I was deposited in a straight line pattern. Collagen IV, perlecan and fibronection staining patterns were similar with an interconnected net like pattern on the surface of the glass (Fig 4.19).

4.2.10 Immunostaining for secreted ECM proteins on collagen type I and solubilised muscle matrix coated etched glass substrates (section 2.11.2)

To determine whether C2C12 cells synthesize and secrete different amounts of ECM proteins on collagen type I and solubilised muscle matrix under serum free culture conditions, C2C12 cells were grown on etched glass coverslips for 3 days in proliferation medium and immunostained using antibodies against collagen type IV and fibronectin (Fig 4.20). Immunostaining revealed patchy staining for fibronectin and collagen type IV on solubilised muscle matrix coated coverslips suggesting presence of both these matrix molecules in the matrix extract (Fig 4.20 a, d). C2C12 cells secreted similar amounts of fibronectin on both collagen type I and solubilised musscle matrix coated substrates as the fibronectin staining intensity appeared similar on both substrates (Fig 5.20. b, c). However, collagen type IV staining was stronger when the cells were cultured on muscle matrix coated substrates when compared to that seen when the cells were cultured on collagen I substrate (Fig 5.20. e, f).

4.3 Discussion

This chapter provides a first report where a serum free culture system has been used to promote myoblast proliferation and differentiation on solubilized and three-dimensional

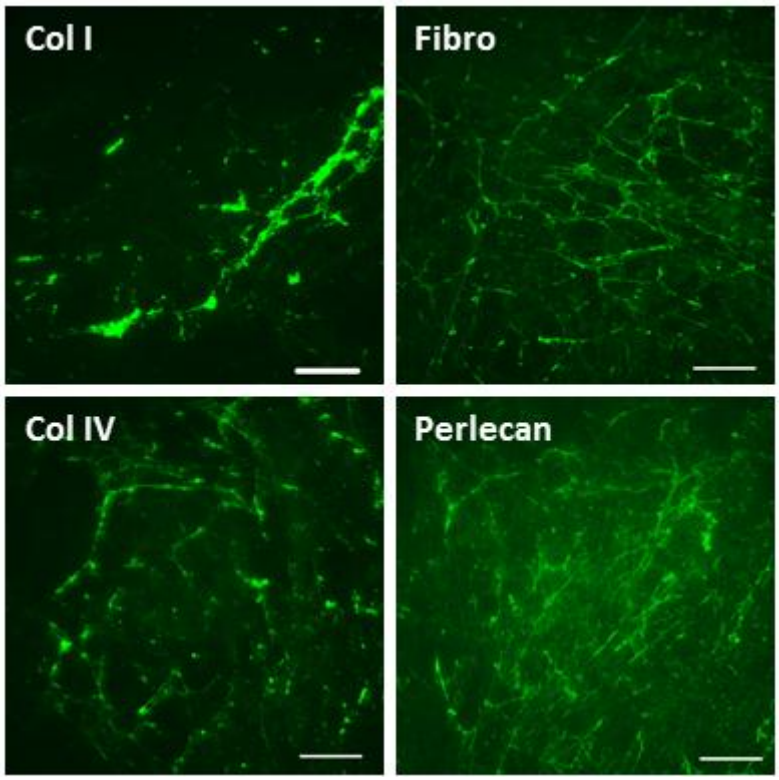

Figure 4.19. Secretion and deposition of matrix proteins by C2C12 cells under serum free conditions on etched glass. C2C12 cells ($3.5x10^3$ cells/cm^2) were seeded on etched glass coverslips ($13mm^2$) placed in the wells of a 12-well plate and cultured for 3 days in serum free medium. After 3 days, the cells were stripped using NH_4OH/TX-100 and coverslips were fixed and stained with antibodies recognising Collagen I, Fibronectin, Collagen IV and Perlecan which were all rabbit polyclonal antibodies. Secondary antibody was a goat anti-rabbit alexafluor 488 conjugated antibody. Nuclei are stained with DAPI (blue). Scale bar-50μm.

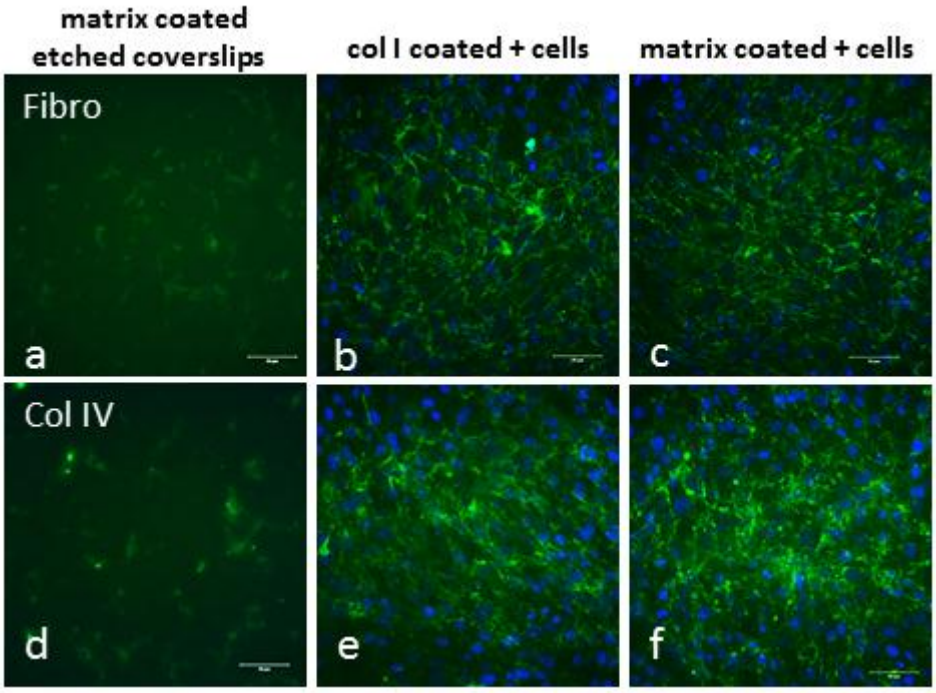

Figure 4.20. Secretion of matrix proteins under serum free conditions on collagen I and solubilized muscle matrix on etched glass. C2C12 cells ($3.5x10^3$ cells/cm^2) were seeded on etched glass coverslips placed in wells of a 24-well plate coated with either collagen I (b, e) (10 µg/cm^2) or solubilised muscle matrix (c, f) (10 µg/cm^2), and cultured for 3 days in serum free medium. Coverslips were fixed with 4% paraformaldehyde and stained with the antibodies against fibronectin (a-c) and Collagen type IV (d-f), both rabbit polyclonal antibodies. Secondary antibody used was goat anti-rabbit alexafluor 488 conjugated for both primary antibodies. Nuclei are stained with DAPI (blue). Scale bar-50 µm. Coverslips without cells (a, d), coated with solubilised muscle matrix and stained for Collagen type IV and fibronectin were used as positive controls.

skeletal muscle matrices. In the serum free system C2C12 mouse myoblasts proliferated on a muscle matrix substrate prepared from solubilized acellular muscle, but seemed to progress towards differentiation at a lower confluency when compared to C2C12 cells cultured on collagen I and fibronectin coated surfaces. Gene expression data of a selection of genes covering different aspects of the differentiation pathway suggest a similar differentiation pattern on muscle matrix and fibronectin and visually the alignment of myosin expressing myotubes on muscle matrix and fibronectin are comparable. Furthermore, three-dimensional acellular muscle matrix supported cell growth and migration and also provided physical and chemical signals for cell alignment/orientation, suggesting that *in vivo* it is the muscle ECM that directs cell positioning. The serum free system used here has removed any possibility that soluble ECM molecules in the culture medium have affected cell behaviour, or have modulated the contribution of the matrix protein substrates to myoblast differentiation.

A number of transformed cell lines such as mouse C2C12 and rat L6 have been routinely used to investigate underlying molecular mechanisms of myoblast fusion and myotube formation [275-277]. Furthermore, these cell types have also been useful to screen drugs against metabolic syndromes [278] and inflammatory muscle diseases [279]. The advantages of using these cell lines over primary muscle myoblasts are their easy availability, and ability to grow indefinitely for a longer period of time. In recent years two groups have reported the growth and differentiation of C2C12 myoblasts on solubilized skeletal muscle ECM [174] [175]. DeQuach et al (2010) used SDS to decellularise porcine muscle and demonstrated retention of collagens, fibrinogen, fibrillin-1 and -5, the proteoglycans decorin, and HS GAGs [174]. Stern et al (2009) used trypsin and Triton X-100 to decellularise quadriceps and hamstring muscle [175]. Both studies reported better differentiation as measured by increased myotube size and more nuclei per myofibre in cells cultured on substrates of decellularised muscle matrix compared to collagen I substrates. However, care must be taken in interpreting these studies as both used media supplemented with foetal bovine serum (FBS) for proliferation and horse serum (HS) for differentiation. These sera add an ill-defined mixture of growth factors and ECM proteins to the medium, therefore assessing the

ability of acellular muscle ECM to support myoblast proliferation and differentiation in the presence of serum introduces confounding factors.

In this study, the ability of a skeletal muscle derived ECM to support myoblast growth and differentiation was assessed using defined serum free medium in two-dimensional and three-dimensional cultures. This enabled the muscle matrix to be compared to purified collagen I and fibronectin in the absence of confounding variables. We found under our serum free conditions C2C12 myoblasts adhered to, and maintained their characteristic stellate shape, on substrates of fibronectin, collagen I and solubilised muscle matrix (Fig 4.1). However, C2C12 myoblast proliferation was slower on muscle matrix, and plateaued at day 4; whereas proliferation on collagen I and fibronectin continued until day 6, such that the number of cells on the pure matrix protein substrates was approximately 1.5 times that on muscle matrix (Fig 4.2). It is possible the slower growth and earlier plateau in cell number on the muscle matrix substrate was due to adult muscle-specific factors in the matrix substrate that directed the cells to differentiate, even though the growth factors in the medium were designed to stimulate proliferation. Slow proliferation is not necessarily a disadvantage, as it may allow time for the cells to become organised and aligned prior to differentiation. The work of Ricotti et al (2012) [280] supports this suggestion. They evaluated the proliferation and differentiation of two myoblast cell lines on synthetic substrates comprising electrospun poly (hydroxybutyrate) (PHB) sub-micron fibers either highly oriented or randomly aligned, or films of PHB. They demonstrated that myoblasts proliferated more slowly but differentiated to form longer myotubes expressing higher levels of the genes characteristic of a differentiated phenotype when grown on PHB aligned nanofibres compared to randomly aligned nanofibres or PHB films [280].

In our study immunofluorescent analyses revealed MyHCB was expressed in C2C12 myotubes in serum free media on days 4 and 6, with striations apparent by day 6, indicating the formation of sarcomeres (Fig 4.4). Myotubes appeared to thicken from day 4 to day 6 on substrates of collagen and muscle-matrix but this was not statistically significant (Fig 4.5). Myotubes on collagen I substrate were randomly oriented, whereas myotubes at day 6 of differentiation were better aligned with less branching on

fibronectin and matrix coated surfaces. The alignment of myotubes is an important pre-requisite to form a functional muscle. Parallel alignment of myotubes could potentially enhance myotube striations and promote better differentiation [281]. Others have described C2C12 cells cultured on fibronectin substrates as elongating, aligning and fusing earlier than cells cultured on laminin and gelatin (denatured collagen) coated substrates [282]. Vaz et al (2012) performed the time-lapse imaging of C2C12 cells cultured on fibronectin and gelatin coated surfaces and found that C2C12 cells on fibronectin coated surfaces migrated further and with 'directionality', whereas cells on gelatin moved randomly [282]. It is expected that directional migration will assist cell alignment and hence myotube formation.

Our results were in agreement to the previous studies where C2C12 cells have been cultured on muscle matrix coated surfaces [174, 175]. Both studies reported increased myotube size and more nuclei per myofibre in cells cultured on decellularised muscle matrix compared to collagen I although De Quach et al (2010) reported no difference in the number of myotubes on both surfaces [174] while Stern et al (2009) reported fewer myotubes on muscle matrix coated surfaces [175]. To form a functional muscle, contractility of the myotubes is an essential phenomenon as this is a key function of muscle cells *in vivo*. In our studies, although the myotubes were not electrically stimulated to generate active contractile force, they were able to generate unidirectional spontaneous contractions, clearly suggesting the functionality of myotubes under serum free culture conditions (data not shown). It was difficult to maintain myotubes in culture beyond 8 days as myotubes cultured on rigid glass substrates have a greater tendency to detach from the surface due to sustained actinomyosin contractions [283].

A number of genes are involved at different stages of muscle differentiation and we chose to investigate a selection of genes that spanned differentiation from myoblasts through to myotubes. Myogenic regulatory factors (MRFs) are transcription regulators that control the process of muscle differentiation. *Myf5* is the first regulatory factor to be expressed during mouse embryogenesis and is a marker of committed satellite cells and myoblasts, whereas *myogenin* is more directly involved in the differentiation process and triggers the expression of myotube specific genes [197]. Myosin, the muscle

contractile protein, consists of four light chains and two heavy chains. Myosin heavy chain exists in different isoforms: *MYH3* is an embryonic form whereas *MYH1* and *MYH7* are adult isoforms, *MYH1* being present in fast-twitch fibres and *MYH7* is in slow-twitch muscle fibres [284, 285]. Cardiac actin (*ACTC1*) is expressed during early differentiation of skeletal muscle and is then down regulated as skeletal muscle alpha actin (*ACTA1*) is expressed [286]. Muscle alpha actin is the major actin isoform in muscle and is classified as a late differentiation marker [284].

The myoblast marker, *Myf5,* was expressed when the gene expression profile of the differentiation markers was first assessed at differentiation day 1, as expected (Fig 4.10-4.12), and showed no change over time in C2C12 myoblasts cultured on collagen I, but decreased by day 8 in myoblasts cultured on muscle-matrix and fibronectin. This is consistent with Brown et al (2012) who found that *Myf5* decreased in C2C12 cells as differentiation proceeded [287]. These authors also found *MYOG* levels increased when C2C12 cells were placed in differentiating conditions, but decreased as the cells became well differentiated, which is similar to our findings of *MYOG* expression levels in C2C12 cells on collagen and fibronectin (Fig 4.10 and 4.11). Wilschut et al (2010) measured the mRNA levels of *Myf5* and *MYOG* genes of primary porcine muscle stem cells cultured on different ECM substrates: collagen I, laminin, fibronectin, gelatin and Matrigel [288]. They found the expression of *Myf5* decreased with cell differentiation regardless of substrate; in contrast the pattern of *MYOG* expression in cells on Matrigel differed markedly. On Matrigel, *MYOG* expression increased in a time dependent manner being significantly higher than that measured from cells cultured on the other substrates at day 5 of differentiation [288]. It is not possible to equate C2C12 cells with primary porcine muscle stem cells in terms of their differentiation, but notably on muscle matrix substrates we similarly found *MYOG* expression levels to be increasing as differentiation progressed (Fig 4.12). Like our solubilised acellular muscle matrix, Matrigel is a complex mixture of ECM proteins obtained from basement membrane extracts of the murine EHS tumor [289]. Stern et al (2009) measured the expression levels of myogenin protein and found the protein levels to be higher in C2C12 cells cultured on skeletal muscle matrix coated surfaces than on uncoated surfaces and this

increased from day 1 to day 3 of differentiation [175]. It is interesting that *MYOG* null (*MYOG*$^{-/-}$) myoblasts that cannot differentiate *in vivo* form myotubes as efficiently as wild-type myoblasts when in tissue culture on a gelatin substrate [290]. These data suggest *in vitro* the requirements for myogenin are not as stringent as they are *in vivo,* and possibly factors in complex matrices act to maintain expression of this protein further into the differentiation pathway than is usually seen *in vitro*.

The mRNA levels for other early differentiation markers, *MYH3* and *ACTC1,* was found to have increased at day 4 of differentiation on all three surfaces, but decreased by day 8 and the drop in expression was more pronounced on muscle matrix and fibronectin substrates than on collagen I substrates (Fig 4.10-4.12). It is thought that *Myf5* initiates the expression of *MYH3* and MyoD enhances *MYH3* expression. MyoD is expressed slightly later than *Myf5,* appearing in myoblasts and myocytes but decreasing markedly in myotubes [197]. It therefore might be expected that the decrease in *Myf5* expression is followed a day or two later by a corresponding decrease in *MYH3* expression and this is what was observed by Brown et al. (2012) in their study with C2C12 cells [287]. The time points of our study do not allow such a detailed interpretation, but our data with cells grown on fibronectin and muscle matrix are consistent with that earlier report [287]. Interestingly, an early peak in *MYH3* expression followed by only a slight decline was also observed in human muscle myoblasts cultured on gelatin substrates [284], which is consistent with our data for cells on collagen I. The decrease in *ACTC1* expression levels by day 8 on all three surfaces is probably associated with an increased expression of other actin isoforms, a conclusion that is supported by the expression pattern observed for *ACTA1* on all substrates (Fig 4.10-4.12).

Expression of myosin (*MYH1*) and (*MYH7*) and skeletal muscle actin (*ACTA1*) increased in a time dependent manner suggesting the maturation of myotubes, but the increase in *MYH1* expression at day 4 was higher on muscle matrix than on collagen I or fibronectin which suggests that myotubes on muscle matrix are transiting faster towards a more differentiated phenotype. Thus, like Brown et al (2012) concluded from their study of the expression patterns of 6 myosin heavy chain isoforms during C2C12 cell differentiation [287]; our data also shows a temporal pattern of expression. The

expression levels of *MYH3* and *ACTC1* peak early and then decline whereas *MYH1*, *MYH7* and *ACTA1* are expressed either at increasing levels at day 8 or at the same level as day 4. A difference between our data and their study was in the expression levels of *MYH7;* they observed similar declines in *MYH7* and *MYH3* expression over the same time frame, and hence grouped *MYH7* with the "early" expressing isoforms [287]. From our data grouping *MYH7* with adult isoforms is appropriate and this is a better fit with the known *in vivo* expression patterns of these myosin heavy chain genes. It is possible that culturing C2C12 cells on matrix proteins directs gene expression to fit more closely with what occurs *in vivo*.

Solubilization of an ECM destroys the positional information provided to cells by the location of molecules in an intact matrix, and may also disrupt protein-protein interactions which influence protein conformation. To examine how an intact muscle matrix affects C2C12 and HSMM cell proliferation and differentiation, we seeded acellular matrices with well-preserved 3D structure with C2C12 cells and HSMMs in serum-free medium (Fig 4.13-4.14 and 4.17). Interestingly, the C2C12 myoblasts lined up longitudinally, or organised into circular patterns, depending on the alignment of the endomysial matrix "tubes" that *in vivo* surround the muscle fibres. Thus, particular matrix proteins were providing cues to direct myoblast adhesion and spreading in specific locations on the acellular matrices (Fig 4.14). Similarly, HSMMs were also well spread with elongated actin fibres (Fig 4.17). A recent study described the lack of full functional recovery of volumetric muscle injuries in rats treated with muscle autografts and it was suggested this may have been because no attention was paid to the alignment of the grafts in accordance with the muscle fibres in the injury bed [291]. Our data indicates that myoblasts are directed by matrix signals to align in certain ways and if autografts are incorrectly orientated then cell positioning on these grafts will also be incorrect for the regeneration of a contracting muscle. Others have used acellular muscle matrix as grafts and describe the population of these matrices by host cells that are induced to differentiate into multinucleated myofibres [292]. In a similar study both blood vessels and myofibres were seen to penetrate further into the acellular scaffold as time progressed, but full function was not achieved 42 days post grafting [25]. We also

saw myoblast migration into the acellular matrices in our *ex vivo* cultures as well as evidence of differentiation. All these studies illustrate the importance of the ECM in directing myogenesis.

The significance of cell-matrix interactions in the formation of functional muscle tissue is also illustrated by the work of Hinds and colleagues (2011) [218]. Engineered muscle bundles were cultured on Matrigel substrates of varying concentrations of matrigel (10%, 20%, 30% and 40%) and two matrix proteins: collagen I and fibrinogen. They studied several parameters for muscle contractility including contractile force measurements and kinetics. Results showed a maximum force generation using fibrinogen and 40% matrigel combination. Further, they also measured the tetanic force of the engineered muscle bundles cultured on: (a) standard Matrigel and (b) growth factor reduced (GFR) Matrigel containing reduced levels of IGF-1, PDGF and TGF-β and found that there were no significant differences in the tetanic force kinetics. The authors proposed that enhanced force generation was a result of myotube-matrix interactions, possibly by the myotubes binding to laminin (a major component of Matrigel) via α7 integrin [218]. Although measurement of the mechanical properties of the acellular matrix was beyond the scope of our study but considering that laminin α2 chain was preserved in the matrix and cells adhered and proliferated on the 3D matrix, it is possible that the decellularised muscle tissue prepared by our method would assist in the formation of functional muscle if tested *in vivo*.

Due to the inherited genetic anomalies in transformed cell types like C2C12, it is important to use primary muscle cells to provide a more relevant system. Although, primary cells grow more slowly than a cell line and can be maintained in culture for a limited number of passages, they are very relevant for translating basic research to a clinical setting. Hence, HSMMs were also used for functional characterisation of the matrix. Interestingly, HSMMs showed a slight increase in proliferation when cultured on muscle matrix coated surfaces (Fig 4.15). These cells more readily formed myotubes when they were seeded at high density (Fig 4.16). At low cell density ($6x10^3$ cells/cm^2) myotubes were only formed on muscle matrix coated surfaces, however at higher cell densities ($15x10^3$ cells/cm^2) similar no of myotubes were formed on both surfaces. Cell

density plays a key role in regulating skeletal muscle myogenesis as has been reported by previous studies [293, 294]. Kaspar et al (2005) showed that C2C12 cells when seeded at a density of 2.5 x 10^4 cells/cm^2, expressed myogenin and α-skeletal actin at significantly higher levels than cells seeded at 0.3 x 10^4 cells/cm^2 [293]. Lindon et al (2001) investigated the induction of myogenin gene expression at high (4 x 10^4 cells/cm^2) and low cell densities (0.4 x 10^4 cells/cm^2) and demonstrated that induction of myogenin was inhibited by Myf5 at a lower cell density [294].

Our serum free medium supported excellent C2C12 cell growth and C2C12 cells were found to secrete major ECM proteins (Fig 4.18-4.19). Secreted ECM proteins play an important role in muscle differentiation as shown by Chan et al (2007) [295]. They conducted a proteomic study on C2C12 cells cultured in a serum free medium to elucidate the proteins secreted during myogenic differentiation. In total, 80 non-redundant proteins were identified, out of which 27 were secreted proteins. The majority of the secreted proteins were ECM proteins and proteoglycans including fibronectin, pro-collagen isoforms, biglycan, heparan sulphate and various matrix metalloproteinases (MMPs) [295]. We obtained similar results: immunocytochemical analyses revealed the secretion of collagen type I, collagen type IV, fibronectin and perlecan after three days in serum free medium. A decrease in immunostaining was observed for all the ECM proteins tested including collagens type I and IV, as the myoblasts differentiated. This observation is in agreement with a previous study by Kuhl et al (1982) which showed that myoblasts have a tendency to produce more collagen than myotubes [296]. The downregulation of perlecan during muscle differentiation has also been reported [297]. Immunostaining showed that C2C12 cells cultured on solubilized muscle matrix and collagen I coated substrates secreted two major basement membrane proteins: collagen type IV and fibronectin (Fig 4.20). An increase in collagen type IV staining intensity was observed when cells were cultured on solubilized muscle matrix coated substrates, compared to those on collagen I, suggesting more deposition of this protein on matrix coated substrates.

4.4 Conclusion

In summary, our results demonstrated the acellular skeletal muscle matrix (prepared in chapter 3) supported proliferation and differentiation of C2C12 murine myoblasts in a serum free culture system both in 2D and 3D *in vitro* cultures.

4.5 Future directions

The primary function of a muscle is to generate active force and thus it would be useful to investigate the active tension generating ability of myotubes formed in this study. Another useful experiment to perform would be to measure the glucose and lactate concentrations in the media to assess the metabolic activity of the cells under serum-free culture conditions.

Chapter 5:

Silk fibroin as a potential biomaterial for human skeletal muscle myoblast differentiation

5.1 Introduction

Artificial ECMs or scaffolds used in tissue engineering frequently contain structural ECM proteins like collagen, fibronectin, elastin, fibrin, and laminin [124] and some scaffolds are comprised entirely of one or more of these ECM proteins. These natural scaffolds have advantages over their synthetic counterparts in that their physiological activities, mechanical properties and biodegradability are similar to natural tissues. However, sourcing these proteins from animal tissues is a major disadvantage if the scaffold is to be used clinically. Silk, a natural biopolymer has emerged as an alternative biomaterial.

In recent years silk, usually obtained from the larvae of various Lepidoptera species, has been used as a potential biomaterial for myoblast growth and differentiation *in vitro*. In one study, silk fibroin was combined with tropoelastin to provide an insoluble biocomposite material with tunable elastic and mechanical properties [298]. The researchers tested the ability of these hybrid materials to support cell growth and differentiation by C2C12 and human mesenchymal stem cell cultures on different silk-tropoelastin composites varying in their protein content. Their findings showed that C2C12 cells proliferated and differentiated much better on substrates having high stiffness and low surface roughness [298]. On the other hand, human mesenchymal stem cells preferred substrates having high surface roughness, high tropoelastin content and more pronounced nano-topographical features [298]. In another study, silk fibroin was blended with polyurethane (PU) in different ratios to make composite films of different tensile strength and mechanical properties. Biocompatibility of the silk fibroin/PU films was tested by C2C12 cell culture and cell adhesion, proliferation and differentiation was examined on these films [299]. As the silk fibroin content increased, the stiffness of the films also increased. The films with the highest silk fibroin content supported better adhesion and myogenic differentiation, which was marked by upregulation of the muscle marker genes: sarcomeric actin and α-actin. Micropatterned spider-silk derived films have also been found to support myoblast adhesion and orientation on structured films [300]. Shen et al (2013) prepared PU scaffold with microchannel patterns and coated it with either silk fibroin or gelatin to give PU/silk fibroin or PU/Gel microchannel films

[281]. Silk fibroin or gelatin coating improved the hydrophilicity of the PU films. Myoblasts seeded on PU/Silk fibroin proliferated at a higher rate and showed better differentiation when compared to myoblasts on the PU/Gel films [281]. When 0.1% sericin, the protein coating the silk fibroin was used as a supplement in a serum free medium to assess muscle cell differentiation, sericin supported less myotube differentiation than cultures in foetal bovine serum with sparsely distributed sarcomeric structures within the myotubes [268]. Silk sutures have also been utilized as support structures on laminin coated polydimethylsiloxane substrates to obtain cylindrical muscle-like constructs called "myooids". These myooids expressed muscle specific proteins, generated active tension upon electric pulse stimulation and possessed a sarcomeric structure [269].

Most of the studies conducted to date evaluating silk biomaterials for their ability to support myogenesis have been done on silk fibroin obtained from *Bombyx mori*. Not much research has been carried out on silk scaffolds obtained from *Antherea mylitta Samia ricini* and *Antherea assamensis*, other species of silkworm. It is only recently that silk fibroin scaffolds derived from other families of silkworm, for example the S*aturniidae* family (which includes *A. mylitta*, *S. ricini* and *A. assamensis*) are gaining attention as an alternative silk biomaterial [138]. Pal et al (2013) prepared silk fibroin 2D films and 3D scaffolds from *S. ricini* [138]. They investigated the molecular composition of the fibroin, its thermal properties and did biochemical characterizations of the scaffolds. SDS-PAGE analysis revealed that silk fibroin from *S. ricini* is a heterodimer of 245 kDa and 205 kDa subunits. The scaffolds showed good thermal stability, "swellability" and were found to be compatible when fibroblasts and human osteoblast like cells were cultured on these scaffolds [138]. Kar et al (2013) solubilised silk fibroin from the gland of *A. assamensis* and evaluated its biochemical and biophysical characteristics [140]. Their results showed that fibroin protein from *A. assamensis* consisted of two polypeptides of 250kDa each linked by disulphide bond. The dissolved fibroin solution attained a random coil structure as revealed by the fourier transform infrared spectroscopy and X-ray diffraction studies [140]. They also tested the cytocompatibility of the 2D matrices by growing MG-63 human osteoblast like cells on

these matrices and obtained favourable outcomes [140].

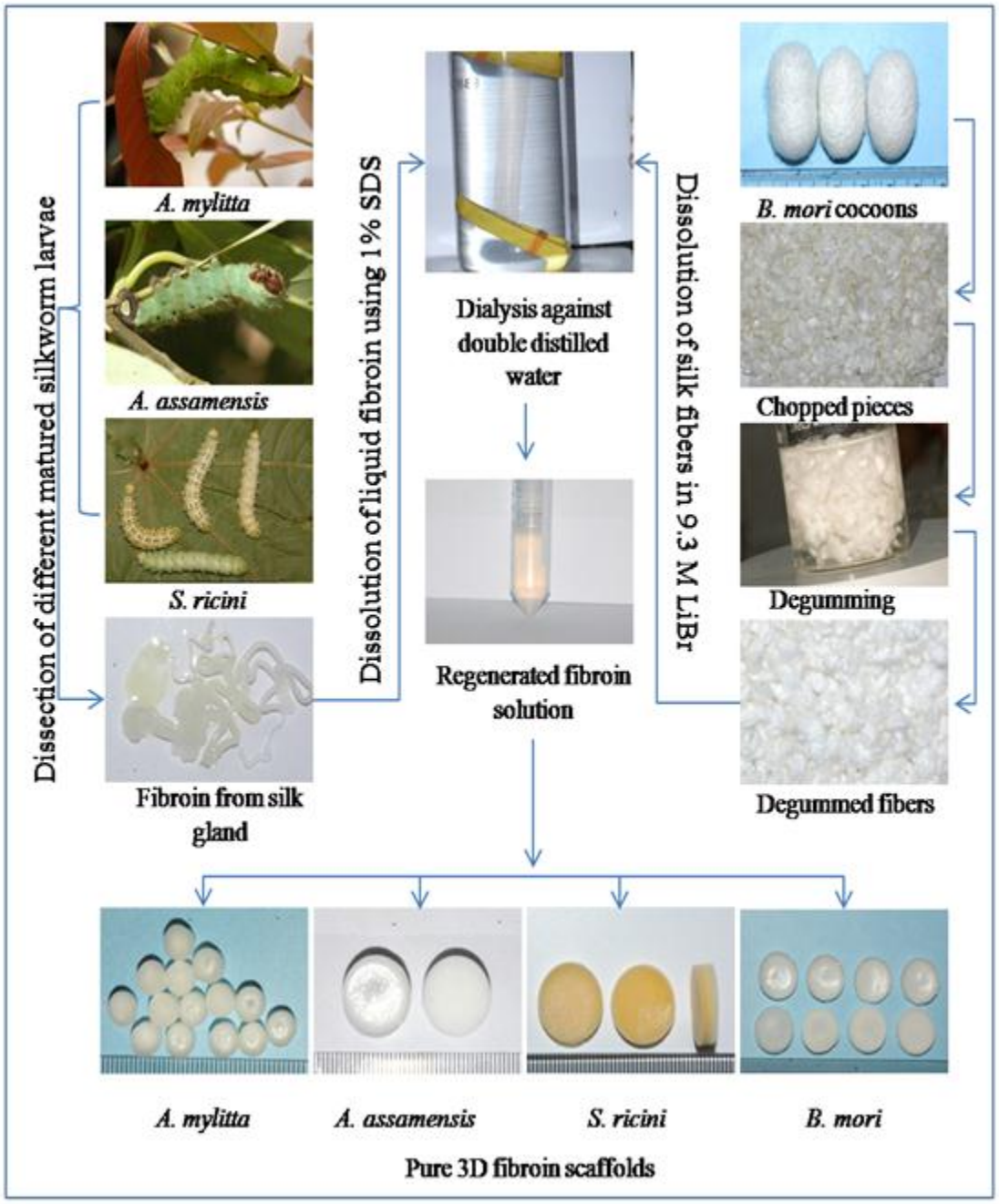

Figure 5.1. Schematic representation of silk protein fibroin isolation from mulberry and different non-mulberry species and preparation of 3D fibroin scaffolds.

Fibroin cryogels from *A. assamensis* have also been tested as a potential biomaterial for liver tissue engineering [147]. Patra et al (2012) investigated the potential of fibroin silk scaffold obtained from *A. mylitta* for preparation of a cardiac patch *in vitro* using neonatal rat cardiomyocytes [141]. Their results indicated that cardiomyocytes attach and spread much faster on *A. mylitta* silk than *B. mori* silk. Furthermore, cells cultured on 3D *A. mylitta* scaffolds expressed connexin 43, exhibited well-organized and aligned sarcomeres and were able to induce spontaneous contractions which lasted for about 20 days in culture [141].

These examples illustrate the usefulness of silk for supporting myoblast growth and differentiation, but no comparative study has been conducted of silk fibroin scaffolds, where the silk has been derived from different insect species (Figure 5.1). This chapter describes the use of four different scaffolds of silk fibroin from the mulberry, *Bombyx mori*, and non-mulberry varieties *Antheraea mylitta*, *Antheraea assamensis/assama* and *Philosamia/Samia ricini* to investigate the attachment, growth, proliferation and differentiation of muscle cells (from both mouse and human) in 2D and 3D cultures.

5.2 Results

5.2.1 Solubilisation of silk fibroin (section 2.9.2)

Briefly, silk fibroin scaffolds were solubilised in PBS for 30 min at 42ºC to give a fibroin solution, which was clarified by centrifugation and the protein concentration of supernatants was measured using a BCA assay (section 2.3.2.1). The scaffolds used for solubilisation were 6 mm in diameter and 3 mm in height. Table 5.1 shows the amount of protein solubilised and the % recovery of solubilised silk fibroin protein/scaffold for each type of silk.

A. assamensis silk gave the maximum amount of solubilised silk fibroin protein with a yield of 2.83 mg which equated to a 72.56 % recovery of the protein in solution. *B. mori* silk was also found to be readily soluble in PBS giving a % recovery of 64.42. *A. mylitta* and *S. ricini* silk scaffolds were found to be the least soluble with % recoveries of 26.9 and 7.5 respectively. All the solubilised proteins were stored at 4ºC until further use.

Interestingly, after 4 days of storage at 4 ºC, *B. mori* silk fibroin at 6 mg/ml formed a gel.

Table 5.1 Solubilised silk fibroin yield from all four silk scaffolds

Type of silk and starting dry weight/ scaffold before solubilisation (mg)	Absorbance at 560 nm	Concentration (mg/ml)	Total yield of solubilised fibroin protein/scaffold (mg)	% recovery
Bm (5.2)	0.533	6.7	3.35	64.42
Am (2.7)	0.117	1.45	0.725	26.85
Aa (3.9)	0.452	5.76	2.83	72.56
Sr (2.3)	0.030	0.35	0.175	7.6

5.2.2 Cyto-compatibility of different silk fibroins in serum-free culture conditions

To assess the ability of solubilised silk proteins to support cell adhesion and cell growth in serum free culture, the murine myoblast cells, C2C12 were cultured on silk fibroin coated plastic dishes in serum free medium for 4 days (Fig. 5.2). Cells maintained their spindle-shaped morphology, adhered to and proliferated well on all 4 silk substrates and by day 4 the cells became confluent on *B. mori*, *A. mylitta* and *S. ricini*, however on *A. assamensis* the cells did not achieve confluency (Fig 5.2). The staining of these cultures with rhodamine phalloidin indicated that F-actin containing stress fibres were oriented in parallel suggesting aligned, elongated cells. This was particularly the case for cells on *B. mori* and *A. mylitta* substrates but less so for cells on *A. assamensis* substrates. On uncoated plastic dishes cells appear rounded in morphology and clustered together (chapter 4, Fig 4.1). The relative number of metabolically active C2C12 cells on these silk protein substrates over a 3-day period was determined by an alamar blue assay (section 2.10.2) (Fig 5.3). At day 1 and 2 after seeding, there was no significant difference in the cell numbers on the different silk substrates or on substrates of the two

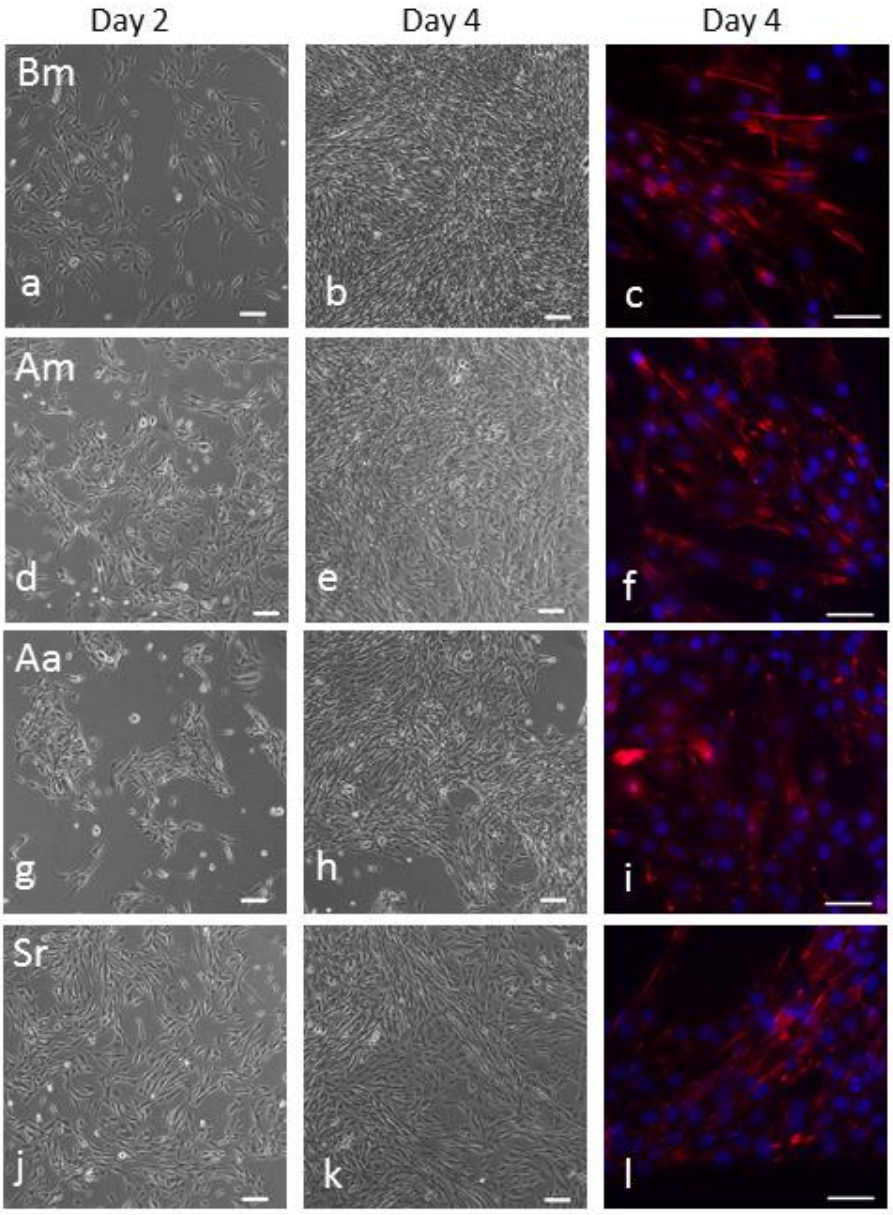

Figure 5.2. Solubilised silk fibroin as a substrate supported C2C12 proliferation under serum free conditions. C2C12 cells ($3.5x10^3$ cells/cm^2) were seeded in wells of a 24-well plate coated with silk fibroin (10 µg/cm^2) and cultured for 4 days in serum free medium. Phase contrast images of proliferating C2C12 cells cultured on Bm (a-b), Am (d-e), Aa (g-h) and Sr (j-k) were captured at day 2 and 4 after seeding with a Zeiss Axiovert bright field microscope at a magnification of 120x using Spot Advanced software. F-actin at day 4 was visualized using rhodamine phalloidin. Images were taken using a Zeiss Axioskop fluorescent microscope. Nuclei are stained with DAPI (blue). Scale bars - 100 µm for a-l. *Am: A. mylitta; Bm: B.mori; Aa: A.assamensis; Sr: S.ricini*

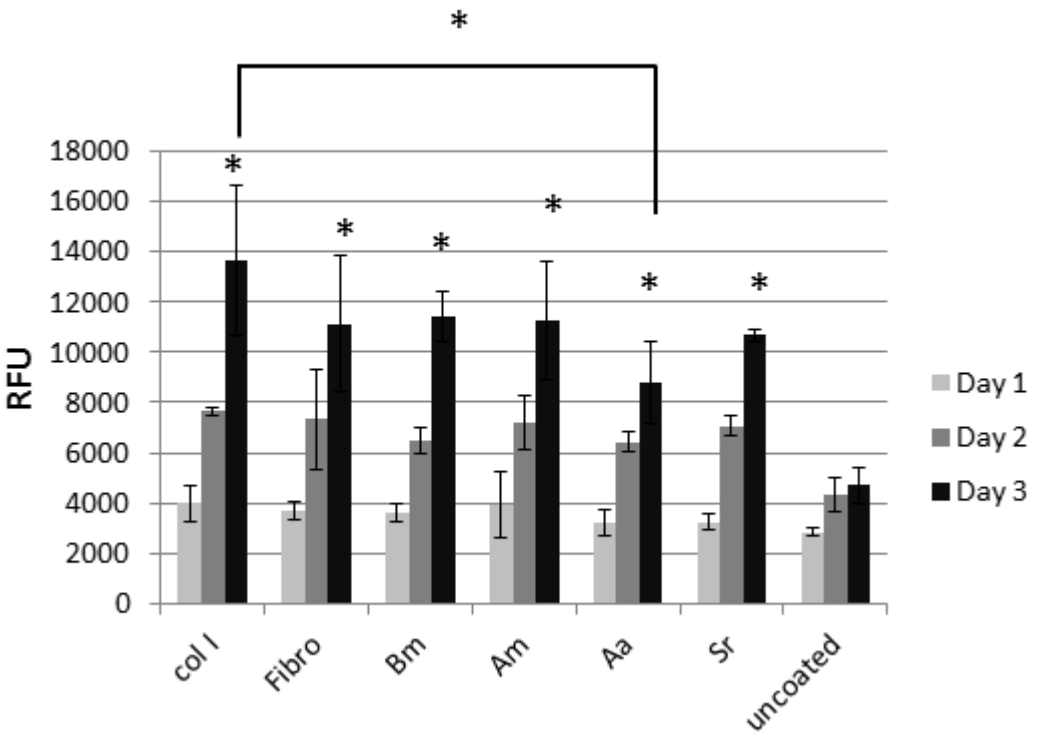

Figure 5.3. Solubilised silk fibroin as a substrate supported C2C12 proliferation under serum free conditions. C2C12 cells ($3.5x10^3$ cells/cm^2) were seeded in wells of a 24-well plate coated with silk fibroin (10 µg/cm^2) and cultured for 3 days in serum free medium. The cell metabolic activities of C2C12 cells on four different silk fibroins, two ECM proteins and tissue culture plastic in SkGM-2 medium are assessed using the Alamar Blue assay. At the indicated times Alamar Blue dye is added and absorbance measured. The relative fluorescence units are plotted as a measure of cell metabolic activity. The data are mean ± SD (n=4). * p≤0.05.Am: *A. mylitta;* Bm: *B. mori;* Aa: *A. assamensis;* Sr: *S. ricini;* Col I: *collagen I;* Fibro: *Fibronectin*

ECM proteins: collagen I and fibronectin, compared to the cell numbers on uncoated plastic. However, at day 3 the number of metabolically active cells was significantly higher on all substrates except on *A. assamensis* substrates, when compared to that on uncoated plastic. No significant differences in relative cell numbers were found among the 4 silk substrates, but there was a difference in the number of cells on collagen I where relative cell number was significantly higher than *A. assamensis* (Fig 5.3).

5.2.3 C2C12 myoblasts fuse to form multinucleated myotubes on all 4 silk substrates

To examine the effect of solubilised silk fibroin on the differentiation of C2C12 myoblasts, cells were cultured on *B. mori*, *A. mylitta*, *A. assamensis* and *S. ricini* silk fibroin coated etched glass surfaces for 12 days. They were cultured in serum free proliferation medium (section 2.7.5.3) until almost confluent (90% confluency) (proliferation day 4), and then switched into serum-free differentiation medium (section 2.7.3) for the remaining 8 days (differentiation day 8). Phase contrast microscopy of the cells after 4 days in differentiation medium clearly showed fusion of myoblasts into myotubes with a similar capacity on all four silk substrates (Figure 5.4. a-h).

Immunostaining with a mAb to myosin heavy chain 7 (MyHCB) (section 2.7.12) revealed that the myoblasts differentiated and fused to form myotubes on all the silk fibroin substrates with similar capacity (Figure 5.5). Immunostaining with an antibody against fibronectin, revealed deposition of fibronectin on the glass surface and on the edges of, and around, some myotubes. DAPI staining indicated the majority of the nuclei were inside the myosin expressing myotubes, but a small proportion of nuclei were not within the myotubes indicating some cells remained unfused. To determine the number of cells proliferating 4 days after switching the medium to a differentiation medium, an EdU assay (section 2.7.11) was performed. The EdU staining nuclei, which indicated these cells were proliferating were $\leq$ 5.0% of the total number of cells on all 4 solubilised silk proteins suggesting the majority of cells were committed to differentiation (Table 5.2). The EdU experiment was performed twice and the results shown in Table 5.2 are from one of those experiments.

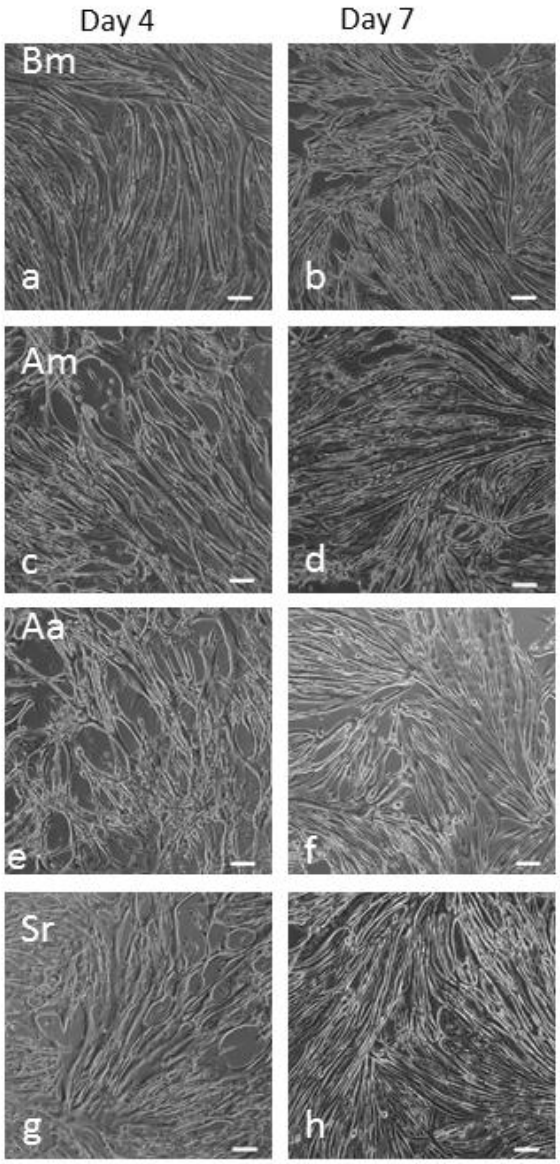

Figure 5.4 Phase contrast images of C2C12 cells cultured on silk fibroins in serum free differentiation medium. C2C12 cells ($3.5x10^3$ cells/cm^2) were seeded in wells of a 24-well plate coated with the indicated silk fibroins (10 µg/cm^2) and cultured for 4 days in serum free proliferation medium. After 4 days, the medium was changed to a differentiation medium and the cells were cultured for another 7 days. Images were captured at day 4 and 7 of differentiation with a Zeiss Axiovert bright field microscope at a magnification of 120x using Spot Advanced software. Scale bars - 100 µm. *Am: A. mylitta; Bm: B.mori; Aa: A.assamensis; Sr: S.ricini*

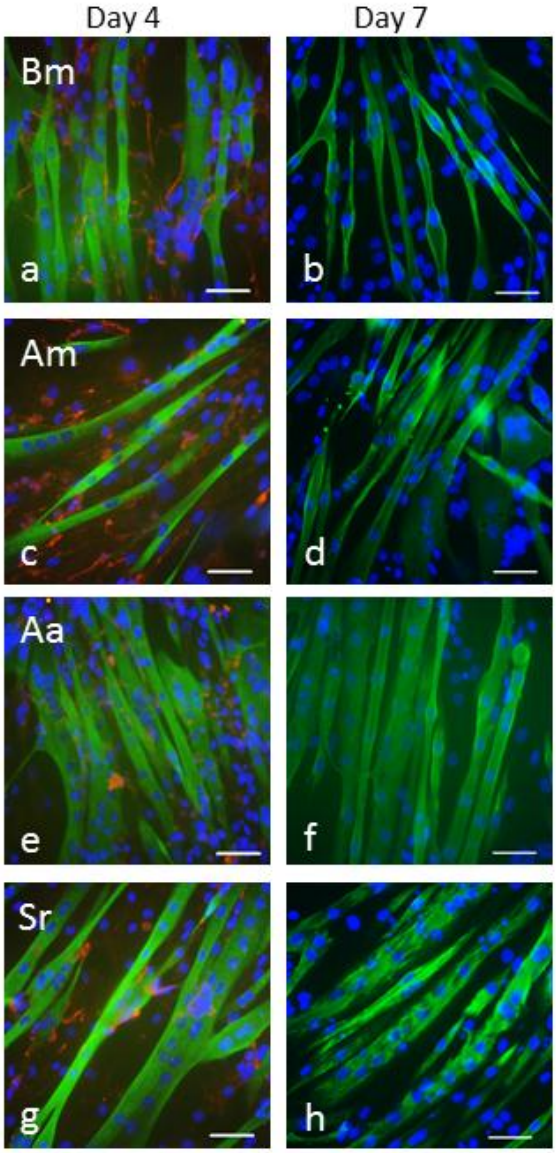

Figure 5.5. Immunofluorescence images showed differentiation of C2C12 cells cultured on silk fibroin substrates in serum free differentiation medium. C2C12 cells ($3.5x10^3$ cells/cm^2) were seeded in wells of a 24-well plate coated with indicated silk fibroins (10 µg/cm^2) and cultured for 4 days in serum free proliferation medium. After 4 days, the medium was changed to a differentiation medium and the cells were cultured for another 7 days. Post-differentiation, cells were fixed with 4% paraformaldehyde and stained with myosin (green) and fibronectin (red) imaged using a Zeiss Axioskop fluorescent microscope at a magnification of 480x using Spot Advanced software.The antibody recognising myosin and fibronectin were respectively mouse mAB (NOQ7.5.4D) and rabbit polyclonal antibody. The secondary antibodies used were a goat anti-mouse alexafluor 488 conjugated antibody and a goat anti-rabbit alexafluor 546 conjugated antibody. Scale bars - 50 µm for a-h. *Am: A. mylitta; Bm: B.mori; Aa: A.assamensis; Sr: S.ricini*

Table 5.2 EdU assay to assess the number of proliferating cells in C2C12 cell

Type of silk	*B. mori*	*A. mylitta*	*A. assamensis*	*S. ricini*
% of proliferating cells	3.0	3.2	3.3	5.0

5.2.4 Secretion of matrix proteins in 2D serum free cultures (section 2.11.2)

To determine whether C2C12 cells synthesize and secrete ECM proteins under serum free culture conditions, C2C12 cells were grown on etched glass coverslips coated with solubilised silk fibroin from *B. mori*, *A. mylitta*, *A. assamensis* or *S. ricini* for 3 days in proliferation medium. Immunostaining was performed using antibodies against collagens type I, type IV, type VI, fibronectin and perlecan (Fig 5.6-5.9). Although immunostaining revealed all of these molecules were expressed, the different silk fibroins appeared to trigger different levels of expression of these ECM molecules. A stronger staining was observed for collagen type I on *B. mori* and *A. mylitta* silk fibroin when compared to *A. assamensis* and *S. ricini*. A similar staining intensity was observed for the collagen type IV antibody on all 4 silk fibroin substrates. Collagen type VI staining intensity appeared to be the strongest on *B. mori* silk fibroin, followed by *S. ricini* and similar staining intensities were observed on *A. mylitta* and *A. assamensis* silk fibroin. The matrix glycoprotein, fibronectin was almost equally expressed on *B. mori*, *A. mylitta* and *S. ricini* silk fibroin substrates with similar staining intensities, while on *A. assamensis* there were low levels of staining with the anti-fibronectin antibody. Perlecan staining intensity was the strongest of all five matrix proteins on *A. assamensis* and *B. mori* silk fibroin substrates where it appeared to be staining a filamentous web like lattice. Although the staining pattern was similar on *A. mylitta* and *S. ricini* silk fibroins, the intensity of staining was lower on these two substrates (Fig 5.6-5.9).

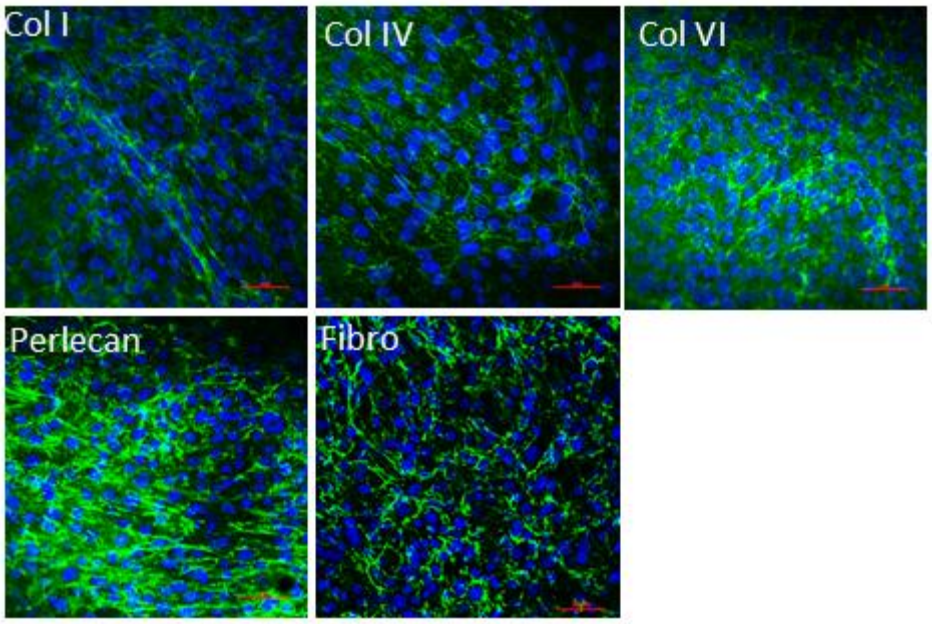

Figure 5.6. Immunofluorescence revealed secretion of ECM proteins by C2C12 cells on *B. mori* silk fibroin in serum free medium. C2C12 cells ($3.5x10^3/cm^2$) were seeded in wells of a 24-well plate coated with *B. mori* silk fibroin ($10\mu g/cm^2$) and cultured for 3 days in serum free medium. Cells were fixed using 4% paraformaldehyde and stained for antibodies recognising collagens type I, type IV, type VI, perlecan and fibronectin (all rabbit polyclonal antibodies) and imaged using Nikon A1 confocal microscope. The secondary antibody used was a goat anti-rabbit alexafluor 488 conjugated antibody. Nuclei are stained with DAPI (blue). Scale bars- 50 μm.

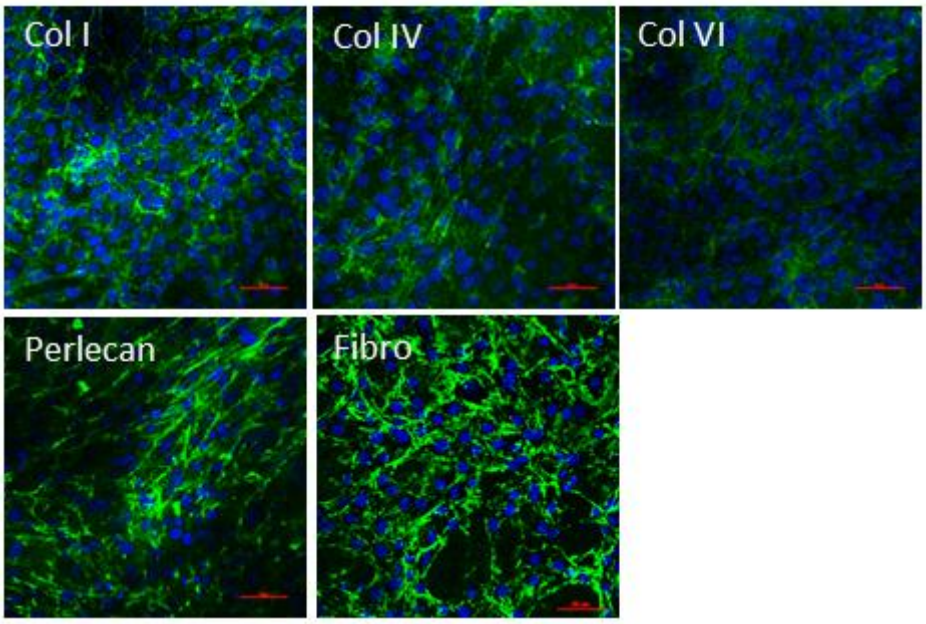

Figure 5.7. Immunofluorescence revealed secretion of ECM proteins by C2C12 cells on *A. mylitta* silk fibroin in serum free medium. C2C12 cells ($3.5x10^3/cm^2$) were seeded in wells of a 24-well plate coated with *A. mylitta* silk fibroin ($10\mu g/cm^2$) and cultured for 3 days in serum free medium. Cells were fixed using 4% paraformaldehyde and stained for antibodies recognising collagens type I, type IV, type VI, perlecan and fibronectin (all rabbit polyclonal antibodies) and imaged using Nikon A1 confocal microscope. The secondary antibody used was a goat anti-rabbit alexafluor 488 conjugated antibody. Nuclei are stained with DAPI (blue). Scale bars- 50 µm.

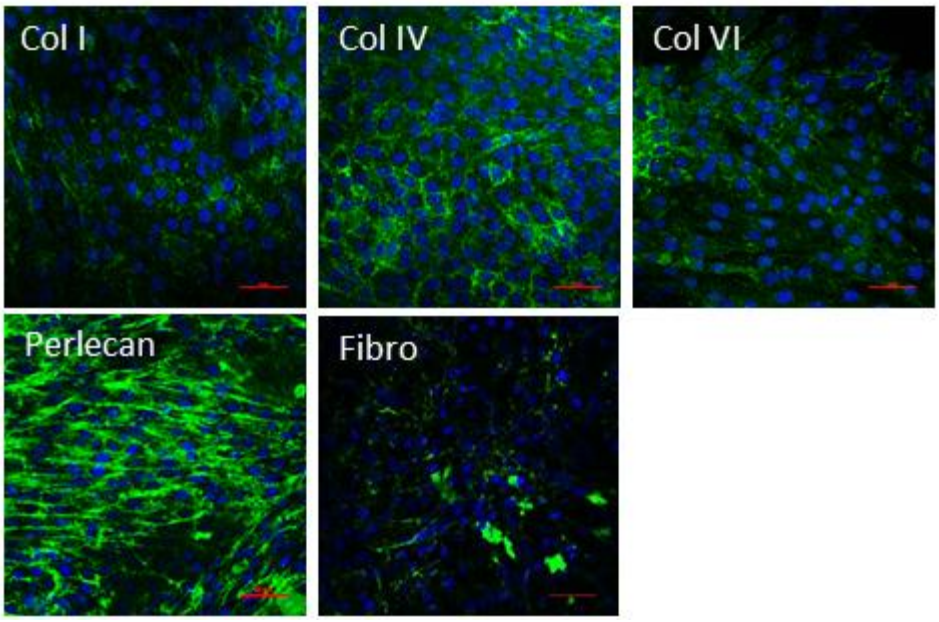

Figure 5.8. Immunofluorescence revealed secretion of ECM proteins by C2C12 cells on *A. assamensis* silk fibroin in serum free medium. C2C12 cells ($3.5x10^3/cm^2$) were seeded in wells of a 24-well plate coated with *A. assamensis* silk fibroin ($10\mu g/cm^2$) and cultured for 3 days in serum free medium. Cells were fixed using 4% paraformaldehyde and stained for antibodies recognising collagens type I, type IV, type VI, perlecan and fibronectin (all rabbit polyclonal antibodies) and imaged using Nikon A1 confocal microscope. The secondary antibody used was a goat anti-rabbit alexafluor 488 conjugated antibody. Nuclei are stained with DAPI (blue). Scale bars- 50 µm.

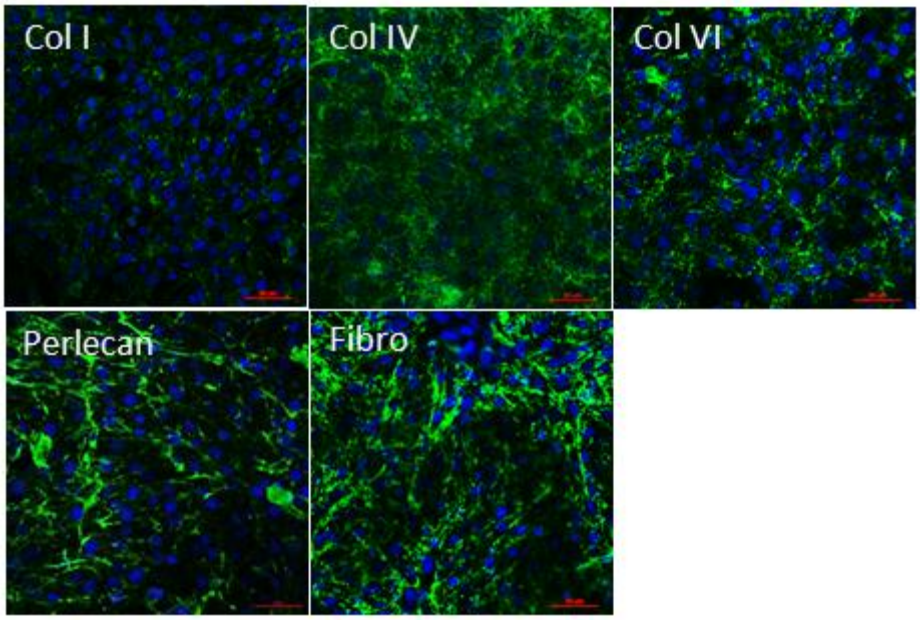

Figure 5.9. Immunofluorescence revealed secretion of ECM proteins by C2C12 cells on *S. ricini* silk fibroin in serum free medium. C2C12 cells ($3.5x10^3/cm^2$) were seeded in wells of a 24-well plate coated with *S. ricini* silk fibroin ($10\mu g/cm^2$) and cultured for 3 days in serum free medium. Cells were fixed using 4% paraformaldehyde and stained for antibodies recognising collagens type I, type IV, type VI, perlecan and fibronectin (all rabbit polyclonal antibodies) and imaged using Nikon A1 confocal microscope. The secondary antibody used was a goat anti-rabbit alexafluor 488 conjugated antibody. Nuclei are stained with DAPI (blue). Scale bars- 50 µm.

5.2.5 Proliferation of Human skeletal muscle myoblasts (HSMMs) on 2D silk fibroin substrates (section 2.7.5.2)

As a first step in assessing which, if any, of these silk fibroin substrates could be useful for human muscle repair their compatibility with primary human myoblasts was examined. To assess the ability of solubilised silk proteins to support cell adhesion and growth of HSMMs, cells were cultured for 11 days in SkGM-2 proliferation medium on each of the four silk substrates or on either of two ECM coating proteins, collagen I and fibronectin, or on tissue culture plastic (TCP) and relative cell number was measured using the alamarBlue assay (section 2.10.2) (Fig 5.10). HSMMs cultures on all silk fibroin and matrix protein substrates exhibited similar metabolic activity at all investigated time points up to 8 days of culture, hence no significant differences were observed in the relative cell numbers on all substrates when compared to TCP. However, at day 11 in culture the metabolic activity of HSMMs cultured on *A. mylitta* silk fibroin was significantly higher than that of all other substrates.

5.2.6 Differentiation of HSMMs on 2D silk fibroin substrates

To examine the effects of silk proteins on differentiation of HSMMs, cells were cultured at a higher cell number ($15x10^3$ cells/cm^2) on each of the four silk substrates coated onto etched glass, or either: collagen I or fibronectin. They were cultured in SkGM-2 proliferation medium until proliferation day 3 when they were almost confluent (90%-100% confluency), and then switched into differentiation medium containing DMEM/F12/2% HS for the remaining 10 days (differentiation day 10). Immunostaining with a mAb to myosin heavy chain 7 (MyHCB) (section 2.7.12) revealed that myotubes were organized and parallel to each other on all substrates at day 7 of differentiation. The data for the silk substrates are shown in Fig 5.11. DAPI staining showed the clustering of nuclei within the myotubes (>2 nuclei close to each other) and nuclei were elongated. Striations were first visible in the myotubes by day 7 and by day 10 striations were evident in myotubes on all silk substrates. Antibody staining patterns of GLUT 4 (a marker for functional myotubes) revealed that GLUT 4 was present along the entire

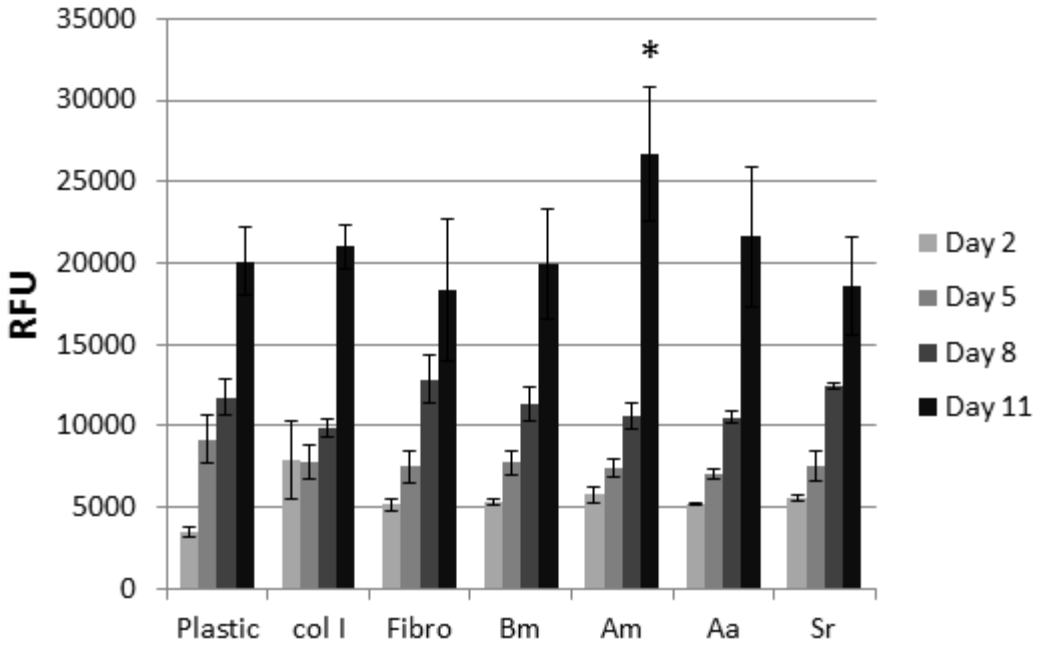

Figure 5.10. Proliferation of human skeletal muscle myoblasts (HSMMs) on four silk fibroins, two ECM protein substrates and tissue culture plastic in SkGM-2 medium assessed using alamar Blue dye assay over a 11 day period. HSMMs ($10^3/cm^2$) were seeded to the wells of a 48-well plate coated with either Bm (10 µg/cm^2), Am (10 µg/cm^2), Aa (10 µg/cm^2), Sr (10 µg/cm^2), collagen I (10 µg/cm^2), fibronectin (10 µg/cm^2) or uncoated plastic and cultured for 11 days in SkGM-2 medium. After the respective time points alamar Blue dye was added to the wells and absorbance measured at 600nm. Relative fluorescence units were plotted as a measure of cell proliferation. Data represented as mean ± SD (n=4). One-way ANOVA was performed and significance (p) values shown at each time point. p*<0.05. *Am: A. mylitta; Bm: B.mori; Aa: A.assamensis; Sr: S.ricini*

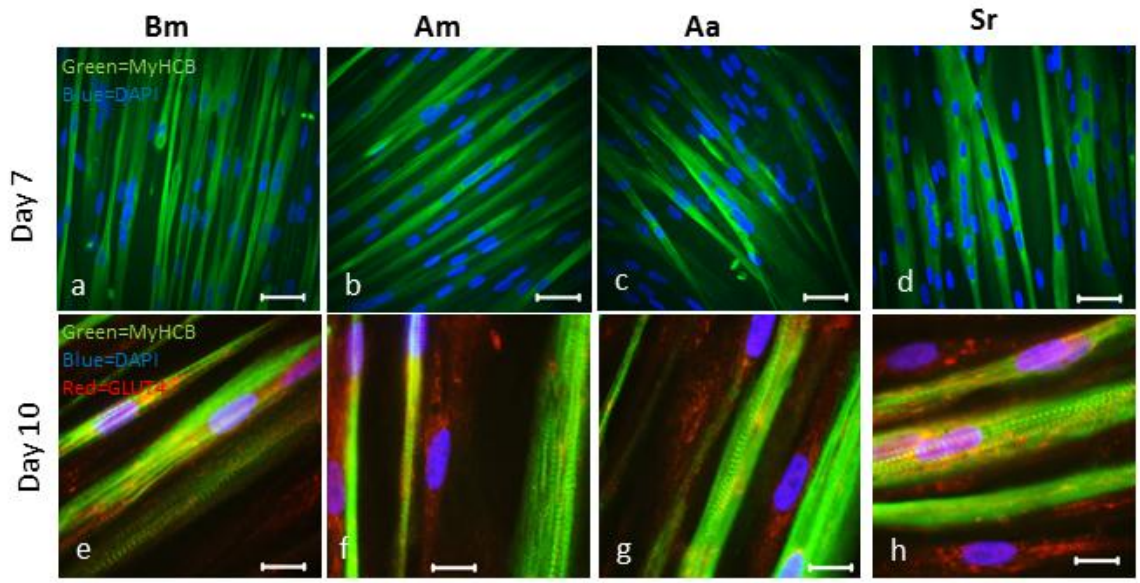

Figure 5.11. Immunofluorescence images show differentiation of HSMMs cultured on silk fibroin substrates in DMEM/F12/2%HS differentiation medium. HSMMs ($15x10^3/cm^2$) were seeded in wells of a 24 well plate coated with indicated silk fibroins (10 µg/cm^2) and cultured for 4 days in SkGM-2 proliferation medium. After 4 days, the medium was changed to a differentiation medium and the cells were cultured for another 10 days. Post-differentiation, cells were fixed with 4% paraformaldehyde and stained with anti-myosin (green) and anti-GLUT4 (red) antibodies and imaged using a Zeiss Axioskop fluorescent microscope. The antibodies recognising myosin and GLUT4 were respectively a mouse mAb (NOQ7.5.4D) and a rabbit polyclonal antibody. The secondary antibodies used were a goat anti-mouse alexafluor 488 conjugated antibody and a goat anti-rabbit alexafluor 546 conjugated antibody. Nuclei are stained with DAPI (blue). Scale bars-50 µm for a-d and 25 µm for e-h. *Am: A. mylitta; Bm: B.mori; Aa: A.assamensis; Sr: S.ricini*

length of the myotube although perinuclear accumulation was also noted on all silk substrates (Fig 5.11 e-h).

To quantify the differentiation of myotubes, fusion indices were calculated from the immunofluorescent images of MyHCB positive myotubes by calculating the number of nuclei within the myotubes (only regions with ≥ 2 nuclei were considered) relative to the total number of nuclei within a field of view (Figure 5.12. A). The results show that the percentage of nuclei within myotubes was similar (ranging from 77%-81%) on collagen I, fibronectin, *B. mori*, *A. mylitta*, *and S. ricini* with no significant differences observed between them. However, on *A. assamensis*, the percentage of nuclei within myotubes was significantly lower than that of HSMMs on other substrates being around 57% of all nuclei. The number of myotubes formed per field of view was also counted and this was similar on collagen I, fibronectin, *B. mori*, *A. mylitta*, *and S. ricini* with no significant differences observed (Figure 5.12 B). On *A. assamensis* silk fibroin, the number of myotubes formed was significantly lower than all other substrates.

5.2.7 HSMM cell adhesion and spreading on four silk 3D scaffolds (section 2.13.1)

Three dimensional, porous silk scaffolds were also tested; these scaffolds were 14 mm in diameter and 4 mm in height. To determine, HSMM cell spreading on 3D silk scaffolds, HSMMs at $7.5x10^4$ cells were cultured for 2 days on *B. mori*, *A. mylitta*, *A. assamensis* or *S. ricini* silk scaffolds in SkGM-2 proliferation medium and stained with Rhodamine phalloidin to detect F-actin (Fig 5.13). Confocal imaging was performed to visualize stress fibre arrangement.

Cells appeared well spread on all four silk scaffolds with distinct actin fibres and a similar actin fibre arrangement on *A. mylitta, A. assamensis* and *S. ricini* scaffolds. Here the cells appeared to be oriented around the scaffold pores (Fig 5.13 d, f and h), but HSMMs on *B. mori* scaffolds showed a different F-actin arrangement with fibres oriented in parallel along the pores and in places crossing over the pores of the scaffold (Fig 5.13 b). The images in Figure 5.13 are merged from several z-stack images (5 µm each stack, 150-200 µm into the scaffold) and are representative of six fields of view

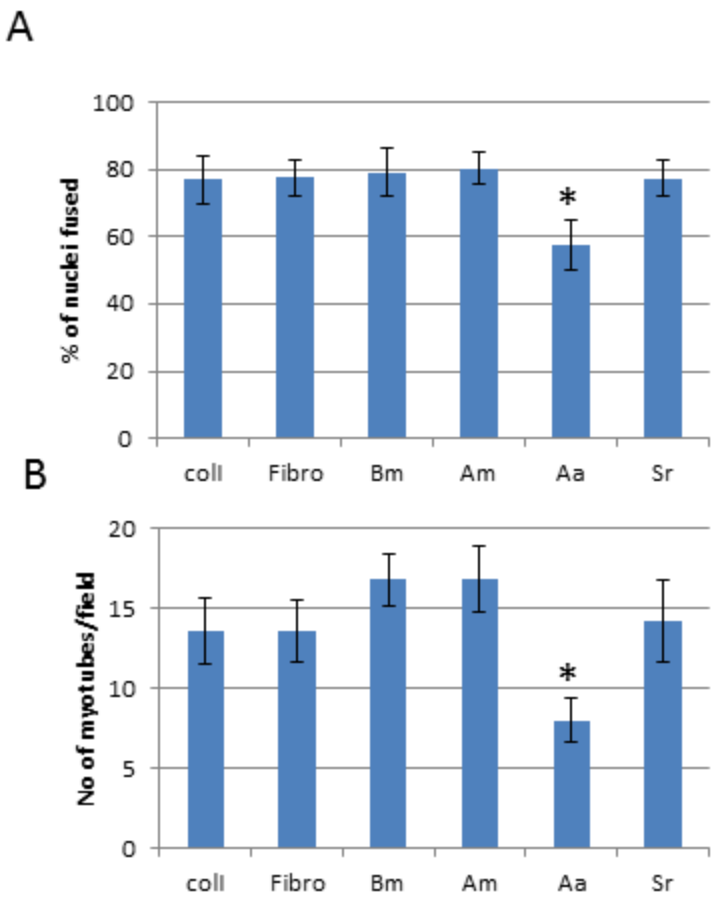

Figure 5. 12 Fusion index and myotube numbers for HSMMs on substrates of silk fibroin proteins or two ECM proteins at day 7 of differentiation. (A) Fusion index was calculated from MyHCB positive myotubes as the ratio of number of nuclei inside the myotubes versus total number of nuclei in 6 random fields of view. (B) Number of myotubes were determined in 6 random fields of view. Data represented as mean ± SD (n=6) from two independent experiments. * shows p≤0.05. *Am: A. mylitta; Bm: B.mori; Aa: A.assamensis; Sr: S.ricini*

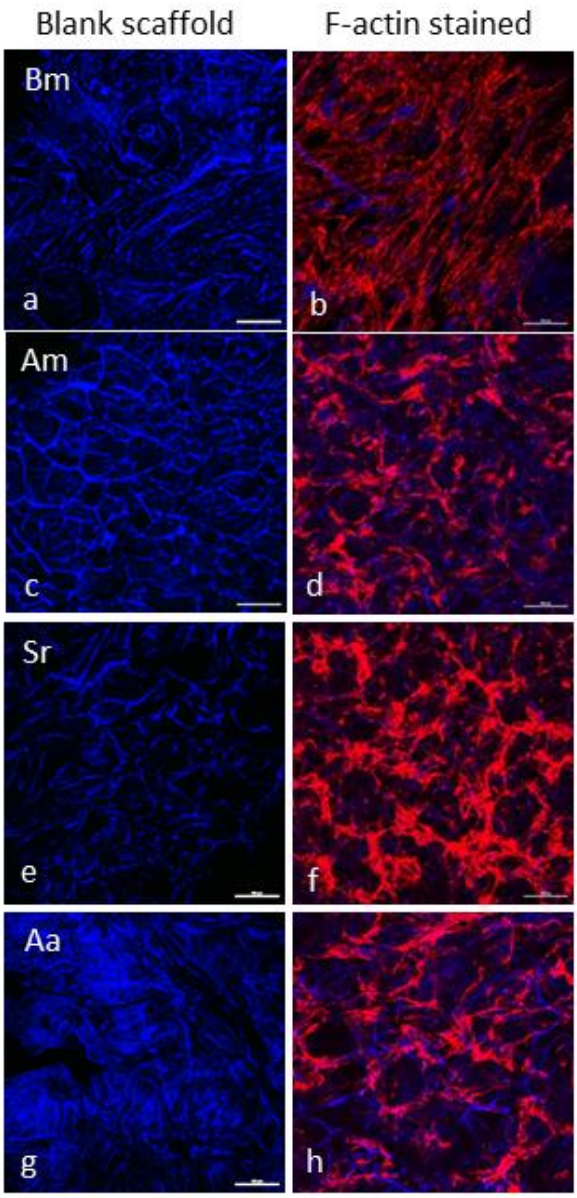

Figure 5.13. HSMMs cell adhesion and spreading on 3D silk scaffolds. HSMMs ($7.5x10^4$) were cultured on 3D silk scaffolds: Bm (b), Am (d), Sr (f) and Aa (h) for 2 days in SkGM-2 proliferation medium, fixed with 4% paraformaldehyde and stained with rhodamine phalloidin for F-actin staining and imaged using Nikon A1 confocal microscope. The images represented are merged images of several z-stack images (5 µm each stack, 150-200 µm deep into the scaffold). Blank scaffolds (a, c, e, g) stained with Rhodamine phalloidin (red) and DAPI (blue). Scale bars 50 µm. Shown is a representative image of six fields of view. *Am: A. mylitta; Bm: B.mori; Aa: A.assamensis; Sr: S.ricini*

taken across the scaffolds. Staining of blank scaffolds with DAPI and Rhodamine phalloidin revealed their porous nature (Fig 5.13 a, c, e and g).

5.2.8 HSMM cell adhesion on solubilized muscle matrix coated *B. mori* silk scaffold

To examine whether coating the silk scaffolds with solubilised skeletal muscle matrix (prepared in chapter 3) would affect cell behaviour, *B. mori* silk scaffolds were coated with solubilized muscle matrix (200 µg/scaffold) for 2 h at 37ºC and HSMMs were cultured for 5 days in SkGM-2 medium on either matrix coated *B. mori* scaffolds or *B. mori* scaffolds alone (section 2.13.1) (Fig 5.14).

Morphological staining of the cytoskeletal F-actin fibres by Rhodamine phalloidin showed well distributed cells across the entire scaffold on *B. mori* silk and matrix coated *B. mori* silk scaffolds (Fig 5.14 a, c). Interestingly, the matrix coated scaffolds, appeared to support a higher cell density even though the same number of cells were seeded on both scaffold types. High magnification images of the respective scaffolds confirmed that cells were distributed in a more compact arrangement on matrix coated *B. mori* scaffolds, or may have grown at a faster rate compared to cells on uncoated *B. mori* scaffolds (Fig 5.14).

5.2.9 Matrix deposition by HSMMs on four silk 3D scaffolds

To determine if like the C2C12 cells, HSMMs deposited ECM proteins onto the 3D silk scaffolds, HSMMs were cultured for 2 days in SkGM-2 proliferation medium on 3D silk scaffolds and immunostaining was performed to detect the presence of the matrix proteins, fibronectin and perlecan. Immunofluorescence images revealed deposition of both fibronectin and perlecan on all four silk scaffolds with comparable signal intensities (Fig 5.15 a-h). Close examination of the images show that matrix proteins were forming a mesh or lattice across the entire scaffold with interconnections going into the scaffold.

5.2.10 Scanning electron microscopy (SEM) of 3D silk scaffolds (section 2.13.3)

To observe the ultrastructure of the scaffolds and the arrangement of HSMMs on the scaffolds, SEM was performed on all four silk scaffolds with and without HSMM cells

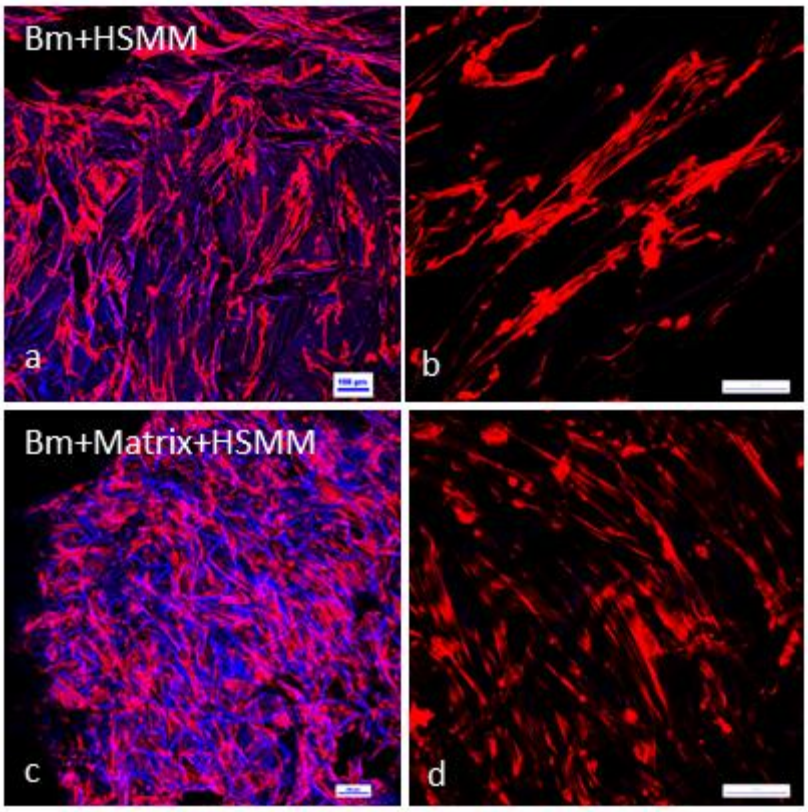

Figure 5.14. HSMMs cell adhesion and spreading on muscle matrix coated *B. mori* (3D) silk scaffolds. HSMMs ($7.5x10^4$) were cultured on either *B. mori* silk scaffold (a-b) or *B. mori* scaffold coated with solubilised muscle matrix (c-d) (200 µg/scaffold) for 5 days in SkGM-2 proliferation medium, fixed with 4% paraformaldehyde and stained with Rhodamine phalloidin to visualize F-actin and imaged using a Nikon A1 confocal microscope. (b, d) are high magnification images of a selected area of the respective images (a, c). The images represented are merged images of several z-stack images (5 µm each stack, 150-200 µm deep into the scaffold) taken across the scaffolds. Nuclei and scaffolds are stained with DAPI (a, c). Scale bars -100 µm

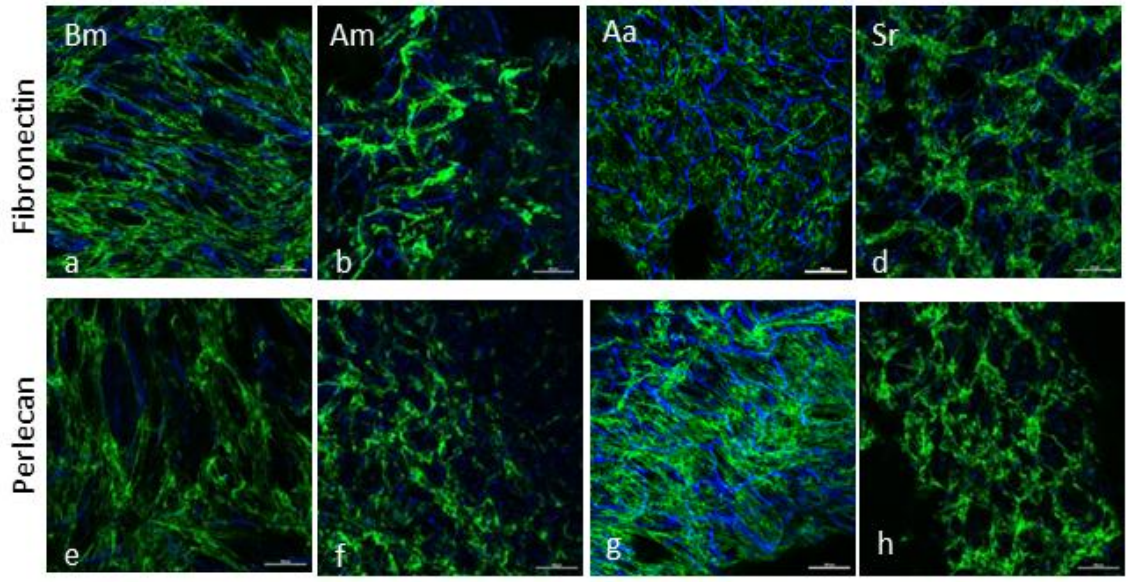

Figure 5.15. Immunofluorescence revealed secretion of ECM proteins by HSMMs on 3D silk scaffolds. HSMMs ($7.5x10^4$ cells/scaffold) were seeded onto the scaffolds and cultured for 2 days in SkGM-2 medium. Cells were fixed using 4% paraformaldehyde and stained with antibodies recognising fibronectin (a-d) and perlecan (e-h) and imaged using a Nikon A1 confocal microscope. The images represented in the figure are merged images of several z-stack images (5 µm each stack, 150-200 µm deep into the scaffold). The antibodies recognising fibronectin and perlecan were rabbit polyclonal antibodies. The secondary antibody used was a goat anti-rabbit alexafluor 488 conjugated antibody. Nuclei are stained with DAPI (blue). Scale bars- 50 µm for a-h. *Am: A. mylitta; Bm: B.mori; Aa: A.assamensis; Sr: S.ricini*

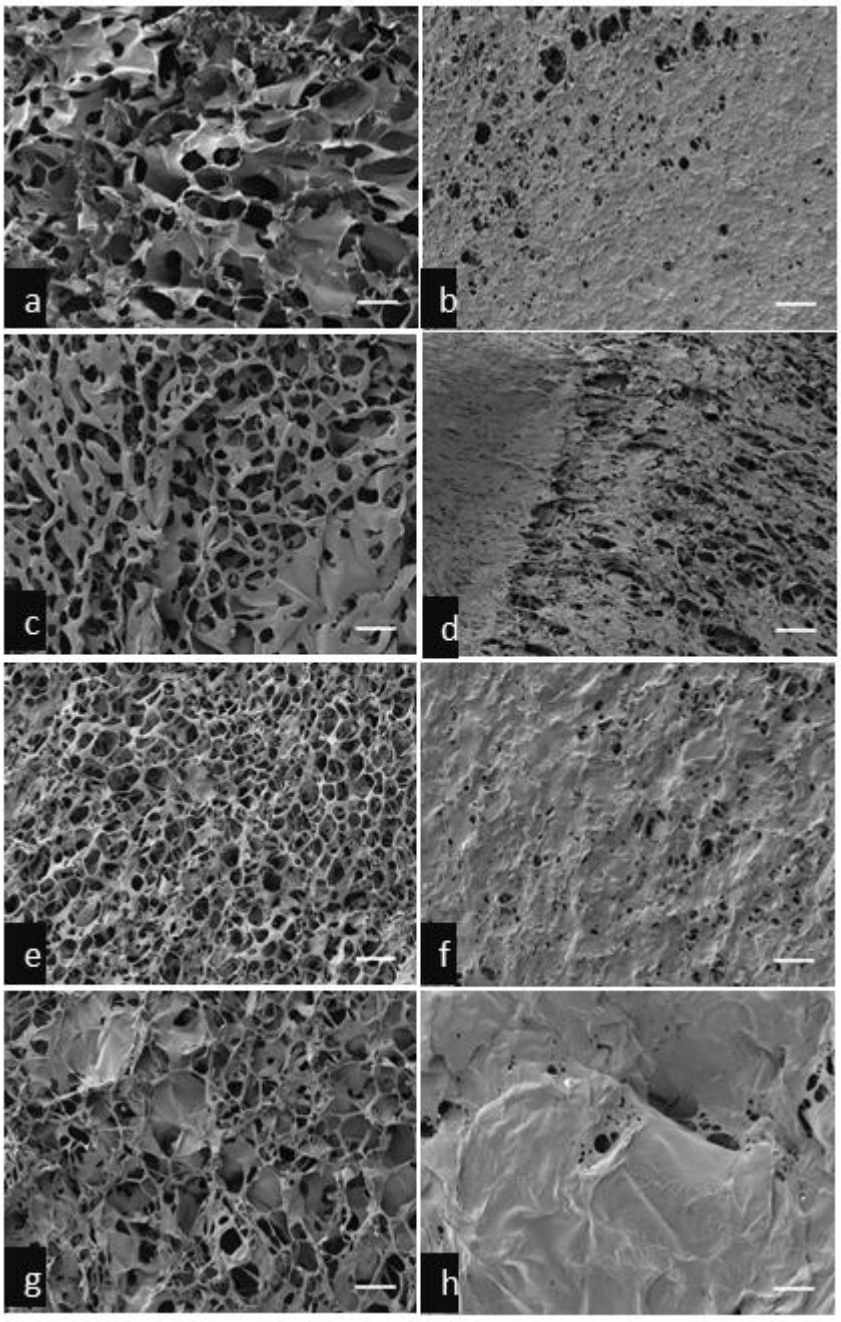

Figure 5.16. Scanning electron micrographs of 3D silk scaffolds. Blank scaffolds (without cells) reveal the porous nature of the scaffolds: Bm, Am, Sr and Aa (a, c, e, g) respectively. At day 5 after seeding, HSMMs formed a cell sheet on all four scaffolds covering almost the entire scaffold suggesting that scaffolds supported cell adhesion and growth (b, d, f, h). Scale bar-100 µm for a-h. *Am: A. mylitta; Bm: B.mori; Aa: A.assamensis; Sr: S.ricini*

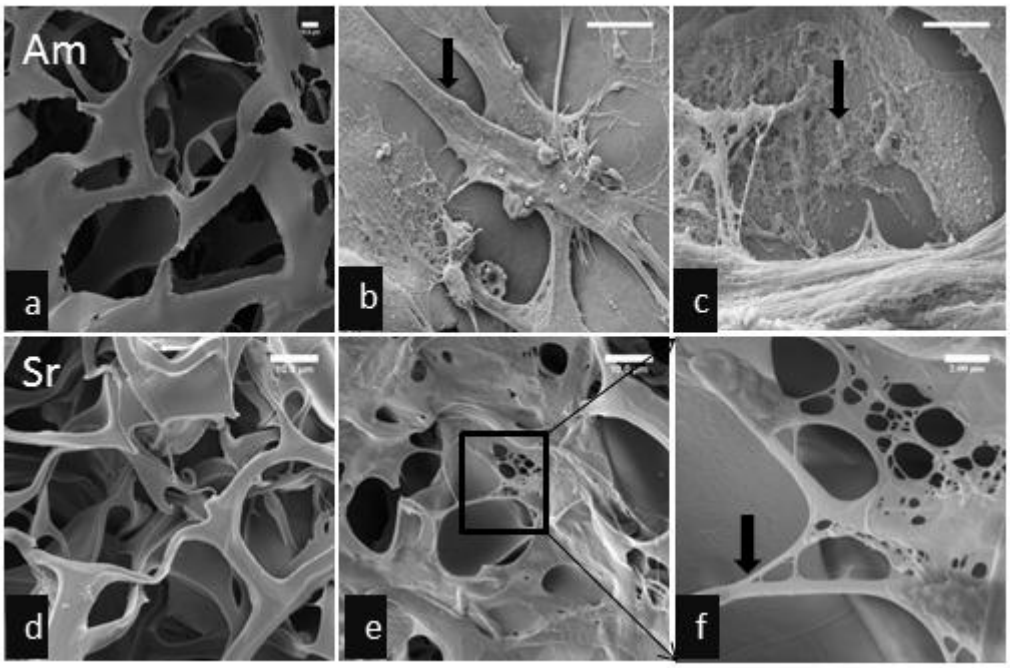

Figure 5.17. Scanning electron micrographs of 3D silk scaffolds. High magnification images of blank scaffolds, Am and Sr show the interconnected pores in silk scaffolds (a, d). At day 2 after seeding, HSMMs adhere to the silk scaffolds and spread on Am scaffold (b, arrow shows a well spread cell), matrix deposition (arrow) can be seen (c); cells formed a sheet on Sr scaffold (e); magnified image of the box show cell projections (arrow) attached to the scaffold (f). Scale bar-10 µm for (a-b, d-e) and 2 µm for c and f. *Am: A. mylitta; Sr: S.ricini*

at days 2 and 5 after seeding (Fig 5.16-5.17). All four scaffolds appeared porous with pores ranging in diameter from 50-120 µm on *A. mylitta*, 30-110 µm on *B. mori*, 30-90 µm on *S. ricini* and *A. assamensi*s scaffolds. SEM images of blank scaffolds revealed the interconnected porous nature of the scaffolds. HSMMs formed a cell sheet on all four scaffolds, covering almost the entire scaffold after 5 days of seeding (Fig 5.16). Upon closer examination of cells on an *A. mylitta* scaffold, the cell morphology can be seen: cells appeared well spread, flat and elongated with many focal contact points and deposition of matrix can be seen. On *S. ricini* scaffold, cells appeared to be growing like thick sheets covering the porous structure of the scaffolds (Fig 5.17).

5.2.11 HSMMs differentiation on 3D silk scaffolds section (2.13.1)

To assess the differentiation of HSMMs on 3D silk scaffolds, HSMMs were seeded at a higher cell number ($5x10^5$ cells per 14 mm diameter scaffold) on *B. mori*, *A. mylitta*, *A. assamensis* or *S. ricini* silk scaffolds and maintained in SKGM-2 proliferation medium for 4 days, and for a further 4 days in differentiation medium comprising of DMEM/F12/2%HS (Fig 5.18). Slow muscle myosin (MyHCB) immunostaining revealed that HSMMs fused and formed multinucleated myotubes on all four scaffolds but there were far less MyHCB positive myotubes on *S. ricini* scaffolds compared to scaffolds from the other insect species. The confocal imaging of the myotubes indicated that they were not confined to the same focal plane and suggested that myotubes formed as a result of fusion with cells at different depths in the 3D scaffolds (Fig 5.19). The parallel alignment of the MyHCB positive myotubes on *B. mori*, *A. mylitta* and *A. assamensis* was striking. Interestingly, on *A. assamensis* scaffolds there appeared to be two layers of myotubes, one at a 90º orientation to the other (Fig 5.18 and 5.19).

5.2.12 Partially solubilised (or Unfixed) *B. mori* scaffold supported HSMM differentiation (section 2.13.1)

Interestingly, when the *B. mori* scaffolds were not fixed with ethanol, but were placed in medium for cell culture experiments without fixation the scaffolds started to partially solubilise. HSMMs were seeded on these scaffolds at ($1x10^5$ cells/scaffold) and cultured for 11 days in proliferation medium and 7 days in differentiation medium. Visualization

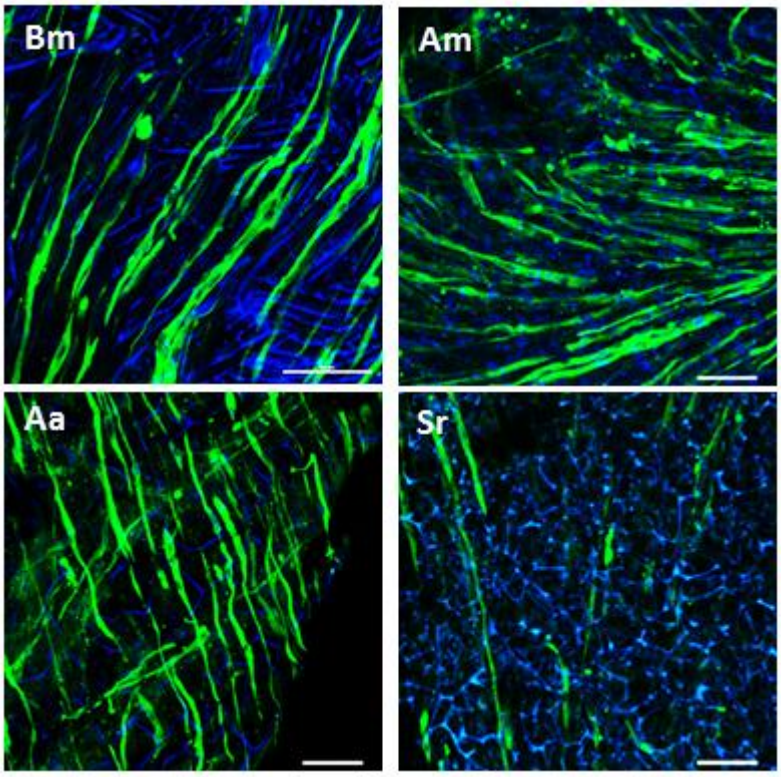

Figure 5.18. Immuonostained images revealed HSMMs differentiation on 3D silk scaffolds. HSMMs ($5x10^5$) were cultured for 4 days in SkGM-2 proliferation medium on ethanol fixed and sterilized Bm, Am, Aa and Sr silk scaffolds, and then the medium was changed to a differentiation medium DMEM/F12/2%HS for a further 4 days. Post differentiation, scaffolds were fixed using 4% paraformaldehyde and stained with anti-myosin, mouse mAb (NOQ.5.4.D), followed by a goat anti-mouse alexafluor 488 conjugated secondary antibody. Images were captured using a Nikon A1 confocal microscope. Represented are merged images of several z-stack images (5 µm each stack, 150-200 µm deep into scaffold). Nuclei are stained with DAPI (blue) Scale bars -100 µm. *Am: A. mylitta; Bm: B.mori; Aa: A.assamensis; Sr: S.ricini*

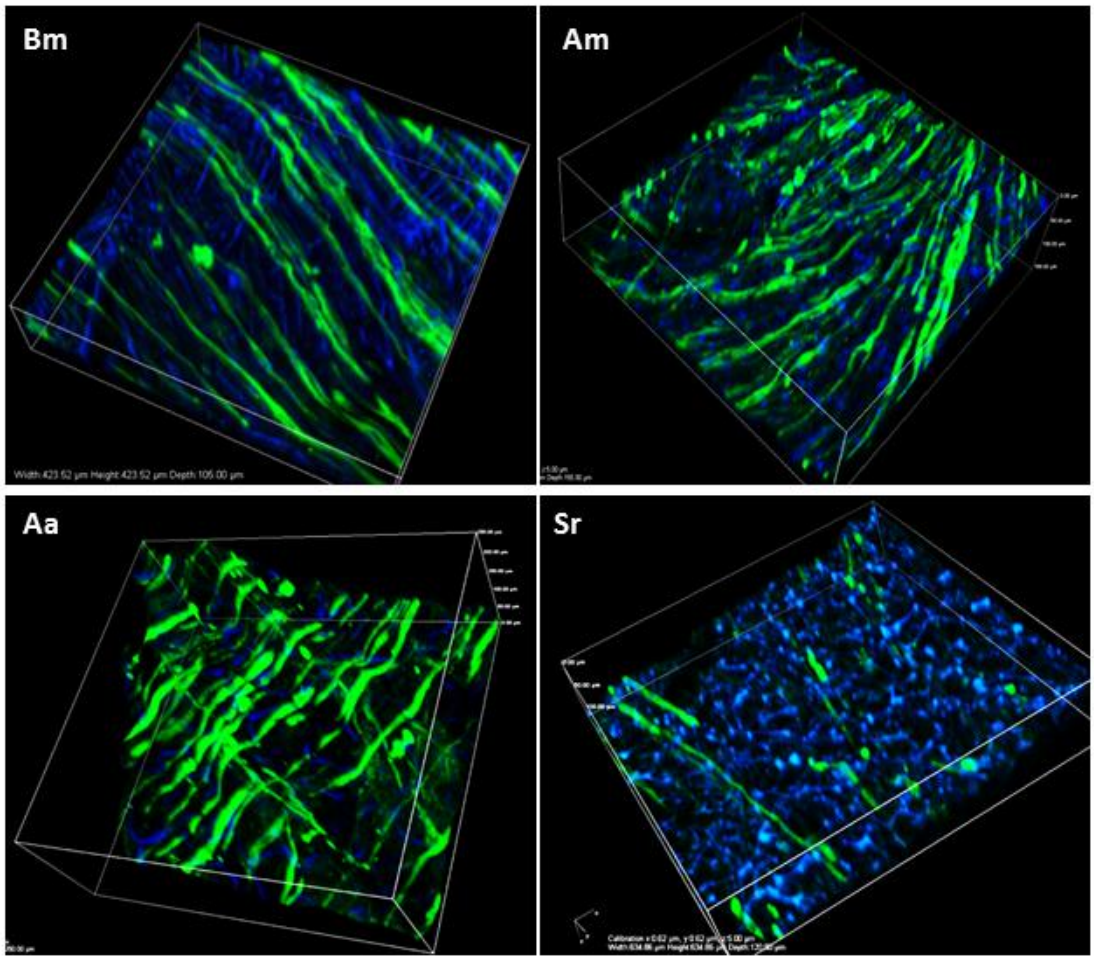

Figure 5.19 Immuonostained 3D images revealed HSMMs differentiation on 3D silk scaffolds. HSMMs ($5x10^5$) were cultured for 4 days in SkGM-2 proliferation medium on ethanol fixed and sterilized Bm, Am, Aa and Sr silk scaffolds, and then the medium was changed to a differentiation medium DMEM/F12/2%HS for a further 4 days. Post differentiation, scaffolds were fixed using 4% paraformaldehyde and stained with anti-myosin, mouse mAb (NOQ.5.4.D), followed by a goat anti-mouse alexafluor 488 conjugated secondary antibody. Images were captured using a Nikon A1 confocal microscope. Represented are 3D merged images of several z-stack images (5 µm each stack, spanning 100-250 µm deep into scaffold). Nuclei are stained with DAPI (blue) Scale bars -100 µm. Note the formation of myotubes in different planes and moving into the scaffolds. *Am: A. mylitta; Bm: B.mori; Aa: A.assamensis; Sr: S.ricini*

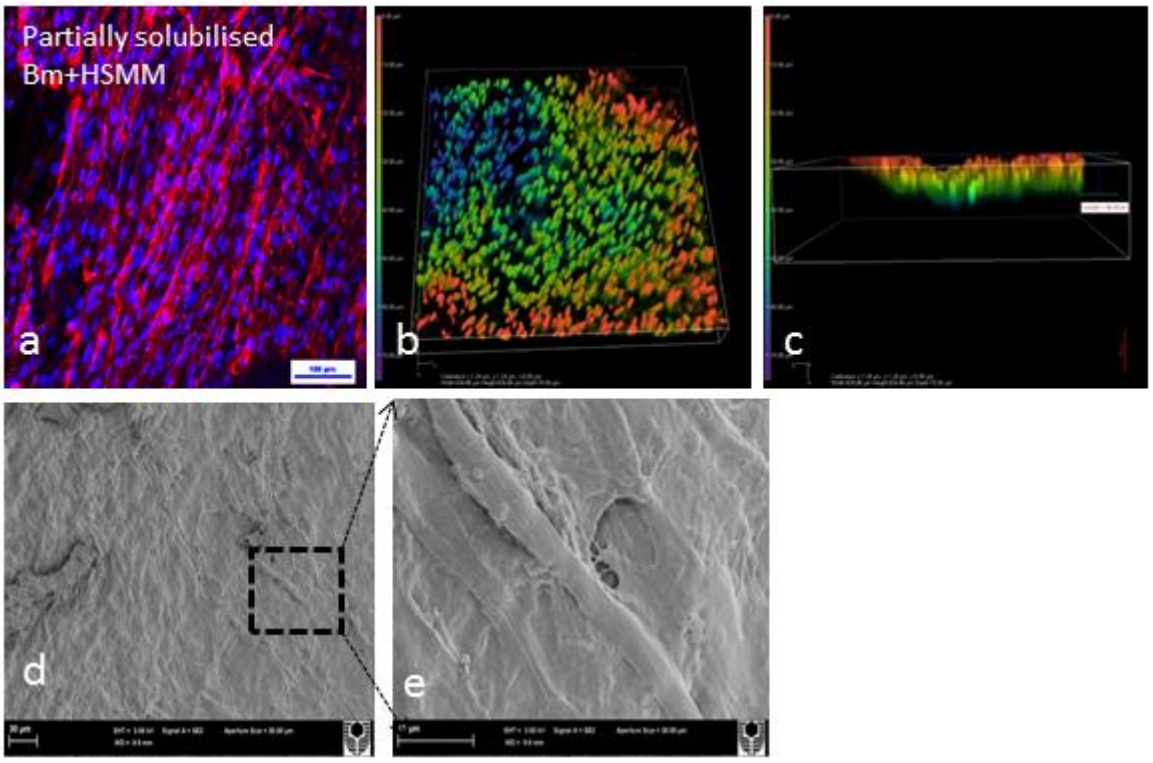

Figure 5.20. HSMMs differentiation on unfixed *B. mori* silk scaffolds. HSMMs ($7.5x10^4$) were cultured on unfixed *B. mori* silk scaffolds (3D) for 11 days in SkGM-2 proliferation medium and then the medium was changed to a differentiation medium and cells were cultured for another 7 days. After cell differentiation, scaffolds were fixed with 4% paraformaldehyde and stained with Rhodamine phalloidin and imaged using a Nikon A1 confocal microscope (a); the colour coded images show the distribution and migration of cells into the scaffold (b and c); SEM images show myotube like structures on partially solubilised silk scaffolds (d, e). Nuclei are stained with DAPI (blue). Scale bar - 100 µm for a-c; 30 µm for d and 10 µm for e.

of the cells by rhodamine phalloidin and DAPI staining revealed multinucleated cells with elongated nuclei and F-actin fibres aligned in parallel orientation, which suggested that cells were differentiating (Fig 5.20. a). The 3D colour coded image indicated that cells were distributed up to a depth of 67 µm into the scaffold (Fig 5.20. b, c). SEM images of these scaffolds clearly showed that cells covered the entire scaffold surface and myoblasts had fused to form myotube like structures by day 15 of culture (Fig 5.20. d-e).

5.2.13 qPCR Experimental workup:

(a) RNA concentration and quality (section 2.8.2)

HSMMs were cultured under 2D conditions on the silk substrates. RNA was isolated from HSMMs cultured for 4 days in SKGM-2 proliferation medium or for 4 days in SKGM-2 proliferation medium plus 1, 7 or 14 days in differentiation medium on wells coated with *B. mori*, *A. mylitta*, *A. assamensis, S. ricini*, collagen I or tissue culture plastic. The ISOLATE RNA KIT was used for this purpose. Since the RNA was to be used for qPCR experiments, RNA concentration and purity was assessed by measuring the absorbance spectrophotometrically and obtaining the ratio of A_{260}/A_{280} nm. For all the RNA samples, A_{260}/A_{280} values were between 1.8 and 2.1.

The genes expressed by HSMMs cultured under 3D conditions were also examined by qPCR. RNA was isolated from HSMMs cultured for 4 days in proliferation medium or for 4 days in differentiation medium on either *B. mori* or *A. mylitta* 3D scaffolds using the TRIZOL method. For all the RNA samples, A_{260}/A_{280} values were between 1.7 and 2.1.

(b) Melt Curve Analysis (section 2.8.5)

Melt curve analysis was performed as described previously (chapter 4, section 4.3.3). As can be seen in Figure 5.20, melt curve histograms for three reference genes and four genes of interest respectively from cDNA samples from HSMMs cultured on silk fibroin coated 2D substrates at days 1 and 7 of differentiation, a prominent single peak was detected for each primer pair indicating gene specific annealing.

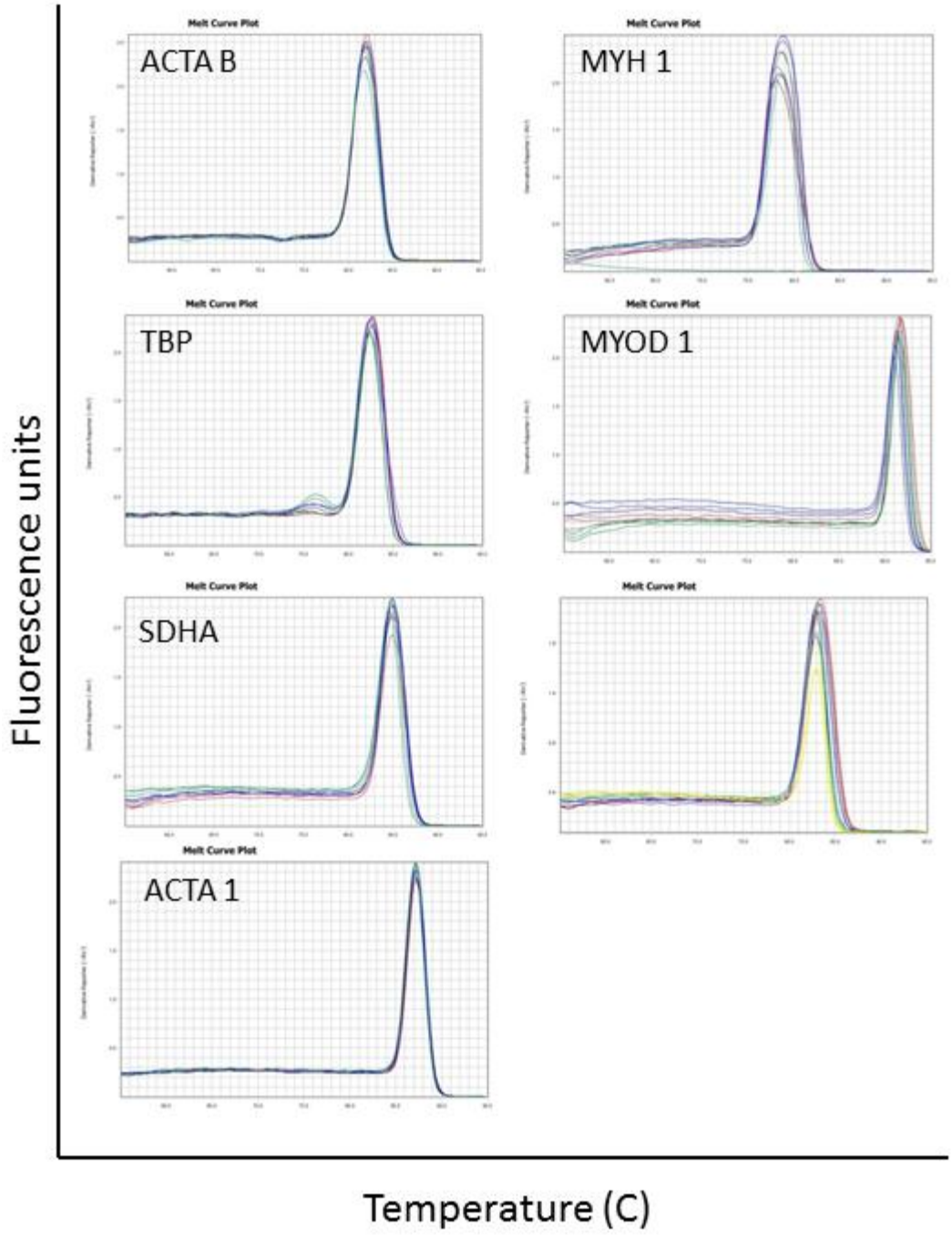

Figure 5.21 Melt curve analysis of reference genes for HSMMs cultured on solubilised silk fibroin. To assess the specificity of the primers, melt curve analysis was performed after every qRT-PCR run. Fluorescence (y-axis) is plotted versus temperature (x-axis). Melt curves show the temperature where two strands of DNA separate.

(c) Primer efficiency calculations (section 2.8.6)

Briefly, five-fold dilutions (1/5, 1/25, 1/125 and 1/625) of neat cDNA (from cultures day 3 of proliferation and 7 of differentiation) were prepared and were amplified for each primer pair (three reference genes and five genes of interest, Table 2.5) in a qPCR reaction. The reaction efficiencies derived from these experiments are shown in Table 5.3.

Table 5.3 Primer efficiencies of reference genes and genes of interest

Gene symbol	Amplification efficiency (%)
SDHA	88
ACTAB	93
TBP	108
$MYOD_1$	101
MYF5	110
MYH 1	67
MYH 3	-
ACTA 1	94

(d) Validation of reference genes using Bestkeeper analysis (section 2.8.7)

qRT PCR was performed on cDNA samples obtained from HSMMs cultured on *B. mori* and *A. mylitta* silk fibroin 3D scaffolds in DMEM/F12/2% HS medium at day 2 and day 10 of differentiation. C_T values obtained after performing the qRT-PCR were placed in the Bestkeeper software and analysed. Three reference genes (*SDHA, TBP* and *ACTAB*) were evaluated before performing the baseline correction for gene expression.

On *A. mylitta* scaffold, *TBP* was found to be the most stable reference gene with CV±SD values of 1.79±0.50. The expression levels of *SDHA* and *ACTAB* were also within acceptable limits with values of 3.35±0.89 and 3.61±0.71 respectively. Similarly, on *B.*

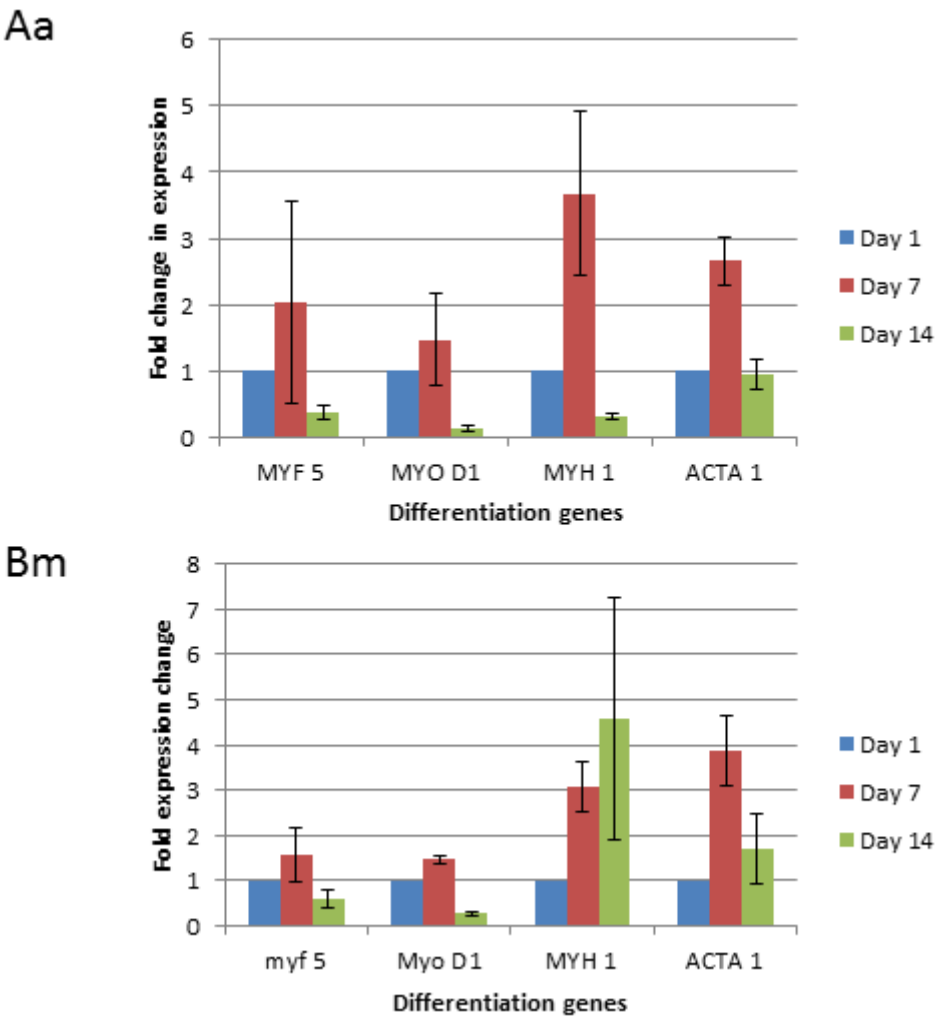

Figure 5.22. Quantitative real-time PCR was used to determine the expression of four differentiation markers in differentiating HSMMs grown on Aa and Bm solubilised silk scaffolds. HSMMs ($6x10^3$ cells/cm^2) were seeded on Aa and Bm coated wells in a 12-well plate and cultured for 4 days in SKGM-2 proliferation medium. Then the medium was changed to a differentiation medium DMEM/F12/2%HS and cells were cultured for 14 days in differentiation medium. RNA was isolated from cells at days 1, 7 and 14 of differentiation. Relative expression levels for *MYF5, MYOD1, MYH1 and ACTA1* were normalized to the C_t value of the reference gene (*TBP)* and fold change was determined using $2^{-delta\ delta}$ C_t method. Day 7 and 14 differentiation expression levels were normalized to Day 1 of differentiation. Mean ± SE of 4 biological replicates are shown. *Bm: B.mori; Aa: A.assamensis.*

mori scaffold, *TBP* was the most stable reference gene with a value of 1.94±0.55, followed by *ACTAB* and *SDHA* with values of 2.30±0.65 and 2.94±0.60.

5.2.14 Relative mRNA levels of myogenic markers in HSMMs on 2D silk substrates (section 2.12)

Further, mRNA levels of muscle transcription factors, myogenic factor 5 (*MYF5)* and myogenic determinant protein-1 (*MYOD1*) and heavy chain myosin (*MYH1)* and skeletal muscle actin-α (*ACTA1*) was assessed using qRT PCR. *TBP* was used as a reference gene after validation using Bestkeeper analysis. Gene expression on days 7 (in differentiation medium) and 14 (in differentiation medium) was assessed when HSMMs ($6x10^3/cm^2$) were cultured on *B. mori* and *A. assamensis* silk fibroin substrates. The baseline expression of the differentiation genes was set at 1.

On both *B. mori* and *A. assamensis* silk fibroin substrates, *MYF5, MYOD1,* and *ACTA*1 showed a similar trend with an increase in the expression levels at day 7 of differentiation but by day 14 the expression levels of *MYF5, MYOD1* were below the baseline expression at day 1 while *ACTA1* levels remained close to the baseline level at day 14 (Fig 5.22). In contrast, the expression pattern of *MYH1* differed on the two silk substrates. On *A. assamensis* silk fibroin, the expression of *MYH1* was three fold higher on day 7 of differentiation than that at day 1 and then it dropped by day 14 of differentiation to below the baseline. However, on *B. mori* silk fibroin the expression of *MYH1* was also three-fold baseline at day 7, but increased to five-fold baseline at day 14 (Fig 5.22).

5.2.15 Gene expression of myogenic markers in HSMMs on *B. mori* and *A. mylitta* 3D silk scaffolds (section 2.13.4)

Since, cell behaviour may be altered when cells are cultured in a 3D microenvironment; the mRNA levels of *MYF5, MYOD1, MYH1 and ACTA1* were measured using qRT PCR when HSMMs ($5x10^5$/scaffold) were cultured on *B. mori* and *A. mylitta* silk fibroin 3D scaffolds. *TBP* was used as a reference gene and gene expression on day 10 (in

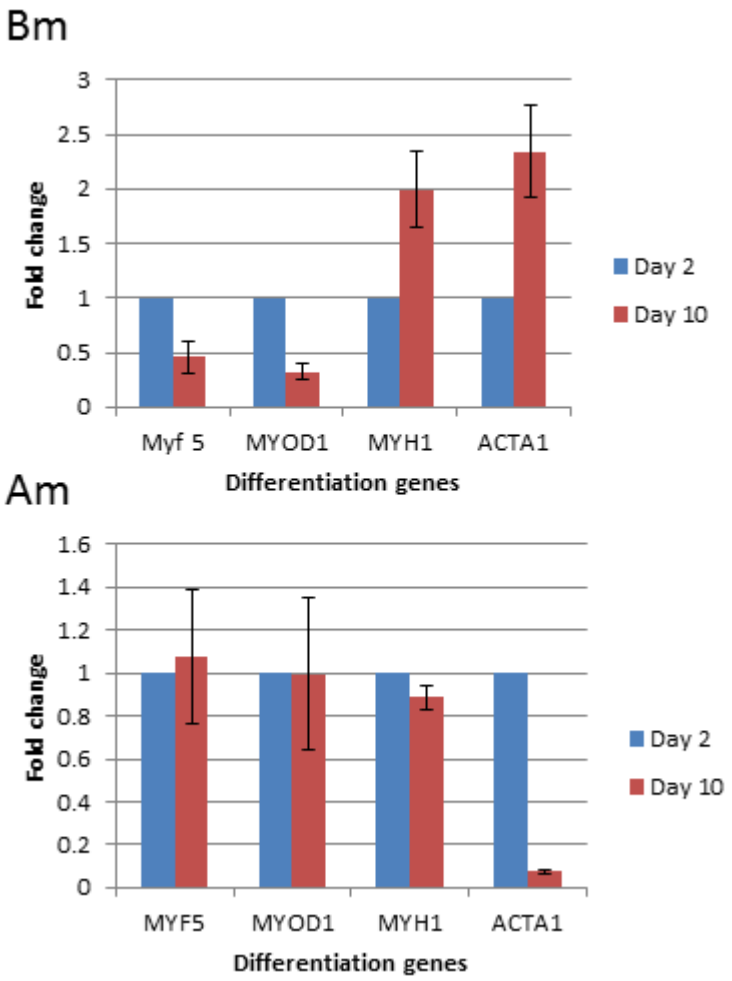

Figure 5.23. Quantitative real-time PCR was used to determine the expression of four differentiation markers in differentiating HSMMs grown on Bm and Am 3D silk scaffolds. HSMMs ($5x10^5$ cells/scaffold) were seeded on Bm and Am 3D silk scaffolds and cultured for 6 days in SKGM-2 proliferation medium. Then the medium was changed to a differentiation medium DMEM/F12/2%HS and cells were cultured for another 10 days in differentiation medium. RNA was isolated from cells at days 2 and 10 of differentiation. Relative expression levels for *MYF5, MYOD1, MYH1 and ACTA1* were normalized to the C_t value of the reference gene (*TBP)* and fold change was determined using $2^{-\text{delta delta}}$ C_t method. Day 10 differentiation expression levels were normalized to Day 2 of differentiation. Mean ± SE of 4 biological replicates are shown. *Am: A. mylitta; Bm: B.mori.*

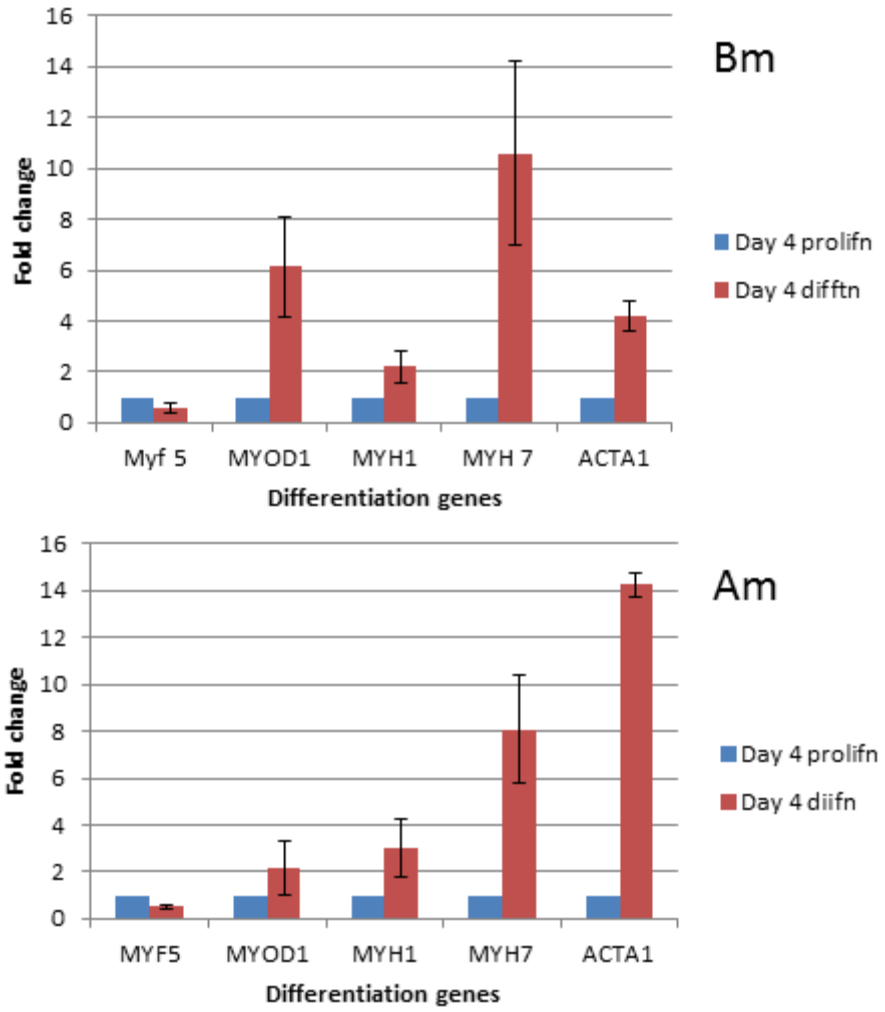

Figure 5.24. Quantitative real-time PCR was used to determine the expression of five differentiation markers in differentiating HSMMs grown on Bm and Am 3D silk scaffolds. HSMMs ($5x10^5$ cells/scaffold) were seeded on Bm and Am 3D silk scaffolds and cultured for 4 days in SKGM-2 proliferation medium. Then the medium was changed to a differentiation medium DMEM/F12/2%HS and cells were cultured for 4 days in differentiation medium. RNA was isolated from cells at day 4 of proliferation and day 4 of differentiation. Relative expression levels for *MYF5, MYOD1, MYH1, MYH3, and ACTA1* were normalized to the C_t value of the reference gene (*TBP)* and fold change was determined using $2^{-\text{delta delta}}$ C_t method. Day 4 differentiation expression levels were normalized to Day 4 proliferation. Mean ± SE of 4 biological replicates are shown. *Am: A. mylitta; Bm: B.mori.*

differentiation medium) was assessed by normalizing expression relative to that at day 2 of differentiation (Fig 5.23).

On *A. mylitta* 3D silk scaffold, *MYF5*, *MYOD1* and *MYH1* levels at day 10 of differentiation were similar to the levels at day 2 of differentiation. However, there was a marked decrease in the expression levels of *ACTA1* at day 10 of differentiation. On *B. mori* 3D silk scaffold, *MYF5* and *MYOD1* expression levels went down at day 10 of differentiation whereas, the muscle myosin and actin isoforms, *MYH 1* and *ACTA 1* increased. Since there was no significant change in the expression levels of myosin isoforms and actin isoforms decreased drastically on *A. mylitta* scaffolds, it was hypothesized that at many cells may have already crossed the threshold and were oriented towards a more mature differentiated phenotype than cells on *B. mori* scaffolds where the *MYH 1*and *ACTA1* showed an increase at day 10 of differentiation. Therefore, to capture the early stages of differentiations, qRT-PCR was performed on day 4 (in differentiation medium) with normalizing to the baseline expression at day 4 of proliferation that is immediately before cells were stimulated to differentiation.

The results are shown in Fig 5.24. On *B. mori* and *A. mylitta* scaffolds, *MYF5* mRNA levels went down on both the scaffolds as the cells preceded towards differentiation and *MyoD1* expression increased. On both scaffolds, a time dependent increase was observed in *ACTA1, MYH1 and MYH7* levels indicative of mature myotubes. Although the increase in levels of *ACTA1* mRNA was much higher on *A. mylitta* scaffolds than on *B. mori* scaffolds possibly suggesting early differentiation of HSMMs on *A. mylitta* scaffolds (Fig 5.24).

5.2.16 3D muscle like tissue growth

To visualize the formation of a 3D muscle-like tissue, HSMMs were seeded at ($5x10^5$ cells per 14 mm diameter scaffold) on *B. mori* silk scaffolds and maintained in SkGM-2 proliferation medium for 4 days, and for a further 4 days in differentiation medium comprising of DMEM/F12/2%HS (Fig 5.25). The confocal images of a large area of the scaffold and myosin immunostaining (secton 2.13.2) suggested that myotubes were formed and covered a very large area of the scaffold i.e. 1.58 mm x 1.218 mm. The

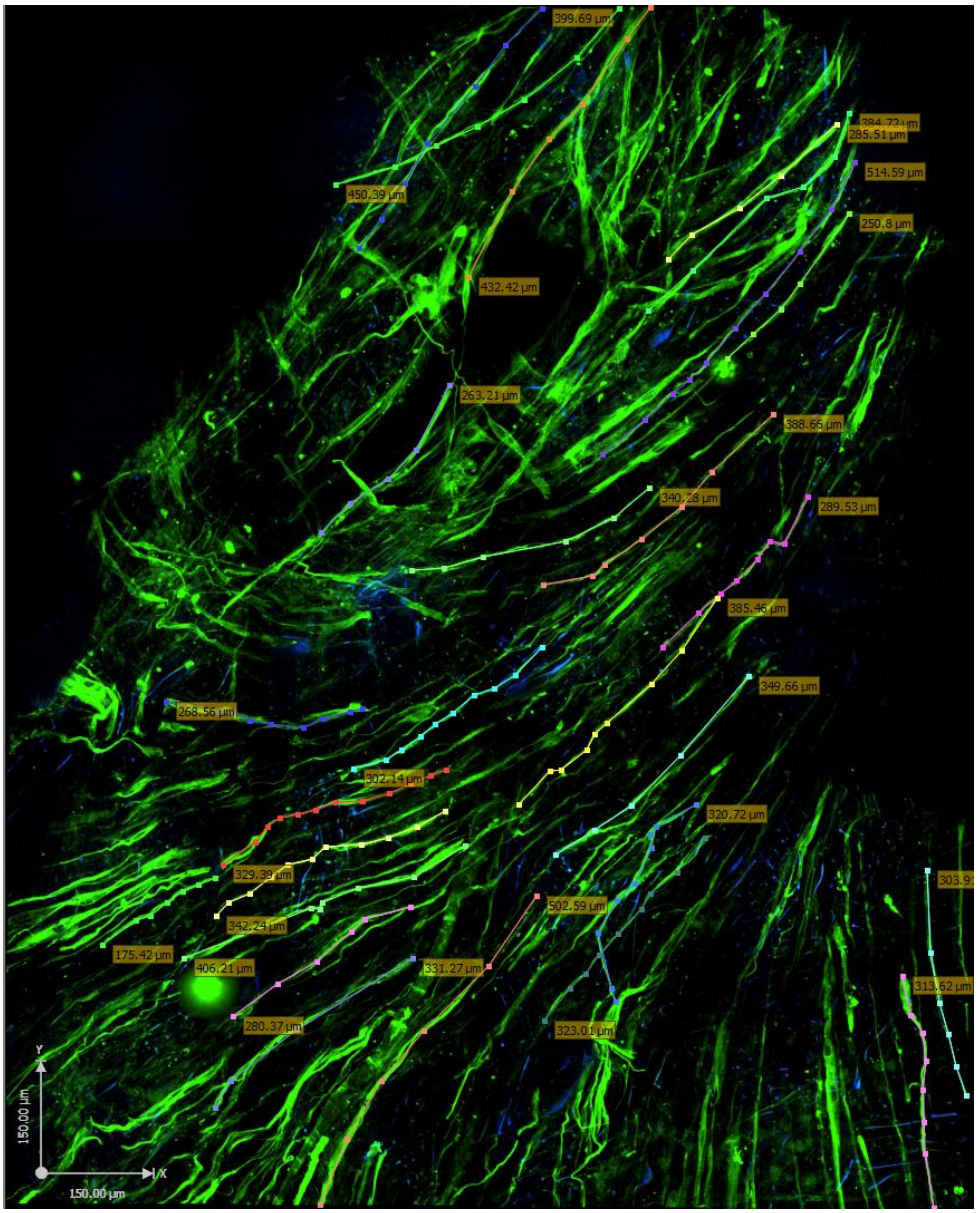

Figure 5.25. Two-dimensional view of a confocal z-stack of multichannel images of 3D muscle-like tissue on *B.mori* scaffolds. HSMMs ($5x10^5$) were cultured for 4 days in SkGM-2 proliferation medium on ethanol fixed and sterilized *B. mori* silk scaffolds, and then the medium was changed to a differentiation medium DMEM/F12/2%HS for a further 4 days. Post differentiation, scaffolds were fixed using 4% paraformaldehyde and stained with anti-myosin, mouse mAb (NOQ.5.4.D), followed by a goat anti-mouse alexafluor 488 conjugated secondary antibody. Images were captured using an Ultraview spinning disc confocal microscope. To capture a large area and to get an estimate of the coverage of the myotubes on scaffold surface, 50 z-stack images of 2.5 µm each stack were stitched together using the Volocity software. Note the extensive coverage of myotubes on the scaffold surface with x-axis (1.58 mm), y-axis (1.213 mm) and z-stack (125 µm). Scale bar-150 µm.

length of the myotubes was also measured using the Volocity software and the analysis revealed that myotubes formed were very long with an average length of 347 μm ±7.2 (Fig 5.25).

5.3 Discussion

This chapter describes the *in vitro* examination of four silk fibroins extracted from different silkworms, for their potential as biomaterials. The results showed that all four silk proteins, when solubilised and used as a substrate, promoted cell growth, proliferation and differentiation of C2C12 myoblasts in 2D serum free cultures. Silk fibroin substrates also supported the differentiation of primary human skeletal muscle myoblasts (HSMMs). These cells were shown to express myosin heavy chain and Glucose transporter 4, both muscle differentiation markers and the fusion of myoblasts to form myotubes was evident on all four silk fibroin materials. Interestingly, myoblasts cultured on 3D silk fibroin scaffolds deposited matrix proteins within a few days of culture to coat the scaffold framework. Although the rate of myoblast differentiation may be expected to be primarily regulated by the deposited matrix proteins, the evidence suggested that *A. mylitta* fibroin scaffolds promoted more rapid differentiation than *B. mori* scaffolds.

Previous studies with silk as a potential biomaterial for skeletal muscle tissue engineering have used the murine myoblast cell line, C2C12 as the model cell type. In this study, in addition to C2C12 cells, HSMMs were also used to test the biocompatibility of silk fibroin biomaterials in 2D and 3D cultures. Additionally, a serum-free culture system was used with the C2C12 cells to better assess the role of these different silk proteins in regulating cell growth and differentiation.

Initially, solubilised silk fibroin was used to coat tissue culture plastic and its ability to support myoblast adhesion and proliferation was assessed microscopically. Phase contrast micrographs showed that C2C12 myoblasts adhered and maintained their characteristic stellate shape on all solubilised silk matrices (Fig 5.2). The viability and proliferation of C2C12 cells was evaluated over a 3 day period; C2C12 cells were sub-confluent at 3 days in a 96-well plate but after this time point contact inhibition altered

the rate of growth. These proliferation assays indicated an equivalent growth pattern on all fibroin films, collagen type I and fibronectin, and this was comparable to uncoated plastic on day 1 and 2 after seeding but at day 3 there was significantly higher growth on all silk matrices compared to tissue culture plastic (Fig 5.3). Although on *A. assamensis* silk C2C12 cells did grow more slowly than on the other protein substrates. We further tested the proliferation of HSMMs on silk and ECM protein substrates (Fig 5.10). Time points for assessing HSMM proliferation were day 2, 5, 8 and 11 as the doubling time of HSMMs was more than 42 hours (data not shown). The growth rate of HSMMs was similar on all silk fibroin substrates and was comparable to that on the ECM protein substrates and uncoated plastic until day 8. However, by day 11 of proliferation the number of cells on *A. mylitta* silk fibroin was higher than that on all other substrates.

Immunostaining showed that both, C2C12 myotubes and the HSMM derived myotubes stained positively for myosin (slow skeletal heavy chain, MyHCB) (Fig 5.5 and Fig 5.11). However, there was a difference in the orientation of myotubes derived from two muscle cell types. HSMM derived myotubes appeared more numerous and aligned in a parallel orientation on all silk substrates, which could potentially promote better differentiation and enhance myotube striations [281]. In contrast, C2C12 myotubes were thicker, having more nuclei per myofibre and were not as well aligned on the fibroin coated glass surfaces (compare Fig 5.5 and Fig 5.11). A similar finding was observed by Cheng et al (2014); they found that as primary human skeletal muscle cells (HSkM) differentiated, the diameter of these myotubes decreased, while C2C12 myotubes diameter increased [301]. In our study, HSMM derived myotubes expressed GLUT4, which has been used as a marker for mature, functional myotubes. Guillet-Deniau et al (1994) found that GLUT4 appeared only in spontaneously contracting myotubes cultured on an extracellular matrix and was located in small intracellular vesicles [302]. After a short exposure to insulin, GLUT4 was translocated to the plasma membrane of the myotubes [302]. An intracellular and cell surface location for GLUT4 matches our data for HSMMs on silk fibroin substrates. Although this suggests these myotubes were mature, contractile performance of the myotubes was not assessed. The extent of HSMM differentiation was further investigated by means of fusion index and counting the

number of myotubes formed on silk substrates. The results showed that myoblasts fused with similar capacities on three silk substrates: *B. mori*, *A. mylitta* and *S. ricini* and the two ECM protein substrates: collagen I and fibronectin with between 77%-80% of the nuclei within the myotubes and the number of myotubes per field of view being between 13 to 17 for all substrates. However, on the *A. assamensis* silk substrate, both the fusion index and number of myotubes formed were significantly lower than on other substrates. These findings were curious given that *A. mylitta* silk fibroin is known to have an integrin binding peptide, RGD, in its amino acid sequence whereas *B. mori* does not. Whether the other non-mulberry species also have the RGD peptide in their silk fibroins is unclear [138, 140].

Given that C2C12 cells were shown to secrete ECM proteins onto etched glass, it was also possible that they also secreted these proteins onto the silk substrates thereby providing their own microenvironment. Immunofluorescence analyses revealed that C2C12 cells secreted major ECM proteins like collagens type I, IV and VI, fibronectin and perlecan although not all these silk fibroin substrates triggered the same level of ECM protein deposition (Fig 5.6-5.9). The reason for the differential production/deposition of ECM proteins on different silk substrates may be due to differences in the structure of these silk fibroins. Immunostaining results similarly showed that all four silk scaffolds in their 3D form supported matrix protein deposition by HSMMs (Fig 5.15). Scanning electron microscopy images of HSMMs on an *A. mylitta* scaffold further supported the immunofluorescence observations, as clear protein deposition can be seen (Fig 5.17 c). Secreted ECM proteins play an important role in muscle differentiation. Chan et al (2007) [295] performed a proteomic analysis of C2C12 cells cultured in serum free medium and identified 80 non-redundant proteins, of which 27 were secretory proteins. Some of these secretory proteins were molecules involved in ECM remodelling, cell proliferation, migration, and signalling [295]. For a biomaterial to be successful as an implanted graft, it should support the resident progenitor cells to synthesize and deposit their own matrix and to form a natural ECM which would better support tissue repair.

Other researchers have used a hybrid scaffold of cell derived ECM and a silk fibroin for nerve tissue engineering *in vivo*. In particular, Gu et al (2014) used silk fibroin scaffolds coated with Schwann cell derived ECM proteins to successfully repair a 10 mm gap in the sciatic nerve of rats [303]. These researchers cultured Schwann cells in the presence of ascorbic acid on silk fibroin/chitosan conduits for a period of 14 days and then decellularized the scaffolds leaving cell deposited fibronectin and laminin on the scaffolds. These ECM coated scaffolds were then implanted in a rat model of sciatic nerve injury and the repair outcomes compared to those of Silk fibroin/Chitosan scaffolds or an acellular nerve graft. After 12 weeks functionality was significantly better in either the Schwann cell-derived ECM modified scaffold or the acellular nerve graft than the scaffold only group [303]. Since all four silk fibroins in our study, both in a solubilised form as 2D substrates and as 3D scaffolds supported the deposition of ECM proteins by myoblasts, these scaffolds with their deposited skeletal muscle cell derived ECM may similarly perform better *in vivo* to repair volumetric muscle loss than silk scaffolds that lack ECM proteins.

It is necessary to evaluate the cell responses in a 3D microenvironment as the information obtained from 2D cell culture is potentially not complete due to a difference in the cell niche encountered by cells in a 3D environment. Moreover, the arrangement of membrane proteins responsible for cell-ECM and cell-cell interactions can be very different between 3D and 2D substrates [304]. The geometry of the 3D scaffolds can have an impact on the "stemness" and behaviour of stem cells as compared to a flat 2D substrate. A recent study by Wei et al (2014) showed that mouse embryonic stem cells cultured on collagen, chitosan and PLGA based 3D scaffolds revealed better maintenance of stem cell like phenotype which was marked by an increase in the number of G0/G1 phase cells, up-regulation of *Oct4* and down-regulation of *Sox2* genes and higher clonal formation ability as compared to the cells cultured on a 2D substrate [304]. In addition, 3D scaffolds mimic *in vivo* situations as they offer better nutrient and gaseous exchange, and removal of waste products is much more effective in a 3D scenario.

To investigate in *in vitro* assays, whether coating silk scaffolds with solubilised muscle matrix (chapter 3) would alter cell adhesion and spreading, HSMMs were cultured on muscle matrix coated *B. mori* 3D silk scaffolds. Cytoskeletal staining for actin fibres revealed that after 5 days in culture, HSMMs appeared well distributed and elongated on both, the matrix coated *B. mori* scaffolds and uncoated *B. mori* scaffolds (Fig 5.14). However, a higher cell density and better cell alignment was achieved on matrix coated scaffolds. Other workers have found that coating biomaterials with ECM proteins enhances cell proliferation and differentiation. In one such study, silk scaffolds obtained from *B. mori* were combined with the ECM proteins: collagen type I, type IV and fibronectin and evaluated for their potential in bladder tissue regeneration [305]. Two structurally distinct silk scaffolds were prepared: smooth, compact multi-laminates and rough, porous lamellar-like sheets and then coated with the ECM proteins. Interestingly, the rough, porous sheets coated with fibronectin promoted the highest attachment of human bladder smooth muscle cells, urothelial cells, murine embryonic stem cells and induced pluripotent stem cells when compared to the other scaffolds [305]. Immunohistochemistry and real time RT-PCR analysis revealed that the fibronectin coated silk scaffolds also supported the contractile differentiation of smooth muscle cells which was marked by a significant up-regulation of α-actin and SM22α mRNA and protein expression levels following TGFβ1 stimulation [305]. This indicating the fibronectin-coated rough porous scaffolds best assisted embryonic stem cells and iPS cell differentiation toward both urothelial and smooth muscle lineages [305]. The decellularized muscle matrix, prepared in our study (chapter 3) is a mixture of structural collagens, glycoproteins, including fibronectin and proteoglycans, and although the HSMMs were not stimulated to differentiate on the muscle matrix coated *B. mori* scaffolds, the alignment and density of these cells suggested that they were proceeding to differentiation more rapidly than HSMMs on the uncoated *B. mori* scaffolds. Given the findings of Franck et al (2013) [305], this should have been investigated further.

F-actin staining and SEM images illustrated that HSMMs adhered to and spread evenly on 3D silk scaffolds and formed a cell sheet by day 5 in culture (Fig 5.13. and Fig 5.16-5.17). Immunostaining against slow skeletal muscle myosin (MyHCB) showed

differentiation of HSMMs on the 3D scaffolds was triggered more readily on some scaffolds than on others (Fig 5.18 and 5.19). On *B. mori* scaffolds HSMMs formed extremely long, well aligned myotubes, whereas the myotubes formed on *A. mylitta* scaffolds appeared thicker and much shorter. Myosin expressing myotubes on scaffolds from *A. assamensis* were perpendicularly oriented in 2 layers on the 3D scaffolds and *S. ricini* silk fibroin poorly supported differentiation of HSMMs (Fig 5.18 and 5.19). This result was surprising given that on *S. ricini* 2D silk fibroin substrates the fusion index and myotube number were not different from those observed on *A. mylitta* or *B. mori* substrates. This suggests that the porosity of the scaffolds may have been a contributing factor. Interestingly, the cell sheet covering *S. ricini* scaffolds were quite different in appearance to that on the other silk scaffolds. The SEM images revealed what appeared to be a many cell thick layer (Fig 5.16), whereas the underlying structure of the *A. mylitta*, *B. mori* and *A. assamensis* scaffolds was visible under a much thinner cell layer. Others have shown that optimum pore size architecture is a crucial component of silk fibroin scaffolds. In particular, Zhang et al (2010) reported that human bone marrow mesenchymal stromal cells seeded on silk fibroin scaffolds of different pore sizes were found to prefer scaffolds of a pore size between 100 μm – 300 μm and showed better cell proliferation and ECM production on these scaffolds [306]. Furthermore, *in vivo* transplantation of these silk scaffolds together with the bone marrow mesenchymal stromal cells promoted de novo bone formation [306].

When the *B. mori* scaffold was used without fixation, it started to partially dissolve (Fig 5.19). Remarkably, when HSMMs were cultured on these "partially solubilised" *B. mori* silk scaffolds, they lined up and displayed well aligned F-actin fibres and elongated nuclei along the length of the actin fibres, which suggested differentiation of myoblasts into aligned myotubes (Fig 5.20). A useful property of silk scaffolds that promotes their use as a bio-implant for tissue regeneration purposes is their biodegradability without releasing any toxic products. Testing the biodegradation of the four silk scaffolds used here was beyond the scope of this study, but others have demonstrated their biodegradability under *in vitro* [307, 308] or *in vivo* conditions [151, 152]. Given

scaffolds are bio-degradable *in vivo* the result shown in Fig 5.20 was encouraging as it suggests that partially degraded *B. mori* silk scaffolds can still support myogenesis.

To quantify the extent of differentiation of the HSMMs on the different silk scaffolds, the expression pattern of a number of genes that trigger the differentiation of myoblasts to myotubes were investigated. *MYF5* is the first muscle regulatory factor to be expressed during mouse embryogenesis while *MYOD1* promotes cell cycle withdrawal and induction of differentiation [197]. *MYH 1* and *MYH 7* are adult heavy chain myosin isoforms and *ACTA 1* is muscle actin isoform [284]. In this study, *TBP* was found to be the most stable reference gene which is in accordance with the study conducted by Stern-Straeter et al (2009), where these authors examined the expression of six reference genes: Beta-actin; Beta-2-microglobulin; glyceraldehyde-3-phosphate dehydrogenase; peptidylprolyl isomerase A; TATA box binding protein (*TBP*) and ribosomal protein, and large P0 (*RPLPO*) in human skeletal muscle myoblast cultures [309]. They found that *RPLPO* was the most stable reference gene and *TBP* was the second best. We did not included *RPLPO* in our study; but among *ACTAB*, *SDHA* and *TBP*, the latter was found to be the best reference gene.

There were some differences observed in the gene expression profile of HSMMs in 2D and 3D cultures (Fig 5.22-5.24). The lower number of cells seeded in 2D cultures ($6x10^3$) as compared to the cell numbers seeded on 3D scaffolds ($5x10^5$) may have been a contributing factor as well as the nature of the supporting protein. In 2D cultures of HSMMs on *A. assamensis* and *B. mori* silk fibroin, *MYF5*, *MYOD1* and *ACTA1* showed a similar pattern of expression where the levels increased by day 7 of differentiation and then decreased at day 14 of differentiation, with *ACTA 1* levels remaining close to the baseline.

The anti-myosin immunostaining data indicated that HSMMs differentiated very well on *A. mylitta* and *B. mori* scaffolds (Fig 5.18), hence we examined the gene expression prolife of differentiation markers on these two silk scaffolds. Since it is not easy to visualize the formation of myotubes on 3D scaffolds, the differentiation was assessed after culturing HSMMs for 17 days (7 days in proliferation and then 10 days in

differentiation medium), giving them maximum time to differentiate. Firstly, the differentiation was assessed at day 10 of differentiation (Fig 5.23). The results suggested that on *A. mylitta* 3D silk scaffolds, the cells are differentiating early as there was virtually no change in the expression of *MYF5, MYOD1* and *MYH1* while *ACTA1* shows a significant decrease at this time point. The data also suggested that cells on *B. mori* scaffold were still differentiating as there was a concomitant increase in *MYH1* and *ACTA1* levels (Fig 5.23). This is a possible scenario as the cells were in proliferation medium for 7 days and then for a further 10 days in differentiation medium and we chose day 2 differentiation levels as our normalization levels. With the higher cell number ($5x10^5$ cells/scaffold) it is very likely that myoblasts may have fused earlier than expected. Hence to capture the early stages of differentiation, another experiment was conducted where cells were cultured for 8 days: 4 days in proliferation medium and 4 days in differentiation medium. On both scaffolds, a decrease in *MYF5* levels and an increase in *MYOD1* levels suggested that cells had ceased proliferation. *MYH7* showed a 10 fold and 8 fold increase on *B. mori* and *A. mylitta* respectively which correlated with the protein expression levels of this gene product (MyHCB) (Fig 5.18). The other myosin isoform, *MYH1* showed only a slight increase on both silk scaffolds but *ACTA1* levels were much higher on *A. mylitta* than on *B. mori* (Fig 5.24). The cells may be differentiating early on *A. mylitta* as the silk fibroin from this silkworm species possesses an integrin binding RGD peptide and others have shown that neonatal cardiomyocytes cultured on *B. mori* and *A. mylitta* silk scaffolds attach and spread much faster on *A. mylitta* silk than *B. mori* silk. Furthermore, the cardiomyocytes cultured on *A. mylitta* scaffolds differentiated towards a more mature phenotype exhibited by well aligned sarcomeres and sustained contractions in culture [141]. Mudera et al (2010) investigated the effect of increasing cell density on the maturation and contractile ability of muscle derived cells in a 3D collagen based model of skeletal muscle [310]. Their results showed that maximal peak force was obtained at an optimum seeding density of $30x10^6$ cells/collagen construct while a distinctive force contraction profile was obtained when cells were seeded at $40x10^6$ cells/collagen construct. A concomitant increase in the myogenic expression profiles of *MYH7* was seen: from 8-fold to 40-fold when cells were seeded at a density of $30x10^6$ and $40x10^6$ cells/collagen construct respectively [310].

Their study showed that cell density in a 3D microenvironment can govern the phenotype of human skeletal muscle cells.

Natural ECM in a functional muscle is highly orientated and muscle fibres extend longitudinally, sometimes up to the length of 35 cm within this natural ECM to form the contractile machinery. In order to form a functional muscle graft, the regenerated fibres should join end to end or else muscle atrophy will occur. Our data suggested that 3D silk fibroin scaffold from *B. mori* was highly supportive of myoblast differentiation and the confocal imaging showed that the myotubes formed were very long, 347 μm in length and cells covered a very large area of the scaffold (1.58 mm x 1.218 mm) (Fig 5.25); myotube formation was a result of the fusion of myoblasts in different planes. Creation of 3D skeletal muscle tissue constructs which mimic the characteristics of the muscle tissue *in vivo* will provide a better system to the research community for skeletal muscle tissue engineering purposes and might fill the gap between 2D and 3D microenvironment. A recent study by Tang-Schomer et al (2014) further supports our observation although their study was focussed on construction of a functional brain-like cortical tissue in 3D *in vitro* cultures [311]. The researchers cultured primary rat cortical neurons on silk fibroin-ECM (collagen) composites and found that compartmentalized and interconnected neural network formation occurred in these silk fibroin based 3D biomaterials. Furthermore, this "brain like" tissue displayed electrophysiological and mechanical properties simulating *in vivo* brain functions and responded to induced injury *in vitro* rendering the applicability of this "brain like" tissue for the assessment of brain disorders like traumatic brain injury [311].

5.4 Conclusion

In summary, our results demonstrated that silk fibroin extracted from four different silkworms was effective in supporting both, mouse and human myoblast proliferation and differentiation under *in vitro* 2D and 3D culture conditions. In a 2D scenario, *A. assamensis* silk fibroin was least able to support proliferation of C2C12 cells and differentiation of HSMMs. All four silk scaffolds supported ECM production by

HSMMs with a similar degree of arrangement of ECM. In 3D cultures, *B. mori* and *A. mylitta* were found to best support HSMMs differentiation. As a result, it is proposed that *B. mori* and *A. mylitta* silk scaffolds are most likely to be useful as three dimensional frameworks for skeletal muscle repair in *in vivo* muscle injury models.

5.5 Future Directions

Since these scaffolds showed promising results *in vitro* it will be intriguing to test these silk scaffolds in animal models for the treatment of volumetric muscle loss. Another useful experiment to perform is to evaluate the immune-modulatory properties of these silks scaffolds either *in vitro* using macrophage cultures or in an *in vivo* implantation situation with subsequent analyses of several inflammatory cytokines.

Chapter 6:

Atomic force microscopy: applications in muscle matrix biology

6.1 Introduction

The supramolecular structure of ECM assemblies is responsible for the function of many connective tissues including skeletal muscle. For a better understanding of the role of ECM in muscle repair and regeneration, it is imperative to know more about the ultrastructure of the complex mesh of molecules that make up the ECM. Existing imaging techniques like electron microscopy requires samples to be fixed with strong fixatives like paraformaldehyde or gluatraldehyde which might alter the structure of the samples. Atomic force microscopy provides a better alternative for imaging structural features of ECM, as samples can be imaged without fixing.

A basic atomic force microscope consists of a silicon nitride cantilever to which a sharp silicon tip (radii of 20-60 nm) is attached. It works on the basic principle of tip-sample interactions. The AFM tip scans over the sample surface and the AFM records interactions between the tip and the surface. The cantilever deflects in a z-direction as the tip scans over the surface and this deflection is detected by a photodiode. A computer processes the electrical signal of the photodiode and generates a feedback signal for the piezoscanner to maintain a constant force on the tip. This information is transferred into a topographic image of the surface (Figure 6.1). Atomic Force Microscopes can be operated in different imaging modes – for example contact and tapping modes (also called as intermittent contact mode), depending on the sample: hard materials are imaged with contact mode whereas soft biological samples are imaged using tapping mode.

Contact mode: In this mode, the tip is in permanent physical contact with the sample surface and the force between the tip and the sample surface is kept constant via an electronic feedback loop. Contact mode can be used to image hard and stable samples which are not affected by the frictional force components the tip applies to the sample. A significant disadvantage of Contact Mode are the lateral forces occurring between probe and sample during scanning.

Tapping mode (Intermittent contact mode): In this mode an oscillating tip (near its resonance frequency) is used and the tip is not in contact with the surface for most of the

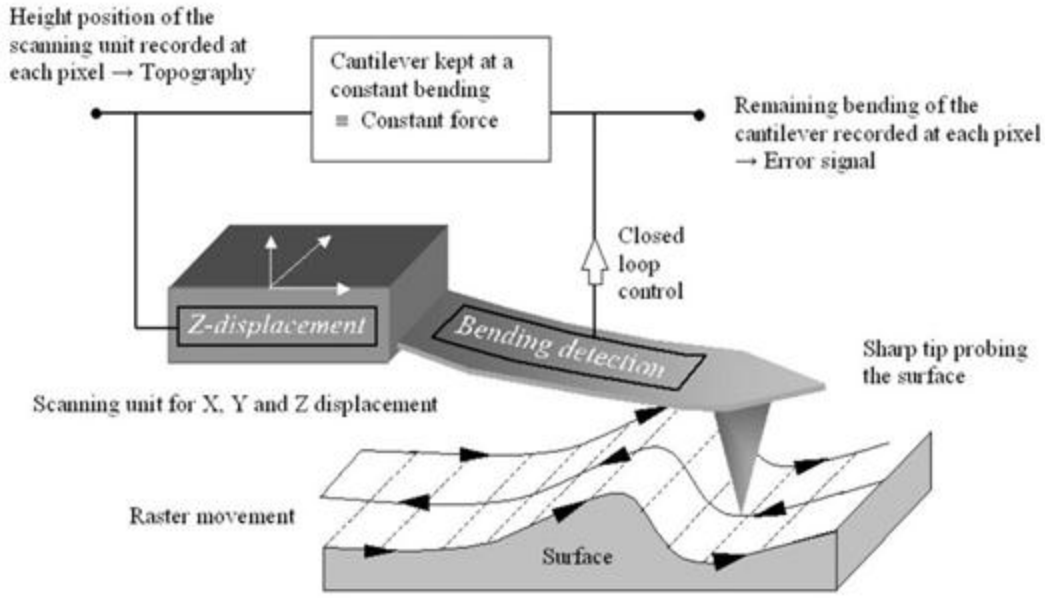

Figure 6.1. Schematic representation of an atomic force microscope. A basic atomic force microscope consists of a silicon nitride cantilever to which a sharp silicon tip (radii of 20-60 nm) is attached. It works on the basic principle of tip-sample interactions. The AFM tip scans over the sample surface and the AFM records interactions between the tip and the surface. The cantilever deflects in z-direction as the tip scans over the surface and this deflection is detected by a photodiode. A computer processes the electrical signal of the photodiode and generates a feedback signal for the piezoscanner to maintain a constant force on the tip. This information is transferred into a topographic image of the surface. Image adapted from University of Neuchatel, Switzerland

oscillation cycle. When the tip (driven by piezo) moves towards the surface, it begins to tap the surface. This leads to an energy loss by the oscillating tip which reduces the amplitude significantly. In Tapping Mode, the amplitude of the oscillation is used as a feedback parameter for imaging the topography of the sample. Tapping Mode can be done in air and also in fluids and thus is suitable for imaging biological specimens. Lateral forces, which occur during scanning in contact mode, are nearly non-existent in tapping mode.

It is also possible to combine the high-resolution topographical imaging capabilities of an atomic force microscope with the optical imaging abilities of a confocal microscope. Using this technique it is possible to determine the biochemical composition of the matrix along with the topographic image. Another useful AFM technique in matrix biology is 'force volume' imaging. In this mode, the tip measures individual forces at different points on the matrix and these individual force curves are combined to produce a volume image. This can be very useful to determine the elasticity of different cells or extracellular matrices in tissues.

Here in this chapter, AFM imaging of undifferentiated C2C12 myoblasts and differentiated myotubes on collagen I matrix was performed to investigate the cell-matrix and cell-cell interactions at molecular level and to get a quantitative estimate of the height of the cells when spread on collagen I. The ultrastructure of the skeletal muscle matrix of mice was also visualized; both the control muscle and muscle decellularized using the PLA_2 method were imaged. A thin layer of fibronectin coated on glass and gelatin gels crosslinked with heparin (2% w/v) were imaged to get an insight into any change in the gel structure after modification with GAGs. We also attempted to biochemically analyse the decellularised matrix obtained in chapter 3 using the picoTREC imaging technique. Finally, "force volume" imaging was also performed on the decellularised matrix to determine the elasticity of the acellular muscle matrix.

6.2 Supplementary Materials and Methods

6.2.1 Cell culture or muscle tissue sectioning

C2C12 (Passage 15) cells ($5x10^4$) were seeded on collagen I (10.0 µg/cm^2) coated cover-slips in growth medium (DMEM/10% FBS) and maintained at 37ºC and 5% CO_2. After 24 h (80% confluence), cells were transferred to differentiation medium (DMEM/2% horse serum) and were cultured for 5 days. Cells at day 1 after seeding and day 5 after differentiation were fixed in 4% paraformaldehyde for 10 min and stored in PBS at 4ºC until imaging. Muscle sections (triceps or gastrocnemius) were cut (10 µm) using a cryostat.

6.2.2 Preparation of gelatine gel

Gelatine (500 mg) was dissolved in 10 ml of hot water to yield a solution of 50 mg/ml. This gelatine solution (6 ml) was pipetted in to a mould and incubated at 4ºC O/N to allow gel formation.

6.2.2.1 Cross linking the gelatine gel with GAGs

The gelatine gels each containing 50 mg of gelatine were incubated in 20 ml of 40% v/v ethanol containing 50 mM 2-morphilinoethane sulfonic acid (MES) pH 5.5 for 10 min at RT. Gels were subsequently immersed in 20 ml 40% v/v ethanol containing 50 mM MES pH 5.5 and 2% Heparin (w/v) for 4h at RT with 24mM of 1-Ethyl-3-[3-dimethylaminopropyl] carbodiimide hydrochloride (EDC, Sigma-Aldrich). N-hydroxy succinimide (NHS, Sigma-Alrdich) was added in an EDC: NHS ratio of 5:1 and incubated overnight at RT. Next day, the gels were washed twice in 0.1M Na_2HPO_4 (pH 9.1) for 1h. Finally to remove uncoupled heparin from the gels were washed twice in 1M NaCl for 2h, 2M NaCl for 1 day (6 changes of washing solution) followed by washing with distilled water. Gels incubated without heparin in the presence of EDC/NHS were used as controls.

6.2.3 AFM Probes used for imaging

NCH probes (NanoWorld, Neuchatel, Switzerland) for tapping mode in liquid and DNP probes (Bruker, Billerica, MA) for contact mode in air

NCH probes:specifications (www.nanoworld.com)

Cantilever Data	Value	Range*
Thickness	4.0 µm	3.5 - 4.5
Mean Width	30 µm	25 - 35
Length	125 µm	120 - 130
Force Constant	42 N/m	21 - 78
Resonance Frequency	320 kHz	250 - 390

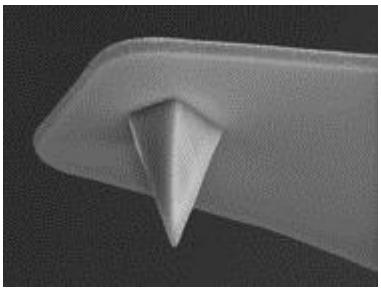
Schematic of a tip

DNP probes:specifications (http://www.brukerafmprobes.com)

Material:	Silicon Nitride
Geometry:	Triangular
Cantilevers Number:	4
Cantilever Thickness (Nom):	0.6 µm
Cantilever Thickness (RNG):	0.55 - 0.65 µm
Back Side Coating:	Reflective Gold
Top Layer Back:	45 ± 5 nm of Ti/Au

Shape	Resonant Freq. kHz			Spring Const. N/m			Length µm			Width µm		
	Nom.	Min.	Max.	Nom.	Min.	Max.	Nom.	Min.	Max.	Nom.	Min.	Max.
A Triangular	65	50	80	0.35	0.175	0.7	120	115	125	25	20	30
B Triangular	23	16	28	0.12	0.06	0.24	205	200	210	40	35	45
C Triangular	56	40	75	0.24	0.12	0.48	120	115	120	20	15	25
D Triangular	18	12	24	0.06	0.03	0.12	205	200	210	25	20	30

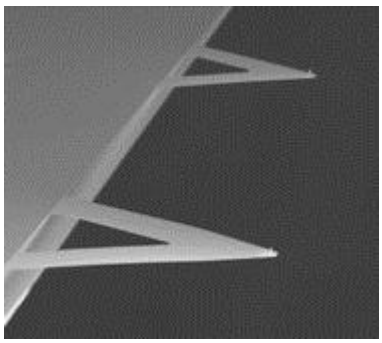
Schematic of cantilevers

6.2.4 Mounting the cantilever on scanner

A cantilever was mounted on the scanner with tip positioned at the edge of the scanner centre point. The Scanner was then placed in an inverted position on the microscope stage and the laser spot was aligned on the cantilever.

6.2.5 Sample mounting

Firstly, a silicon wafer was placed on the fluid cell assembly and then the cover-slip ($24mm^2$) either containing C2C12 cells (undifferentiated or differentiated) or muscle sections was placed on the silicon wafer and then sealed with an O-ring. The silicon wafer reflects the light from the bright field microscope and makes it easier to view the sample otherwise it is difficult to trace the sample on a cover-glass. PBS was then added drop wise to the fluid cell. The O-ring prevents any leakage of PBS from the fluid cell assembly. The assembly was then carefully slid onto the microscope so that the nose of the scanner is right at the centre of the stage, allowing access to the sample. The laser spot was readjusted on the cantilever to compensate for the shift due to liquid in the flow cell.

6.2.6 AFM imaging

6.2.6.1 Contact mode in air

Images of gelatin gels were acquired using a Nanoscope IIIa (Digital Instruments Inc., Santa Barbara, CA) atomic force microscope with V-shaped silicon nitride cantilever in contact mode and a long range scanner.

6.2.6.2 Tapping mode in liquid

All the samples (except the gelatin gel) were imaged using a PicoPlus AFM (Agilent Technologies, Santa Clara, CA) with tapping mode in liquid using a silicon nitride cantilever with a spring constant of 0.32 N/m. The cantilever was tuned with a frequency range of 1-60 kHz. Cantilever oscillation frequencies and drive amplitudes were determined by the Pico Scan 5 software before every scan. Once the desired frequency was reached with a sharp peak obtained, the tune frequency was narrowed down and the tip was retracted by 10 µm and approached with a slower speed. The amplitude voltage to start the scan was between 3V and 5V and when the tip approached the sample, the voltage falls. Once the cantilever reached the surface of the sample, the set-point was lowered and the scan rate was decreased which enabled the collection of high resolution images. All the images were obtained only after optimising the gain settings (integral and proportional gains were close to 1). Height, amplitude and phase images at different scan areas of 80 μm^2, 50 μm^2, 10 μm^2 and 2 μm^2 were captured between scan rates of 1 to 5 Hz using the software Pico Scan 5. All reported images were acquired with 512 × 512 pixels definition. Depending on the area of the scan, either a long range scanner or a short range scanner was used.

6.2.7 picoTREC Measurements

6.2.7.1 AFM tip functionalization

Amine groups were introduced onto inert AFM tips using the vapour phase deposition method [312]. Briefly, AFM tips (Type VI Mac Levers, Agilent Technologies) were washed in methanol (3 times), dried and then washed again with chloroform (100 %) for 5 min and dried. Tips were then placed in a desiccator to remove all air and moisture from the tips. After complete drying, tips were placed on para-film in a petri-dish ($35mm^2$) with 30 µl of fresh 3-(Aminopropyl) triethylsiloxane (APTES (99%), Sigma Aldrich) and 10 µl of tetraethyl-ammonium chloride (TEA (0.5%), Sigma Aldrich) and incubated for 2 h at RT.

6.2.7.2 Antibody linking to the tips

Antibody coupling to the AFM tips is a three step protocol where firstly, an amine group is attached to the AFM tip (see above), followed by linking a flexible cross-linker molecule (NHS-PEG800-aldehyde in this case) and finally the covalent binding of the desired antibody (an anti-collagen I antibody in this case) to the cross-linker [312, 313]. Briefly, 10 µl of an anti-collagen I rabbit polyclonal antibody (Abcam) was diluted in 100 µl of sterile PBS and then centrifuged in a Ultra 15 centrifugal filter unit (Amicon, Millipore) at 10,000 g for 10 min at 4ºC to remove the sodium azide from the antibody mixture. The heterobifunctional cross-linker NHS-PEG_{800}-aldehyde (Sigma-Aldrich) was covalently bound to the amine groups on the tips at a concentration of 6.6 mg/mL in chloroform with 1% (vol/vol) triethylamine for 2h at RT. Tips were then placed in a 1 mg/ml antibody solution (25µl) and 2 µl of sodium cyanoborohydride ($NaCNBH_3$) solution (32 mg $NaCNBH_3$, 50 µl of 100 mM NaOH in 450 µl MilliQ water) for 2 h. Subsequently, 5 µl of 1 M ethanolamine-hydrochloride (Sigma-Aldrich) was added to the solution for 10 min to quench any remaining aldehyde groups. Finally, the probes were washed and stored in PBS buffer at 4°C.

6.2.7.3 Simultaneous topography and recognition imaging (TREC) measurements

This procedure uses a receptor functionalised tip on a magnetic-coated cantilever (MAC probe) driven by a magnetic field (MAC mode). For AFM topography and recognition measurements, MAC probes (nominal spring constant 0.2 – 0.9 N/m) modified with the collagen I antibody as described were used for imaging. Gastrocnemius muscle sections (thickness, 20 µm) on glass coverslips were placed in a fluid cell filled with PBS at RT. MAC mode non-contact images were acquired using a PicoPlus AFM and a picoTREC^{TM} box (Agilent Technologies), spanning regions of interest less than 5 × 5 μm^2. Cantilevers were tuned to a very low drive frequency (3.5 kHz) at scanning speeds of 1 line/s (or slower) using full amplitude feedback. For the MAC mode probes, the thermal noise method was used for calibration and spring constants were found to be between 0.2 and 0.9 N/m.

6.2.8 Force spectroscopy and force volume imaging

To measure the elastic forces of the gastrocnemius muscle samples, PicoPlus AFM was used according to the protocol described earlier to capture topographic images (tapping mode in liquid). In AFM "force spectroscopy" experiments, the cantilever and tip were moved towards the sample until they were in contact, and then retracted again while the force of the interaction between the tip and sample was measured (Figure 6.2). This step was then repeated at different locations of the sample to build up a map of tip-surface interactions. The Topograph and spectroscopy sweep (SPS) option was selected in the buffer assignment window and an SPS sweep was performed at every 32^{nd} and 16^{th} point using contact mode and tapping mode in liquid. Closest SPS curve was extracted to load a spectroscopy sweep of the closest data point. Seven to eight data points were examined and the raw data collected for cantilever deflection and z-piezo movement for every force curve was then subsequently analysed using a custom MATLAB script. The elastic modulus of the muscle samples was then determined by fitting the modified Hertz model to force indentation curves.

6.2.9 Image Analysis

All the images acquired using AFM were analysed using the Gwyddion data analysis software version 2.31 (http://gwyddion.net/). Standard gwyddion tools were used for plane levelling and line correction of images. Some images were also modified using the 'scar' correction tool to remove the background noise.

6.3 Results

6.3.1 Fine structure of cells and cell-matrix interactions were visualized using AFM

Undifferentiated C2C12 cells (day 1 in proliferation media) and differentiated myotubes (day 5 in differentiation media) (section 6.2.1) were visualized using AFM by tapping mode in liquid (section 6.2.6.2).

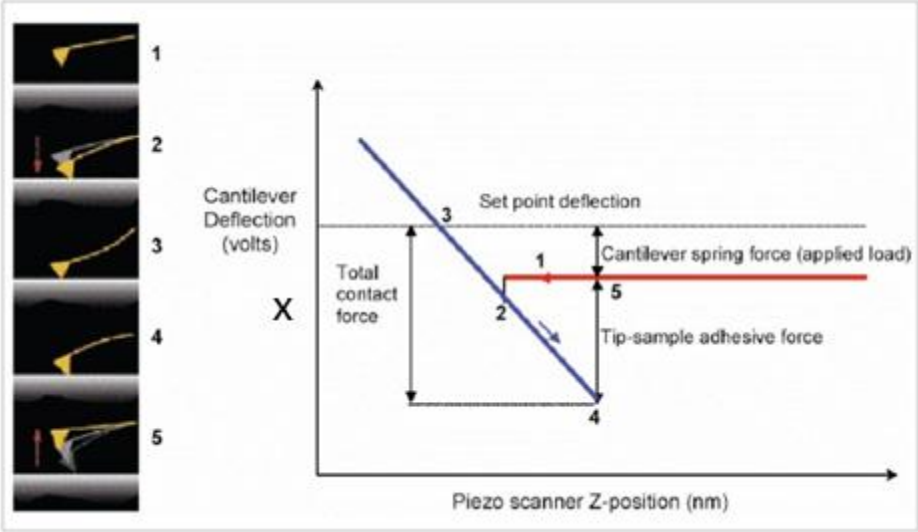

Figure 6.2. Force distance curve to map tip-sample interactions. An AFM force-distance curve is a plot of tip-sample interaction forces vs. tip-sample distance. The schematic diagram shows the movement of the cantilever and tip during the force spectroscopy experiment-towards the sample (the approach part, shown in red) and the withdraw part (the retract part, shown in blue). A force curve is obtained by the graphing of force (cantilever deflection, calculated in volts) plotted on y-axis versus the piezoelectric position (as a distance) plotted on x-axis. The tip-sample force is given by Hooke's law: F=Kx where k is the spring constant of the cantilever, and x is the deflection of the cantilever. (Image adapted from Bruker.com)

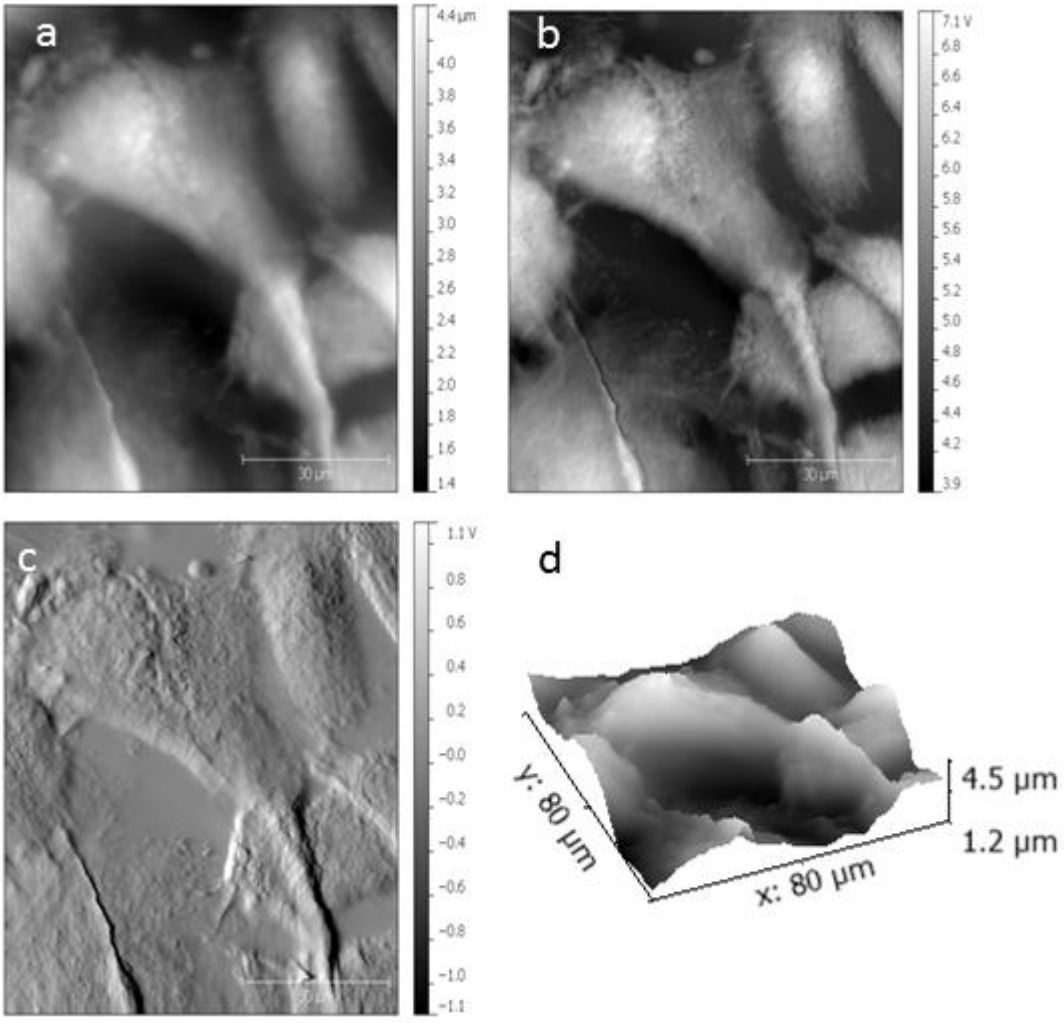

Figure 6.3. AFM imaging of C2C12 myoblasts on collagen I coated coverslips. C2C12 cells ($5x10^4$) were plated on collagen I coated cover-slips in growth medium (DMEM/10% FBS). After 24 h (80% confluence), cells were fixed using 4% paraformaldehyde and imaged by AFM with tapping mode in liquid (PBS) using a silicon nitride cantilever with a spring constant of 0.32 N/m and a long range scanner. Topography (a), amplitude (b) and phase images (c) at scan sizes of 80 μm were captured at an initial scan rate of 1.97Hz. (d) 3D representation of cells providing an estimate of their height as they sit on the glass surface.

Atomic force micrographs show single cell high resolution images where undifferentiated C2C12 cells were well spread and attached to the collagen I coated plastic surface (Figure 6.3). The AFM topography image provides estimates of both lateral (xy) and height (z) measurements of cells (Fig 6.3. a). AFM deflection or amplitude images show how the tip is deflected as it encounters sample topography (Fig 6.3 b). AFM phase images highlight sharp features of the cells (like the edges). It also provides qualitative information about hardness and elasticity of the surface as the phase signal depends on the surface properties of the object and can be affected by relative softness or hardness or chemical nature of the surface (Fig 6.3. c). The AFM 3D image provided information about the height of the individual cells spread on the collagen coated surface. The height was 3.3 μm (Fig 6.3. d).

Differentiated myotubes (section 6.2.1) were captured at different stages of their development. Fully fused myotubes appeared elongated and spindle shaped in appearance with tube like structures at the ends (short arrow, Fig 6.4. b). It was also possible to visualize the fusion process of two myoblasts where microprocesses (thin fibrous extensions) of varying lengths at the ends of the two fusing myoblasts were seen (long arrow, Fig 6.4 b). The AFM 3D images also provided information about the height of these myotubes and in this case the height was 3.4 μm (Figure 6.4 d) which is very similar to that of the undifferentiated cells (Fig 6.3. d).

6.3.2 Muscle matrix ultrastructure visualized using AFM

As the goal was to characterize the structure of the matrix in skeletal muscle tissue, AFM was used to examine the 3D ultrastructure of the skeletal muscle tissue sections. Triceps muscles from 12 week old mice were decellularized using the PLA_2 method (section 2.2.2.3) and a comparison of the tissue structure was done before and after the decellularization using AFM.

The amplitude image shows the sections containing cells attached to the matrix with flat and even images of individual myofibres (Figure 6.5 a). The Topography image shows clear intercellular spaces between the two myofibres (arrow) (Figure 6.5 b) possibly showing the endomysium around a single muscle fibre. It is represented as a map of

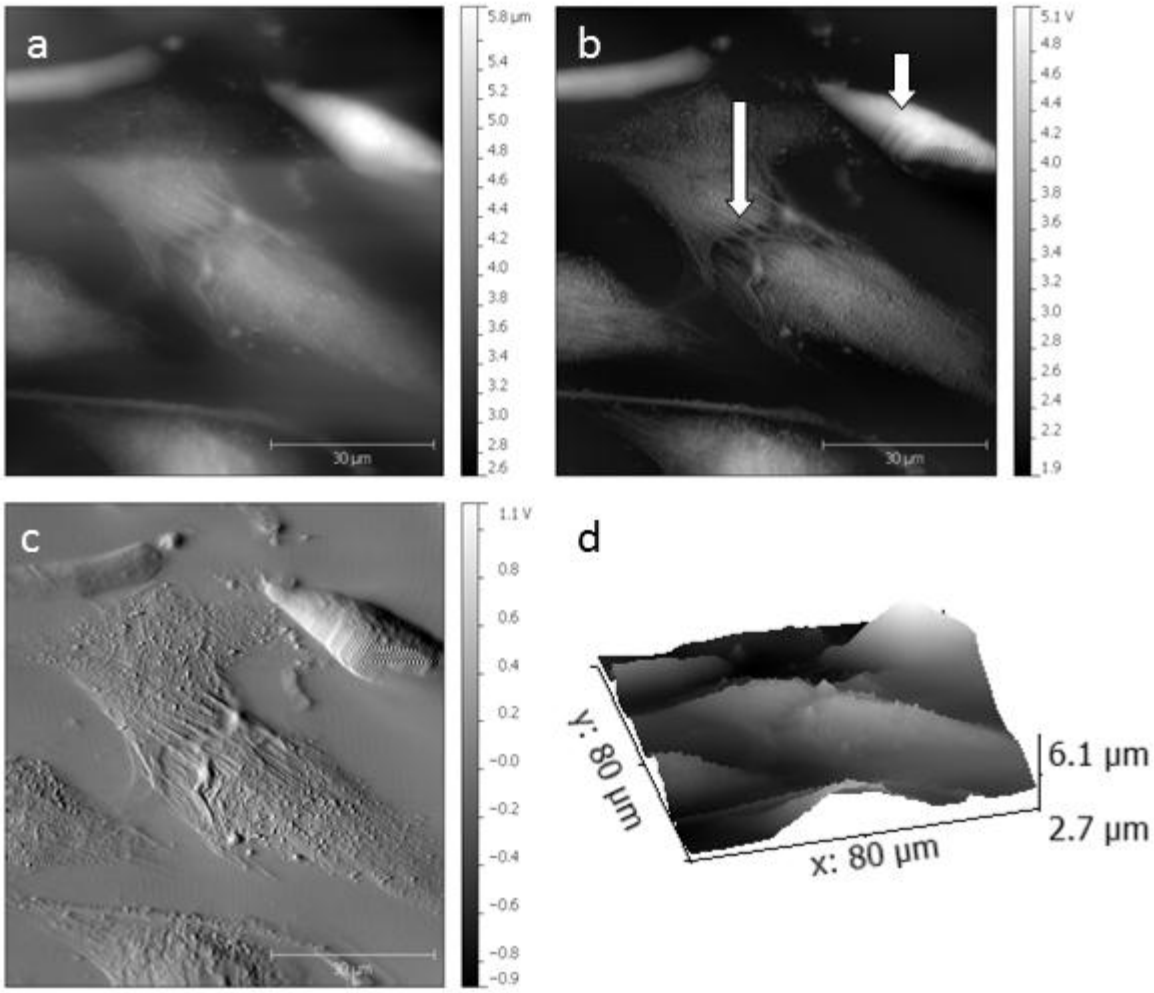

Figure 6.4. AFM imaging of differentiated C2C12 myotubes on collagen I coated coverslips. C2C12 cells ($5x10^4$) were plated on collagen I coated coverslips in growth medium (DMEM/10% FBS). After 24 h (80% confluence), cells were transferred to differentiation medium (DMEM/2% horse serum), cultured for 5 days, fixed using 4% paraformaldehyde and imaged by AFM with tapping mode in liquid (PBS) using a silicon nitride cantilever with a spring constant of 0.32 N/m and a long range scanner. (a) Topography, (b) amplitude and (c) phase images at scan sizes of 80 μm were captured at an initial scan rate of 1.97Hz. (d) 3D representation of cells providing an estimate of their height as they sit on the glass surface. Long arrow represents the point of fusion between two myoblasts.

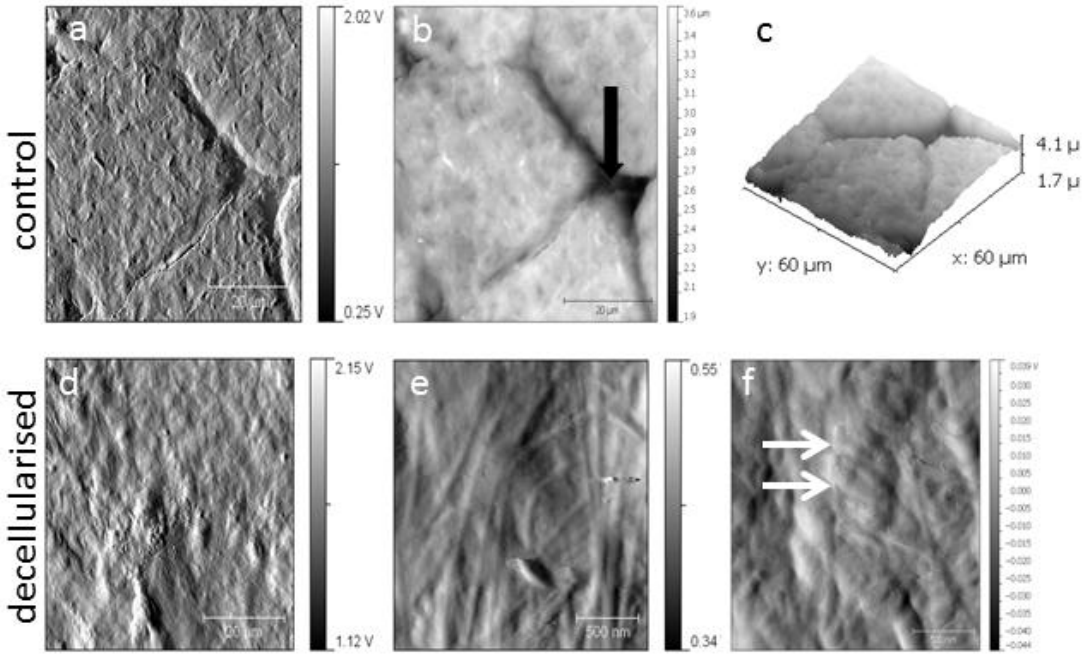

Figure 6.5. AFM imaging of the triceps muscles of mice (control and PLA_2 decellularised) revealed the ultrastructural details of the extracellular matrix. Muscle sections were imaged using a PicoPlus AFM with tapping mode in liquid using a Silicon Nitride cantilever with a spring constant of 0.32 N/m and a long range scanner for control sections (a, b) and PLA_2 decellularised sections (d, e and f). (c) 3D representation of muscle fibres providing an estimate of their height as they sit on the glass surface. Arrow represents the endomysium around single muscle fibre. Amplitude (a, d) and topography (b, e, f) images at scan sizes of 60 µm (a, b and d) and 2 µm (e-f) were captured at an initial scan rate of 1.97Hz. Arrow in (f) points to collagen fibres.

differently coloured pixels with a colour bar relating colour to height, with black being low and white high on the scan. The 3D image provides information about the height of the individual myofibres and in the image shown this is 2.4 µm (Figure 6.5 c).

After decellularisation of muscle sections with PLA_2, the surface appeared rough with several ridges seen along the whole section (Fig 6.5 d-e). A root mean square (rms) value which is a measure of the roughness of the surface was 0.717 µm for decellularized sections as compared to 0.415 µm for the control sections. A longitudianl scan of the tissue section at a higher resolution with a scan area of $2\mu m^2$ reveals an intricate network of collagen fibres in the matrix (Fig 6.5 e). The topography image reveals the characteristic banding pattern of collagen I bundles with a 67 nm gap/overlap region (white arrows Fig 6.5 f).

6.3.3 AFM imaging of natural ECM proteins and scaffolds

Fibronectin (2 $\mu g/cm^2$) was coated onto the glass surface for 2 hr at RT and then the glass coverslip was imaged using a PicoPlus AFM. Gelatin gel (50 mg/ml) (section 6.2.2) was imaged either alone or when modified using 2 % heparin (section 6.2.2.1) using a Nanoscope IIIa AFM. A topographic image of fibronectin coating the glass surface showed that the fibronectin layer was not evenly spread across the glass surface and there were areas left uncoated (arrow, Fig 6.6 a). A height map of the same scan area reveals a 60 nm thick fibronectin coating on the glass surface (Fig 6.6 d). The surface scanning of gelatin gel revealed the smooth surface of the gel (Fig 6.6 b) and the respective height map of the gel showed the indentations on this surface to be 4 nm deep (Fig 6.6 e). After modifying the gelatin gel with heparan sulphate, the surface appeared rougher with gaps appearing in the gel (Fig 6.6 c) and the height map showed bigger indentations of 8 nm deep (Fig 6.6 f).

6.3.4 picoTREC imaging of muscle sections (section 6.2.7.3)

TREC imaging was applied to the control gastrocnemius muscle sections in PBS buffer using collagen I antibody functionalized tips. PBS has a pH of 7.4 which closely mimics the physiological pH and thus serves as an ideal fluid for imaging conditions. Measurements were made in small areas on the muscle sections varying from 5 μm^2 to

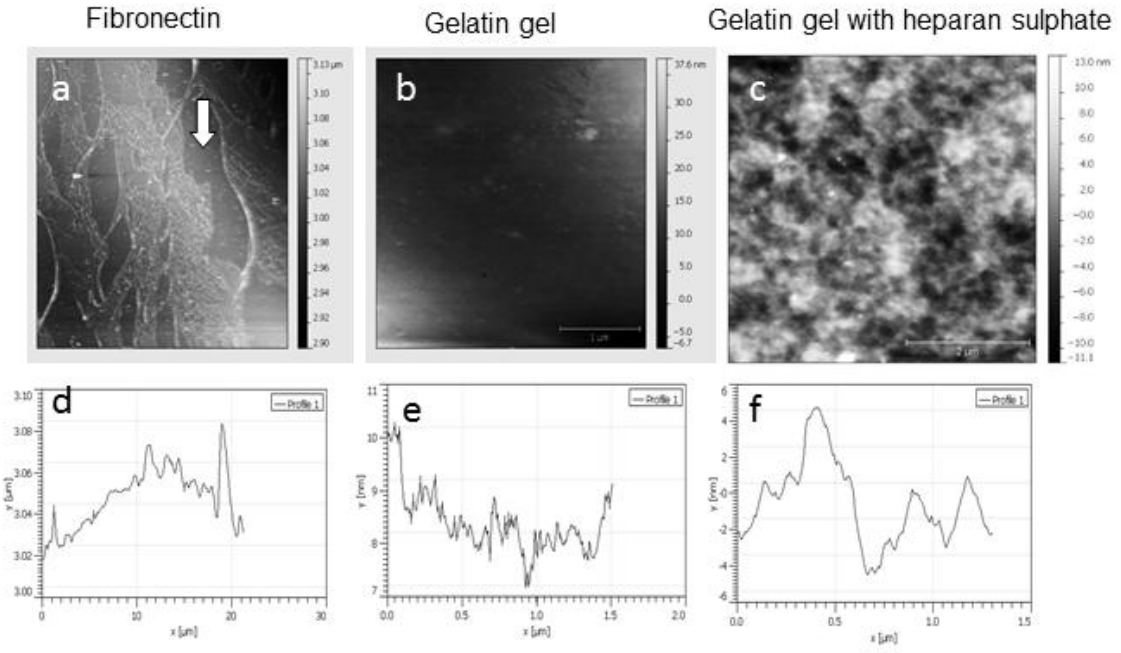

Figure 6.6.AFM imaging of different scaffolds with their height maps. Topographic images of Fibronectin (2 µg/cm^2) coated on glass (a), gelatin gel (b) and gelatin gel modified with heparan sulfate (c); imaged using a Nanoscope IIIa atomic force microscope with V-shaped silicon nitride cantilevers in contact mode and a long range scanner. Respective height maps of the above three surfaces (d-f).

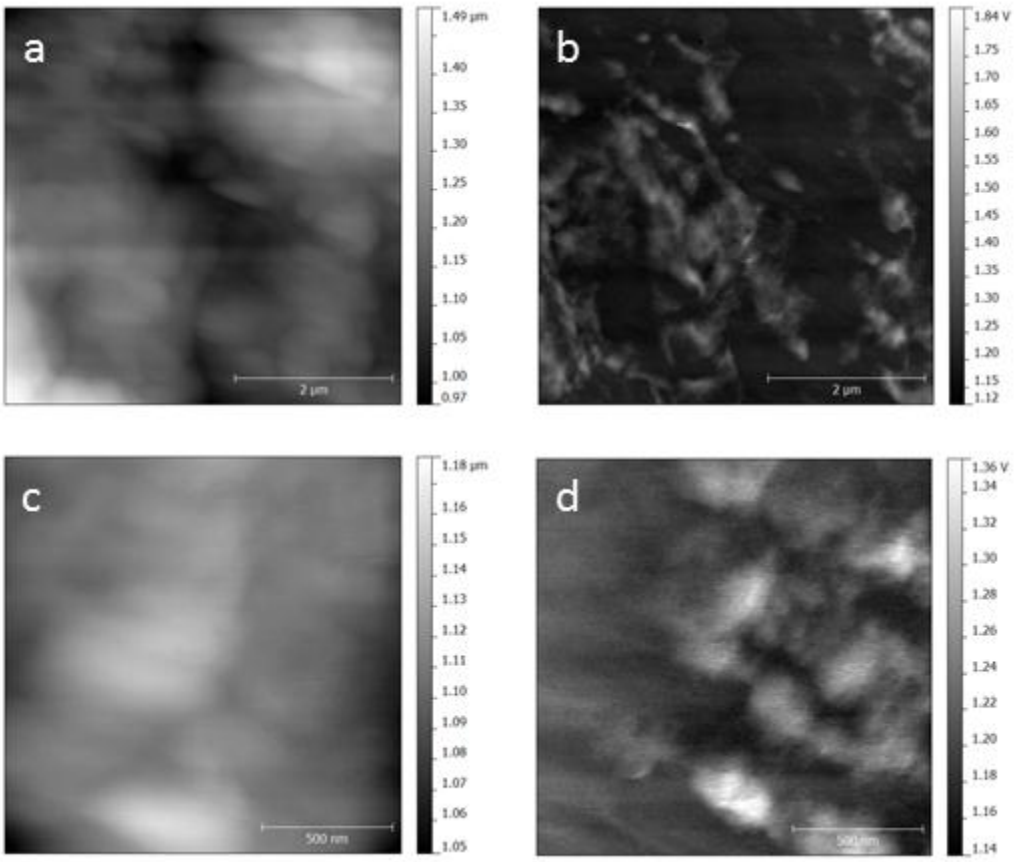

Figure 6.7. AFM imaging of the gastrocnemius muscles of mice using MAC mode in PBS. Muscle sections were imaged using a PicoPlus AFM with tapping mode in liquid using MAC mode probes with a spring constant of 0.2 -0.9 N/m and a short range scanner. Images on the left (a, c) are topographic images while images on the right (b, d) are their respective recognition images. (a and b) are acquired with a tip oscillation amplitude of 22 nm, c and d with 33 nm.

1.5 μm^2 and with amplitudes from 20nm-50nm. Fig 6.7 (a, c) shows the topographic image of the muscle section, with respective TREC images of the same area of muscle section in Fig 6.7 (b, d). Recognition spots were very difficult to interpret in these images.

6.3.5 Force spectroscopy imaging of muscle sections (section 6.2.8)

Gastrocnemius muscle sections (10 µm) were imaged using the topograph and SPS option in the PicoScan software. The result shows (Figure 6.8 a and b), a topographic image of the muscle section (20 μm^2) and the corresponding points where the spectroscopy sweeps were performed with contact mode (section 6.2.6.1) imaging and tapping mode (section 6.2.2.2) imaging in PBS. Calculation of the elastic modulus of the muscle samples was not possible due to the excessive number of force curves taken per image and there was no MATLAB script available to convert those force curves to yield a Young's modulus (Y) value. Agilent Technologies, the manufacturer of the microscope were contacted regarding a programme for the direct conversion of the force curves, but they did not have a programme for this application. If the experiments were performed now, it would have been easier to map the elasticity of the samples using new AFM imaging systems, which have more advanced features. For example, WITec alpha 300s scanning near field optical microscope (SNOM) is now available and it can provide force spectroscopy data in real time.

6.4 Discussion

The application of AFM imaging in cell biology is still in its infancy but in recent years it has gained huge attention. The aim of this chapter was to obtain images of myoblasts undergoing the process of fusion to provide insights into the muscle differentiation processes. Also performed was high-resolution imaging of the control muscle and PLA_2 decellularised matrix to investigate the ultrastructure and surface roughness of the remaining matrix.

Frequently, the interaction between the hard surface of a tip and soft cell surface makes it difficult to obtain good resolution images using AFM [314]. Therefore, the C2C12

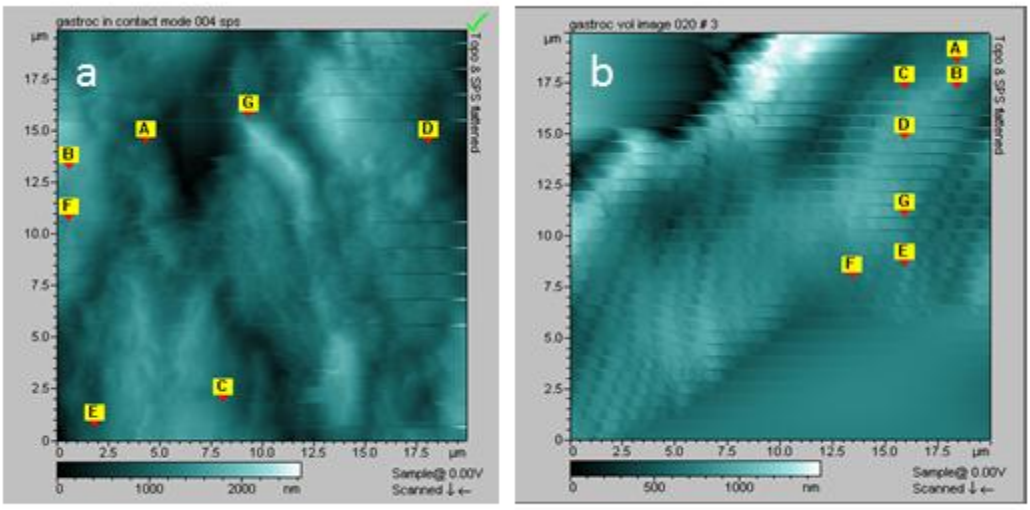

Figure 6.8. AFM force volume imaging of the gastrocnemius muscles of mice using contact and tapping mode in PBS. Muscle sections (10 µm) were imaged using a PicoPlus AFM with contact mode and tapping mode in liquid using silicon nitride cantilevers with a spring constant of 0.36 N/m and a long range scanner. Only the respective topographic images were shown in the above figure. (a) Contact mode imaging in PBS. (b) Tapping mode imaging in PBS. The letters A, B ….. G denote the points where respective force curves were taken on the muscle section.

cells were fixed with paraformaldehyde as fixing made cell surfaces more rigid and easier to image. The images obtained revealed the cell shape and micro-structure at the point of cell fixation (Fig 6.3 and 6.4). 3D images of the myoblasts and myotubes shows that there was not a significant difference in the height of individual cells. Intercellular interactions between myoblasts during the fusion process have also been captured by others using an AFM [314]. However, the images obtained were generated using contact mode in liquid. Contact mode imaging is not the preferred mode of AFM imaging when softer surfaces like cells are imaged, as frictional forces generated by lateral tip-sample interactions can damage the cells [315]. The images of myoblasts and myotubes in this chapter were obtained using tapping mode in liquid and as a consequence better resolution images were captured compared to those published by Kim et al (2008) [314]. Time lapse imaging of C2C12 myoblasts at various stages of the cell cycle was performed to capture myoblast cell fusion and cell division in real time by Stadler and colleagues [316]. Although, these researchers succeeded in capturing images of myoblasts undergoing fusion, only a few images of cell division were taken because of difficulties associated with myoblasts being loosely adhered to the substratum. It is clear from the above studies that AFM imaging is a difficult technique and requires a lot of user time to obtain good images and useful information from those images.

Cryo-sectioned control muscle tissues and PLA_2 decellularized muscle were imaged in PBS as cryo-sectioning preserves the native protein structure of the samples during sample preparation and imaging in PBS keeps the pH at a physiological level [224]. High resolution images were obtained and they revealed minute changes in the nanotopography (surface structure) of the muscle samples as the AFM tip encountered the collagen and elastic fibres in the muscle (Fig 6.5). Root mean square (rms) value of the control and PLA_2 decellularized muscle tissue revealed that after decellularisation the remaining ECM was much rougher than the control muscle. Tissue section AFM has been used to visualize the macromolecular structures of fibrillar collagens in skin, cartilage and intervertebral disc; elastic fibres in the aorta and lung, as well as the intracellular organelles like desmosomes and mitochondria [224] but it had not been used for imaging muscle matrix.

The AFM images provided useful information about the topography of different scaffolds. The ECM molecule fibronectin coated on glass and heparan sulfate cross-linked gelatin gels were imaged with AFM. A marked increase was observed in the surface roughness of heparan sulfate modified gelatin gels (Fig 6.6). The nanotopography of a synthetic surface plays a key role in determining cell adhesion, proliferation and differentiation and recent studies suggested that cells respond to these nano-topographical features [317-319]. It is likely that the observed differences in the nanotopography of the gelatin gels with or without immobilized heparin sulfate will alter cell behavior when cells are seeded on these gels *in vitro*. Designing synthetic scaffolds which mimic the natural ECM in their structure can markedly increase the regenerative response of cells when seeded on these scaffolds. From our data, it is clear that AFM images will assist in understanding the nanotopography of both natural ECMs and their synthetic scaffold mimics.

picoTREC measurements were made using an anti-collagen I antibody tethered to the AFM tip. It was not possible to interpret the data obtained by picoTREC measurements (Fig 6.7), as it is not clear that the respective recognition images in Fig 6.7 are true recognition events and not an artefact because the control experiments to verify the specificity of the antibody-protein interaction were not performed. If experiments with an excess of antibody in the imaging medium were performed and this resulted in a significant decrease in the molecular recognition events, then it is possible to be more certain of the specificity of the interactions recorded. Due to lack of this experiment, the data presented here gave an idea about the picoTREC technique and its applicability in muscle matrix biology. Creasey et al (2011) performed antibody recognition imaging on human lens capsules to examine protein aggregates in pseudoexfoliation syndrome [320]. An example of a true molecular recognition signal can be seen in “Fig 3” of their article. In their experiments, when a tip oscillation amplitude of 30 nm was applied, a recognition area in relation to the topography features was observed and with a tip oscillation amplitude of 54 nm, a reduction in recognition was observed. In our experiments the amplitudes of 22 nm and 33 nm were examined and visual differences were observed in the recognition images.

With the aim of measuring the elastic properties of the muscle, force spectroscopy was performed on the gastrocnemius muscle sections. Topographic images and the force curves at marked points were obtained but a mathematical value for the elastic modulus could not be calculated due to unavailability of the MATLAB script (Fig 6.8). Decellularized muscle scaffolds have been prepared for transplantation into animal models [292, 321]; but, the elastic properties of the obtained ECM scaffolds were not evaluated. Darling et al (2010) measured the biomechanical properties (elastic moduli) of the pericellular matrix and ECM of articular cartilage obtained from human, porcine and murine knee joints *in situ* using AFM [322]. Elastic properties of the pericellular matrix were evaluated for regions surrounding cell voids in the middle zone of articular cartilage while ECM elastic moduli were evaluated in regions visually devoid of pericellular matrix. Of the three species examined, the elastic moduli of the ECM and the pericellular matrix of human articular cartilage was the highest while porcine cartilage exhibited the softest mechanical properties and murine samples showed a value in between [322]. This study suggests that the elastic modulus of ECM can vary between different species. Ghosh et al (2007) investigated the mechanical properties of adult human dermal fibroblasts (AHDF) cultured on hydrogels that were composed of hyaluronan and fibronectin in different proportions to impart different viscoelastic properties to the hydrogels [323]. Measurements of the elastic modulus, cellular traction forces and cytoskeleton structure revealed that cells on stiffer substrates had a higher modulus and a better organized actin cytoskeleton, which exerted larger traction forces on the substrate. Furthermore, as an implication of this modulation of cellular mechanics, cells migrated faster on softer substrates and proliferated better on stiffer ones [323]. These two studies and those conducted by Engler et al (2004, 2006) [164, 228], underline the fact that it is important to evaluate the decellularized muscle scaffolds for their elastic properties, before they are used for xenogeneic transplantation purpose or in the clinic for muscle injury repair. Only limited work with AFM has been done on ECM scaffolds and AFM has only occasionally been applied to measure the elastic forces of muscle samples. Designing scaffolds of matching stiffness to muscle tissue and implanting these scaffolds at the muscle injury site may improve cell-scaffold interactions and enhance the outcome of muscle repair processes.

6.5 Conclusion

Our data indicate that AFM imaging method can be useful for analyses of:

- Cell-matrix interactions at nanometer levels, including the height and width of cells and capturing information of the different stages of skeletal muscle differentiation *in vitro;*
- Three dimensional *in-situ* imaging of skeletal muscle sections and visualization of fine ultrastructure, e.g. collagen fibrils in natural muscle ECM and PLA_2 decellularised ECM, and
- AFM provides an additional tool to visualise synthetic scaffolds that have been modified, with ECM proteins for example, to enhance their functional attributes.

Chapter 7:

Conclusion and Future Perspectives

7.0 Conclusion and Future perspectives

The results presented in this thesis corroborate the importance of cell-matrix interactions and their role in supporting the proliferation and differentiation of both mouse and human myoblasts. This conclusion is based on evidence from experiments where ECM derived from skeletal muscle or natural silk fibroins were used as substrates in 2D and 3D serum/serum free *in vitro* cultures.

Several skeletal muscle decellularisation methods have previously been published by others. These methods report varying degrees of success in the removal of DNA and the preservation of ECM molecules in the decellularised matrix [174-176]. This current study is the first report of a decellularised skeletal muscle matrix with intact well-preserved proteoglycans (perlecan and decorin) and a heparan sulphate epitope recognised by the antibody, EV3C3. When solubilized, this ECM supported mouse and human myoblast proliferation and differentiation in a serum free culture system. In contrast to the previous studies conducted using C2C12 cells and solubilised skeletal muscle matrix [174, 175], our data showed that C2C12 cells proliferated at a slower rate on the solubilised skeletal muscle matrix than on pure collagen I or fibronectin. This may be attributed to the presence of some growth factors in the solubilized skeletal muscle matrix, for example, myostatin (a TGF-β family member) negatively regulates the growth of C2C12 myoblasts and Thomas et al (2000) showed that when C2C12 myoblasts were incubated with myostatin, proliferation of myoblasts decreased [324]. Although the cells proliferated at a slower rate on the solubilised ECM substrate, the alignment of myotubes was much better on the muscle matrix coated surfaces compared to collagen I substrates and comparable to fibronectin coated surfaces. Although the differentiated cells expressed slow muscle myosin (MyHCB) on all three substrates qPCR data indicated that the expression of myosin heavy chains, *MYH1* and *MYH7*, and skeletal muscle actin (*ACTA1*), increased in a time dependent manner on all three substrates suggesting the maturation of myotubes. However, the increase in *MYH1* expression at day 4 was higher on muscle matrix than on collagen I or fibronectin which suggested that myotubes on muscle matrix were transiting faster towards a more differentiated phenotype.

This difference in cell growth on solubilized muscle matrix from other reports may be attributable to the fact that in the previous two studies DMEM/10 % FBS medium was used for cell culture experiments while we used a completely serum-free medium containing known concentrations of growth factors for all cultures of C2C12 mouse myoblasts. The presence of sera in tissue culture medium introduces variables and makes it difficult to assess the response of cells to the muscle matrix substrates. Soluble ECM molecules in the serum, like fibronectin and vitronectin, will bind to the matrix substrate thereby masking the characteristic signals of the muscle matrix. Moreover, any growth regulatory functions of molecules like myostatin that are contained in the muscle matrix may be suppressed by the growth stimulating components of serum. In our hands major basement membrane components that contribute to the "satellite cell niche", like collagens type IV and type VI were retained in the decellularised muscle matrix. Thus in our study components that control satellite cell quiescence were present in the muscle matrix substrates and these would have contributed to the signalling milieu regulating cell growth. We also found that the myoblasts secreted their own matrix proteins onto the substrate. Although only fibronectin and collagen IV were examined, it was clear that different amounts of these matrix molecules were secreted depending on the substrate. These subtle differences attributable to signals from the different substrates would be lost in the presence of serum.

Perhaps the most interesting data generated from the investigation of cell-matrix interactions, was the patterning of C2C12 cells and HSMMs on the acellular 3D muscle matrix. Cells were aligned in concentric patterns around the transversely cut muscle fibres, whereas when the acellular muscle matrix was cut along the length of the tissue the seeded cells aligned in longitudinal patterns. This clearly indicated that cells can follow the matrix "cues" left after decellularisation. It also suggests that it is the arrangement of muscle matrix molecules in intact muscle that directs/maintains the aligned myotubes. Hence, when this 3D pattern is disrupted by solubilizing the matrix, this information is lost. These findings may have practical implications as aligned ECM grafts, compared to grafts placed in random orientations, at the injury site should lead to better regenerative outcomes for muscle injuries [291]. The data also suggested that on

the 3D whole muscle scaffolds, the cells were not only present on the surface of the scaffold but they also migrated into the scaffold by as much as138 μm. Cell migration is an important prerequisite for myoblasts to make cell-cell contacts, fuse and form multinucleated myotubes. However, a functioning muscle requires directional cell migration and myotube alignment, cell behaviours that from our data seem to be determined at least in part by the matrix substrate.

This study found that when solubilised silk fibroin, prepared from four different silkworms: *A. mylitta, B. mori, S. ricini and A. assamensis* was used as substrates, C2C12 cell and HSMM proliferation was comparable to that seen when purified ECM proteins like collage type I and fibronectin were used as substrates. This data suggests that silk fibroin can be used as an alternative protein substrate for cell culture studies. Secretion of ECM proteins was also seen on silk fibroin substrates but different silks triggered the deposition of different amounts of these proteins. The signalling pathways causing this effect are unclear, but it is likely to involve differences in the structures of fibroin proteins.

Another interesting finding was when an artificial scaffold (*B. mori* silk fibroin in this case) was coated with a tissue derived decellularised ECM (skeletal muscle ECM in this case), this "hybrid scaffold" better supported spreading and adhesion of HSMMs. The artificial scaffold provided a platform for cell adhesion and spreading while the ECM coating provided a complex mixture of fibrous proteins, glycoproteins, proteoglycans and possibly some growth factors like bFGF (associated with these proteoglycans) which the cells would encounter if they were present inside the body. Like the muscle matrix these silks scaffolds also supported the deposition of ECM proteins by HSMMs at very early stages of their cell cycle (day 2 after seeding). The arrangement of the deposited proteins was three-dimensional and appeared as "lattice" which presumably assisted the cells to align and fuse.

In this study, unfixed 3D silk scaffolds when used for cell culture experiments partially dissolved and failed to maintain their original structure. Remarkably, HSMMs lined up with well aligned F-actin fibres and differentiated to form well aligned myotubes on this

partially dissolved scaffold. This experiment is pertinent to the *in-vivo* situation because, as silk scaffolds are biodegradable, if they are to be used in muscle repair *in vivo,* it is important to understand the extent to which a biodegrading scaffold can still support HSMM differentiation. That is if a silk scaffold implant is placed at the muscle injury site the muscle construct should not collapse as the silk slowly biodegrades.

The final areas of the investigation involved the testing of silk scaffolds in 3D *in vitro* cultures with a view to use them in future as biomaterials in *in vivo* animal models of muscle repair. Natural ECM in a functional muscle is highly orientated and muscle fibres extend longitudinally within this natural ECM to form the contractile machinery. In order to form a functional muscle graft, the regenerated fibres should join end to end to avoid muscle atrophy. Our data suggested that 3D silk fibroin scaffolds prepared from *B. mori* was highly supportive of myoblast differentiation. Confocal imaging showed that very long myotubes were formed, in the order of 347 μm in length, and cells covered a large area of the scaffold. It was also apparent that myotube formation was a result of the fusion of myoblasts in different planes. All of which points to the potential of this biomaterial for muscle repair.

Given that it appears silk fibroin scaffolds are potential biomaterials for use in skeletal muscle regeneration, we envisage that multilayered silk fibroin porous sheets of 5 cm length and 5 mm in thickness, prepared from silk fibroin from *B. mori* or *A. mylitta* silkworms, could be packed together to give a silk fibroin bio-composite material. This material could be implanted in a large animal model of muscle injury either alone, or in combination with a coating of soluble ECM derived from skeletal muscle. These scaffolds would be tested either pre-seeded with cells or without cells. The first approach would require seeding of myogenic progenitor cells/fibroblasts, or progenitor cells and fibroblasts in a co-culture onto the scaffold *in vitro* using our serum-free culture system and then transplanting the scaffold into the animal. These thin sheets of silk fibroin would allow cell migration into the scaffold (as our data suggests that HSMMs migrate into the scaffolds) and the thin and porous nature of the scaffolds will also allow in-growth of blood vessels into the functional graft. Serum free culture of cells to be used for transplantation provides an additional advantage that it does not

contain any animal derived proteins, so it minimizes the chances of evoking an immunologic response. It does not have to face the stringent regulatory approvals, for example from the FDA, to be used for clinical purposes because there is no risk of transferring viruses or disease from animals to man, with a serum free culture system. In future, after further testing on human myoblasts this serum-free culture system could also be useful for manufacturing cells for muscle transplantation purposes. The second approach requires the scaffold to be placed at the injury site and be populated by the resident myogenic progenitor cells residing inside the body. To cover all the necessary requirements of a functional implant, a thorough examination of the regeneration process at the site of implant is warranted. The graft site should be assessed for cell growth, re-innervation, and vascularization, infiltration of pro/anti-inflammatory cytokines and the contraction ability of the graft. A large animal model is ideal to assess the efficacy and safety of the biomaterial pre-clinically, before being used as a clinical bio-implant. Moreover, another important factor to be assessed in future studies as far as regenerative outcomes are concerned is the age of the animal as it is known that middle aged people between 40-80 years lose 20%-30% of the regenerative capacity of the muscles [3].

Previously, thin sheets of porcine SIS-ECM were successfully implanted to repair volumetric muscle loss in a patient and the regenerated muscle tissue had greater functionality than was obtained without the implant [129]. Although porcine SIS-ECM has been approved by the FDA for clinical use, there is one study which suggests this SIS-ECM is not a complete acellular matrix and this may have possible implications in human transplantation [217]. Providing the animal studies produce favourable results, using silk fibroin based scaffolds as described should avoid the issues associated with the use of a porcine ECM.

It is also very important to determine the elasticity of the decellularised scaffolds as it has been shown that substrates of different elasticity can determine the stem cell phenotype seeded on those substrates [228]. Elasticity of the muscle derived scaffold can play a major role in myogenic differentiation. Our study showed that AFM could be used to measure the elastic profile of solubilised muscle matrix coated silk fibroin

scaffold. Silk scaffolds are generally considered to be very rigid, but we predict that the muscle matrix would form an elastic layer onto the scaffold. These experiments are easier to perform now with advanced AFM instruments and imaging applications like PeakForce QNM (Bruker Scientific). It is now possible to quantify the mechanical properties of cells and ECM in real time at a very high resolution (http://www.bruker.jp/axx). AFM can be a very useful technique in the field of muscle matrix biology as it is possible to investigate the cell-matrix interactions at nanometer levels under physiological conditions. Our data suggested that it is pertinent to study the ultrastructure of a decellularized matrix and artificial scaffolds as cells in their natural/artificial environments can sense ECM structures in the nanometre scale and respond to these nanostructures [318, 319, 325].

In the last decade or so, decellularized muscle ECM scaffolds have been prepared from a selection of muscles and transplanted into animal injury models. The numbers of published reports in this area have been gradually increasing [25, 130, 214, 215, 291, 292, 321, 326-328]. Although the field of skeletal muscle tissue engineering has progressed, there are still a number of significant challenges before we can think of translating the idea of a skeletal muscle scaffold, prepared off-the-shelf, into a treatment for patients in the clinic. However, the field of tissue engineering as a whole, has made a significant progress and successful clinical transplantation of bio-artificial tissues including pulmonary valves, bladders, urethra and tracheas is underway [329-333].

We are optimistic that the data obtained from this thesis will contribute to the long term goal of developing therapeutic options to improve muscle function in people suffering from muscle mass loss due to a traumatic injury.

References:

[1] Carrel A. On the Permanent Life of Tissues Outside of the Organism. J Exp Med. 1912;15:516-28.

[2] Patrick CW, Jr., Chauvin PB, Hobley J, Reece GP. Preadipocyte seeded PLGA scaffolds for adipose tissue engineering. Tissue Eng. 1999;5:139-51.

[3] Carmeli E, Coleman R, Reznick AZ. The biochemistry of aging muscle. Exp Gerontol. 2002;37:477-89.

[4] Grounds MD. Age-associated changes in the response of skeletal muscle cells to exercise and regeneration. Ann N Y Acad Sci. 1998;854:78-91.

[5] Brack AS, Rando TA. Intrinsic changes and extrinsic influences of myogenic stem cell function during aging. Stem Cell Rev. 2007;3:226-37.

[6] Conboy IM, Conboy MJ, Smythe GM, Rando TA. Notch-mediated restoration of regenerative potential to aged muscle. Science. 2003;302:1575-7.

[7] Conboy IM, Conboy MJ, Wagers AJ, Girma ER, Weissman IL, Rando TA. Rejuvenation of aged progenitor cells by exposure to a young systemic environment. Nature. 2005;433:760-4.

[8] Conboy IM, Rando TA. Aging, stem cells and tissue regeneration: lessons from muscle. Cell Cycle. 2005;4:407-10.

[9] Jarvinen TA, Jarvinen TL, Kaariainen M, Kalimo H, Jarvinen M. Muscle injuries: biology and treatment. Am J Sports Med. 2005;33:745-64.

[10] Porter KR, Palade GE. Studies on the endoplasmic reticulum. III. Its form and distribution in striated muscle cells. J Biophys Biochem Cytol. 1957;3:269-300.

[11] Hanson J, Huxley HE. Structural Basis of the Cross-Striations in Muscle. Nature. 1953;172:530-2.

[12] Huxley AF. Muscle. Annu Rev Physiol. 1964;26:131-52.

[13] van Putte C, Regan J, Russo A. Seeley's anatomy & physiology McGraw Hill, New York. 2014;10th edition Pg 270, Chapter 9 Muscular System (65-308).

[14] Mauro A. Satellite cell of skeletal muscle fibers. J Biophys Biochem Cytol. 1961;9:493-5.

[15] Schröder JM. The fine structure of de-and reinnervated muscle spindles. Acta Neuropathol (Berl). 1974;30:129-44.

[16] Scharner J, Zammit P. The muscle satellite cell at 50: the formative years. Skeletal Muscle. 2011;1:28.

[17] Tennyson VM, Brzin M, Kremzner LT. Acetylcholinesterase activity in the myotube and muscle satellite cell of the fetal rabbit. An electron microscopic-cytochemical and biochemical study. J Histochem Cytochem. 1973;21:634-52.

[18] Lagord C, Soulet L, Bonavaud S, Bassaglia Y, Rey C, Barlovatz-Meimon G, et al. Differential myogenicity of satellite cells isolated from extensor digitorum longus (EDL) and soleus rat muscles revealed in vitro. Cell Tissue Res. 1998;291:455-68.

[19] Dhawan J, Rando TA. Stem cells in postnatal myogenesis: molecular mechanisms of satellite cell quiescence, activation and replenishment. Trends Cell Biol. 2005;15:666-73.

[20] Gopinath SD, Rando TA. Stem cell review series: aging of the skeletal muscle stem cell niche. Aging Cell. 2008;7:590-8.

[21] Tedesco FS, Dellavalle A, Diaz-Manera J, Messina G, Cossu G. Repairing skeletal muscle: regenerative potential of skeletal muscle stem cells. J Clin Invest. 2010;120:11-9.

[22] Quintero AJ, Wright VJ, Fu FH, Huard J. Stem Cells for the Treatment of Skeletal Muscle Injury. Clin Sports Med. 2009;28:1-11.

[23] Sun D, Martinez CO, Ochoa O, Ruiz-Willhite L, Bonilla JR, Centonze VE, et al. Bone marrow-derived cell regulation of skeletal muscle regeneration. The FASEB Journal. 2009;23:382-95.

[24] Ten Broek RW, Grefte S, Von den Hoff JW. Regulatory factors and cell populations involved in skeletal muscle regeneration. J Cell Physiol. 2010;224:7-16.

[25] Merritt EK, Cannon MV, Hammers DW, Le LN, Gokhale R, Sarathy A, et al. Repair of traumatic skeletal muscle injury with bone-marrow-derived mesenchymal stem cells seeded on extracellular matrix. Tissue Eng Part A. 2010;16:2871-81.

[26] Huard J, Li Y, Fu FH. Muscle injuries and repair: current trends in research. J Bone Joint Surg Am. 2002;84-A:822-32.

[27] Reid MB, Li YP. Cytokines and oxidative signalling in skeletal muscle. Acta Physiol Scand. 2001;171:225-32.

[28] Tidball JG, Villalta SA. Regulatory interactions between muscle and the immune system during muscle regeneration. Am J Physiol Regul Integr Comp Physiol. 2010;298:R1173-87.

[29] Cantini M, Giurisato E, Radu C, Tiozzo S, Pampinella F, Senigaglia D, et al. Macrophage-secreted myogenic factors: a promising tool for greatly enhancing the proliferative capacity of myoblasts in vitro and in vivo. Neurol Sci. 2002;23:189-94.

[30] Cantini M, Massimino ML, Rapizzi E, Rossini K, Catani C, Dalla Libera L, et al. Human satellite cell proliferation in vitro is regulated by autocrine secretion of IL-6 stimulated by a soluble factor(s) released by activated monocytes. Biochem Biophys Res Commun. 1995;216:49-53.

[31] Sonnet C, Lafuste P, Arnold L, Brigitte M, Poron F, Authier FJ, et al. Human macrophages rescue myoblasts and myotubes from apoptosis through a set of adhesion molecular systems. J Cell Sci. 2006;119:2497-507.

[32] Nagata Y, Partridge TA, Matsuda R, Zammit PS. Entry of muscle satellite cells into the cell cycle requires sphingolipid signaling. J Cell Biol. 2006;174:245-53.

[33] Allen RE, Sheehan SM, Taylor RG, Kendall TL, Rice GM. Hepatocyte growth factor activates quiescent skeletal muscle satellite cells in vitro. J Cell Physiol. 1995;165:307-12.

[34] Schmalbruch H. The morphology of regeneration of skeletal muscles in the rat. Tissue Cell. 1976;8:673-92.

[35] Tatsumi R, Anderson JE, Nevoret CJ, Halevy O, Allen RE. HGF/SF is present in normal adult skeletal muscle and is capable of activating satellite cells. Dev Biol. 1998;194:114-28.

[36] Menetrey J, Kasemkijwattana C, Day CS, Bosch P, Vogt M, Fu FH, et al. Growth factors improve muscle healing in vivo. J Bone Joint Surg Br. 2000;82:131-7.

[37] Allen RE, Dodson MV, Luiten LS. Regulation of skeletal muscle satellite cell proliferation by bovine pituitary fibroblast growth factor. Exp Cell Res. 1984;152:154-60.

[38] Sato K, Li Y, Foster W, Fukushima K, Badlani N, Adachi N, et al. Improvement of muscle healing through enhancement of muscle regeneration and prevention of fibrosis. Muscle Nerve. 2003;28:365-72.

[39] Chakravarthy MV, Abraha TW, Schwartz RJ, Fiorotto ML, Booth FW. Insulin-like Growth Factor-I Extends in VitroReplicative Life Span of Skeletal Muscle Satellite Cells by Enhancing G1/S Cell Cycle Progression via the Activation of Phosphatidylinositol 3′-Kinase/Akt Signaling Pathway. J Biol Chem. 2000;275:35942-52.

[40] Suzuki S, Yamanouchi K, Soeta C, Katakai Y, Harada R, Naito K, et al. Skeletal muscle injury induces hepatocyte growth factor expression in spleen. Biochem Biophys Res Commun. 2002;292:709-14.

[41] Tatsumi R, Hattori A, Ikeuchi Y, Anderson JE, Allen RE. Release of hepatocyte growth factor from mechanically stretched skeletal muscle satellite cells and role of pH and nitric oxide. Mol Biol Cell. 2002;13:2909-18.

[42] Miller KJ, Thaloor D, Matteson S, Pavlath GK. Hepatocyte growth factor affects satellite cell activation and differentiation in regenerating skeletal muscle. Am J Physiol Cell Physiol. 2000;278:C174-81.

[43] Gordon KJ, Blobe GC. Role of transforming growth factor-β superfamily signaling pathways in human disease. Biochimica et Biophysica Acta (BBA) - Molecular Basis of Disease. 2008;1782:197-228.

[44] Kollias HD, McDermott JC. Transforming growth factor-beta and myostatin signaling in skeletal muscle. J Appl Physiol. 2008;104:579-87.

[45] Liu D, Black BL, Derynck R. TGF-beta inhibits muscle differentiation through functional repression of myogenic transcription factors by Smad3. Genes Dev. 2001;15:2950-66.

[46] Davis RL, Weintraub H, Lassar AB. Expression of a single transfected cDNA converts fibroblasts to myoblasts. Cell. 1987;51:987-1000.

[47] Edmondson DG, Olson EN. A gene with homology to the myc similarity region of MyoD1 is expressed during myogenesis and is sufficient to activate the muscle differentiation program. Genes Dev. 1989;3:628-40.

[48] Rhodes SJ, Konieczny SF. Identification of MRF4: a new member of the muscle regulatory factor gene family. Genes Dev. 1989;3:2050-61.

[49] Massari ME, Murre C. Helix-Loop-Helix Proteins: Regulators of Transcription in Eucaryotic Organisms. Mol Cell Biol. 2000;20:429-40.

[50] Ott MO, Bober E, Lyons G, Arnold H, Buckingham M. Early expression of the myogenic regulatory gene, myf-5, in precursor cells of skeletal muscle in the mouse embryo. Development. 1991;111:1097-107.

[51] Tajbakhsh S, Rocancourt D, Cossu G, Buckingham M. Redefining the Genetic Hierarchies Controlling Skeletal Myogenesis: Pax-3 and Myf-5 Act Upstream of MyoD. Cell.89:127-38.

[52] Rudnicki MA, Braun T, Hinuma S, Jaenisch R. Inactivation of MyoD in mice leads to up-regulation of the myogenic HLH gene Myf-5 and results in apparently normal muscle development. Cell. 1992;71:383-90.

[53] Braun T, Bober E, Arnold HH. Inhibition of muscle differentiation by the adenovirus E1a protein: repression of the transcriptional activating function of the HLH protein Myf-5. Genes Dev. 1992;6:888-902.

[54] Rudnicki MA, Schnegelsberg PNJ, Stead RH, Braun T, Arnold H-H, Jaenisch R. MyoD or Myf-5 is required for the formation of skeletal muscle. Cell. 1993;75:1351-9.

[55] Hasty P, Bradley A, Morris JH, Edmondson DG, Venuti JM, Olson EN, et al. Muscle deficiency and neonatal death in mice with a targeted mutation in the myogenin gene. Nature. 1993;364:501-6.

[56] Kjaer M. Role of extracellular matrix in adaptation of tendon and skeletal muscle to mechanical loading. Physiol Rev. 2004;84:649-98.

[57] Borg TK, Caulfield JB. Morphology of connective tissue in skeletal muscle. Tissue Cell. 1980;12:197-207.

[58] Purslow PP, Trotter JA. The morphology and mechanical properties of endomysium in series-fibred muscles: variations with muscle length. J Muscle Res Cell Motil. 1994;15:299-308.

[59] Trotter JA, Purslow PP. Functional morphology of the endomysium in series fibered muscles. J Morphol. 1992;212:109-22.

[60] Järvinen TAH, Józsa L, Kannus P, Järvinen TLN, Järvinen M. Organization and distribution of intramuscular connective tissue in normal and immobilized skeletal muscles. J Muscle Res Cell Motil. 2002;23:245-54.

[61] Passerieux E, Rossignol R, Chopard A, Carnino A, Marini JF, Letellier T, et al. Structural organization of the perimysium in bovine skeletal muscle: Junctional plates and associated intracellular subdomains. J Struct Biol. 2006;154:206-16.

[62] Gillies AR, Lieber RL. Structure and function of the skeletal muscle extracellular matrix. Muscle Nerve. 2011;44:318-31.

[63] Gao Y, Waas AM, Faulkner JA, Kostrominova TY, Wineman AS. Micromechanical modeling of the epimysium of the skeletal muscles. J Biomech. 2008;41:1-10.

[64] Rich A, Crick FH. The molecular structure of collagen. J Mol Biol. 1961;3:483-506.

[65] Veit G, Kobbe B, Keene DR, Paulsson M, Koch M, Wagener R. Collagen XXVIII, a Novel von Willebrand Factor A Domain-containing Protein with Many Imperfections in the Collagenous Domain. J Biol Chem. 2006;281:3494-504.

[66] Brazel D, OberbÄUmer I, Dieringer H, Babel W, Glanville RW, Deutzmann R, et al. Completion of the amino acid sequence of the α1 chain of human basement membrane collagen (type IV) reveals 21 non-triplet interruptions located within the collagenous domain. Eur J Biochem. 1987;168:529-36.

[67] Ricard-Blum S, Ruggiero F. The collagen superfamily: from the extracellular matrix to the cell membrane. Pathol Biol (Paris). 2005;53:430-42.

[68] Light N, Champion AE. Characterization of muscle epimysium, perimysium and endomysium collagens. Biochem J. 1984;219:1017-26.

[69] Gelse K, Pöschl E, Aigner T. Collagens—structure, function, and biosynthesis. Adv Drug Deliv Rev. 2003;55:1531-46.

[70] Petersen TE, Thøgersen HC, Skorstengaard K, Vibe-Pedersen K, Sahl P, Sottrup-Jensen L, et al. Partial primary structure of bovine plasma fibronectin: Three types of internal homology. Proc Natl Acad Sci U S A. 1983;80:137-41.

[71] Mosesson MW, Umfleet RA. The Cold-insoluble Globulin of Human Plasma. J Biol Chem. 1970;245:5728-36.

[72] George EL, Georges-Labouesse EN, Patel-King RS, Rayburn H, Hynes RO. Defects in mesoderm, neural tube and vascular development in mouse embryos lacking fibronectin. Development. 1993;119:1079-91.

[73] Labat-Robert J. Cell–Matrix interactions, the role of fibronectin and integrins. A survey. Pathol Biol (Paris). 2012;60:15-9.

[74] Grounds MD. Complexity of Extracellular Matrix and Skeletal Muscle Regeneration. Adv Muscle Res. 2008;3.

[75] Miner JH, Li C, Patton BL. Laminins α2 and α4 in Pancreatic Acinar Basement Membranes Are Required for Basal Receptor Localization. J Histochem Cytochem. 2004;52:153-6.

[76] Grounds MD, Sorokin L, White J. Strength at the extracellular matrix–muscle interface. Scand J Med Sci Sports. 2005;15:381-91.

[77] Yurchenco PD, Amenta PS, Patton BL. Basement membrane assembly, stability and activities observed through a developmental lens. Matrix Biol. 2004;22:521-38.

[78] Tome FM, Evangelista T, Leclerc A, Sunada Y, Manole E, Estournet B, et al. Congenital muscular dystrophy with merosin deficiency. C R Acad Sci III. 1994;317:351-7.

[79] Mithieux SM, Weiss AS. Elastin. In: David ADP, John MS, editors. Adv Protein Chem: Academic Press; 2005. p. 437-61.

[80] Kielty CM, Sherratt MJ, Shuttleworth CA. Elastic fibres. J Cell Sci. 2002;115:2817-28.

[81] Toonkool P, Regan DG, Kuchel PW, Morris MB, Weiss AS. Thermodynamic and hydrodynamic properties of human tropoelastin. Analytical ultracentrifuge and pulsed field-gradient spin-echo NMR studies. J Biol Chem. 2001;276:28042-50.

[82] Wu WJ, Vrhovski B, Weiss AS. Glycosaminoglycans Mediate the Coacervation of Human Tropoelastin through Dominant Charge Interactions Involving Lysine Side Chains. J Biol Chem. 1999;274:21719-24.

[83] Reinboth B, Hanssen E, Cleary EG, Gibson MA. Molecular interactions of biglycan and decorin with elastic fiber components: biglycan forms a ternary complex with tropoelastin and microfibril-associated glycoprotein 1. J Biol Chem. 2002;277:3950-7.

[84] Brandan E, Gutierrez J. Role of skeletal muscle proteoglycans during myogenesis. Matrix Biol. 2013;32:289-97.

[85] Sugahara K, Mikami T, Uyama T, Mizuguchi S, Nomura K, Kitagawa H. Recent advances in the structural biology of chondroitin sulfate and dermatan sulfate. Curr Opin Struct Biol. 2003;13:612-20.

[86] Coombe DR, Kett WC. Heparan sulfate-protein interactions: therapeutic potential through structure-function insights. Cell Mol Life Sci. 2005;62:410-24.

[87] Ferdous Z, Grande-Allen KJ. Utility and control of proteoglycans in tissue engineering. Tissue Eng. 2007;13:1893-904.

[88] Barbosa I, Morin C, Garcia S, Duchesnay A, Oudghir M, Jenniskens G, et al. A synthetic glycosaminoglycan mimetic (RGTA) modifies natural glycosaminoglycan species during myogenesis. J Cell Sci. 2005;118:253-64.

[89] Bianco P, Fisher LW, Young MF, Termine JD, Robey PG. Expression and localization of the two small proteoglycans biglycan and decorin in developing human skeletal and non-skeletal tissues. J Histochem Cytochem. 1990;38:1549-63.

[90] Casar JC, McKechnie BA, Fallon JR, Young MF, Brandan E. Transient up-regulation of biglycan during skeletal muscle regeneration: delayed fiber growth along with decorin increase in biglycan-deficient mice. Dev Biol. 2004;268:358-71.

[91] Lechner BE, Lim JH, Mercado ML, Fallon JR. Developmental regulation of biglycan expression in muscle and tendon. Muscle Nerve. 2006;34:347-55.

[92] Tufvesson E, Westergren-Thorsson G. Tumour necrosis factor-α interacts with biglycan and decorin. FEBS Lett. 2002;530:124-8.

[93] Ungefroren H, Krull NB. Transcriptional Regulation of the Human Biglycan Gene. J Biol Chem. 1996;271:15787-95.

[94] Bowe MA, Mendis DB, Fallon JR. The Small Leucine-Rich Repeat Proteoglycan Biglycan Binds to α-Dystroglycan and Is Upregulated in Dystrophic Muscle. J Cell Biol. 2000;148:801-10.

[95] Schönherr E, Witsch-Prehm P, Harrach B, Robenek H, Rauterberg J, Kresse H. Interaction of Biglycan with Type I Collagen. J Biol Chem. 1995;270:2776-83.

[96] Wiberg C, Heinegård D, Wenglén C, Timpl R, Mörgelin M. Biglycan Organizes Collagen VI into Hexagonal-like Networks Resembling Tissue Structures. J Biol Chem. 2002;277:49120-6.

[97] Reinboth B, Hanssen E, Cleary EG, Gibson MA. Molecular Interactions of Biglycan and Decorin with Elastic Fiber Components. J Biol Chem. 2002;277:3950-7.

[98] Paulsson M, Yurchenco PD, Ruben GC, Engel J, Timpl R. Structure of low density heparan sulfate proteoglycan isolated from a mouse tumor basement membrane. J Mol Biol. 1987;197:297-313.

[99] Fujiwara S, Wiedemann H, Timpl R, Lustig A, Engel J. Structure and interactions of heparan sulfate proteoglycans from a mouse tumor basement membrane. Eur J Biochem. 1984;143:145-57.

[100] Hassell JR, Robey PG, Barrach HJ, Wilczek J, Rennard SI, Martin GR. Isolation of a heparan sulfate-containing proteoglycan from basement membrane. Proc Natl Acad Sci U S A. 1980;77:4494-8.

[101] Peng HB, Ali AA, Daggett DF, Rauvala H, Hassell JR, Smalheiser NR. The relationship between perlecan and dystroglycan and its implication in the formation of the neuromuscular junction. Cell Adhes Commun. 1998;5:475-89.

[102] Peng HB, Xie H, Rossi SG, Rotundo RL. Acetylcholinesterase Clustering at the Neuromuscular Junction Involves Perlecan and Dystroglycan. J Cell Biol. 1999;145:911-21.

[103] Arikawa Hirasawa E. Absence of acetylcholinesterase at the neuromuscular junctions of perlecan-null mice. Nat Neurosci. 2002;5:119.

[104] Costell M, Gustafsson E, Aszodi A, Morgelin M, Bloch W, Hunziker E, et al. Perlecan maintains the integrity of cartilage and some basement membranes. J Cell Biol. 1999;147:1109-22.

[105] Zoeller JJ, McQuillan A, Whitelock J, Ho S-Y, Iozzo RV. A central function for perlecan in skeletal muscle and cardiovascular development. J Cell Biol. 2008;181:381-94.

[106] Kamimura K, Ueno K, Nakagawa J, Hamada R, Saitoe M, Maeda N. Perlecan regulates bidirectional Wnt signaling at the Drosophila neuromuscular junction. J Cell Biol. 2013;200:219-33.

[107] Krusius T, Ruoslahti E. Primary structure of an extracellular matrix proteoglycan core protein deduced from cloned cDNA. Proc Natl Acad Sci U S A. 1986;83:7683-7.

[108] McPherron AC, Lawler AM, Lee S-J. Regulation of skeletal muscle mass in mice by a new TGF-p superfamily member. Nature. 1997;387:83-90.

[109] Miura T, Kishioka Y, Wakamatsu J-i, Hattori A, Hennebry A, Berry CJ, et al. Decorin binds myostatin and modulates its activity to muscle cells. Biochem Biophys Res Commun. 2006;340:675-80.

[110] Li Y, Li J, Zhu J, Sun B, Branca M, Tang Y, et al. Decorin gene transfer promotes muscle cell differentiation and muscle regeneration. Mol Ther. 2007;15:1616-22.

[111] Schmidt G, Hausser H, Kresse H. Interaction of the small proteoglycan decorin with fibronectin. Involvement of the sequence NKISK of the core protein. Biochem J. 1991;280 (Pt 2):411-4.

[112] Goetsch KP, Kallmeyer K, Niesler CU. Decorin modulates collagen I-stimulated, but not fibronectin-stimulated, migration of C2C12 myoblasts. Matrix Biol. 2011;30:109-17.

[113] Hauschka SD, Konigsberg IR. The influence of collagen on the development of muscle clones. Proc Natl Acad Sci U S A. 1966;55:119-26.

[114] Hartley RS, Yablonka-Reuveni Z. Long-term maintenance of primary myogenic cultures on a reconstituted basement membrane. In Vitro Cell Dev Biol. 1990;26:955-61.

[115] Kricker JA, Towne CL, Firth SM, Herington AC, Upton Z. Structural and functional evidence for the interaction of insulin-like growth factors (IGFs) and IGF binding proteins with vitronectin. Endocrinology. 2003;144:2807-15.

[116] Fiorotto ML, Schwartz RJ, Delaughter MC. Persistent IGF-I overexpression in skeletal muscle transiently enhances DNA accretion and growth. FASEB J. 2003;17:59-60.

[117] Kujawa MJ, Pechak DG, Fiszman MY, Caplan AI. Hyaluronic acid bonded to cell culture surfaces inhibits the program of myogenesis. Dev Biol. 1986;113:10-6.

[118] Roisman I, Zarzhevsky N, Reznick AZ. Effect of growth hormone on oxidative stress in immobilized muscles of old animals. In: Reznick AZ, Packer L, Sen CK, Holloszy JO, Jackson MJ, editors. Oxidative Stress in Skeletal Muscle: Birkhäuser Basel; 1998. p. 215-21.

[119] Bach AD, Beier JP, Stern-Staeter J, Horch RE. Skeletal muscle tissue engineering. J Cell Mol Med. 2004;8:413-22.

[120] Vilquin JT. Myoblast transplantation: clinical trials and perspectives. Mini-review. Acta Myol. 2005;24:119-27.

[121] Beier JP, Klumpp D, Rudisile M, Dersch R, Wendorff JH, Bleiziffer O, et al. Collagen matrices from sponge to nano: new perspectives for tissue engineering of skeletal muscle. BMC Biotechnol. 2009;9:34.

[122] Geutjes PJ, Daamen WF, Buma P, Feitz WF, Faraj KA, van Kuppevelt TH. From Molecules to Matrix: Construction and Evaluation of Molecularly Defined Bioscaffolds. In: Fisher JP, editor. Tissue Engineering: Springer US; 2007. p. 279-95.

[123] Koning M, Harmsen MC, van Luyn MJ, Werker PM. Current opportunities and challenges in skeletal muscle tissue engineering. J Tissue Eng Regen Med. 2009;3:407-15.

[124] Koning M, Harmsen MC, van Luyn MJA, Werker PMN. Current opportunities and challenges in skeletal muscle tissue engineering. J Tissue Eng Regen Med. 2009;3:407-15.

[125] Shapiro L, Cohen S. Novel alginate sponges for cell culture and transplantation. Biomaterials. 1997;18:583-90.

[126] Guerret S, Govignon E, Hartmann DJ, Ronfard V. Long-term remodeling of a bilayered living human skin equivalent (Apligraf) grafted onto nude mice: immunolocalization of human cells and characterization of extracellular matrix. Wound Repair Regen. 2003;11:35-45.

[127] Jux C, Wohlsein P, Bruegmann M, Zutz M, Franzbach B, Bertram H. A new biological matrix for septal occlusion. J Interv Cardiol. 2003;16:149-52.

[128] Sculean A, Berakdar M, Chiantella GC, Donos N, Arweiler NB, Brecx M. Healing of intrabony defects following treatment with a bovine-derived xenograft and collagen membrane. A controlled clinical study. J Clin Periodontol. 2003;30:73-80.

[129] Mase VJ, Jr., Hsu JR, Wolf SE, Wenke JC, Baer DG, Owens J, et al. Clinical application of an acellular biologic scaffold for surgical repair of a large, traumatic quadriceps femoris muscle defect. Orthopedics. 2010;33:511.

[130] Valentin JE, Turner NJ, Gilbert TW, Badylak SF. Functional skeletal muscle formation with a biologic scaffold. Biomaterials. 2010;31:7475-84.

[131] Rosso F, Marino G, Giordano A, Barbarisi M, Parmeggiani D, Barbarisi A. Smart materials as scaffolds for tissue engineering. J Cell Physiol. 2005;203:465-70.

[132] Mahendran B, Ghosh SK, Kundu SC. Molecular phylogeny of silk-producing insects based on 16S ribosomal RNA and cytochrome oxidase subunit I genes. Journal of Genetics. 2006;85:31-8.

[133] Nayak S, Talukdar S, Kundu S. Potential of 2D crosslinked sericin membranes with improved biostability for skin tissue engineering. Cell Tissue Res. 2012;347:783-94.

[134] Zhou C-Z, Confalonieri F, Medina N, Zivanovic Y, Esnault C, Yang T, et al. Fine organization of Bombyx mori fibroin heavy chain gene. Nucleic Acids Res. 2000;28:2413-9.

[135] Tanaka K, Inoue S, Mizuno S. Hydrophobic interaction of P25, containing Asn-linked oligosaccharide chains, with the H-L complex of silk fibroin produced by Bombyx mori. Insect Biochem Mol Biol. 1999;29:269-76.

[136] Fu C, Shao Z, Fritz V. Animal silks: their structures, properties and artificial production. Chem Commun. 2009:6515-29.

[137] Kundu SC, Kundu B, Talukdar S, Bano S, Nayak S, Kundu J, et al. Nonmulberry silk biopolymers. Biopolymers. 2012;97:455-67.

[138] Pal S, Kundu J, Talukdar S, Thomas T, Kundu SC. An Emerging Functional Natural Silk Biomaterial from the only Domesticated Non-mulberry Silkworm Samia ricini. Macromol Biosci. 2013;13:1020-35.

[139] Mandal BB, Das S, Choudhury K, Kundu SC. Implication of silk film RGD availability and surface roughness on cytoskeletal organization and proliferation of primary rat bone marrow cells. Tissue Eng Part A. 2010; 16:2391-403. .

[140] Kar S, Talukdar S, Pal S, Nayak S, Paranjape P, Kundu SC. Silk gland fibroin from indian muga silkworm Antheraea assama as potential biomaterial. TERM. 2013;10:200-10.

[141] Patra C, Talukdar S, Novoyatleva T, Velagala SR, Mühlfeld C, Kundu B, et al. Silk protein fibroin from Antheraea mylitta for cardiac tissue engineering. Biomaterials. 2012;33:2673-80.

[142] Meinel L, Fajardo R, Hofmann S, Langer R, Chen J, Snyder B, et al. Silk implants for the healing of critical size bone defects. Bone. 2005;37:688-98.

[143] Meinel L, Kaplan DL. Silk constructs for delivery of musculoskeletal therapeutics. Adv Drug Deliv Rev. 2012;64:1111-22.

[144] Kim HJ, Kim U-J, Kim HS, Li C, Wada M, Leisk GG, et al. Bone tissue engineering with premineralized silk scaffolds. Bone. 2008;42:1226-34.

[145] Bhardwaj N, Nguyen QT, Chen AC, Kaplan DL, Sah RL, Kundu SC. Potential of 3-D tissue constructs engineered from bovine chondrocytes/silk fibroin-chitosan for in vitro cartilage tissue engineering. Biomaterials. 2011;32:5773-81.

[146] Talukdar S, Nguyen QT, Chen AC, Sah RL, Kundu SC. Effect of initial cell seeding density on 3D-engineered silk fibroin scaffolds for articular cartilage tissue engineering. Biomaterials. 2011;32:8927-37.

[147] Banani K, Kundu SC. Bio-inspired fabrication of fibroin cryogels from the muga silkworm Antheraea assamensis for liver tissue engineering. Biomed Mater. 2013;8:055003.

[148] Talukdar S, Kundu SC. A Non-Mulberry Silk Fibroin Protein Based 3D In Vitro Tumor Model for Evaluation of Anticancer Drug Activity. Adv Funct Mater. 2012;22:4778-88.

[149] Talukdar S, Kundu SC. Engineered 3D Silk-Based Metastasis Models: Interactions Between Human Breast Adenocarcinoma, Mesenchymal Stem Cells and Osteoblast-Like Cells. Adv Funct Mater. 2013;23:5249-60.

[150] Panilaitis B, Altman GH, Chen J, Jin H-J, Karageorgiou V, Kaplan DL. Macrophage responses to silk. Biomaterials. 2003;24:3079-85.

[151] Wang Y, Rudym DD, Walsh A, Abrahamsen L, Kim H-J, Kim HS, et al. In vivo degradation of three-dimensional silk fibroin scaffolds. Biomaterials. 2008;29:3415-28.

[152] Zhou J, Cao C, Ma X, Hu L, Chen L, Wang C. In vitro and in vivo degradation behavior of aqueous-derived electrospun silk fibroin scaffolds. Polym Degrad Stab. 2010;95:1679-85.

[153] Arnaoutova I, George J, Kleinman H, Benton G. The endothelial cell tube formation assay on basement membrane turns 20: state of the science and the art. Angiogenesis. 2009;12:267-74.

[154] McGrath AM, Novikova LN, Novikov LN, Wiberg M. BD™ PuraMatrix™ peptide hydrogel seeded with Schwann cells for peripheral nerve regeneration. Brain Res Bull. 2010;83:207-13.

[155] Rossi CA, Pozzobon M, De Coppi P. Advances in musculoskeletal tissue engineering: moving towards therapy. Organogenesis. 2010;6:167-72.

[156] Song JJ, Ott HC. Organ engineering based on decellularized matrix scaffolds. Trends Mol Med. 2011.

[157] Place ES, Evans ND, Stevens MM. Complexity in biomaterials for tissue engineering. Nat Mater. 2009;8:457-70.

[158] Rossi CA, Pozzobon M, De Coppi P. Advances in musculoskeletal tissue engineering: Moving towards therapy. Organogenesis. 2010;6:167-72.

[159] Lee SJ, Lee IW, Lee YM, Lee HB, Khang G. Macroporous biodegradable natural/synthetic hybrid scaffolds as small intestine submucosa impregnated poly(D,L-lactide-co-glycolide) for tissue-engineered bone. J Biomater Sci Polym Ed. 2004;15:1003-17.

[160] Stankus JJ, Freytes DO, Badylak SF, Wagner WR. Hybrid nanofibrous scaffolds from electrospinning of a synthetic biodegradable elastomer and urinary bladder matrix. J Biomater Sci Polym Ed. 2008;19:635-52.

[161] Gilmore KJ, Kita M, Han Y, Gelmi A, Higgins MJ, Moulton SE, et al. Skeletal muscle cell proliferation and differentiation on polypyrrole substrates doped with extracellular matrix components. Biomaterials. 2009;30:5292-304.

[162] Luong-Van E, Grøndahl L, Song S, Nurcombe V, Cool S. The in vivo assessment of a novel scaffold containing heparan sulfate for tissue engineering with human mesenchymal stem cells. J Mol Histol. 2007;38:459-68.

[163] Kaji H, Ishibashi T, Nagamine K, Kanzaki M, Nishizawa M. Electrically induced contraction of C2C12 myotubes cultured on a porous membrane-based substrate with muscle tissue-like stiffness. Biomaterials. 2010;31:6981-6.

[164] Engler AJ, Griffin MA, Sen S, Bonnemann CG, Sweeney HL, Discher DE. Myotubes differentiate optimally on substrates with tissue-like stiffness: pathological implications for soft or stiff microenvironments. J Cell Biol. 2004;166:877-87.

[165] Borselli C, Cezar CA, Shvartsman D, Vandenburgh HH, Mooney DJ. The role of multifunctional delivery scaffold in the ability of cultured myoblasts to promote muscle regeneration. Biomaterials. 2011;32:8905-14.

[166] Crapo PM, Gilbert TW, Badylak SF. An overview of tissue and whole organ decellularization processes. Biomaterials. 2011;32:3233-43.

[167] Grauss RW, Hazekamp MG, Oppenhuizen F, van Munsteren CJ, Gittenberger-de Groot AC, DeRuiter MC. Histological evaluation of decellularised porcine aortic valves: matrix changes due to different decellularisation methods. Eur J Cardiothorac Surg. 2005;27:566-71.

[168] Kasimir MT, Rieder E, Seebacher G, Silberhumer G, Wolner E, Weigel G, et al. Comparison of different decellularization procedures of porcine heart valves. Int J Artif Organs. 2003;26:421-7.

[169] Rieder E, Kasimir MT, Silberhumer G, Seebacher G, Wolner E, Simon P, et al. Decellularization protocols of porcine heart valves differ importantly in efficiency of

cell removal and susceptibility of the matrix to recellularization with human vascular cells. J Thorac Cardiovasc Surg. 2004;127:399-405.

[170] Conklin BS, Richter ER, Kreutziger KL, Zhong DS, Chen C. Development and evaluation of a novel decellularized vascular xenograft. Med Eng Phys. 2002;24:173-83.

[171] Schmidt CE, Baier JM. Acellular vascular tissues: natural biomaterials for tissue repair and tissue engineering. Biomaterials. 2000;21:2215-31.

[172] Cartmell JS, Dunn MG. Effect of chemical treatments on tendon cellularity and mechanical properties. J Biomed Mater Res. 2000;49:134-40.

[173] Woods T, Gratzer PF. Effectiveness of three extraction techniques in the development of a decellularized bone-anterior cruciate ligament-bone graft. Biomaterials. 2005;26:7339-49.

[174] DeQuach JA, Mezzano V, Miglani A, Lange S, Keller GM, Sheikh F, et al. Simple and High Yielding Method for Preparing Tissue Specific Extracellular Matrix Coatings for Cell Culture. PLoS One. 2010;5:e13039.

[175] Stern MM, Myers RL, Hammam N, Stern KA, Eberli D, Kritchevsky SB, et al. The influence of extracellular matrix derived from skeletal muscle tissue on the proliferation and differentiation of myogenic progenitor cells ex vivo. Biomaterials. 2009;30:2393-9.

[176] Gillies AR, Smith LR, Lieber RL, Varghese S. Method for decellularizing skeletal muscle without detergents or proteolytic enzymes. Tissue Eng Part C Methods. 2011;17:383-9.

[177] Reing JE, Brown BN, Daly KA, Freund JM, Gilbert TW, Hsiong SX, et al. The effects of processing methods upon mechanical and biologic properties of porcine dermal extracellular matrix scaffolds. Biomaterials. 2010;31:8626-33.

[178] Gilbert TW, Sellaro TL, Badylak SF. Decellularization of tissues and organs. Biomaterials. 2006;27:3675-83.

[179] Keane TJ, Londono R, Turner NJ, Badylak SF. Consequences of ineffective decellularization of biologic scaffolds on the host response. Biomaterials. 2012;33:1771-81.

[180] Brown BN, Freund JM, Han L, Rubin JP, Reing JE, Jeffries EM, et al. Comparison of three methods for the derivation of a biologic scaffold composed of adipose tissue extracellular matrix. Tissue Eng Part C Methods. 2011;17:411-21.

[181] Levy RJ, Vyavahare N, Ogle M, Ashworth P, Bianco R, Schoen FJ. Inhibition of cusp and aortic wall calcification in ethanol- and aluminum-treated bioprosthetic heart

valves in sheep: background, mechanisms, and synergism. J Heart Valve Dis. 2003;12:209-16; discussion 16.

[182] Cortiella J, Niles J, Cantu A, Brettler A, Pham A, Vargas G, et al. Influence of acellular natural lung matrix on murine embryonic stem cell differentiation and tissue formation. Tissue Eng Part A. 2010;16:2565-80.

[183] Gulati AK. Long-term retention of regenerative capability after denervation of skeletal muscle, and dependency of late differentiation on innervation. Anat Rec. 1988;220:429-34.

[184] Prasertsung I, Kanokpanont S, Bunaprasert T, Thanakit V, Damrongsakkul S. Development of acellular dermis from porcine skin using periodic pressurized technique. J Biomed Mater Res B Appl Biomater. 2008;85:210-9.

[185] Funamoto S, Nam K, Kimura T, Murakoshi A, Hashimoto Y, Niwaya K, et al. The use of high-hydrostatic pressure treatment to decellularize blood vessels. Biomaterials. 2010;31:3590-5.

[186] Hopkinson A, Shanmuganathan VA, Gray T, Yeung AM, Lowe J, James DK, et al. Optimization of amniotic membrane (AM) denuding for tissue engineering. Tissue Eng Part C Methods. 2008;14:371-81.

[187] Meyer SR, Chiu B, Churchill TA, Zhu L, Lakey JR, Ross DB. Comparison of aortic valve allograft decellularization techniques in the rat. J Biomed Mater Res A. 2006;79:254-62.

[188] Yang B, Zhang Y, Zhou L, Sun Z, Zheng J, Chen Y, et al. Development of a porcine bladder acellular matrix with well-preserved extracellular bioactive factors for tissue engineering. Tissue Eng Part C Methods. 2010;16:1201-11.

[189] Deeken CR, White AK, Bachman SL, Ramshaw BJ, Cleveland DS, Loy TS, et al. Method of preparing a decellularized porcine tendon using tributyl phosphate. J Biomed Mater Res B Appl Biomater. 2011;96:199-206.

[190] Gui L, Chan SA, Breuer CK, Niklason LE. Novel utilization of serum in tissue decellularization. Tissue Eng Part C Methods. 2010;16:173-84.

[191] Ott HC, Matthiesen TS, Goh SK, Black LD, Kren SM, Netoff TI, et al. Perfusion-decellularized matrix: using nature's platform to engineer a bioartificial heart. Nat Med. 2008;14:213-21.

[192] Uygun BE, Soto-Gutierrez A, Yagi H, Izamis ML, Guzzardi MA, Shulman C, et al. Organ reengineering through development of a transplantable recellularized liver graft using decellularized liver matrix. Nat Med. 2010;16:814-20.

[193] Petersen TH, Calle EA, Zhao L, Lee EJ, Gui L, Raredon MB, et al. Tissue-Engineered Lungs for in Vivo Implantation. Science. 2010;329:538-41.

[194] Turner N, Badylak S. Regeneration of skeletal muscle. Cell Tissue Res. 2012;347:759-74.

[195] Gredinger E, Gerber AN, Tamir Y, Tapscott SJ, Bengal E. Mitogen-activated protein kinase pathway is involved in the differentiation of muscle cells. J Biol Chem. 1998;273:10436-44.

[196] Jones NC, Fedorov YV, Rosenthal RS, Olwin BB. ERK1/2 is required for myoblast proliferation but is dispensable for muscle gene expression and cell fusion. J Cell Physiol. 2001;186:104-15.

[197] Bentzinger CF, Wang YX, Dumont NA, Rudnicki MA. Cellular dynamics in the muscle satellite cell niche. EMBO Rep. 2013;14:1062-72

[198] Huang NF, Thakar KG, Wong M, Kim D, Lee RJ, Song L. Tissue engineering of muscle on micropatterned polymer films. Engineering in Medicine and Biology Society, 2004 IEMBS '04 26th Annual International Conference of the IEEE2004. p. 4966-9.

[199] Gingras J, Rioux RM, Cuvelier D, Geisse NA, Lichtman JW, Whitesides GM, et al. Controlling the orientation and synaptic differentiation of myotubes with micropatterned substrates. Biophys J. 2009;97:2771-9.

[200] Yamamoto Y, Ito A, Kato M, Kawabe Y, Shimizu K, Fujita H, et al. Preparation of artificial skeletal muscle tissues by a magnetic force-based tissue engineering technique. J Biosci Bioeng. 2009;108:538-43.

[201] Rossi CA, Flaibani M, Blaauw B, Pozzobon M, Figallo E, Reggiani C, et al. In vivo tissue engineering of functional skeletal muscle by freshly isolated satellite cells embedded in a photopolymerizable hydrogel. FASEB J. 2011;25:2296-304.

[202] Carsin H, Ainaud P, Le Bever H, Rives J-M, Lakhel A, Stephanazzi J, et al. Cultured epithelial autografts in extensive burn coverage of severely traumatized patients: a five year single-center experience with 30 patients. Burns. 2000;26:379-87.

[203] Hafemann B, Ensslen S, Erdmann C, Niedballa R, Zühlke A, Ghofrani K, et al. Use of a collagen/elastin-membrane for the tissue engineering of dermis. Burns. 1999;25:373-84.

[204] Chou T-D, Chen S-L, Lee T-W, Chen S-G, Cheng T-Y, Lee C-H, et al. Reconstruction of Burn Scar of the Upper Extremities with Artificial Skin. Plast Reconstr Surg. 2001;108:378-84.

[205] Cuono C, Langdon R, Mcguire J. Use of Cultured Epidermal Autografts and Dermal Allografts as Skin Replacement after Burn Injury. Lancet. 1986;1:1123-4.

[206] Brigido SA. The use of an acellular dermal regenerative tissue matrix in the treatment of lower extremity wounds: a prospective 16-week pilot study. Int Wound J. 2006;3:181-7.

[207] Mostow EN, Haraway GD, Dalsing M, Hodde JP, King D. Effectiveness of an extracellular matrix graft (OASIS Wound Matrix) in the treatment of chronic leg ulcers: A randomized clinical trial. J Vasc Surg. 2005;41:837-43.

[208] Zhong SP, Zhang YZ, Lim CT. Tissue scaffolds for skin wound healing and dermal reconstruction. Wiley Interdisciplinary Reviews: Nanomedicine and Nanobiotechnology. 2010;2:510-25.

[209] Ansaloni L, Cambrini P, Catena F, Di Saverio S, Gagliardi S, Gazzotti F, et al. Immune Response to Small Intestinal Submucosa (Surgisis) Implant in Humans: Preliminary Observations. J Invest Surg. 2007;20:237-41.

[210] Ansaloni L, Catena F, Coccolini F, Gazzotti F, D'Alessandro L, Pinna AD. Inguinal hernia repair with porcine small intestine submucosa: 3-year follow-up results of a randomized controlled trial of Lichtenstein's repair with polypropylene mesh versus Surgisis Inguinal Hernia Matrix. Am J Surg. 2009;198:303-12.

[211] Karpelowsky JS, Thomas G, Shun A. Definitive abdominal wall closure using a porcine intestinal submucosa biodegradable membrane in pediatric transplantation. Pediatr Transplant. 2009;13:285-9.

[212] Lee DK. Achilles Tendon Repair with Acellular Tissue Graft Augmentation in Neglected Ruptures. J Foot Ankle Surg. 2007;46:451-5.

[213] Lee DK. A Preliminary Study on the Effects of Acellular Tissue Graft Augmentation in Acute Achilles Tendon Ruptures. J Foot Ankle Surg. 2008;47:8-12.

[214] Turner NJ, Yates AJ, Jr., Weber DJ, Qureshi IR, Stolz DB, Gilbert TW, et al. Xenogeneic extracellular matrix as an inductive scaffold for regeneration of a functioning musculotendinous junction. Tissue Eng Part A. 2010;16:3309-17.

[215] Turner NJ, Badylak JS, Weber DJ, Badylak SF. Biologic Scaffold Remodeling in a Dog Model of Complex Musculoskeletal Injury. J Surg Res. 2012;176:490-502.

[216] Tottey S, Johnson SA, Crapo PM, Reing JE, Zhang L, Jiang H, et al. The effect of source animal age upon extracellular matrix scaffold properties. Biomaterials. 2011;32:128-36.

[217] Zheng MH, Chen J, Kirilak Y, Willers C, Xu J, Wood D. Porcine small intestine submucosa (SIS) is not an acellular collagenous matrix and contains porcine DNA: possible implications in human implantation. J Biomed Mater Res B Appl Biomater. 2005;73:61-7.

[218] Hinds S, Bian W, Dennis RG, Bursac N. The role of extracellular matrix composition in structure and function of bioengineered skeletal muscle. Biomaterials. 2011;32:3575-83.

[219] Das M, Rumsey J, Bhargava N, Gregory C, Riedel L, Kang J, et al. Developing a novel serum-free cell culture model of skeletal muscle differentiation by systematically studying the role of different growth factors in myotube formation. In Vitro Cell Dev Biol - Animal. 2009;45:378-87.

[220] Das M, Rumsey JW, Bhargava N, Stancescu M, Hickman JJ. Skeletal muscle tissue engineering: A maturation model promoting long-term survival of myotubes, structural development of the excitation–contraction coupling apparatus and neonatal myosin heavy chain expression. Biomaterials. 2009;30:5392-402.

[221] Brewer GJ, Boehler MD, Jones TT, Wheeler BC. NbActiv4 medium improvement to Neurobasal/B27 increases neuron synapse densities and network spike rates on multielectrode arrays. J Neurosci Methods. 2008;170:181-7.

[222] Ruprecht J, Nield J. Determining the structure of biological macromolecules by transmission electron microscopy, single particle analysis and 3D reconstruction. Prog Biophys Mol Biol. 2001;75:121-64.

[223] Fotiadis D, Scheuring S, Muller SA, Engel A, Muller DJ. Imaging and manipulation of biological structures with the AFM. Micron. 2002;33:385-97.

[224] Graham HK, Hodson NW, Hoyland JA, Millward-Sadler SJ, Garrod D, Scothern A, et al. Tissue section AFM: In situ ultrastructural imaging of native biomolecules. Matrix Biol. 2010;29:254-60.

[225] Hinterdorfer P, Baumgartner W, Gruber HJ, Schilcher K, Schindler H. Detection and localization of individual antibody-antigen recognition events by atomic force microscopy. Proc Natl Acad Sci U S A. 1996;93:3477-81.

[226] Hoh JH, Hansma PK. Atomic force microscopy for high-resolution imaging in cell biology. Trends Cell Biol. 1992;2:208-13.

[227] Tao NJ, Lindsay SM, Lees S. Measuring the microelastic properties of biological material. Biophys J. 1992;63:1165-9.

[228] Engler AJ, Sen S, Sweeney HL, Discher DE. Matrix elasticity directs stem cell lineage specification. Cell. 2006;126:677-89.

[229] Bissell MJ, Hall HG, Parry G. How does the extracellular matrix direct gene expression? J Theor Biol. 1982;99:31-68.

[230] Geiger B, Bershadsky A, Pankov R, Yamada KM. Transmembrane crosstalk between the extracellular matrix and the cytoskeleton. Nat Rev Mol Cell Biol. 2001;2:793-805.

[231] Cukierman E, Pankov R, Stevens DR, Yamada KM. Taking Cell-Matrix Adhesions to the Third Dimension. Science. 2001;294:1708-12.

[232] Hong H, Stegemann JP. 2D and 3D collagen and fibrin biopolymers promote specific ECM and integrin gene expression by vascular smooth muscle cells. J Biomater Sci Polym Ed. 2008;19:1279-93.

[233] Harley BAC, Kim H-D, Zaman MH, Yannas IV, Lauffenburger DA, Gibson LJ. Microarchitecture of Three-Dimensional Scaffolds Influences Cell Migration Behavior via Junction Interactions. Biophys J. 2008;95:4013-24.

[234] Laemmli UK. Cleavage of Structural Proteins during the Assembly of the Head of Bacteriophage T4. Nature. 1970;227:680-5.

[235] Spandidos A, Wang X, Wang H, Seed B. PrimerBank: a resource of human and mouse PCR primer pairs for gene expression detection and quantification. Nucleic Acids Res. 2010;38:D792-D9.

[236] Andersen CL, Jensen JL, Ørntoft TF. Normalization of Real-Time Quantitative Reverse Transcription-PCR Data: A Model-Based Variance Estimation Approach to Identify Genes Suited for Normalization, Applied to Bladder and Colon Cancer Data Sets. Cancer Res. 2004;64:5245-50.

[237] Pfaffl M, Tichopad A, Prgomet C, Neuvians T. Determination of stable housekeeping genes, differentially regulated target genes and sample integrity: BestKeeper – Excel-based tool using pair-wise correlations. Biotechnol Lett. 2004;26:509-15.

[238] Livak KJ, Schmittgen TD. Analysis of Relative Gene Expression Data Using Real-Time Quantitative PCR and the 2−ΔΔCT Method. Methods. 2001;25:402-8.

[239] Bengtsson M, Ståhlberg A, Rorsman P, Kubista M. Gene expression profiling in single cells from the pancreatic islets of Langerhans reveals lognormal distribution of mRNA levels. Genome Res. 2005;15:1388-92.

[240] Sofia S, McCarthy MB, Gronowicz G, Kaplan DL. Functionalized silk-based biomaterials for bone formation. J Biomed Mater Res. 2001;54:139-48.

[241] Datta A, Ghosh AK, C. Kundu S. Purification and characterization of fibroin from the tropical Saturniid silkworm, Antheraea mylitta. Insect Biochem Mol Biol. 2001;31:1013-8.

[242] Nazarov R, Jin H-J, Kaplan DL. Porous 3-D Scaffolds from Regenerated Silk Fibroin. Biomacromolecules. 2004;5:718-26.

[243] Wang Y, Cui C-B, Yamauchi M, Miguez P, Roach M, Malavarca R, et al. Lineage restriction of human hepatic stem cells to mature fates is made efficient by tissue-specific biomatrix scaffolds. Hepatology. 2011;53:293-305.

[244] Didangelos A, Yin X, Mandal K, Saje A, Smith A, Xu Q, et al. Extracellular Matrix Composition and Remodeling in Human Abdominal Aortic Aneurysms: A Proteomics Approach. Mol Cell Proteom. 2011;10.

[245] Zhang Y, He Y, Bharadwaj S, Hammam N, Carnagey K, Myers R, et al. Tissue-specific extracellular matrix coatings for the promotion of cell proliferation and maintenance of cell phenotype. Biomaterials. 2009;30:4021-8.

[246] Courtman DW, Pereira CA, Kashef V, McComb D, Lee JM, Wilson GJ. Development of a pericardial acellular matrix biomaterial: biochemical and mechanical effects of cell extraction. J Biomed Mater Res. 1994;28:655-66.

[247] Rommel C, Bodine SC, Clarke BA, Rossman R, Nunez L, Stitt TN, et al. Mediation of IGF-1-induced skeletal myotube hypertrophy by PI(3)K/Akt/mTOR and PI(3)K/Akt/GSK3 pathways. Nat Cell Biol. 2001;3:1009-13.

[248] McLennan IS. Localisation of transforming growth factor beta 1 in developing muscles: Implications for connective tissue and fiber type pattern formation. Dev Dyn. 1993;197:281-90.

[249] Cusella-De Angelis MG, Molinari S, Le Donne A, Coletta M, Vivarelli E, Bouche M, et al. Differential response of embryonic and fetal myoblasts to TGF beta: a possible regulatory mechanism of skeletal muscle histogenesis. Development. 1994;120:925-33.

[250] Li Y, Foster W, Deasy BM, Chan Y, Prisk V, Tang Y, et al. Transforming Growth Factor-β1 Induces the Differentiation of Myogenic Cells into Fibrotic Cells in Injured Skeletal Muscle: A Key Event in Muscle Fibrogenesis. Am J Pathol. 2004;164:1007-19.

[251] Urciuolo A, Quarta M, Morbidoni V, Gattazzo F, Molon S, Grumati P, et al. Collagen VI regulates satellite cell self-renewal and muscle regeneration. Nat Commun. 2013;4.

[252] Boppart MD, Burkin DJ, Kaufman SJ. α7β1-Integrin regulates mechanotransduction and prevents skeletal muscle injury. Am J Physiol Cell Ph. 2006;290:C1660-C1665

[253] Bentzinger CF, Barzaghi P, Lin S, Ruegg MA. Overexpression of mini-agrin in skeletal muscle increases muscle integrity and regenerative capacity in laminin-α2-deficient mice. The FASEB Journal. 2005;19:934-42.

[254] Bentzinger CF, Wang Yu X, von Maltzahn J, Soleimani Vahab D, Yin H, Rudnicki Michael A. Fibronectin Regulates Wnt7a Signaling and Satellite Cell Expansion. Cell Stem Cell. 2013;12:75-87.

[255] Danen EHJ, Sonneveld P, Brakebusch C, Fässler R, Sonnenberg A. The fibronectin-binding integrins α5β1 and αvβ3 differentially modulate RhoA–GTP loading, organization of cell matrix adhesions, and fibronectin fibrillogenesis. J Cell Biol. 2002;159:1071-86.

[256] Mayer U. Integrins: Redundant or Important Players in Skeletal Muscle? J Biol Chem. 2003;278:14587-90.

[257] Smits NC, Robbesom AA, Versteeg EMM, van de Westerlo EMA, Dekhuijzen PNR, van Kuppevelt TH. Heterogeneity of Heparan Sulfates in Human Lung. Am J Respir Cell Mol Biol. 2004;30:166-73.

[258] Xu Z, Ichikawa N, Kosaki K, Yamada Y, Sasaki T, Sakai LY, et al. Perlecan deficiency causes muscle hypertrophy, a decrease in myostatin expression, and changes in muscle fiber composition. Matrix Biol. 2010;29:461-70.

[259] Guiraud S, van Wittenberghe L, Georger C, Scherman D, Kichler A. Identification of decorin derived peptides with a zinc dependent anti-myostatin activity. Neuromuscul Disord. 2012;22:1057-68.

[260] Cabello-Verrugio C, Santander C, Cofré C, Acuña MJ, Melo F, Brandan E. The Internal Region Leucine-rich Repeat 6 of Decorin Interacts with Low Density Lipoprotein Receptor-related Protein-1, Modulates Transforming Growth Factor (TGF)-β-dependent Signaling, and Inhibits TGF-β-dependent Fibrotic Response in Skeletal Muscles. J Biol Chem. 2012;287:6773-87.

[261] Faulk DM, Carruthers CA, Warner HJ, Kramer CR, Reing JE, Zhang L, et al. The effect of detergents on the basement membrane complex of a biologic scaffold material. Acta Biomater. 2014;10:183-93.

[262] Schultz GS, Wysocki A. Interactions between extracellular matrix and growth factors in wound healing. Wound Repair Regen. 2009;17:153-62.

[263] Chachques JC, Herreros J, Trainini J, Juffe A, Rendal E, Prosper F, et al. Autologous human serum for cell culture avoids the implantation of cardioverter-defibrillators in cellular cardiomyoplasty. Int J Cardiol. 2004;95, Supplement 1:S29-S33.

[264] Selvaggi TA, Walker RE, Fleisher TA. Development of Antibodies to Fetal Calf Serum With Arthus-Like Reactions in Human Immunodeficiency Virus–Infected Patients Given Syngeneic Lymphocyte Infusions. Blood. 1997;89:776-9.

[265] Lawson MA, Purslow PP. Differentiation of Myoblasts in Serum-Free Media: Effects of Modified Media Are Cell Line-Specific. Cells Tissues Organs. 2000;167:130-7.

[266] Das M, Rumsey JW, Bhargava N, Stancescu M, Hickman JJ. A defined long-term in vitro tissue engineered model of neuromuscular junctions. Biomaterials. 2010;31:4880-8.

[267] Goto S, Miyazaki K, Funabiki T, Yasumitsu H. Serum-Free Culture Conditions for Analysis of Secretory Proteinases during Myogenic Differentiation of Mouse C2C12 Myoblasts. Anal Biochem. 1999;272:135-42.

[268] Fujita H, Endo A, Shimizu K, Nagamori E. Evaluation of serum-free differentiation conditions for C2C12 myoblast cells assessed as to active tension generation capability. Biotechnol Bioeng. 2010;107:894-901.

[269] Fujita H, Shimizu K, Nagamori E. Novel method for fabrication of skeletal muscle construct from the C2C12 myoblast cell line using serum-free medium AIM-V. Biotechnol Bioeng. 2009;103:1034-41.

[270] Podleski TR, Greenberg I, Schlessinger J, Yamada KM. Fibronectin delays the fusion of L6 myoblasts. Exp Cell Res. 1979;122:317-26.

[271] Kühl U, Öcalan M, Timpl R, von der Mark K. Role of laminin and fibronectin in selecting myogenic versus fibrogenic cells from skeletal muscle cells in vitro. Dev Biol. 1986;117:628-35.

[272] Foster RF, Thompson JM, Kaufman SJ. A laminin substrate promotes myogenesis in rat skeletal muscle cultures: Analysis of replication and development using antidesmin and anti-BrdUrd monoclonal antibodies. Dev Biol. 1987;122:11-20.

[273] Kleinman HK, Klebe RJ, Martin GR. Role of collagenous matrices in the adhesion and growth of cells. J Cell Biol. 1981;88:473-85.

[274] Salic A, Mitchison TJ. A chemical method for fast and sensitive detection of DNA synthesis in vivo. Proc Natl Acad Sci U S A. 2008;105:2415-20.

[275] Yaffe D, Feldman M. The formation of hybrid multinucleated muscle fibers from myoblasts of different genetic origin. Dev Biol. 1965;11:300-17.

[276] Yaffe D, Saxel ORA. Serial passaging and differentiation of myogenic cells isolated from dystrophic mouse muscle. Nature. 1977;270:725-7.

[277] Blau HM, Chiu C-P, Webster C. Cytoplasmic activation of human nuclear genes in stable heterocaryons. Cell. 1983;32:1171-80.

[278] Cho YS, Kim CH, Cheon HG. Cell-based assay for screening 11β-hydroxysteroid dehydrogenase 1 inhibitors. Anal Biochem. 2009;392:110-6.

[279] Baudy AR, Saxena N, Gordish H, Hoffman EP, Nagaraju K. A robust in vitro screening assay to identify NF-κB inhibitors for inflammatory muscle diseases. Int Immunopharmacol. 2009;9:1209-14.

[280] Leonardo R, Alessandro P, Giada GG, Gianni C, Donata I, Helena V, et al. Proliferation and skeletal myotube formation capability of C2C12 and H9c2 cells on isotropic and anisotropic electrospun nanofibrous PHB scaffolds. Biomed Mater. 2012;7:035010.

[281] Shen Z, Guo S, Ye D, Chen J, Kang C, Qiu S, et al. Skeletal Muscle Regeneration on Protein-Grafted and Microchannel-Patterned Scaffold for Hypopharyngeal Tissue Engineering. BioMed Res Int. 2013;2013:8.

[282] Vaz R, Martins G, Thorsteinsdóttir S, Rodrigues G. Fibronectin promotes migration, alignment and fusion in an in vitro myoblast cell model. Cell Tissue Res. 2012;348:569-78.

[283] Cooper ST, Maxwell AL, Kizana E, Ghoddusi M, Hardeman EC, Alexander IE, et al. C2C12 Co-culture on a fibroblast substratum enables sustained survival of contractile, highly differentiated myotubes with peripheral nuclei and adult fast myosin expression. Cell Motil Cytoskeleton. 2004;58:200-11.

[284] Stern-Straeter J, Bonaterra GA, Kassner SS, Zügel S, Hörmann K, Kinscherf R, et al. Characterization of human myoblast differentiation for tissue-engineering purposes by quantitative gene expression analysis. J Tissue Eng Regen Med. 2011;5:e197-e206.

[285] Wang M, Yu H, Kim YS, Bidwell CA, Kuang S. Myostatin facilitates slow and inhibits fast myosin heavy chain expression during myogenic differentiation. Biochem Biophys Res Commun. 2012;426:83-8.

[286] Ochala J, Iwamoto H, Ravenscroft G, Laing NG, Nowak KJ. Skeletal and cardiac α-actin isoforms differently modulate myosin cross-bridge formation and myofibre force production. Hum Mol Genet. 2013;22:4398-404.

[287] Brown D, Parr T, Brameld J. Myosin heavy chain mRNA isoforms are expressed in two distinct cohorts during C2C12 myogenesis. J Muscle Res Cell Motil. 2012;32:383-90.

[288] Wilschut KJ, Haagsman HP, Roelen BAJ. Extracellular matrix components direct porcine muscle stem cell behavior. Exp Cell Res. 2010;316:341-52.

[289] Kleinman HK, Martin GR. Matrigel: Basement membrane matrix with biological activity. Semin Cancer Biol. 2005;15:378-86.

[290] Rawls A, Morris JH, Rudnicki M, Braun T, Arnold H-H, Klein WH, et al. Myogenin's Functions Do Not Overlap with Those of MyoD or Myf-5 during Mouse Embryogenesis. Dev Biol. 1995;172:37-50.

[291] Li MTA, Willett NJ, Uhrig BA, Guldberg RE, Warren GL. Functional analysis of limb recovery following autograft treatment of volumetric muscle loss in the quadriceps femoris. J Biomech. 2014;47:2013-21.

[292] Perniconi B, Costa A, Aulino P, Teodori L, Adamo S, Coletti D. The pro-myogenic environment provided by whole organ scale acellular scaffolds from skeletal muscle. Biomaterials. 2011;32:7870-82.

[293] Kaspar P, Pajer P, Sedlak D, Tamaoki T, Dvorak M. c-Myb inhibits myogenic differentiation through repression of MyoD. Exp Cell Res. 2005;309:419-28.

[294] Lindon C, Albagli O, Pinset C, Montarras D. Cell Density-Dependent Induction of Endogenous Myogenin (myf4) Gene Expression by Myf5. Dev Biol. 2001;240:574-84.

[295] Chan XaCY, McDermott JC, Siu KWM. Identification of Secreted Proteins during Skeletal Muscle Development. J Proteome Res. 2007;6:698-710.

[296] Kühl U, Timpl R, von der Mark K. Synthesis of type IV collagen and laminin in cultures of skeletal muscle cells and their assembly on the surface of myotubes. Dev Biol. 1982;93:344-54.

[297] Larraín J, Alvarez J, Hassell JR, Brandan E. Expression of Perlecan, a Proteoglycan That Binds Myogenic Inhibitory Basic Fibroblast Growth Factor, Is Down Regulated during Skeletal Muscle Differentiation. Exp Cell Res. 1997;234:405-12.

[298] Hu X, Park S-H, Gil ES, Xia X-X, Weiss AS, Kaplan DL. The influence of elasticity and surface roughness on myogenic and osteogenic-differentiation of cells on silk-elastin biomaterials. Biomaterials. 2011;32:8979-89.

[299] Park H-s, Gong M-S, Park J-H, Moon S-i, Wall IB, Kim H-W, et al. Silk fibroin–polyurethane blends: Physical properties and effect of silk fibroin content on viscoelasticity, biocompatibility and myoblast differentiation. Acta Biomater. 2013;9:8962-71.

[300] Bauer F, Wohlrab S, Scheibel T. Controllable cell adhesion, growth and orientation on layered silk protein films. Biomater Sci. 2013;1:1244-9.

[301] Cheng CS, El-Abd Y, Bui K, Hyun Y-E, Hughes RH, Kraus WE, et al. Conditions that promote primary human skeletal myoblast culture and muscle differentiation in vitro. Am J Physiol - Cell Ph. 2014;306:C385-C95.

[302] Guillet-Deniau I, Leturque A, Girard J. Expression and cellular localization of glucose transporters (GLUT1, GLUT3, GLUT4) during differentiation of myogenic cells isolated from rat foetuses. J Cell Sci. 1994;107:487-96.

[303] Gu Y, Zhu J, Xue C, Li Z, Ding F, Yang Y, et al. Chitosan/silk fibroin-based, Schwann cell-derived extracellular matrix-modified scaffolds for bridging rat sciatic nerve gaps. Biomaterials. 2014;35:2253-63.

[304] Wei J, Han J, Zhao Y, Cui Y, Wang B, Xiao Z, et al. The importance of three-dimensional scaffold structure on stemness maintenance of mouse embryonic stem cells. Biomaterials. 2014;35:7724-33.

[305] Franck D, Gil ES, Adam RM, Kaplan DL, Chung YG, Estrada CR, Jr., et al. Evaluation of Silk Biomaterials in Combination with Extracellular Matrix Coatings for Bladder Tissue Engineering with Primary and Pluripotent Cells. PloS one. 2013;8:e56237.

[306] Zhang Y, Fan W, Ma Z, Wu C, Fang W, Liu G, et al. The effects of pore architecture in silk fibroin scaffolds on the growth and differentiation of mesenchymal stem cells expressing BMP7. Acta Biomater. 2010;6:3021-8.

[307] Horan RL, Antle K, Collette AL, Wang Y, Huang J, Moreau JE, et al. In vitro degradation of silk fibroin. Biomaterials. 2005;26:3385-93.

[308] Li M, Ogiso M, Minoura N. Enzymatic degradation behavior of porous silk fibroin sheets. Biomaterials. 2003;24:357-65.

[309] Stern-Straeter J, Bonaterra G, Hormann K, Kinscherf R, Goessler U. Identification of valid reference genes during the differentiation of human myoblasts. BMC Mol Biol 2009;10:66.

[310] Mudera V, Smith AST, Brady MA, Lewis MP. The effect of cell density on the maturation and contractile ability of muscle derived cells in a 3D tissue-engineered skeletal muscle model and determination of the cellular and mechanical stimuli required for the synthesis of a postural phenotype. J Cell Physiol. 2010;225:646-53.

[311] Tang-Schomer MD, White JD, Tien LW, Schmitt LI, Valentin TM, Graziano DJ, et al. Bioengineered functional brain-like cortical tissue. Proc Natl Acad Sci U S A. 2014.

[312] Ebner A, Hinterdorfer P, Gruber HJ. Comparison of different aminofunctionalization strategies for attachment of single antibodies to AFM cantilevers. Ultramicroscopy. 2007;107:922-7.

[313] Ebner A, Wildling L, Kamruzzahan ASM, Rankl C, Wruss J, Hahn CD, et al. A New, Simple Method for Linking of Antibodies to Atomic Force Microscopy Tips. Bioconjug Chem. 2007;18:1176-84.

[314] Kim S-J, Kim S, Shin H, Uhm C-S. Intercellular interaction observed by atomic force microscopy. Ultramicroscopy. 2008;108:1148-51.

[315] Jandt KD. Atomic force microscopy of biomaterials surfaces and interfaces. Surf Sci. 2001;491:303-32.

[316] StÄDler B, BlÄTtler TM, Franco-ObregÓN A. Time-lapse imaging of In Vitro myogenesis using atomic force microscopy. J Microsc. 2010;237:63-9.

[317] Dalby MJ, Gadegaard N, Riehle MO, Wilkinson CDW, Curtis ASG. Investigating filopodia sensing using arrays of defined nano-pits down to 35 nm diameter in size. Int J Biochem Cell Biol. 2004;36:2005-15.

[318] Yim EKF, Darling EM, Kulangara K, Guilak F, Leong KW. Nanotopography-induced changes in focal adhesions, cytoskeletal organization, and mechanical properties of human mesenchymal stem cells. Biomaterials. 2010;31:1299-306.

[319] Yim EKF, Reano RM, Pang SW, Yee AF, Chen CS, Leong KW. Nanopattern-induced changes in morphology and motility of smooth muscle cells. Biomaterials. 2005;26:5405-13.

[320] Creasey R, Sharma S, Gibson CT, Craig JE, Ebner A, Becker T, et al. Atomic force microscopy-based antibody recognition imaging of proteins in the pathological deposits in Pseudoexfoliation Syndrome. Ultramicroscopy. 2011;111:1055-61.

[321] Wolf MT, Daly KA, Reing JE, Badylak SF. Biologic scaffold composed of skeletal muscle extracellular matrix. Biomaterials. 2012;33:2916-25.

[322] Darling EM, Wilusz RE, Bolognesi MP, Zauscher S, Guilak F. Spatial Mapping of the Biomechanical Properties of the Pericellular Matrix of Articular Cartilage Measured In Situ via Atomic Force Microscopy. Biophys J. 2010;98:2848-56.

[323] Ghosh K, Pan Z, Guan E, Ge S, Liu Y, Nakamura T, et al. Cell adaptation to a physiologically relevant ECM mimic with different viscoelastic properties. Biomaterials. 2007;28:671-9.

[324] Thomas M, Langley B, Berry C, Sharma M, Kirk S, Bass J, et al. Myostatin, a Negative Regulator of Muscle Growth, Functions by Inhibiting Myoblast Proliferation. J Biol Chem. 2000;275:40235-43.

[325] Yim EKF, Leong KW. Significance of synthetic nanostructures in dictating cellular response. Nanomedicine: Nanotechnology, Biology and Medicine. 2005;1:10-21.

[326] Corona BT, Garg K, Ward CL, McDaniel JS, Walters TJ, Rathbone CR. Autologous minced muscle grafts: a tissue engineering therapy for the volumetric loss of skeletal muscle. Am J Physiol- Cell Ph. 2013;305:C761-C75.

[327] Corona BT, Wu X, Ward CL, McDaniel JS, Rathbone CR, Walters TJ. The promotion of a functional fibrosis in skeletal muscle with volumetric muscle loss injury following the transplantation of muscle-ECM. Biomaterials. 2013;34:3324-35.

[328] Conconi MT, Coppi PD, Bellini S, Zara G, Sabatti M, Marzaro M, et al. Homologous muscle acellular matrix seeded with autologous myoblasts as a tissue-engineering approach to abdominal wall-defect repair. Biomaterials. 2005;26:2567-74.

[329] Atala A, Bauer SB, Soker S, Yoo JJ, Retik AB. Tissue-engineered autologous bladders for patients needing cystoplasty. The Lancet.367:1241-6.

[330] Dohmen PM, Lembcke A, Holinski S, Pruss A, Konertz W. Ten Years of Clinical Results With a Tissue-Engineered Pulmonary Valve. Ann Thorac Surg. 2011;92:1308-14.

[331] Raya-Rivera A, Esquiliano DR, Yoo JJ, Lopez-Bayghen E, Soker S, Atala A. Tissue-engineered autologous urethras for patients who need reconstruction: an observational study. The Lancet.377:1175-82.

[332] Elliott MJ, De Coppi P, Speggiorin S, Roebuck D, Butler CR, Samuel E, et al. Stem-cell-based, tissue engineered tracheal replacement in a child: a 2-year follow-up study. The Lancet.380:994-1000.

[333] Jungebluth P, Alici E, Baiguera S, Le Blanc K, Blomberg P, Bozóky B, et al. Tracheobronchial transplantation with a stem-cell-seeded bioartificial nanocomposite: a proof-of-concept study. The Lancet.378:1997-2004.

Every reasonable effort has been made to acknowledge the owners of copyright material. I would be pleased to hear from any copyright owner who has been omitted or incorrectly acknowledged.